

AD-A069 646

NORTHROP CORP HAWTHORNE CA AIRCRAFT GROUP

F/G 20/4

ANALYSIS OF WIND TUNNEL DATA PERTAINING TO HIGH ANGLE OF ATTACK--ETC(U)

JUL 78 J W HEADLEY

F33615-77-C-3062

UNCLASSIFIED

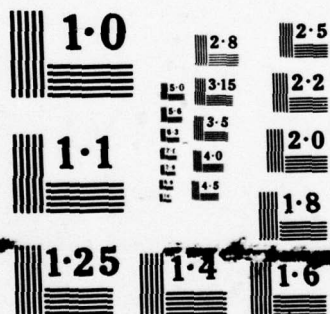
NOR-78-69-VOL-1

AFFDL-TR-78-94-VOL-1

NL

1 OF 2
AD
A089646





NATIONAL BUREAU OF STANDARDS

AD A 069646

AFFDL-TR-78-94
VOLUME I

LEVEL II

2

ANALYSIS OF WIND TUNNEL DATA PERTAINING TO HIGH ANGLE-OF-ATTACK AERODYNAMICS

VOLUME I — Technical Discussion and Analysis of Results

J. W. Headley

NORTHROP CORPORATION AIRCRAFT GROUP
HAWTHORNE, CALIFORNIA

JULY 1978



DDC FILE COPY

Approved for public release; distribution unlimited.

AIR FORCE FLIGHT DYNAMICS LABORATORY
AIR FORCE SYSTEMS COMMAND
WRIGHT-PATTERSON AIR FORCE BASE, OHIO

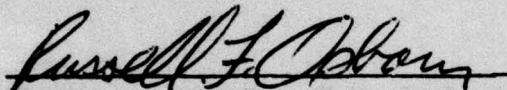
79 06 07 044

NOTICE

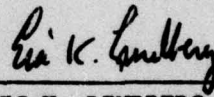
When Government drawings, specifications, or other data are used for any purpose other than in connection with a definitely related Government procurement operation, the United States Government thereby incurs no responsibility nor any obligation whatsoever; and the fact that the government may have formulated, furnished, or in any way supplied the said drawings, specifications, or other data, is not to be regarded by implication or otherwise as in any manner licensing the holder or any other person or corporation, or conveying any rights or permission to manufacture, use, or sell any patented invention that may in any way be related thereto.

This report has been reviewed by the Information Office (OI) and is releasable to the National Technical Information Service (NTIS). At NTIS, it will be available to the general public, including foreign nations.

This technical report has been reviewed and is approved for publication.

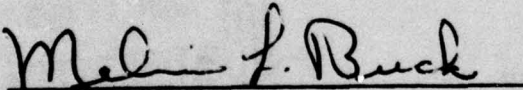


RUSSELL F. OSBORN
Project Engineer
Aerodynamics and Airframe Branch
Aeromechanics Division



ERIC K. LINDBERG, Major, USAF
Chief, Aerodynamics and Airframe Branch
Aeromechanics Division

FOR THE COMMANDER



MELVIN L. BUCK
Acting Chief
Aeromechanics Division

"If your address has changed, if you wish to be removed from our mailing list, or if the addressee is no longer employed by your organization please notify _____, W-PAFB, OH 45433 to help us maintain a current mailing list".

Copies of this report should not be returned unless return is required by security considerations, contractual obligations, or notice on a specific document.

Unclassified

SECURITY CLASSIFICATION OF THIS PAGE (When Data Entered)

19 REPORT DOCUMENTATION PAGE		READ INSTRUCTIONS BEFORE COMPLETING FORM	
1. REPORT NUMBER	2. GOVT ACCESSION NO.	3. RECIPIENT'S CATALOG NUMBER	
18 AFFDL TR-78-94 1 VOL-1			
4. TITLE (and Subtitle)		5. TYPE OF REPORT & PERIOD COVERED	
6 ANALYSIS OF WIND TUNNEL DATA PERTAINING TO HIGH ANGLE OF ATTACK AERODYNAMICS, VOLUME I, TECHNICAL DISCUSSION AND ANALYSIS OF RESULTS		9 Technical Report. Jan 77 - Apr 78	
7. AUTHOR(s)		6. PERFORMING ORG. REPORT NUMBER	
10 Jack W. Headley		NOR-78-09-VOL-1	
9. PERFORMING ORGANIZATION NAME AND ADDRESS		14. CONTRACT OR GRANT NUMBER(s)	
Northrop Corporation Aircraft Group. Hawthorne, California		15 F33615-77-C-3062 nww	
11. CONTROLLING OFFICE NAME AND ADDRESS		10. PROGRAM ELEMENT, PROJECT, TASK AREA & WORK UNIT NUMBERS	
Air Force Flight Dynamics Laboratory (FXM) Air Force Systems Command Wright-Patterson Air Force Base, Ohio		16 2404 10-17	
14. MONITORING AGENCY NAME & ADDRESS (if different from Controlling Office)		12. REPORT DATE	
12 180p.		Jul 1978	
		13. NUMBER OF PAGES	
		168	
		15. SECURITY CLASS. (of this report)	
		Unclassified	
		15a. DECLASSIFICATION/DOWNGRADING SCHEDULE	
16. DISTRIBUTION STATEMENT (of this Report)			
Approved for public release; distribution unlimited			
17. DISTRIBUTION STATEMENT (of the abstract entered in Block 20, if different from Report)			
18. SUPPLEMENTARY NOTES			
19. KEY WORDS (Continue on reverse side if necessary and identify by block number)			
Aerodynamics Forebodies Fighter Aircraft Wing Leading Edge Extensions High Angle of Attack Vertical Tails Wind Tunnel Results Forebody Strakes			
20. ABSTRACT (Continue on reverse side if necessary and identify by block number)			
This report provides a technical discussion and analysis of wind tunnel data obtained from tests conducted on a family of Northrop fighter aircraft. These tests were performed mainly in the Northrop Low Speed Wind Tunnel, and cover the time period between 1966 and 1976. This report concentrates on data in the stall post-stall region, and for convenience is provided in two sections. This volume presents the results of the analysis of wind tunnel data which concentrates on the high angle of attack regime, and on			

DD FORM 1 JAN 73 1473

Unclassified

SECURITY CLASSIFICATION OF THIS PAGE (When Data Entered)

410 275

79 06 07 044

Unclassified

SECURITY CLASSIFICATION OF THIS PAGE(When Data Entered)

three major aircraft components. These components are the nose and forebody, the wing leading edge extension, and the vertical tail. The effects of geometric changes in these components on the aircrafts high angle of attack aerodynamics is analysed. Wherever possible design guidelines which identify the sensitivity of aerodynamic characteristics to geometric parameter variations are presented. Geometric changes or effects which were configuration dependent are also discussed. The second volume, Volume II: "Data Base," contains summaries of the wind tunnel tests which were selected to provide data for the analysis.

SECURITY CLASSIFICATION OF THIS PAGE(When Data Entered)

FOREWORD

This report, "Analysis of Wind Tunnel Data Pertaining to High Angle-of-Attack Aerodynamics" provides a technical discussion and analysis of wind tunnel data obtained from tests conducted on a family of Northrop fighter aircraft. These tests were performed mainly in the Northrop Low Speed Wind Tunnel, and cover the time period between 1966 and 1976. This report concentrates on data in the stall/post-stall region, and for convenience is provided in two sections. The first section, provided in this volume presents the data analysis and from this analysis derives some general guidelines to aid in the design of future fighter aircraft operating in this high angle-of-attack regime. The second volume, Volume II: "Data Base", contains summaries of the wind tunnel tests which were selected to provide data for the analysis.

This report was prepared by the Northrop Corporation, Aircraft Group, Hawthorne, California, under United States Air Force Contract F33615-77-C-3062. The program was administered by the Air Force Flight Dynamics Laboratory, Air Force Systems Command, Wright-Patterson Air Force Base, Ohio. The project engineer was R. F. Osborne (AFFDL/FXM).

The contract work was performed during the period June 1977 to April 1978. The draft of this report was submitted in April 1978.

The author acknowledges his gratitude to O. R. Edwards and A. M. Skow for assistance in data analysis and interpretation during the preparation of this volume. Northrop report number NOR 78-69 has been assigned for internal control.

WTS GAMA DDC TAB Unannounced Justification	By _____ Distribution/ Availability Codes Availand/or Special
---	---

TABLE OF CONTENTS

Section		Page
I	INTRODUCTION	1
	1. CONFIGURATION EVOLUTION, F-5E and F-5F	2
	2. YF-17 SERIES EVOLUTION	3
	a. N300/P530	3
	b. P600/610/YF-17	6
	3. REPORT PRESENTATION	9
II	ANALYSIS OF DATA AND DESIGN GUIDELINES	11
	1. NOSE AND FOREBODY EFFECTS	11
	a. Effects at Zero Sideslip	12
	b. Effects at Non-Zero Sideslip	22
	c. Pointed Noses	25
	Nose Booms	39
	Nose Strakes	44
	d. Blunted Noses	52
	e. Camera Noses	58
	f. Shark Type Noses	66
	g. Forebody Design Guidelines Summary	77
	2. Wing Leading Edge Extensions	82
	a. The Isolated LEX	84
	b. LEX/Wing Combinations	86
	c. Complete Configuration Data	102
	d. Lateral/Directional Effects	119
	e. Summary of Results	130
	3. Vertical Tails	132
	a. Single Vertical Tails	134
	b. Twin Vertical Tails	138
	4. Miscellaneous Configuration Components	143
	a. Wing Leading Edge Discontinuities	143
	b. Wing Upper Surface Fences	146
	c. Wing Leading-Edge Flaps	155
	d. Wing Trailing-Edge Flaps	158
	e. Dorsal/Ventral Fins	160
	f. Decoupled Canards	163
III	CONCLUDING REMARKS	167

LIST OF ILLUSTRATIONS

<u>Figure</u>		<u>Page</u>
1	F-5 Configuration Genealogy	4
2	Northrop F-5E and F-5F Aircraft	5
3	YF-17 Configuration Genealogy	7
4	Northrop YF-17 Aircraft	8
5	Typical Fighter Forebody	11
6	Typical Fighter Forebody Lengths	13
7	Vortex Patterns	14
8	Wind Tunnel/Flight Test Correlation	15
9	F-5F Forebody in Water Tunnel	16
10	Forebody Vortex Patterns	17
11	Lateral/Directional Data at Zero Sideslip Angle	18
12	Idealized Forebody Force System	19
13	Pitching Moments at Zero Sideslip	20
14	Normal Force Data at Zero Sideslip.	21
15	Comparison of Directional Stabilities	23
16	Nose Effect of Stability	24
17	Definition of Nose Fineness Ratio	26
18	Definition of Nose Ellipticity and Apex Angle.	27
19	Effects of Nose Fineness Ratio at Zero Sideslip	29
20	Effect of Nose Apex Angle on Onset Angle	30
21	Effect of Mach Number on Onset Angle of Attack	31
22	Effect on Mach Number on Forebody Length Change	32
23	Vertical Tail Off Data	33
24	Trends in Directional Stability	34
25	Directional Stability, F-5F	35
26	Pitching Moment Due to Sideslip	36
27	F-5F Nose Effect at 40° Angle of Attack	37
28	F-5F Force Vector Rotation with Sideslip Angle at 40° Angle of Attack	38

LIST OF ILLUSTRATIONS (Continued)

<u>Figure</u>		<u>Page</u>
29	F-5F with Flight Test Nose Boom Installed	40
30	Nose Boom Effects at Zero Sideslip, YF-17	41
31	Nose Boom Effects at Sideslip Angle of YF-17	42
32	Nose Boom Effects F-5E/F	43
33	YF-17 Strake Geometry.	44
34	Effect of Nose Boom and Strake	45
35	Nose Strake Effect	46
36	Effect of Strake Configurations at 10° Sideslip.	47
37	Effect of Nose Strake at Zero Sideslip	49
38	Effect of Nose Strake on Directional Stability	50
39	F-5 Strake Geometry Definitions	50
40	Radiused Nose	52
41	Lateral/Directional Effects of Increased Nose Radius at Zero Sideslip	54
42	Pitching Moment Effects Due to Increased Nose Radius at Zero Sideslip	55
43	Effect of Nose Radius Increases on Onset Angle of Attack	56
44	Effect of Nose Radius Increases on Peak Asymmetric Yawing Moments	56
45	Comparison of Peak Asymmetric Data	57
46	Comparison of Onset Angle of Attack Data	57
47	Lateral/Directional Stability Effects	59
48	Effect of β_0 Bias on Directional Stability	60
49	F-5E Camera Nose	61
50	Effect of Camera Nose at Zero Sideslip	62
51	Effect of Camera Nose on Zero Sideslip Asymmetries	63
52	Camera Nose Zero Sideslip Yawing Moments	64
53	Effects of Cross Flow Mach Number	65
54	Directional Stability Comparisons.	67
55	Comparison of Directional Stabilities	68
56	Shark Nose Geometry	69
57	Effect of Shark Nose at Zero Sideslip	70
58	Effect of Shark Nose on Zero Sideslip Pitching Moments.	72

LIST OF ILLUSTRATIONS (Continued)

<u>Figure</u>		<u>Page</u>
59	Effect of Shark Nose on Lateral/Directional Stability.	73
60	Effect of Shark Nose on Pitching Moments in Sideslip	74
61	Surface Oil Flows on F-5F Nose	75
62	F-5F Model in Northrop Water Tunnel	76
63	Onset Angle for Nose Stability	80
64	Range of Nose Stability	80
65	Limiting Regions for Nose Vortex Effects	81
66	F-5A Wing Leading Edge Extension	83
67	Slender Delta Wing Vortex Burst Locations	83
68	Conditions for Trailing Edge Vortex Burst Location	85
69	Lift Characteristic - 75° Delta Wing.	86
70	Wing/Body Geometry	87
71	Effect of Flap Deflection on the Vortex Burst Angle of Attack .	88
72	Basic Wing (LEX Off) Performance L.E. Flaps Deflected . . .	90
73	Triangular LEX Configurations	91
74	Triangular LEX's - Lift Effects	92
75	Triangular LEX's - Pitching Moment Effects	93
76	Summary of Lift Data	94
77	LEX Effect - Empennage Off	96
78	Pitching Moment Effects of LEX	97
79	Comparison of Wing Body and Delta Wing Data	97
80	LEX Pitching Moment Effects	99
81	LEX Strake Geometry.	99
82	Effect of LEX Strakes	100
83	Effect of LEX Planform Shape on Lift	101
84	LEX/Wing/Body Geometry	101
85	Effect of LEX at High Speeds	103
86	Effect of LEX at High Speeds.	105
87	Pitching Moments at Constant Angle of Attack	107
88	a. N300 Lift Data	108
89	b. P530 Lift Data	109
90	c. P600 Lift Data	110

LIST OF ILLUSTRATIONS (Continued)

Figure		Page
91	d. P610 Lift Data	111
92	e. P630 Lift Data	112
93	f. YF-17 Lift Data	113
94	g. F-5E/F Lift Data	114
95	a. Lift Data Summary (Flaps Up)	115
96	b. Lift Data Summary (Flaps Down)	116
97	Effect of LEX Planform Shape (Flaps Down)	117
98	Effect of LEX Strake	118
99	LEX Effect on Wing Body Data	120
100	LEX Effect on Wing Body Data	121
101	Triangular LEX Effects in Sideslip	123
102	Triangular LEX Effect in Sideslip	124
103	Schematic of LEX Effect in Sideslip	126
104	Effect of Reduced LEX Angle of Attack	128
105	Effect of Leading Edge Curvature on Vortex Burst Poing ($\alpha = 25$)	129
106	Linearized LEX Lift Effects	131
107	Single Vertical Tail Configuration	132
108	Effectiveness of a Single Vertical Tail	133
109	Definition of α_c	134
110	Definition of θ_V	135
111	Vertical Tail Effective Range	136
112	Vertical Tail Effective Range as a Function of Wing Blanketing Angle	137
113	Effect of Vertical Tail Area	139
114	Effect of Vertical Tail Area	140
115	Effect of Fore and Aft Location	141
116	Vertical Tail Geometries	142
117	Wing Leading Edge Discontinuities	144
118	Effect of Leading Edge Discontinuities	145
119	Wing Fence Geometry	146
120	Effect of Upper Surface Wing Fences	147

LIST OF ILLUSTRATIONS (Continued)

<u>Figure</u>		<u>Page</u>
121	Effect of Fence Semi-Span Station	147
122	Effect of Upper Surface Wing Fences	148
123	Effect of Fence Semi-Span Station	149
124	Effect of Fence Height	150
125	Effect of Fence Height	150
126	Effect of Fence Chord Length	151
127	Effect of Fence Chord Length	152
128	Effect of Fence Chord Length	152
129	Effect of Fence Chord Length	153
130	Effect of Flap Deflection on C_{LMAX}	154
131	Effect of Flap Deflection on $C_{N\beta DYN. MIN.}$	154
132	Effect of Leading Edge Flap Deflection	156
133	Effect of Leading Edge Flap Deflection	157
134	Effect of T/E Flap Deflection	159
135	Dorsal Fin Geometry	160
136	Typical Ventral Fin	161
137	Ventral Fin Geometry	161
138	Effect of Ventral Fins	162
139	Typical Canard Geometry	163
140	Effect of Decoupled Canards	164
141	Effect of Decoupled Canards	165
142	Effect of Canard Size	165
143	Effect of Canards	166

LIST OF SYMBOLS

α , ALPHA	Angle of Attack
β	Angle of Sideslip
\bar{c}	Mean Aerodynamic Chord (M.A.C.)
C_l , CLLB	Rolling Moment Coefficient
C_n , CLNB	Yawing Moment Coefficient
$C_{l\beta}$	Lateral Stability Coefficient
C_{LM} , C_M	Pitching Moment Coefficient
$C_{m\beta}$	Pitching Moment Coefficient Due to Sideslip
C_N	Normal Force Coefficient
$C_{n\beta}$	Directional Stability Coefficient
$C_{n\beta_{dyn.}}$	Directional Divergence Parameter
CY	Side Force Coefficient
δf	Trailing Edge Flap Deflection Angle
δn	Leading Edge Flap Deflection Angle
l_c	Canard Moment Arm
l_v	Vertical Tail Moment Arm
M	Mach Number

SECTION I

INTRODUCTION

Northrop has designed and manufactured a family of fighter aircraft beginning in 1955 with the N156 and progressing through the T-38, F-5A, F-5B, F-5E, F-5F and finally to the YF-17. This report will concentrate on the last three members of this family, the F-5E, F-5F and YF-17, and their aerodynamic development. Of these three aircraft, both the F-5E and the YF-17 began as advanced versions of the F-5A. The F-5F is a two placed version of the F-5E.

The F-5E/F are closely related aerodynamically to the original F-5A, but the YF-17 passed through several project stages, the N300, P530, P600 and P610 before the final configuration was defined.

The configuration development of these various aircraft covered the time period between 1966 to 1976, when over 18,000 hours of wind tunnel testing were completed both at Northrop (high and low speed) and at various other facilities. These tests covered configuration integration and refinement, control effectiveness, static stability, and store carriage and separation. A wide variety of wings and leading edge extensions, body shapes and empennage configurations were tested in order to achieve the desired high lift stability and control requirements, though not necessarily in parametric form.

A major consideration during these development tests was placed on high maneuverability at subsonic speeds over a greatly increased angle-of-attack range, and to have adequate stability and control in the stall/post stall flight regimes. Thus, an extensive body of test data over a large angle-of-attack range has been accumulated by Northrop for a wide variety of wings, bodies and empennages. Part of this information forms the data base for this report.

It is not the purpose of this report to cover the complete aerodynamic development of these various aircraft. Attention will be focused only on certain components,

components which are of primary importance in the high angle-of-attack flight regime. These components include the forebody, the wing leading edge extensions, the vertical tail, and strakes on the forebody. The wind tunnel test data for geometric variations of these components are discussed and analysed. Based on the results of this analysis, design guidelines are developed for forebody shaping, the use of nose strakes, and wing leading edge extensions. These guidelines will thus be available for use in the development of future fighter aircraft.

Before commencing the data analysis and design guidelines discussion, some clarification of the various aircraft and project types briefly mentioned above, and used extensively throughout the report, will be made. The following paragraphs trace the aerodynamic evolution of the F-5E/F and the YF-17 aircraft, and discuss the various project definitions which make up the YF-17 development background.

1. CONFIGURATION EVOLUTION, F-5E AND F-5F

By the early 1960's, U.S. military planners began to establish requirements for an advanced, higher performance Military Assistance Program (MAP) defense fighter. Anticipating the need for an upgraded version of the F-5A to fill this role, Northrop investigated the adaptation of the new higher thrust General Electric J85-21 engine.

The resulting aircraft designated YF-5-21, was further enhanced with a larger wing leading-edge extension (LEX) for better lift, a maneuvering flap system, and other specialty features which had been individually tailored for countries operating the earlier F-5's. The test bed YF-5B-21 made its flight on March 28, 1969, at Edwards Air Force Base.

In the fall of 1969, a decision was reached to competitively select the most appropriate airplane for the new International Fighter Aircraft (IFA) role. Proposals were prepared and submitted by Lockheed, LTV, McDonnell Douglas, and Northrop. The F-5-21 was selected to be the new IFA. Several aerodynamic features not found on earlier F-5's were incorporated, such as stretching and widening of the fuselage because of the larger engines and inlet ducts, increased wing area and an enlarged

wing leading edge extension. In January 1971, the Air Force changed the model designation of the F-5-21 to the F-5E. The first F-5E made its initial flight on August 11, 1972 at Edwards AFB.

A Full-Scale Development program for a two-place version of the airplane was initiated in April 1973, named the F-5F. The F-5F retained the combat capability and weapon delivery accuracy of the single-place fighter but was also able to serve as an advanced trainer. Major differences were the stretched forward fuselage to accommodate the second crew member. The first F-5F flew at Edwards AFB on September 24, 1974. Figure 1 illustrates the small differences between the F-5A, E and F. Figure 2 shows the F-5 in flight.

2. YF-17 SERIES EVOLUTION

a. N300/P530

In 1965, operations analyses were conducted by Northrop to define the requirements for an advanced F-5 lightweight, multirole, tactical fighter, designated the N300. The N300 possessed certain F-5 configuration characteristics: a wing of F-5 planform, a stretched F-5 fuselage, and a propulsion system of two General Electric engines. Testing and analysis led to a high wing configuration, which increased the ordnance capability.

However, the major impact of relocating the wing was to permit the LEX to extend forward. With the low wing configuration the leading edge of the LEX was fixed by the engine inlet location. By "uncoupling" the wing and the engine intake ducts, the leading edge extension could be greatly increased in area from its previous size (5% of the basic wing area), to sizes around 15% wing area. This was then the beginning in the development of the YF-17 hybrid wing configuration, and the use of vortex lift for high angle-of-attack maneuverability. In 1967, the designation was changed to the P530. The aerodynamically curved, wing leading-edge extensions and their longitudinal slots were increased in size for greater lift and airflow control. Canted twin vertical tails replaced the single vertical to provide the desired lateral directional stability at high angles of attack. Development continued through 1969, where a more refined LEX shape was defined to increase lift and improve the vortex bursting character, thereby enhancing the stability and control characteristics at high angles of attack. The cockpit was moved forward for better pilot visibility and for improved avionics and gun system installations.

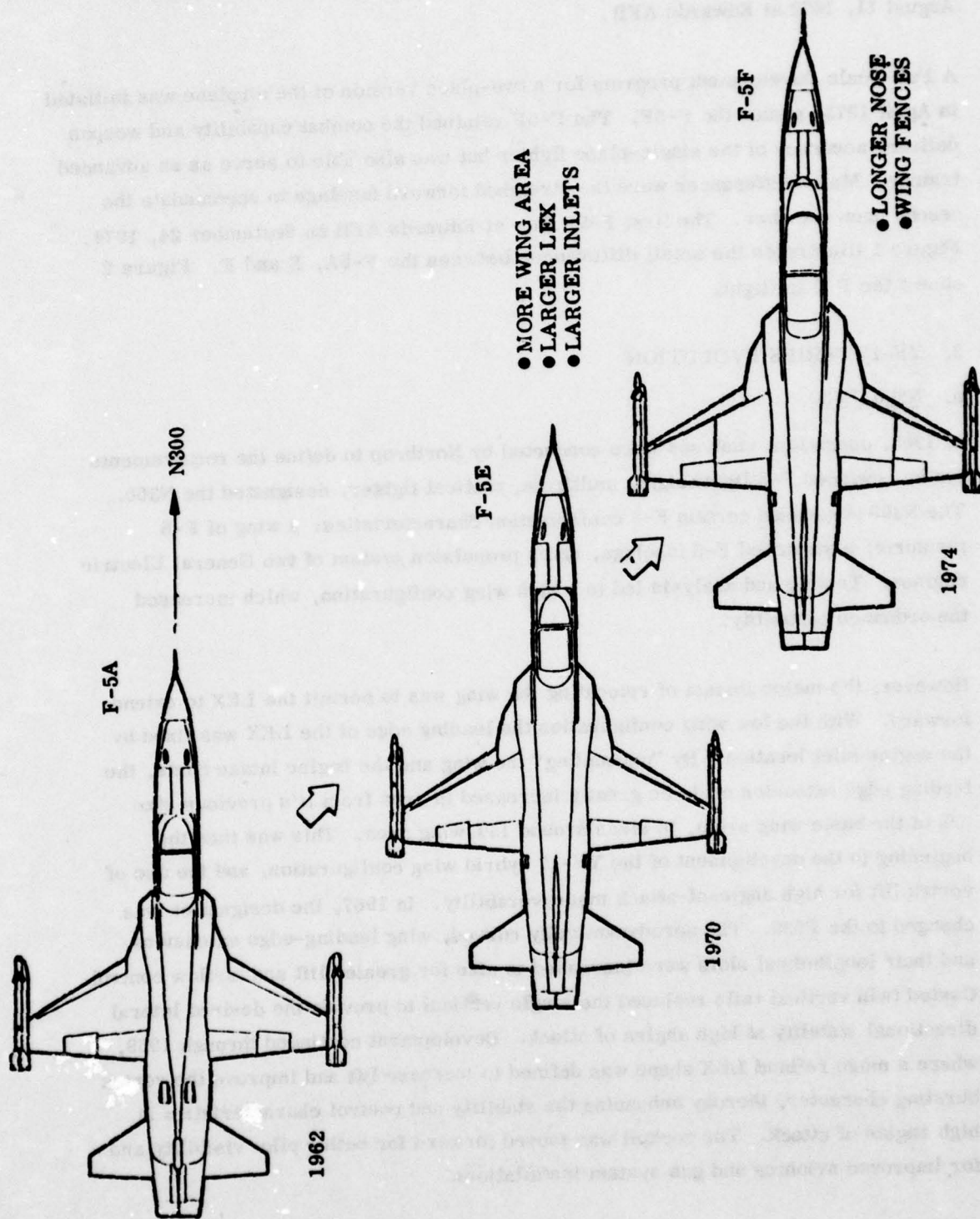


Figure 1. F-5 Configuration Genealogy

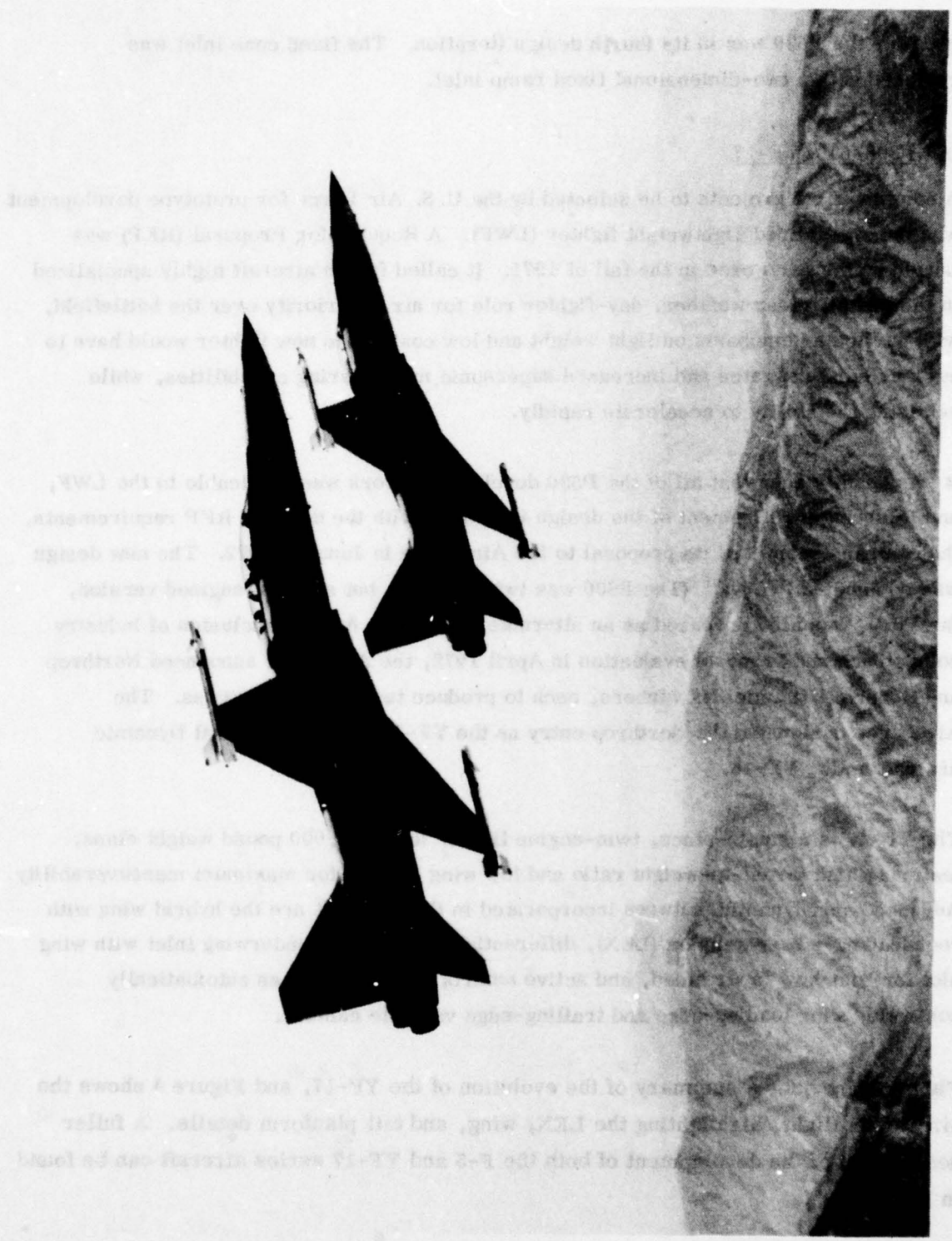


Figure 2. Northrop F-5E and F-5F Aircraft

In 1970, the P530 was in its fourth design iteration. The fixed cone inlet was replaced with a two-dimensional fixed ramp inlet.

b. P600/610/YF-17

Among the first projects to be selected by the U. S. Air Force for prototype development was the specialized lightweight fighter (LWF). A Request for Proposal (RFP) was issued by the Air Force in the fall of 1971. It called for an aircraft highly specialized in the visual, clear weather, day-fighter role for air superiority over the battlefield, with particular emphasis on light weight and low cost. The new fighter would have to sustain high turn rates and increased supersonic maneuvering capabilities, while retaining the ability to accelerate rapidly.

It was readily seen that all of the P530 development work was applicable to the LWF, and following a refinement of the design to comply with the detailed RFP requirements, the company submitted its proposal to the Air Force in January 1972. The new design was designated "P600." (The P600 was twin engined, but a single engined version, the P610, was also proposed as an alternate solution). At the conclusion of industry competition and proposal evaluation in April 1972, the Air Force announced Northrop and General Dynamics as winners, each to produce two flying prototypes. The Air Force designated the Northrop entry as the YF-17, and the General Dynamic aircraft as the YF-16.

The YF-17 is a single-place, twin-engine fighter in the 20,000 pound weight class, featuring high thrust-to-weight ratio and low wing loading for maximum maneuverability. Advanced aerodynamic features incorporated in this aircraft are the hybrid wing with root leading-edge extension (LEX), differential area ruling, underwing inlet with wing slot for boundary layer bleed, and active control features such as automatically controlled wing leading-edge and trailing-edge variable camber.

Figure 3 provides a summary of the evolution of the YF-17, and Figure 4 shows the aircraft in flight, highlighting the LEX, wing, and tail planform details. A fuller description of the development of both the F-5 and YF-17 series aircraft can be found in Reference 1.

1. Anderson, F., "Northrop - An Aeronautical History," Northrop Corporation, July 1976.

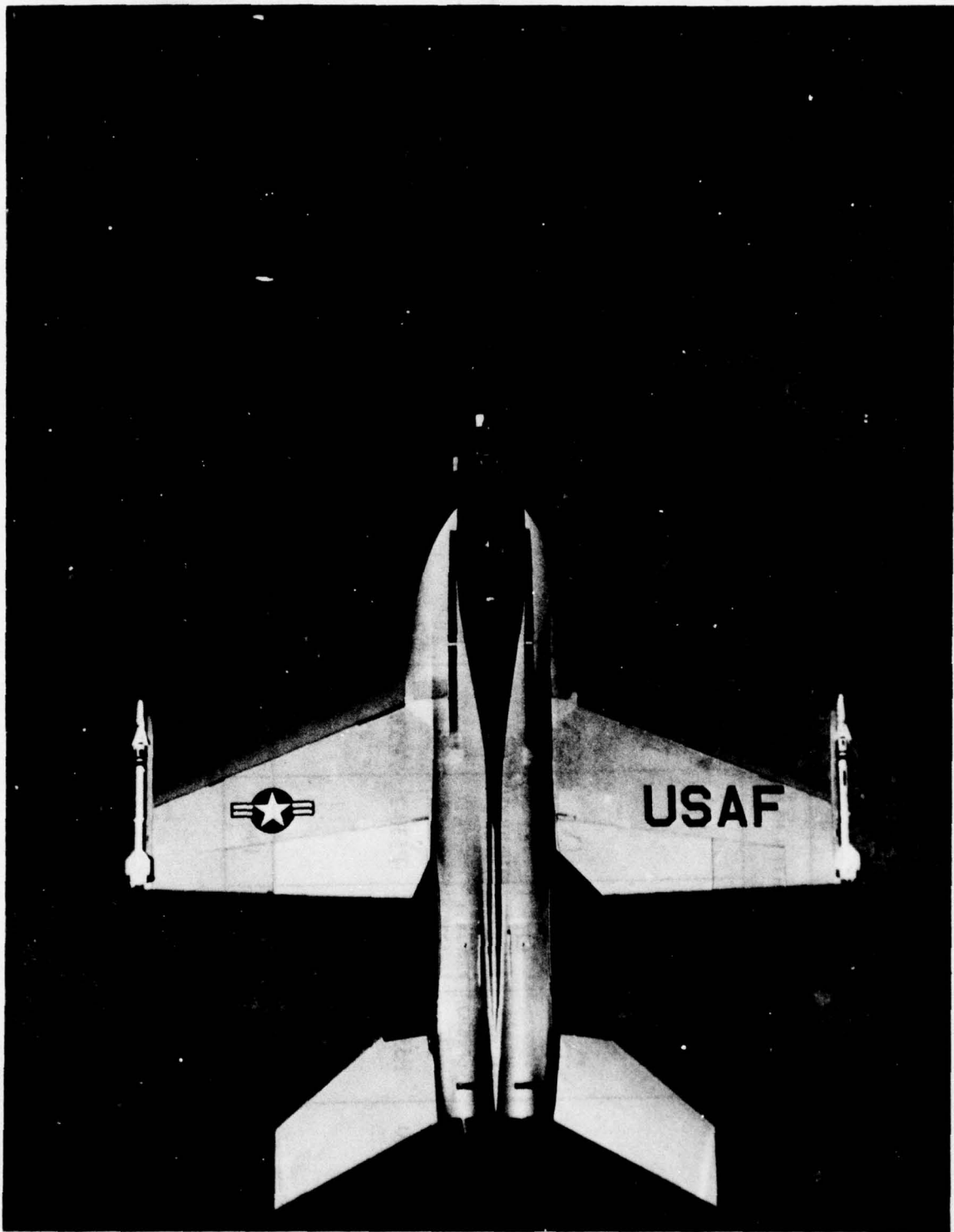


Figure 4. Northrop YF-17 Aircraft

This report covers the aerodynamic development of this hybrid wing, and other features which have significance in the high angle-of-attack region.

3. REPORT PRESENTATION

For convenience the report is presented in two volumes. Volume II contains the data base, and details of wind tunnel test conditions, model configurations and appropriate high angle-of-attack data selected from the available wind tunnel tests.

In this volume, Volume I, an analysis of the test data is presented, together with design guidelines based on empirical relationships developed from this analysis, whenever appropriate.

The following sections of this report will discuss three major aircraft component effects in detail, these being;

- 1) The nose and forebody
- 2) The wing leading edge extension
- 3) The vertical tail

Several other configuration effects (e.g. leading edge discontinuities, using fences, flaps, etc.) are then discussed in lesser detail. Further minor features which were investigated very briefly in the wind tunnel tests, and are therefore not amenable to generalization, are presented only in Volume II. As the great majority of the wind tunnel tests were run only at low speeds, the analytic effort concentrates on the subsonic high angle-of-attack region. Wherever possible, Mach Number effects are presented.

One of the main items of concern is that the results obtained are configuration sensitive, and therefore that the design guidelines derived may have limited general applicability. In an effort to increase the generality of the design guidelines, data from other sources have been combined with the Northrop data wherever possible, and these data are clearly labeled as such when used. Finally, to summarize the main sources of the test results, Table 1 has been prepared. This table indicates from which aircraft series the main body of the data was obtained.

TABLE 1. DATA SOURCES

ITEM	YF-17 Family	F-5 Family
Nose and Forebody	X	X
Wing Leading Edge Extensions	X	X
Vertical Tails	X	X
Leading Edge Discontinuities		X
Wing Fences		X
Leading Edge Flaps	X	X
Trailing Edge Flaps	X	X
Dorsals/Ventrals	X	X
Canards		X

SECTION II

ANALYSIS OF DATA AND DESIGN GUIDELINES

1. NOSE AND FOREBODY EFFECTS

The evolution of fighter aircraft from the piston-engine era to contemporary configurations has seen an ever increasing influence of the nose and forebody region on aircraft flying qualities. In the piston-engine era, the forebody was basically a fairing over the motor, which became shorter and shorter as engine weights increased. Introduction of the jet engine produced a major revision of the fuselage design constraints, with a mid or rearward placement of the engine and the need for a long diffuser ahead of the engine for processing of the inlet airstream. The forebody was used now as a fairing over this diffuser. Increasing speeds, increasing radar requirements and more sophisticated inlet systems were again responsible for a further revision in fuselage concepts. Engines and inlet systems moved rearwards, the nose became longer and more pointed, and the forebody function was now a fairing over the considerable avionics and armament equipment required by the current fighter aircraft. If the forebody is defined as that fuselage region ahead of the C.G., then the forebody length has now become greater than that of the afterbody, as shown in Figure 5.

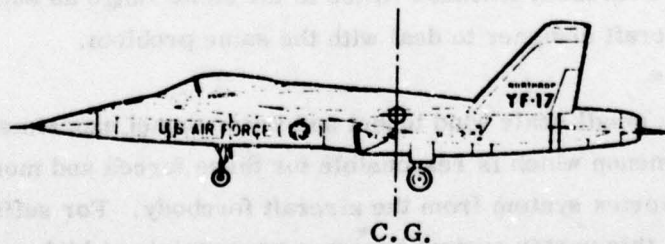


Figure 5. Typical Fighter Forebody

Thus, the size of the forebody has increased progressively until its influence in the complete configuration aerodynamics is now of major importance. This is further illustrated on Figure 6, which shows the configurations used in this study, and presents forebody lengths as a function of the aircraft mean aerodynamic chord.

In addition to this increase in forebody length a similar historical increase in the angle-of-attack range over which fighter aircraft operate has taken place. Development of wing shapes for high maneuverability, and the beneficial effects of the addition of highly swept leading edge extensions has resulted in the increased use of these "hybrid" planforms on contemporary fighters. With such wing planforms, stall angles of attack in the 25° - 35° region are now quite commonplace.

These two effects, the increased forebody length and maneuvering angle of attack envelope have resulted in an increased contribution of the forebody region to the overall aerodynamics of the aircraft.

Before commencing the discussion and analysis of the experimental results, a brief description of the fluid mechanics around the forebody region at high angles of attack will be presented.

a. Effects at Zero Sideslip

One of the detrimental effects of the elongated forebody has been the generation of aerodynamic asymmetries at high angles of attack, which, until recently, had only been considered by missile designers who associated such asymmetries with the long slender missile body. Recent trends in fighter aircraft design have led to aircraft fuselages which have forebody fineness ratios in the same range as some missiles, thus forcing the aircraft designer to deal with the same problem.

It has been shown in small scale wind tunnel and water tunnel experiments that the aerodynamic phenomenon which is responsible for these forces and moments is the growth of a strong vortex system from the aircraft forebody. For sufficiently slender forebodies, this vortex system becomes asymmetric at high angles of attack

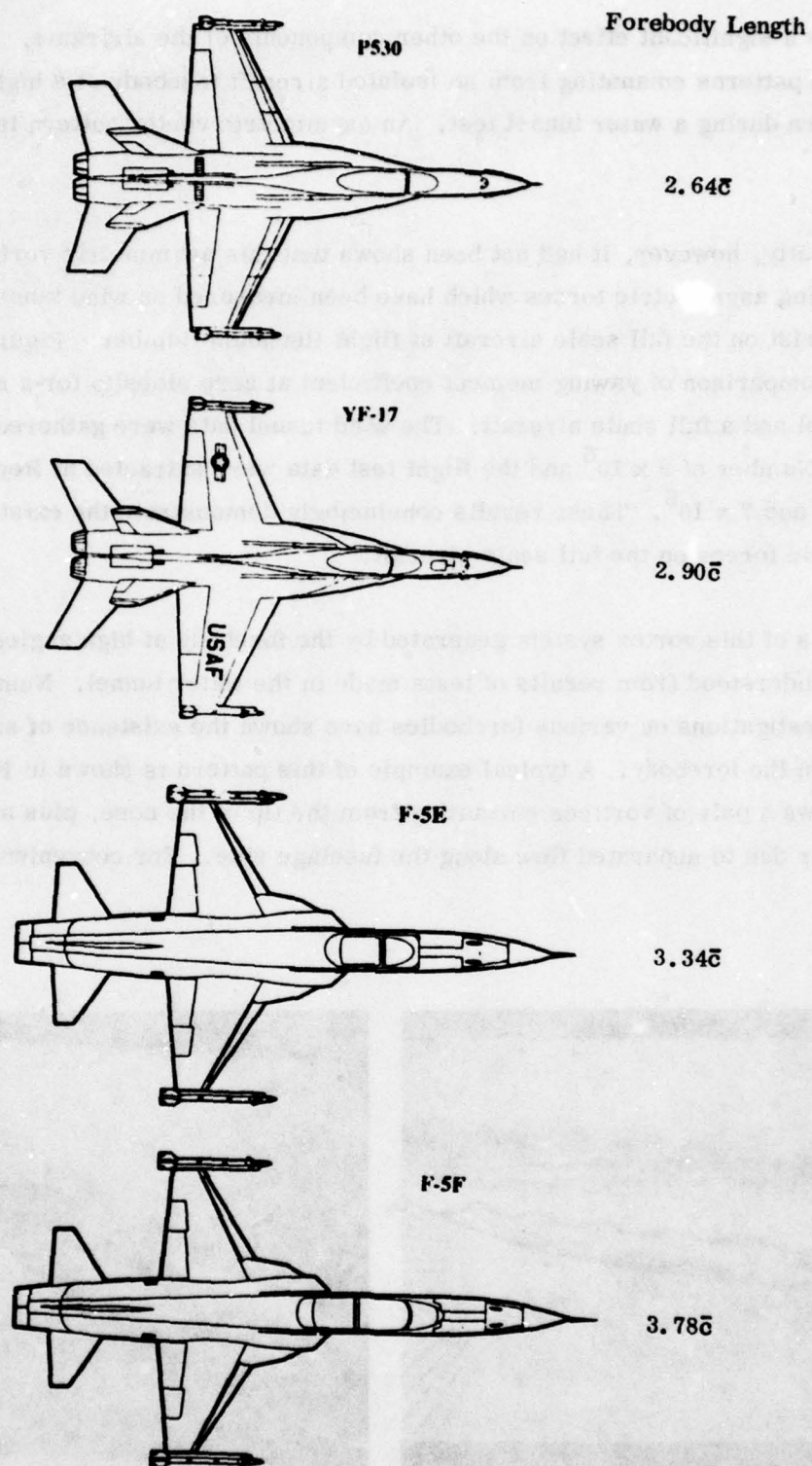


Figure 6. Typical Fighter Forebody Lengths

and exerts a significant effect on the other components of the airframe. Figure 7 shows dye patterns emanating from an isolated aircraft forebody at a high angle of attack taken during a water tunnel test. An asymmetric vortex pattern is clearly shown.

Until recently, however, it had not been shown that this asymmetric vortex system and the resulting asymmetric forces which have been measured on wind tunnel models actually exist on the full scale aircraft at flight Reynolds Number. Figure 8 shows a comparison of yawing moment coefficient at zero sideslip for a small scale wind tunnel and a full scale aircraft. The wind tunnel data were gathered at a Reynolds Number of 2×10^6 and the flight test data were extracted at Reynolds Numbers between 6 and 7×10^6 . These results convincingly demonstrate the existence of the asymmetric forces on the full scale aircraft.

The details of this vortex system generated by the forebody at high angles of attack are best understood from results of tests made in the water tunnel. Numerous water tunnel investigations on various forebodies have shown the existence of similar vortex patterns on the forebody. A typical example of this pattern is shown in Figure 9 which shows a pair of vortices emanating from the tip of the nose, plus a secondary vortex pair due to separated flow along the fuselage side. For convenience in the

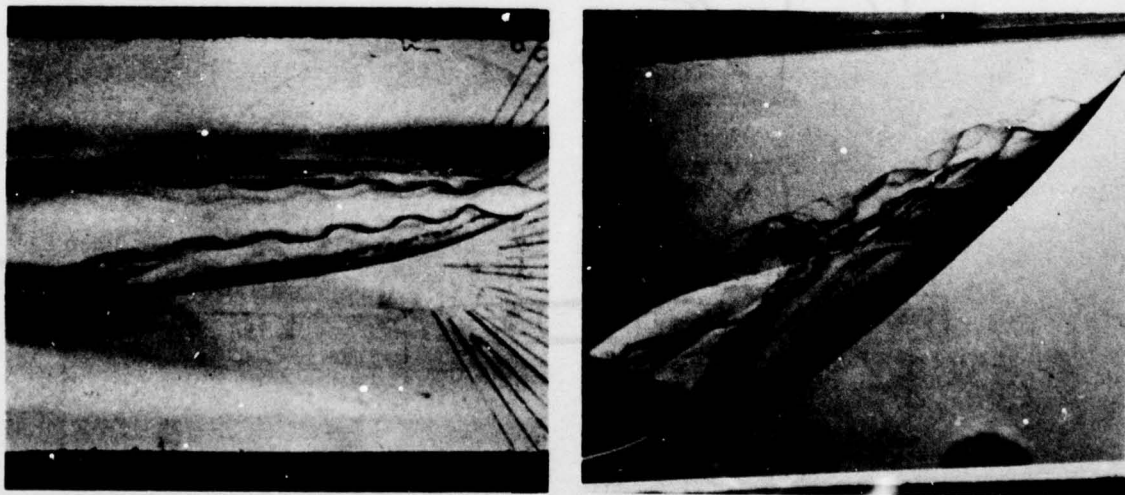


Figure 7. Vortex Patterns

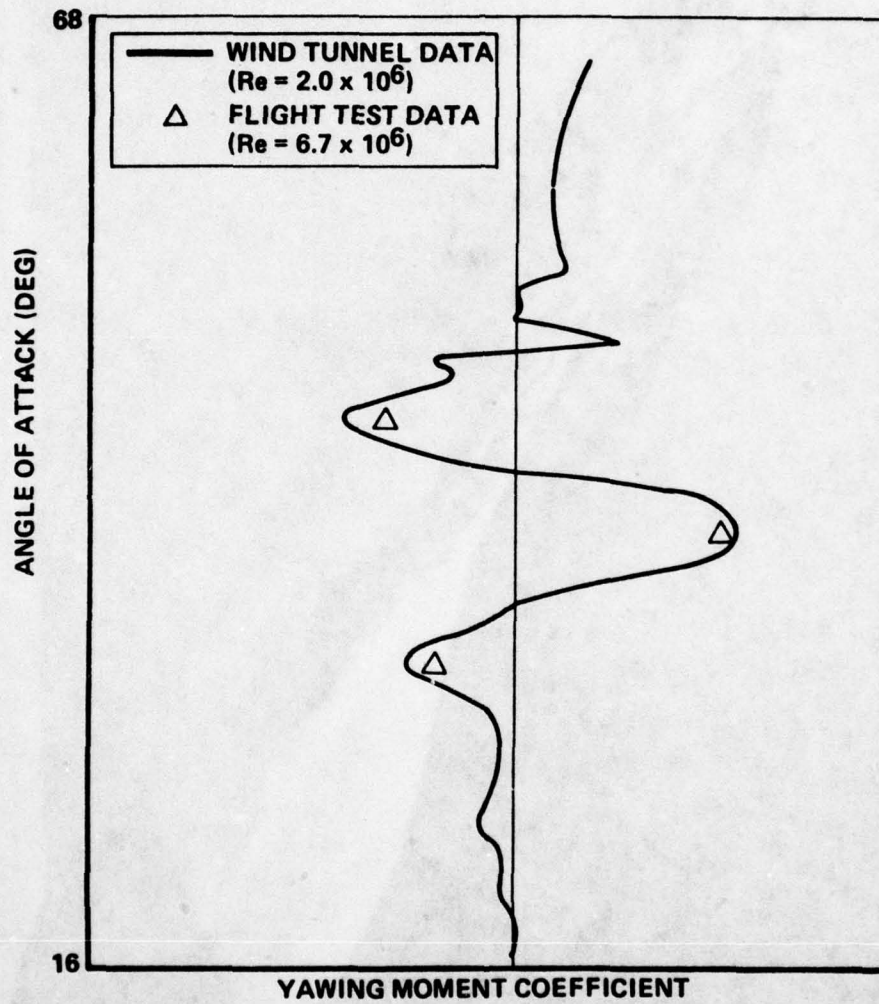


Figure 8. Wind Tunnel/Flight Test Correlation



Figure 9. F-5F Forebody in Water Tunnel

following discussions, the vortex arrangement will be represented by a simplified cross-sectional view of the nose, as shown in Figure 10. This figure illustrates the effects of both a symmetric and an asymmetric vortex pattern around the nose at zero angle of sideslip.

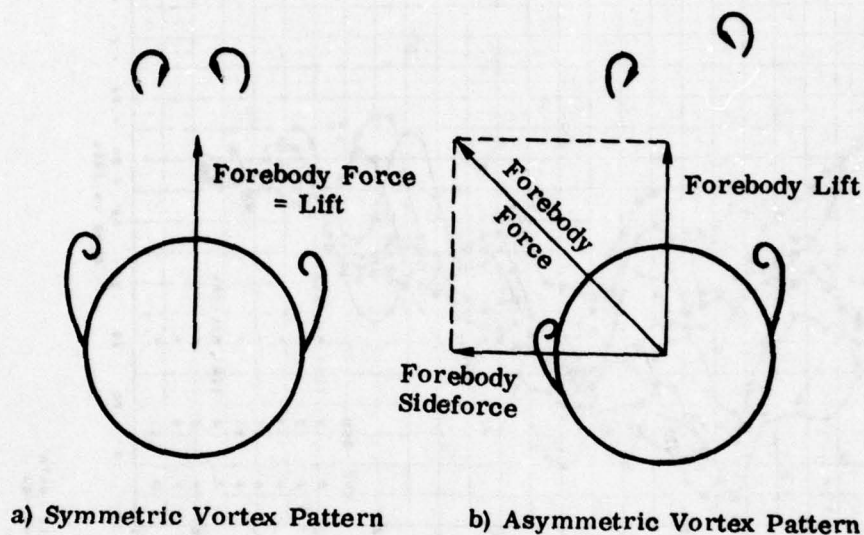
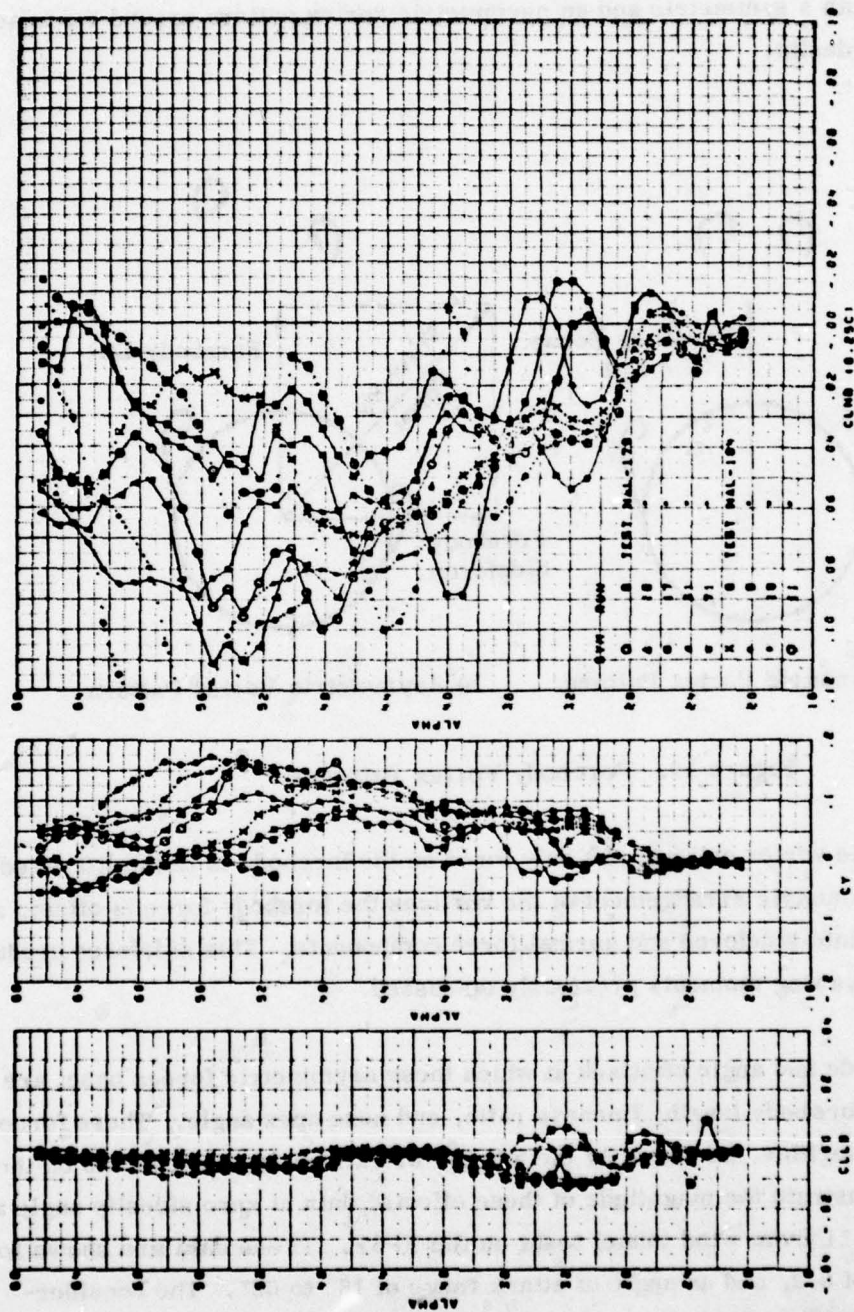


Figure 10. Forebody Vortex Patterns

With a symmetric vortex pattern, the only force on the forebody is in the lift direction; but with the asymmetric arrangement of the vortices the forebody force is offset, and can be resolved into sideforce and normal force components. This sideforce produces the asymmetric yawing moments previously discussed.

Both the magnitude and angle of attack at which these asymmetric forces onset are functions of the forebody length, fineness ratio, and nose apex angle. These forces can be virtually negligible, as shown by the YF-17, or extremely powerful, as on the F-5F. To demonstrate the magnitude of these effects, data at zero sideslip angle are shown in Figure 11 from wind tunnel tests on the F-5F. These data are shown for a Mach number of 0.2, and an angle of attack range of 16° to 68° . The considerable side forces and yawing moments are immediately obvious, beginning at an angle



P-57 BETA ZERO BASIC DATA
P-1-1/L FLAPS-0.0 ONE-00

Figure 11. Lateral/Directional Data at Zero Sideslip Angle

of attack of about 24° . The non-repeatability of these data is caused by small model assembly differences, and slight imperfections on the forebody. Little change in rolling moment is seen, and in general this parameter remains constant throughout the angle-of-attack range. This suggests that the asymmetric forebody vortex patterns do not significantly influence the wing or vertical tail flow fields.

The normal force component of the total forebody force vector also produces effects which have to be considered. Unlike the sideforces which are measured directly in the wind tunnel, the zero sideslip normal force component due to the asymmetric vortex system is indeterminate. Figure 12 illustrates this dilemma. However, the effects of this normal force C_{N_a} can be shown by examination of the pitching moments associated with the wind tunnel data previously shown in Figure 11. These pitching moments are illustrated in Figure 13, where it can be seen that the non-linear longitudinal instabilities above 40° angle of attack coincide with the direction instabilities shown in Figure 11. The normal force data for the same test runs are presented in Figure 14 and shown little change, indicating that the forebody force is small, but its effect is amplified by the long moment arm of the nose.

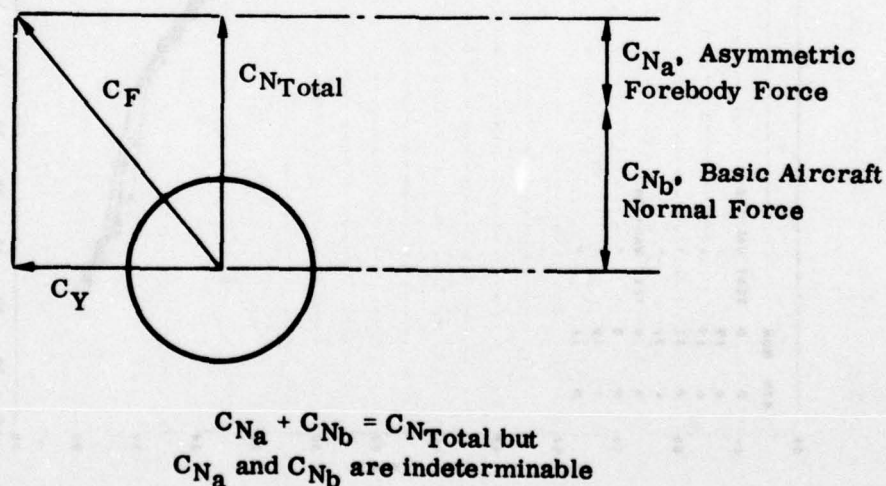


Figure 12. Idealized Forebody Force System

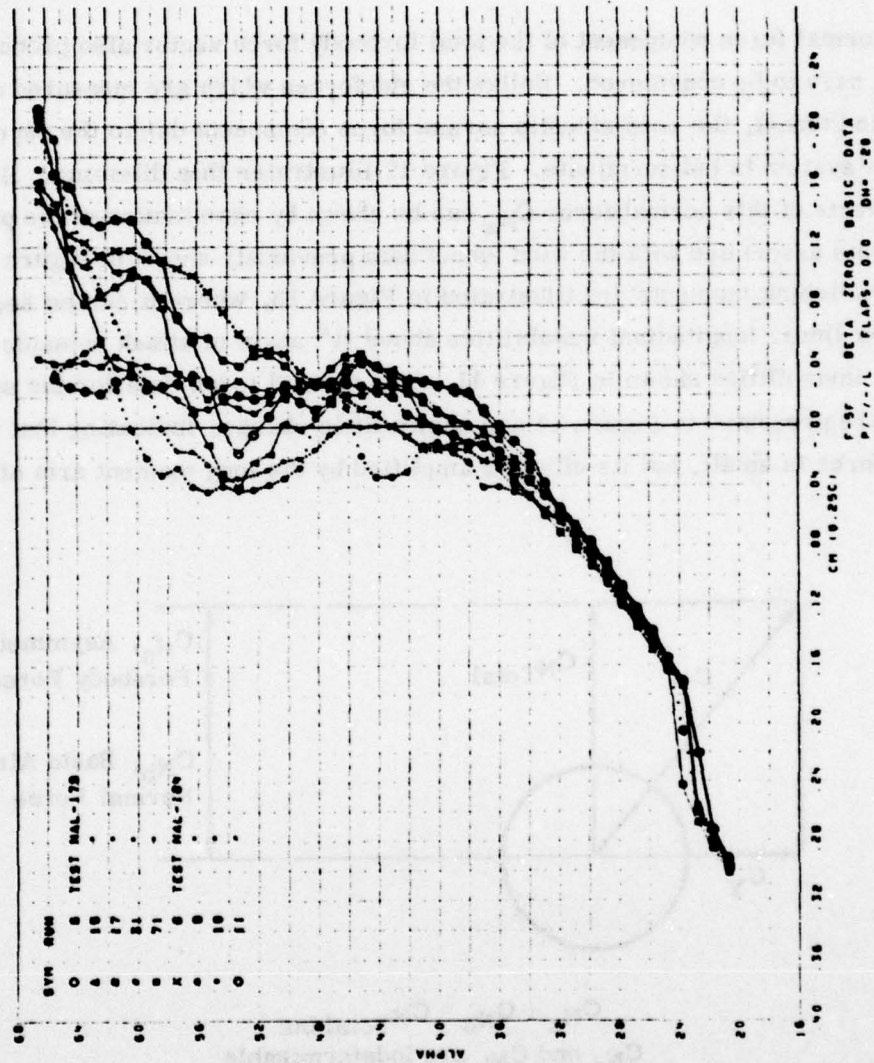


Figure 13. Pitching Moments at Zero Sideslip

The following are the data obtained in the low speed flight regime. The effects of increasing Mach number must also be considered for higher speeds. In general, the effects of Mach number are to provide even increasing regions of separation over the forewing which are followed by shock systems. Above a certain velocity Mach number separation is induced by shock systems faster than the flow velocity.

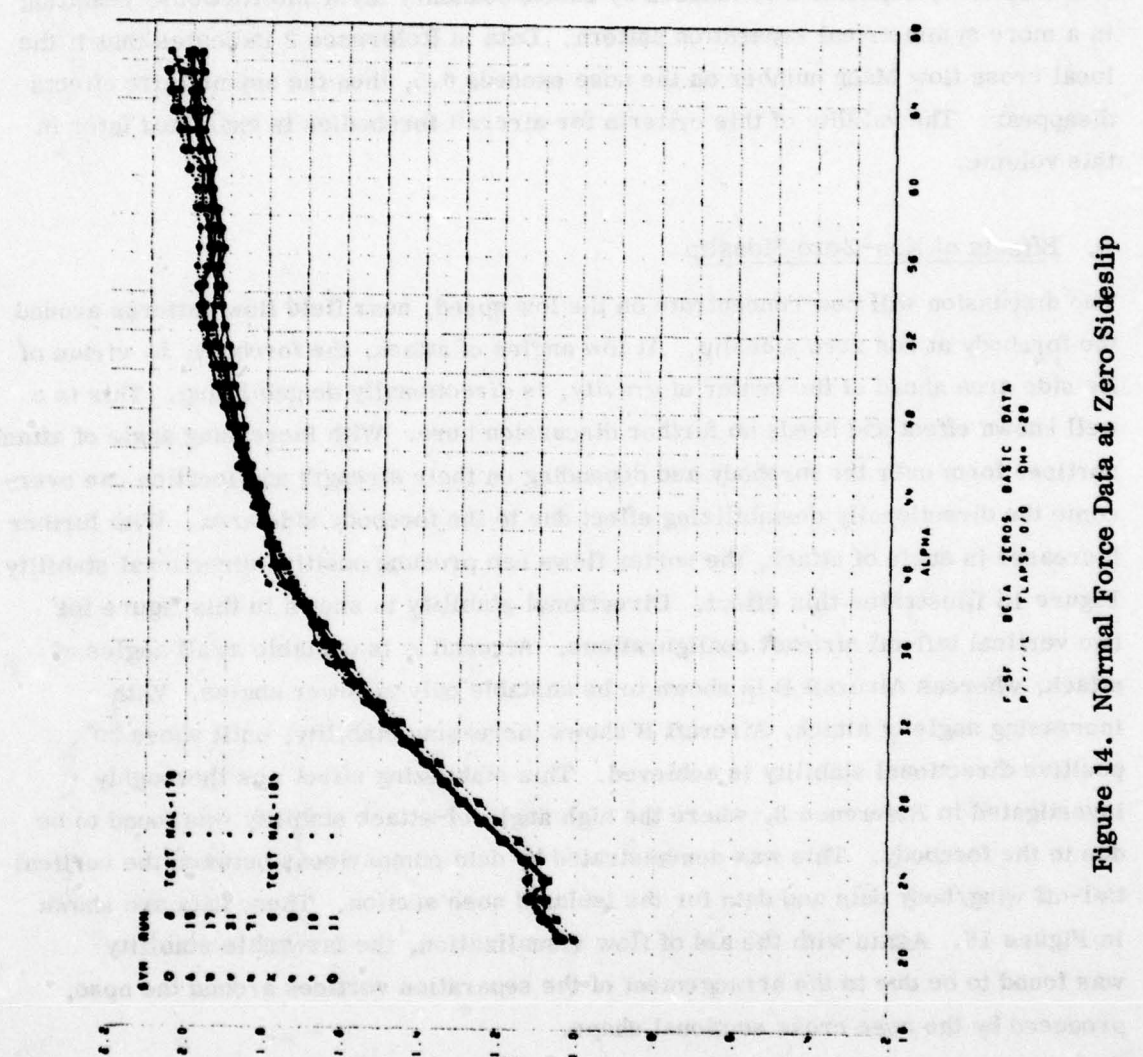


Figure 14. Normal Force Data at Zero Sideslip

The cross-sectional shape of the nose of Aircraft B is an ellipse, with the major axis horizontal. This favorable shape, augmented by the long mouth area of the nose is instrumental in producing the relatively low drag moments at high angles of attack.

3. "Small Scale Problems of Military Aircraft" Agard CP-150, November 1953

4. Chambers, J.H. et al. "Wind Tunnel Free Flight Investigation of a Model of a Spin-Restored Fighter Configuration" NASA TN D-1115 June 1954

The discussions so far has been confined to the low speed flight region. The effects of increasing Mach number must also be considered for fighter aircraft. In general, the effects of Mach number are to provide ever increasing regions of supersonic flow over the forebody which are followed by shock systems. Above a certain critical Mach number, separation is induced by shock/boundary layer interactions, resulting in a more symmetrical separation pattern. Data in Reference 2 indicates that if the local cross flow Mach number on the nose exceeds 0.5, then the asymmetric effects disappear. The validity of this criteria for aircraft forebodies is examined later in this volume.

b. Effects of Non-Zero Sideslip

The discussion will now concentrate on the low speed, near field flow patterns around the forebody at non zero sideslip. At low angles of attack, the forebody, by virtue of its side area ahead of the center of gravity, is directionally destabilizing. This is a well known effect and needs no further discussion here. With increasing angle of attack, vortices form over the forebody and depending on their strength and location can overcome the directionally destabilizing effect due to the forebody side area. With further increases in angle of attack, the vortex flows can produce positive directional stability. Figure 15 illustrates this effect. Directional stability is shown in this figure for two vertical tail-off aircraft configurations. Aircraft A is unstable at all angles of attack, whereas Aircraft B is shown to be unstable only at lower angles. With increasing angle of attack, Aircraft B shows increasing stability, until above 30° , positive directional stability is achieved. This stabilizing effect was thoroughly investigated in Reference 3, where the high angle-of-attack stability was found to be due to the forebody. This was demonstrated by data comparisons between the vertical tail-off wing/body data and data for the isolated nose section. These data are shown in Figure 16. Again with the aid of flow visualization, the favorable stability was found to be due to the arrangement of the separation vortices around the nose, produced by the nose cross sectional shape.

The cross sectional shape of the nose of Aircraft B is an ellipse, with the major axis horizontal. This favorable shape, augmented by the long moment arm of the nose is instrumental in producing the stabilizing yawing moments at high angles of attack.

-
2. "Stall/Spin Problems of Military Aircraft" Agard CP-199, November 1975
 3. Chambers, J.R., et al. "Wind-Tunnel Free-Flight Investigation of a Model of a Spin-Resistant Fighter Configuration" NASA TN D-7716 June 1974

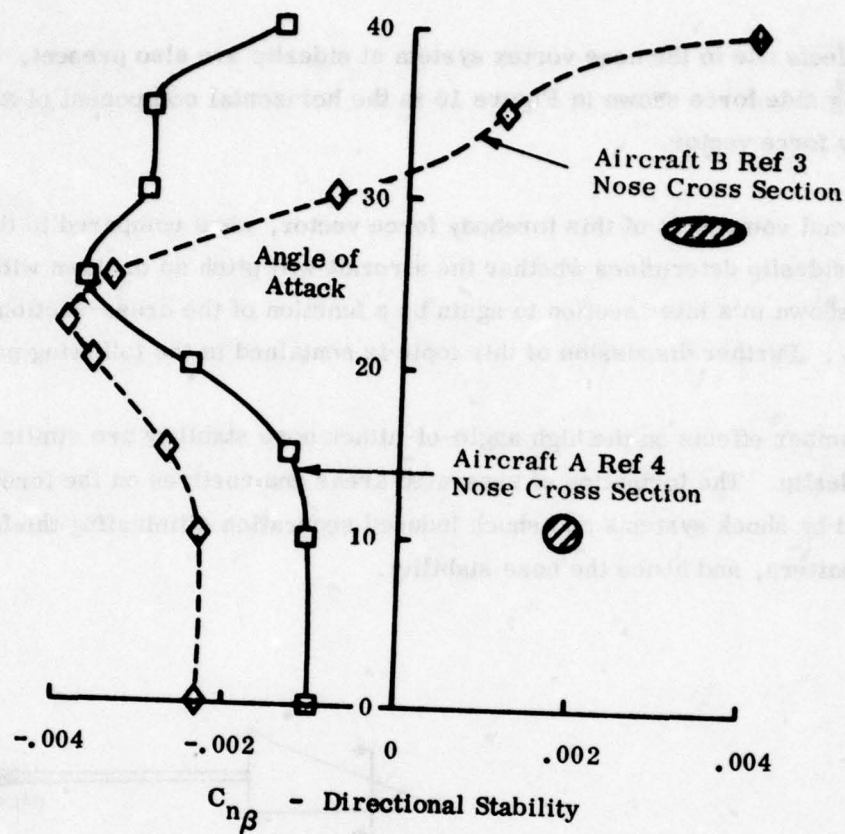


Figure 15. Comparison of Directional Stabilities

4. Chambers, J. R., and Anglin, E. L., "Analysis of Lateral/Directional Stability Characteristics of a Twin-Jet Fighter Airplane at High Angles of Attack," NASA TN D-5361, August 1969.

Pitch effects due to the nose vortex system at sideslip are also present. The restoring side force shown in Figure 16 is the horizontal component of an offset forebody force vector.

The normal component of this forebody force vector, when compared to the normal force at zero sideslip determines whether the aircraft will pitch up or down with sideslip. This will be shown in a later section to again be a function of the cross-sectional shape of the forebody. Further discussion of this topic is contained in the following paragraphs.

Mach number effects on the high angle-of-attack nose stability are similar to those at zero sideslip. The formation of separated areas and vortices on the forebody are replaced by shock systems and shock induced separation eliminating the favorable vortex pattern, and hence the nose stability.

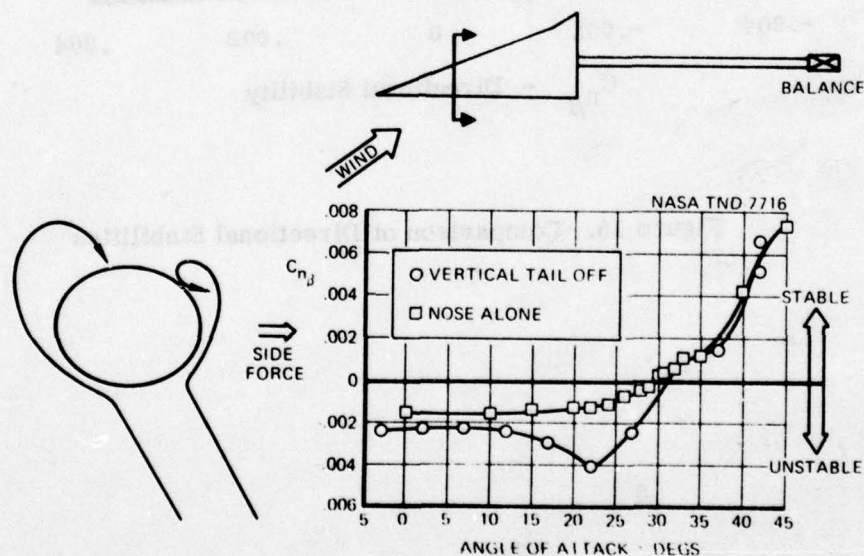


Figure 16. Nose Effect on Stability

c. Pointed Noses

The following sections present an analysis of the available test data on pointed nose configurations and concentrate on the aerodynamic effects due to changes in the geometry of the nose and forebody region. During this analysis, reference is made to various geometric and aerodynamic parameters, which require some explanation. Before beginning the actual analysis, therefore, some discussion and definition of these parameters will be made.

(1) Definitions

(a) Nose Fineness Ratio

The strength of the nose vortex system is proportional to the length of the nose, but if the body is interrupted by a shielding surface, such as a wing or LEX, then no further increase of vortex strength occurs across this region. The important length to consider in assessing the effects of the nose is, therefore, that of the unobstructed region ahead of the wing or LEX, and this is defined as " l ." The fuselage diameter " d " is defined as the width of the fuselage at the beginning of the nose section (measured in the plan view).

These definitions are shown in Figure 17, for both the F-5 and the YF-17. The F-5 forebody is defined as starting at the inlet station, and this is fortuitously coincidental with a scheme used in Reference 5, which defines the nose as starting at a station 4 diameters ahead of the wing trailing edge. This dimensional scheme is also shown in Figure 17. The NASA data reported in Reference 5 are for a similar wing body configuration and these data will be also included in the analysis of nose fineness ratios following.

Although the nose fineness ratio is defined in Figure 17 in terms of the unobstructed length of the forebody, it is important also to consider the physical distance between the nose and the C.G. when assessing the effects of changing l/d values, in particular when investigating yawing moments.

-
5. Jorgensen, L.H., and Nelson, E.R. "Experimental Aerodynamic Characteristics for Slender Bodies with Wings and Tail at Angles of Attack from 0° to 58° and Ma Numbers from 0.6 to 2.0" NASA TM X-3310, March 1976

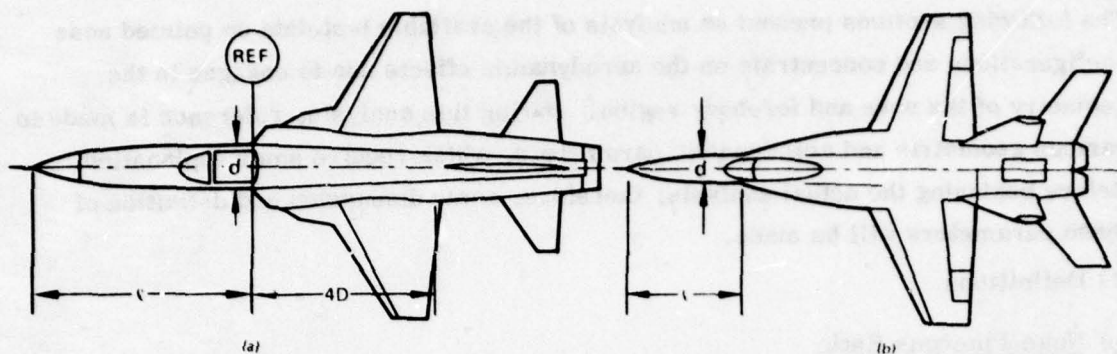


Figure 17. Definition of Nose Fineness Ratio

(b) Nose Ellipticity Ratio

In order to assess the effects of dissimilar forebody cross sectional shapes available in the data base, some common fuselage location is required. Based on the forebody force center of pressure locations derived from the F-5A tests, a station equidistant between the tip of the nose and the canopy was selected as being typical. This is shown in Figure 18.

This definition is also applicable to other aircraft considered in this report.

(c) Nose Apex Angle

The nose apex angle, δ_n , is defined as the angle embraced by the upper and lower surfaces of the tip of the forebody in the profile view. This angle is also defined in Figure 18.

(d) Aerodynamic Parameters

In addition to the usual aerodynamic terms and parameters, which have been presented earlier in the List of Symbols, some other quantities have to be defined. These are as follows:

- 1) Onset angle is that angle of attack at which the asymmetric aerodynamic effects at zero sideslip become apparent. Throughout this report this will be referred to as the onset angle, and will mainly be applicable to the yawing moment data.

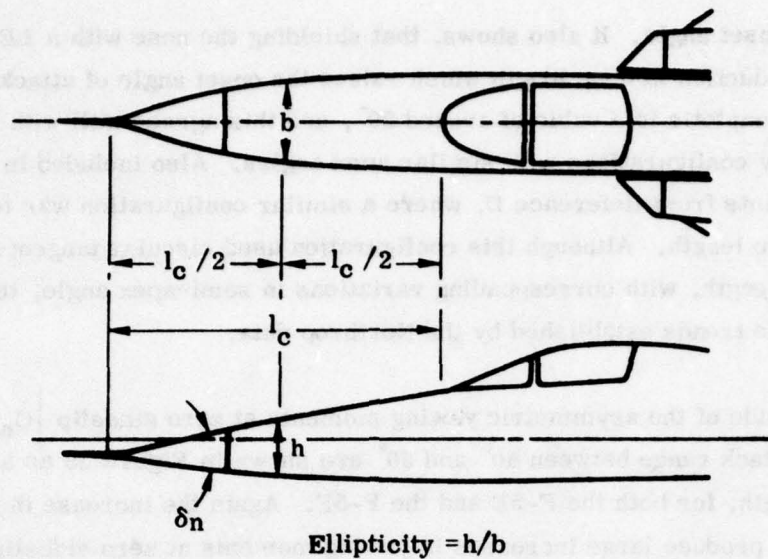


Figure 18. Definition of Nose Ellipticity and Apex Angle

- 2) The peak value of zero sideslip yawing moment is designated as

$$\left| C_{n_0} \right|_{\text{peak}}$$

- 3) Forebody cross flow Mach number, M_{cf} , is defined as

$$M_{cf} = M_{\infty} \sin \alpha$$

where M_{∞} is the free stream Mach number, and α the angle of attack.

(2) Aerodynamic Asymmetries at Zero Sideslip

(a) Onset Angle of Attack

Figure 19 shows the effects of increasing the nose length on the onset angle of attack for various configurations. Increases in nose length are shown to dramatically

lower the onset angle. It also shows, that shielding the nose with a LEX causes an apparent reduction in nose length which raises the onset angle of attack. The data trend is asymptotic to a value of around 20° , and this agrees well with other data for pointed body configurations with similar apex angles. Also included in Figure 19 are data points from Reference D, where a similar configuration was tested with varying nose length. Although this configuration used circular tangent-ogive forebodies of various length, with corresponding variations in semi-apex angle, the data agree well with the trends established by the Northrop data.

The magnitude of the asymmetric yawing moments at zero sideslip $|C_{n_o}|$ peak in the angle-of-attack range between 40° and 50° are shown in Figure 19 as a function of nose length, for both the F-5E and the F-5F. Again the increase in nose length is shown to produce large increases in yawing moments at zero sideslip.

Comparison of asymmetric effects between aircraft in terms of $|C_{n_o}|$ peak values may not be the most suitable scheme. For two aircraft with approximately the same body lengths but varying wing areas, different C_{n_o} values can be obtained simply by using wing area as a non-dimensionalizing factor, whereas the actual forces may be equal. A more consistent trend might be shown if the nose forces could be non-dimensionalized with respect to a more meaningful length such as nose diameter.

Figure 20 presents data for the F-5E/F taken from References 48, 54, and 55 of Volume II. This shows the effect of the nose apex angle on onset angle of attack. At the lower values of nose apex angle, the data correlates well with the circular forebody line of Reference C. At higher nose apex angles the data fall between the circular forebodies data and the elliptic tangent-ogive data also from Reference C. It is apparent that the onset angle/apex angle correlation of circular forebodies is only good for general forebody angles, i. e., the basic nose, and not the more abrupt local nose angles tested.

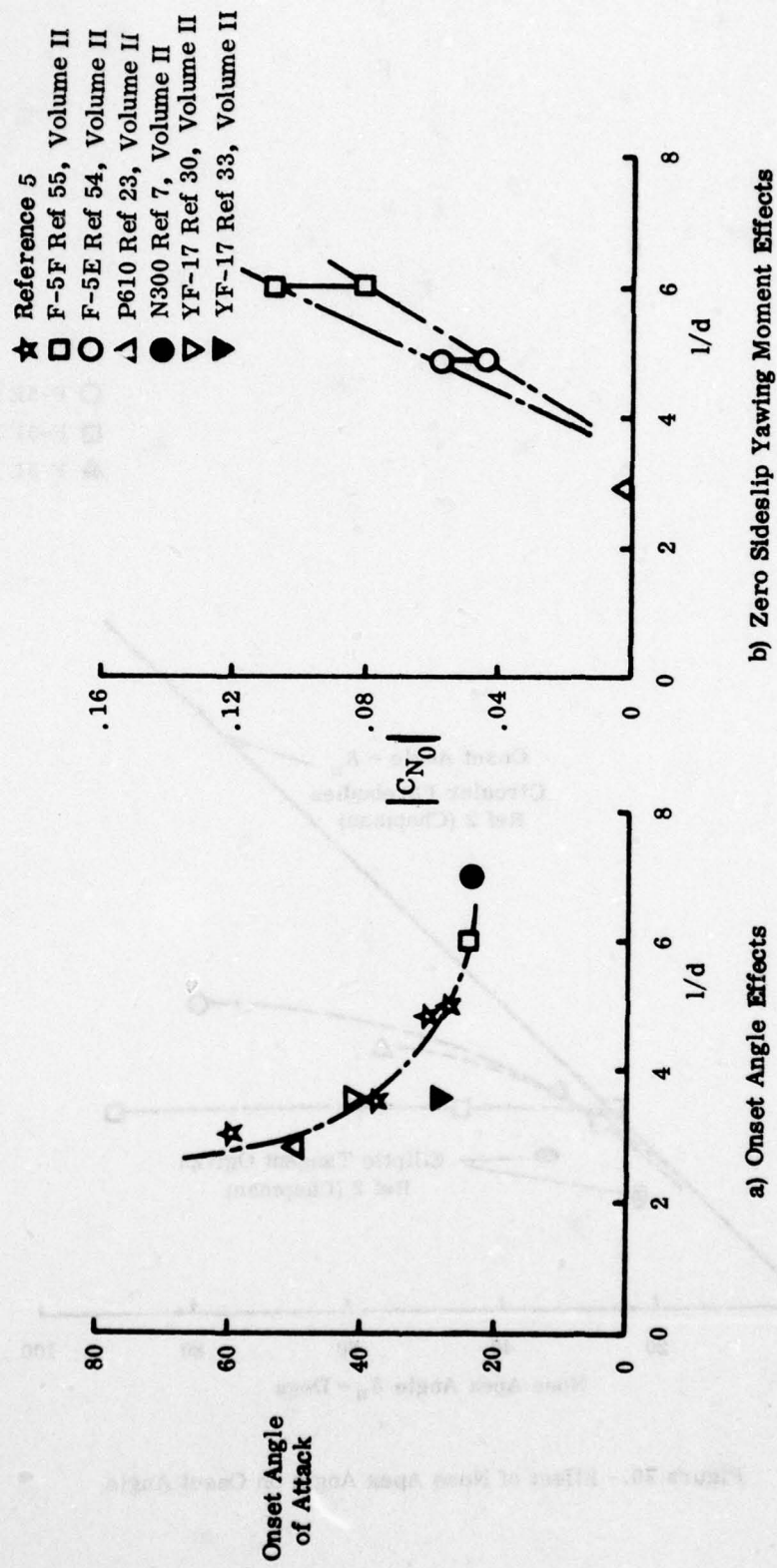


Figure 19. Effects of Nose Fineness Ratio at Zero Sideslip

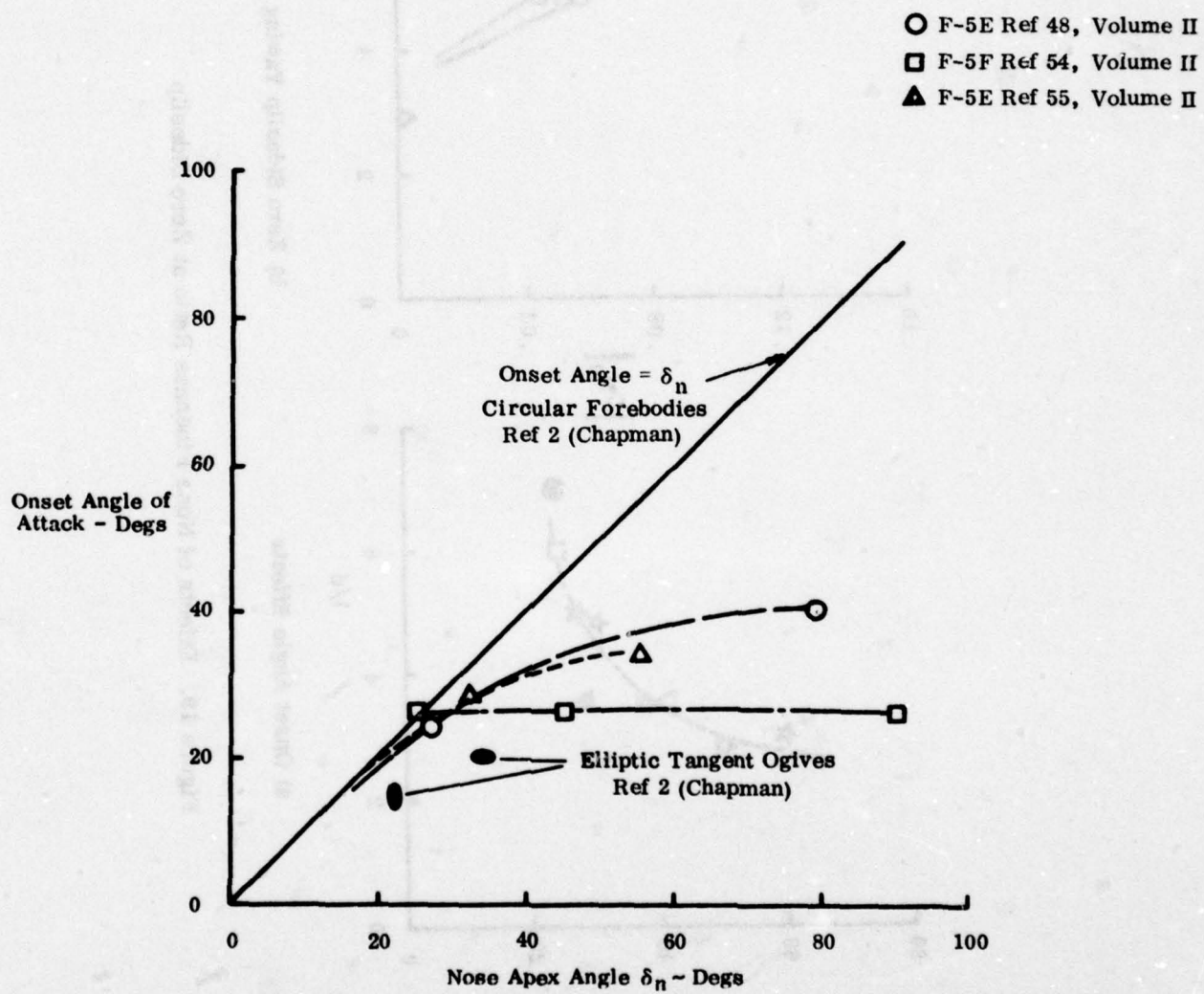


Figure 20. Effect of Nose Apex Angle on Onset Angle

Information on the effects of Mach number on the onset of the asymmetric yawing moments is hampered by the restricted angle-of-attack ranges of the available transonic tests. The onset angle usually exceeds this upper limit of angle-of-attack tested. For the F-5E/F a small amount of test data are available, and this is shown in Figure 21. This figure shows a gradual increase in onset angle of attack with Mach number. The data from Reference 5 provide a data trend beyond that given by the F-5 results, and show that at a Mach number = 1.5 the onset angle is now above 60 degrees, indicating an abrupt increase between a Mach Number = 1.2 and 1.5.

The effect of increasing Mach number across the forebody is that the vortex separation, which occurs in a somewhat random manner at low speeds, is replaced by a more symmetrical shock induced separation pattern after the local Mach number across the forebody exceeds a sonic value.

Chapman et al in Reference 2 reports that if the cross Mach number (M_{CF}) exceeds = 0.5, then the asymmetric forces are no longer present. The angles of attack and free stream Mach numbers to produce this cross flow Mach number have been calculated, and are plotted in Figure 21 for comparison with the F-5 data. The results of this comparison are somewhat inconclusive due to the lack of test data above a free stream Mach number of 1.05.

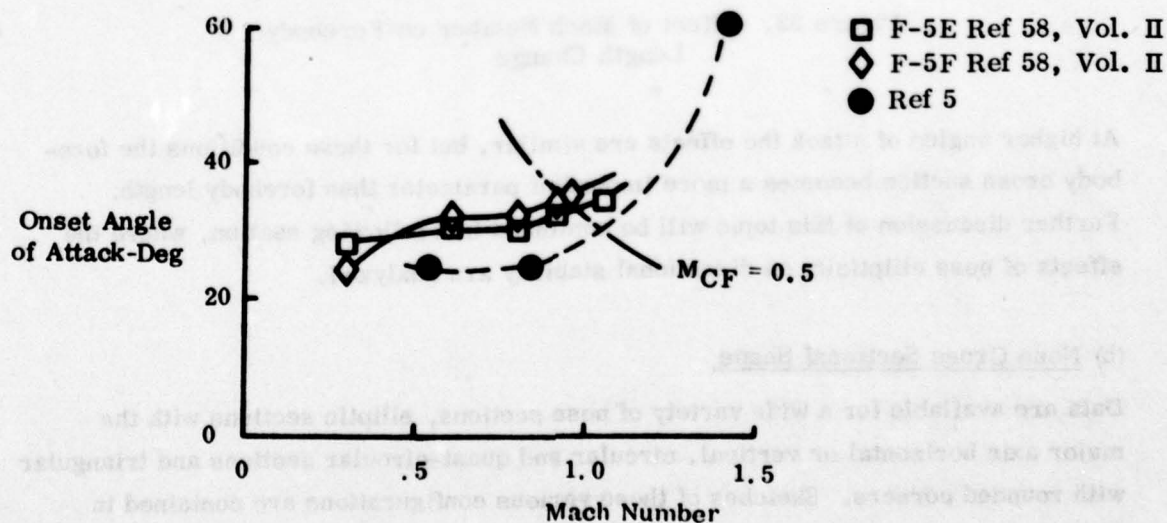


Figure 21. Effect of Mach Number on Onset Angle of Attack

(3) Pointed Nose Configurations

(a) Effect of Forebody Fineness Ratio on Directional Stability

The effects of an increased nose length on directional stability at low angles of attack are straightforward. Due to the increased side area ahead of the C.G., a destabilizing effect is noted. Figure 22 below shows the incremental loss of low angle of attack directional stability between the F-5E and the F-5F. The F-5F forebody is 42.5 inches longer than the forebody of the F-5E. The figure also shows that the loss in stability can be seen to be roughly constant across the Mach Number range of 0.6 to 1.2. All data shown in this figure are for an angle of attack of 5 degrees.

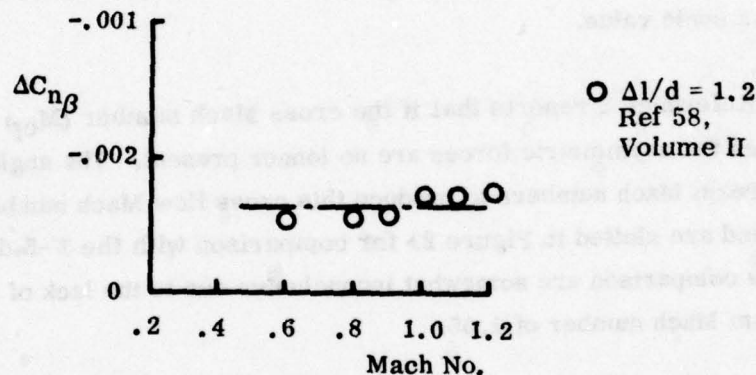
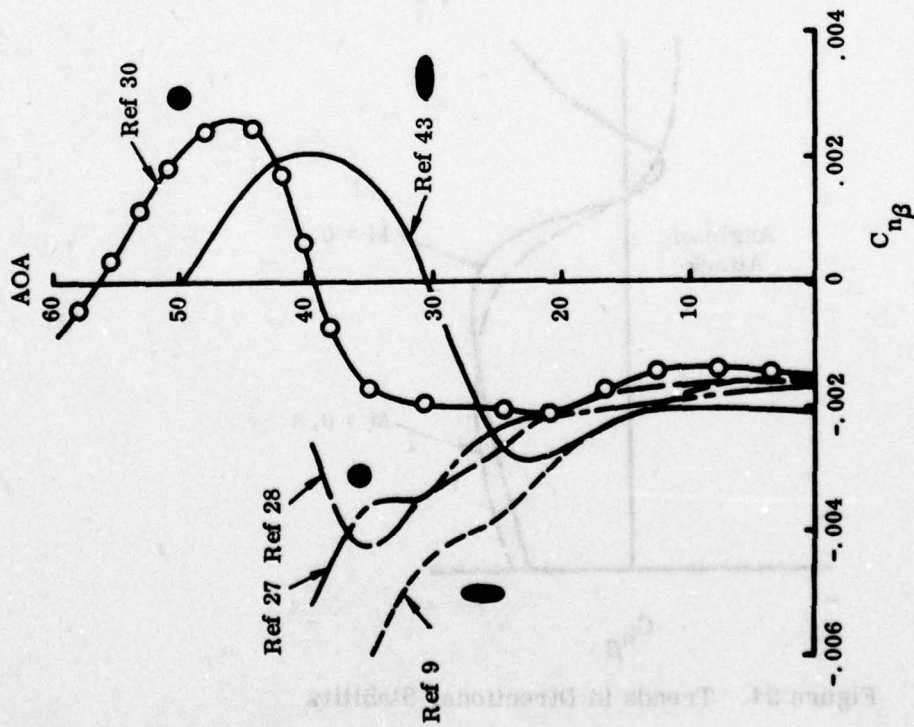


Figure 22. Effect of Mach Number on Forebody Length Change

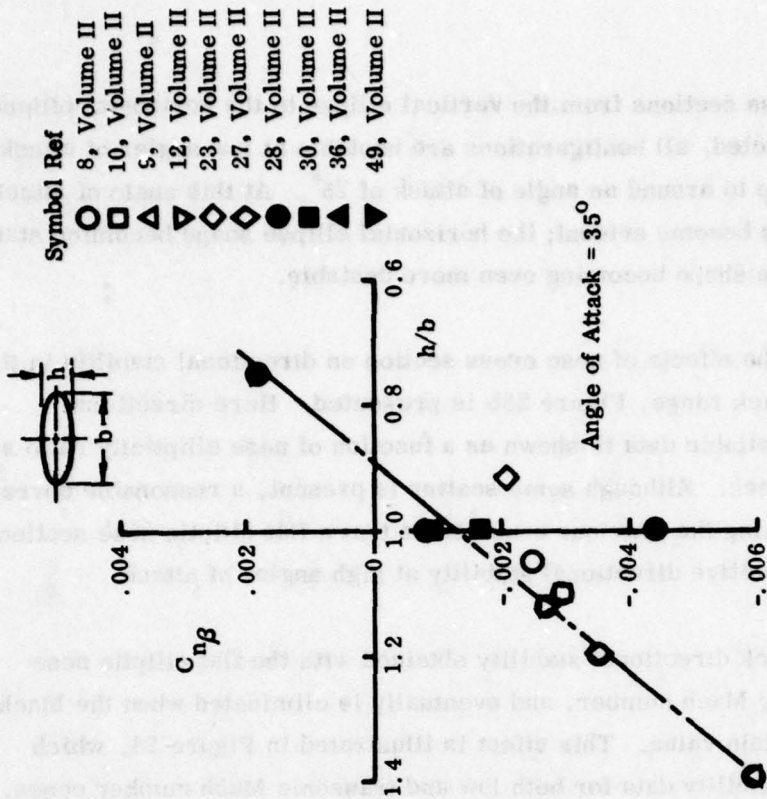
At higher angles of attack the effects are similar, but for these conditions the forebody cross section becomes a more important parameter than forebody length. Further discussion of this topic will be continued in a following section, where the effects of nose ellipticity on directional stability are analyzed.

(b) Nose Cross Sectional Shape

Data are available for a wide variety of nose sections, elliptic sections with the major axis horizontal or vertical, circular and quasi-circular sections and triangular with rounded corners. Sketches of these various configurations are contained in Volume II. In Figure 23a, the effects of nose cross-sectional shape on directional stability are shown for vertical tail off configurations for an angle of attack range up to 60° . For clarity, not all the available data have been presented but the



a) Effect of Nose Shape



b) Effect of Nose Ellipticity on $C_{n\beta}$

Figure 23. Vertical Tail Off Data

full range of nose cross sections from the vertical ellipse to the horizontal ellipse are covered. As expected, all configurations are unstable at low angles of attack, and remain unstable up to around an angle of attack of 25° . At this angle of attack, cross sectional effects become evident; the horizontal ellipse shape becoming stable and the vertical ellipse shape becoming even more unstable.

To further illustrate the effects of nose cross section on directional stability in the post-stall angle of attack range, Figure 23b is presented. Here directional stability for all the available data is shown as a function of nose ellipticity ratio at a constant angle of attack. Although some scatter is present, a reasonable correlation is shown, confirming the previous conclusions that a flat elliptic nose section is required to produce positive directional stability at high angles of attack.

This high angle of attack directional stability obtained with the flat elliptic nose shapes is influenced by Mach number, and eventually is eliminated when the Mach number exceeds a certain value. This effect is illustrated in Figure 24, which presents directional stability data for both low and transonic Mach number cases. The actual effects of Mach number on the F-5F from Reference 59 is shown in

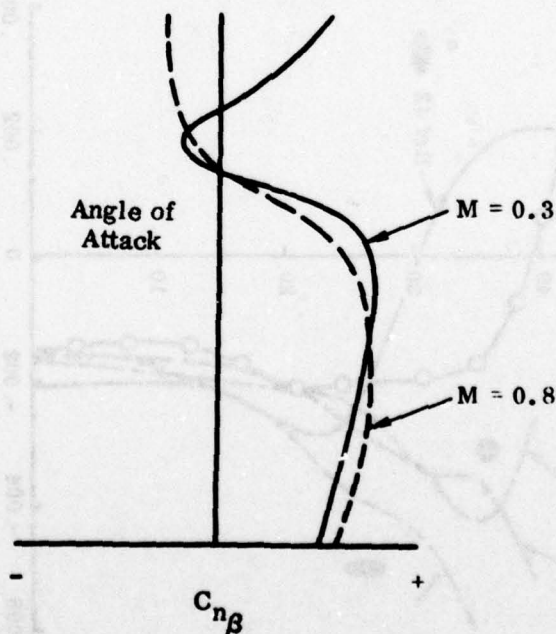


Figure 24. Trends in Directional Stability

Figure 25. This figure presents the three basic stability areas, the low angle of attack stable region, the unstable region around the stall, and the high angle of attack stable area.

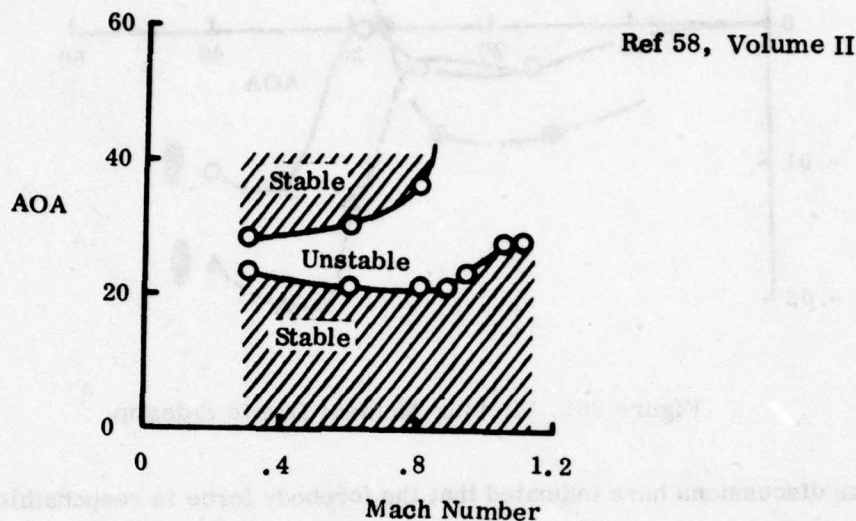


Figure 25. Directional Stability, F-5F

The lower boundary where the aircraft's directional stability is reversed is generally around 20° angle of attack up to $M = 0.8$, after which it gradually increases. The upper boundary where directional stability is regained also increases with Mach Number, until above $M = 0.8$ this upper region of stability is lost.

Any aerodynamic changes to the aircraft forebody, which produce lateral/directional effects, would also be expected to produce an effect in pitching moment, particularly as forces on the forebody act at considerable distance from the moment center.

These pitching moment effects with changes in sideslip angle have been observed since early flight testing of the F-5A, where it was possible to increase or hold the angle of attack by cyclic applications of the rudder pedals at high attitudes. This effect is shown in Figure 26 below, where it can be seen that below the stall a favorable C_{m_β} effect exists (nose down) but above 30° angle of attack the opposite effect exists, and an unstable C_{m_β} is present.

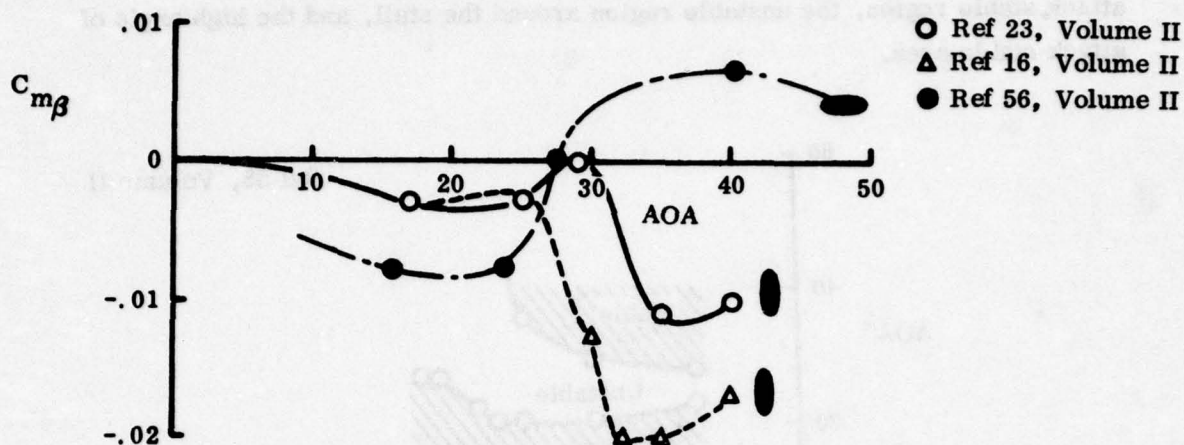
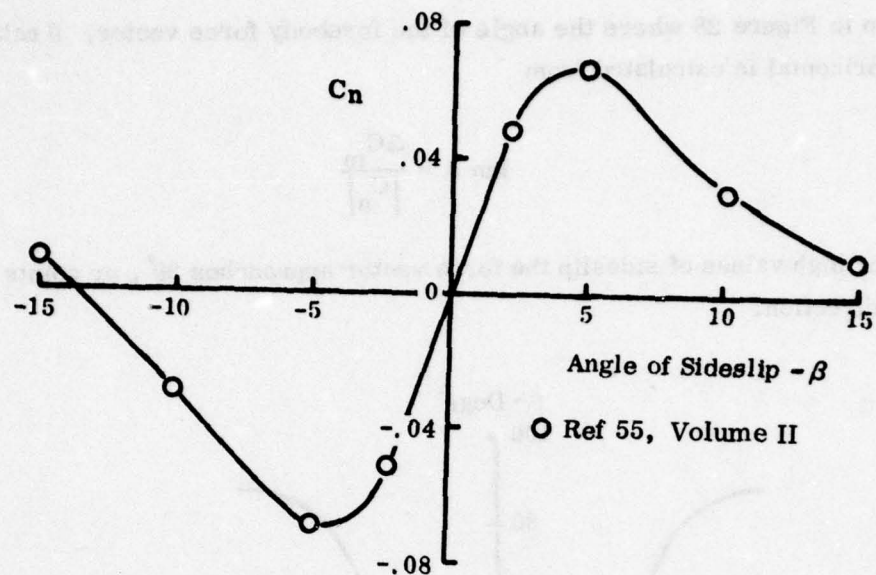


Figure 26. Pitching Moment Due to Sideslip

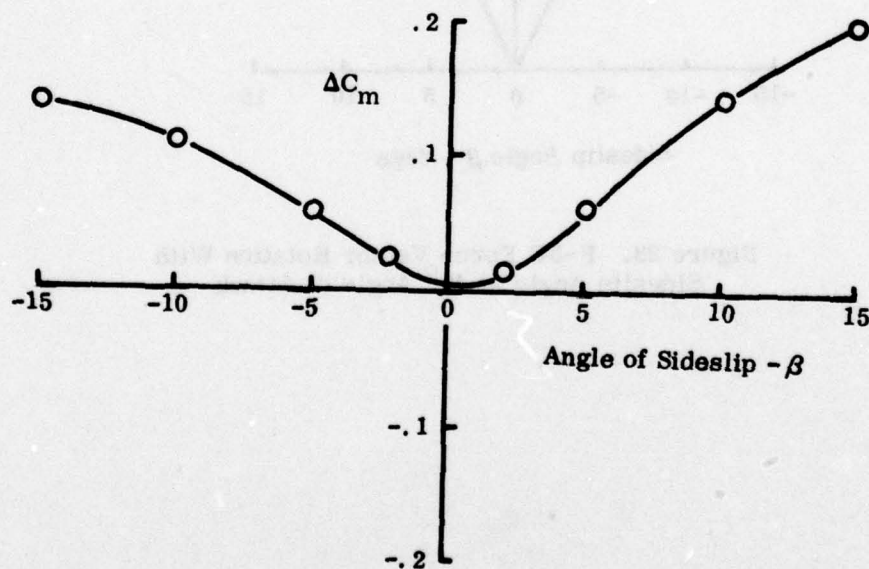
Previous discussions have indicated that the forebody force is responsible for this unstable pitch/yaw coupling on the F-5. For other configurations, aircraft with nose cross sections which are unstable the opposite trends in $C_{m\beta}$ are shown. Data from References 16 and 23, for tall elliptic noses, are also shown in Figure 26, and illustrate this stable pitch yaw coupling at high angles of attack. Thus, a correlation between directional stability and pitching moment exists as a function of nose shape, a flat elliptical nose having a positive $C_{n\beta}$ and a unfavorable $C_{m\beta}$, a tall elliptic nose having the reverse.

As previously mentioned, the stabilizing side force is the lateral component of the forebody force vector, which also has a component in the lift direction. With increasing angle of sideslip, the vortex pattern becomes more asymmetric and the forebody force vector rotates proportionally.

Figure 27 shows data for an F-5F at an angle of attack of 40 degrees, and illustrates this point. The region of strongest directional stability at small angles of sideslip is well demonstrated, with little pitch effect. As sideslip increases the directional stability reduces and pitching moment increases. This can be illustrated



a) Yawing Moments



b) Pitching Moments

Figure 27. F-5F Nose Effects at 40° Angle of Attack

as shown in Figure 28 where the angle of the forebody force vector, θ relative to the horizontal is calculated from

$$\tan \theta = \frac{\Delta C_m}{|C_n|}$$

Thus, for high values of sideslip the force vector approaches 90° , or points in an upward direction.

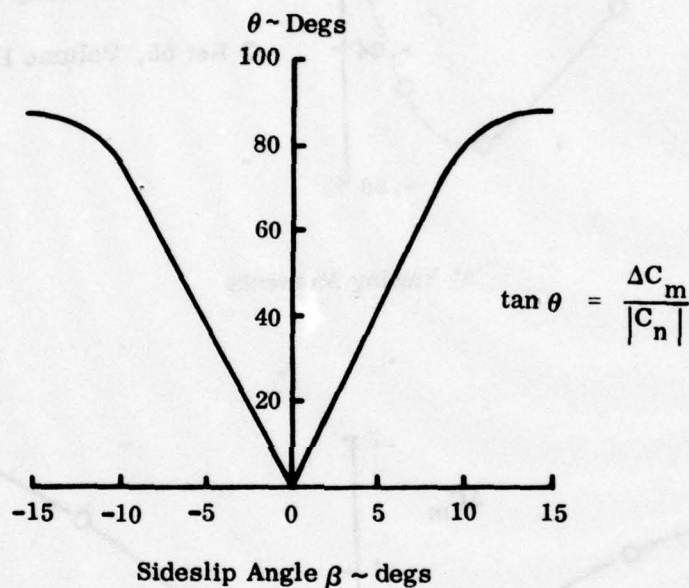


Figure 28. F-5F Force Vector Rotation With Sideslip Angle at 40° Angle of Attack

(4) Nose Booms

Flight testing requirements often result in the addition of a large instrumentation boom to the nose of the aircraft for accurate determination of such quantities as airspeed, altitude, angle of attack and sideslip. Figure 29 shows a typical configuration. This boom, usually over seven feet long and with a four inch base diameter, modifies both the nose shape and the effective fineness ratio, altering the nose vortex system. In addition a vortex pattern is shed by the boom itself.

The effects of adding such a boom were determined on both the YF-17 and the F-5E/F, the main parameter affected is shown to be the directional stability. The results of these low speed wind tunnel tests are given in Figures 30, 31, and 32, and show that the effects of the nose boom are extremely configuration dependent.

Figures 30 and 31 illustrate the effect of the nose boom on the YF-17, at both sideslip angles of 0° and 10° . The following effects are noted,

- 1) Addition of the boom virtually eliminates the small zero sideslip yawing moments present at high angles of attack on the basic nose.
- 2) Addition of the boom makes the aircraft directionally unstable above an angle of attack of 25° .

The F-5E/F test results are presented in Figure 32. A totally different effect is shown relative to the YF-17 data. Addition of the flight test boom to the 5E/F is shown to

- 1) Modify the zero sideslip yawing moments from being biased essentially in one direction to being alternately biased left or right with increasing angle of attack.
- 2) At sideslip, a similar trend is shown. The stable region above an angle of attack of 30° , present on the basic aircraft, is modified by the addition of the nose boom to being a highly oscillatory stable/unstable pattern with increasing angle of attack.

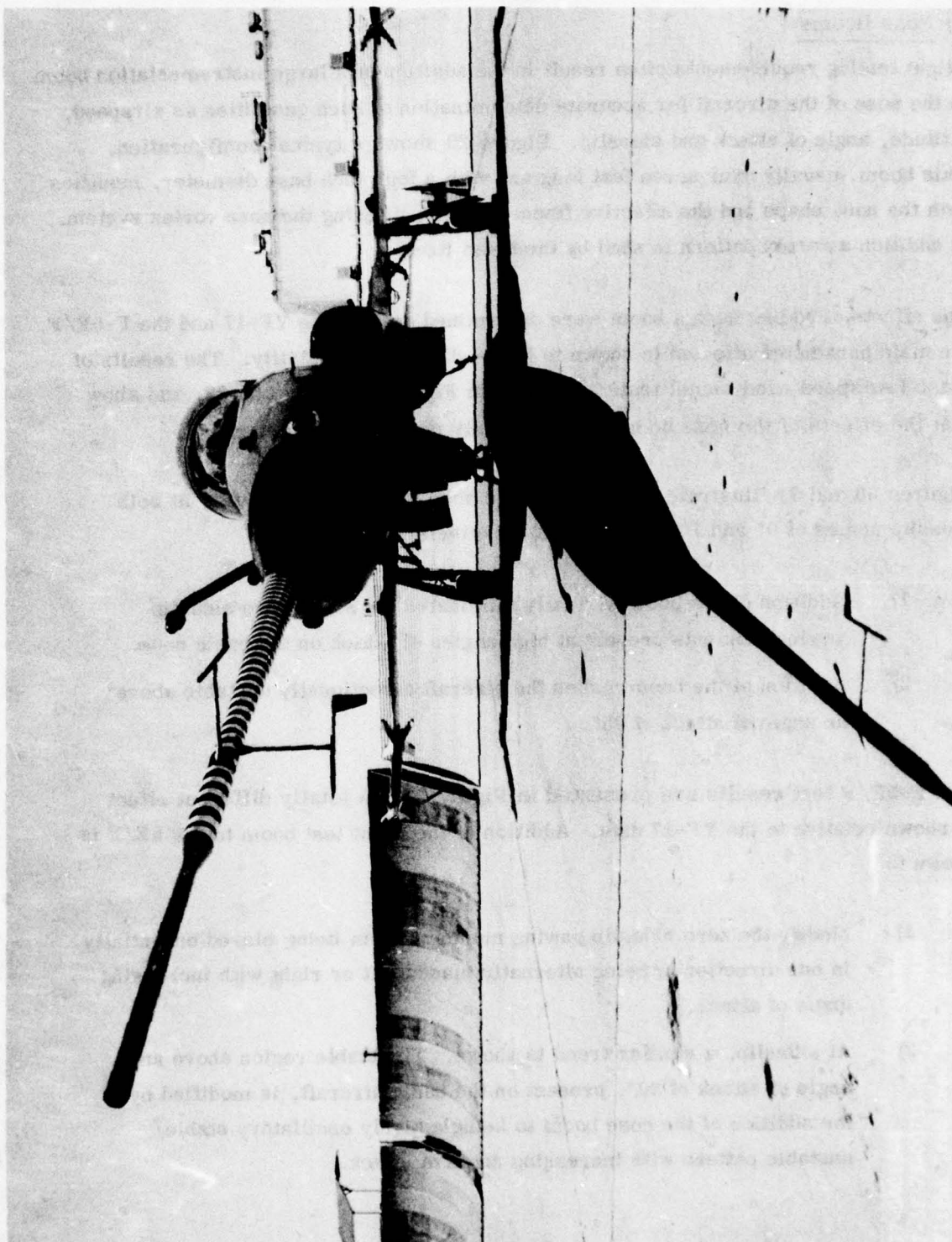


Figure 29. F-5F with Flight Test Nose Boom Installed

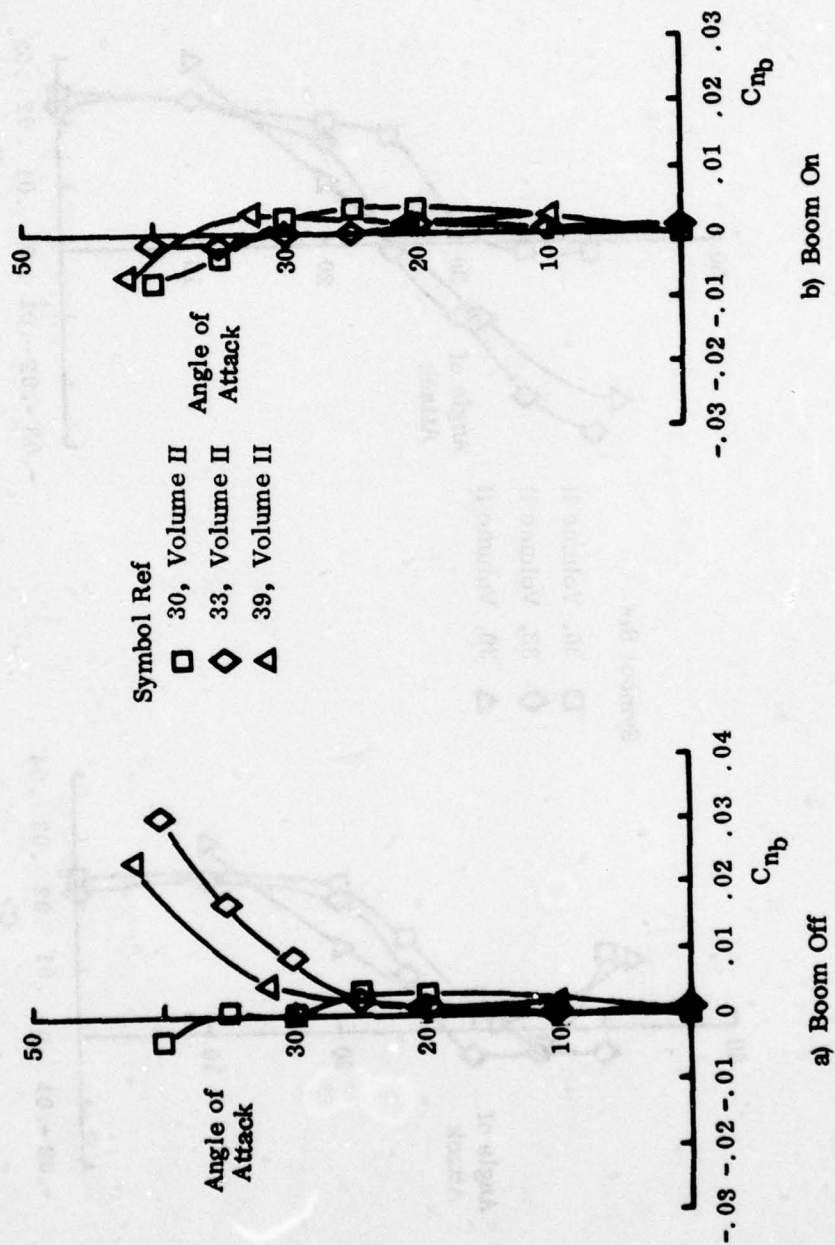


Figure 30. Nose Boom Effects at Zero Sideslip, YF-17

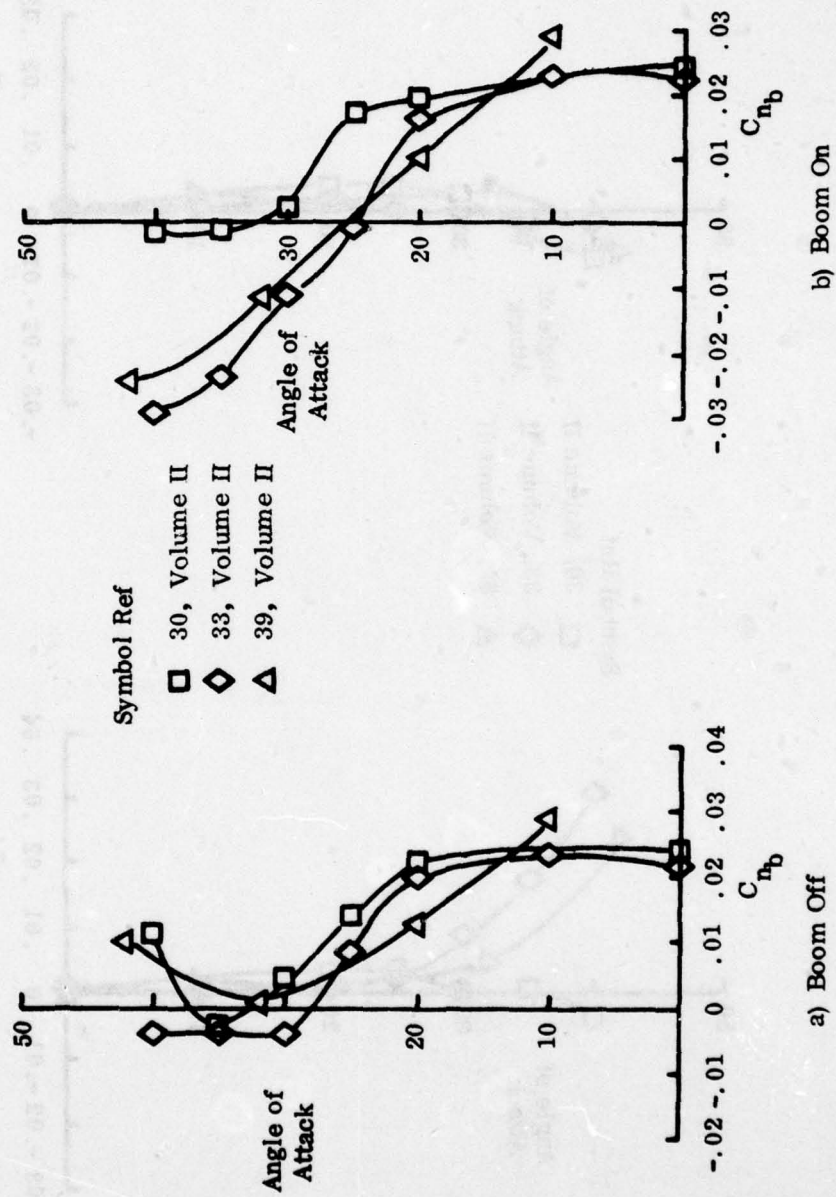
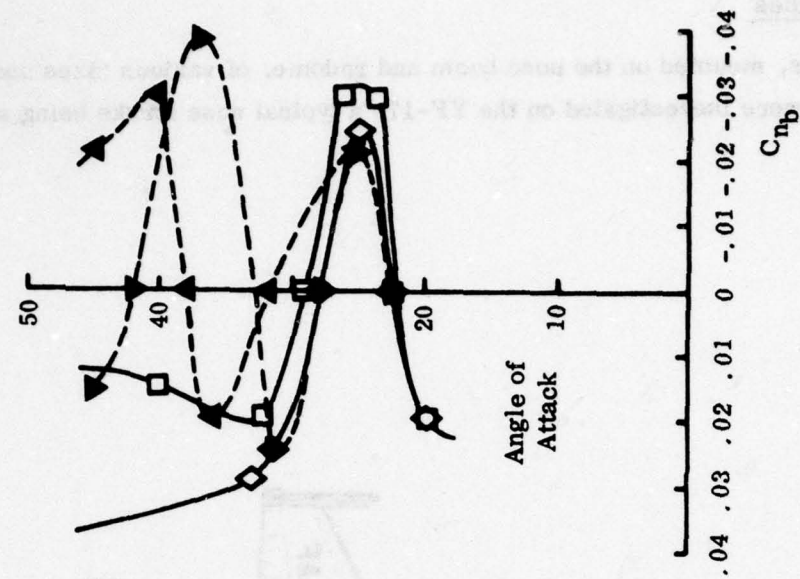
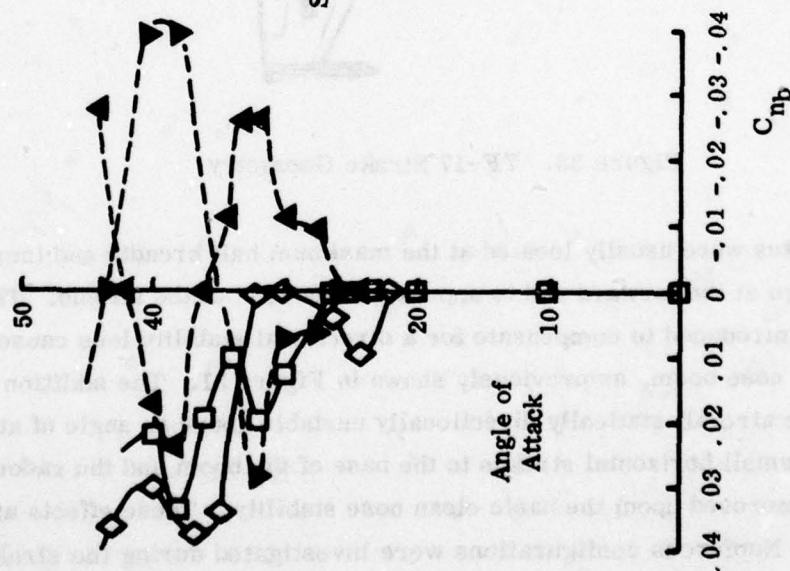


Figure 31. Nose Boom Effects at Sideslip Angle of -10° , YF-17



a) $\beta = 0^\circ$



b) $\beta = 10^\circ$

Figure 32. Nose Boom Effects F-5E/F

(5) Nose Strakes

Small strakes, mounted on the nose boom and radome, of various sizes and orientation, were investigated on the YF-17, a typical nose strake being shown in Figure 33.

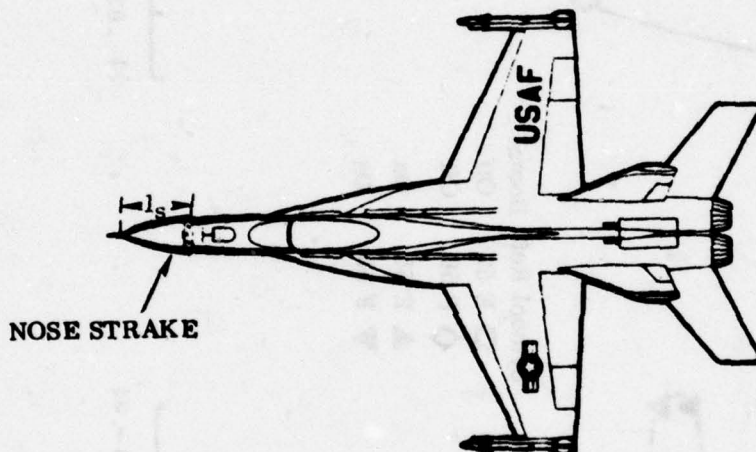


Figure 33. YF-17 Strake Geometry

The nose strakes were usually located at the maximum half breadth and increased in width from zero at the forward end to approximately 2.5" at the aft end. These strakes were introduced to compensate for a directional stability loss caused by the addition of the nose boom, as previously shown in Figure 31. The addition of the boom made the aircraft statically directionally unstable above an angle of attack at 25° . Incorporating small horizontal strakes to the base of the boom and the radome regained (and slightly improved upon) the basic clean nose stability. These effects are shown in Figure 34. Numerous configurations were investigated during the strake optimization tests and these data are used in the following analysis. Figure 35

30. 31, Volume II
 30. 32, Volume II
 30. 33, Volume II

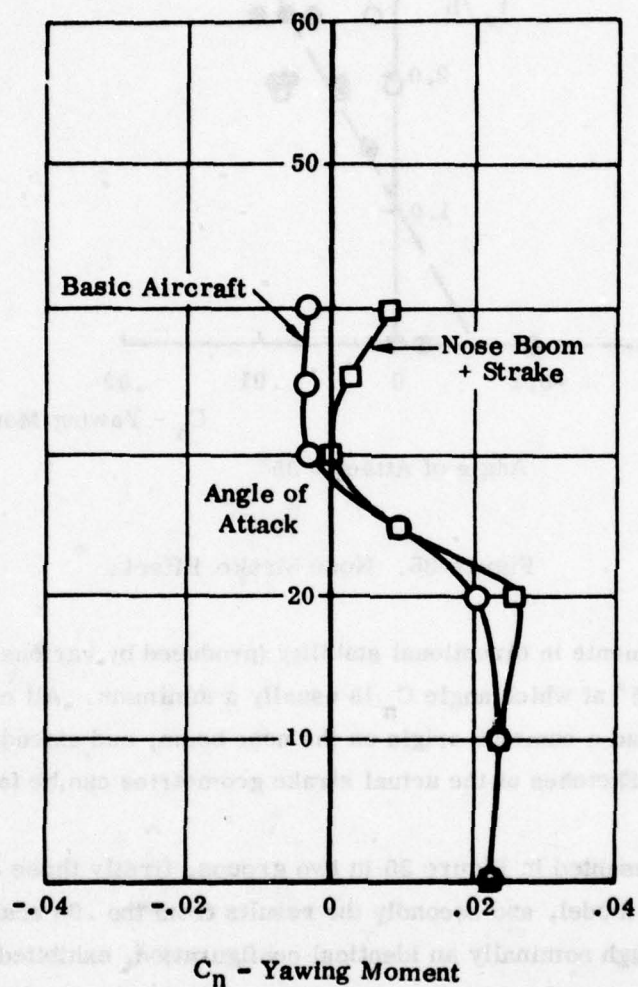


Figure 34. Effect of Nose Boom and Strake

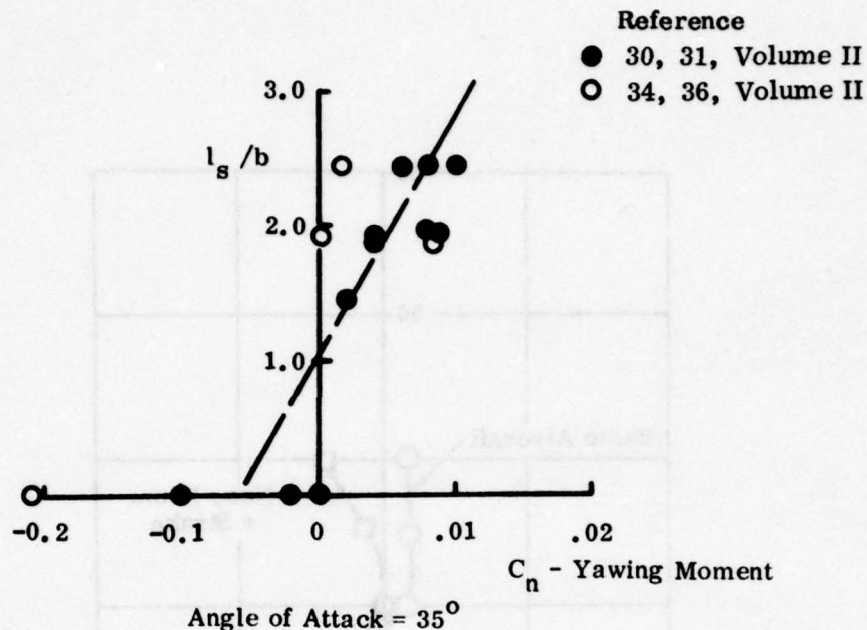


Figure 35. Nose Strake Effect

shows the improvements in directional stability (produced by various strakes) at an angle of attack of 35° at which angle C_n is usually a minimum. All configurations shown in this plot had a common origin on the nose boom, and extended aft the various fuselage stations. Sketches of the actual strake geometries can be found in Volume II.

The results are presented in Figure 35 in two groups, firstly those obtained with the .121 scale model, and secondly the results from the .08 scale model. The latter model, although nominally an identical configuration, exhibited slightly less directional stability than the earlier model. Generally both sets of data show improvements in directional stability with increasing strake length l_s . The required strake length to provide stable directional stability is seen to be at least twice the forebody diameter. Changes in nose strake configuration of this type appeared to have little affect of lateral stability. Figure 36 shows some typical results.

Various forebody strakes, similar to those previously discussed on the YF-17, were investigated on the F-5F during the low speed tests of Reference 54. The

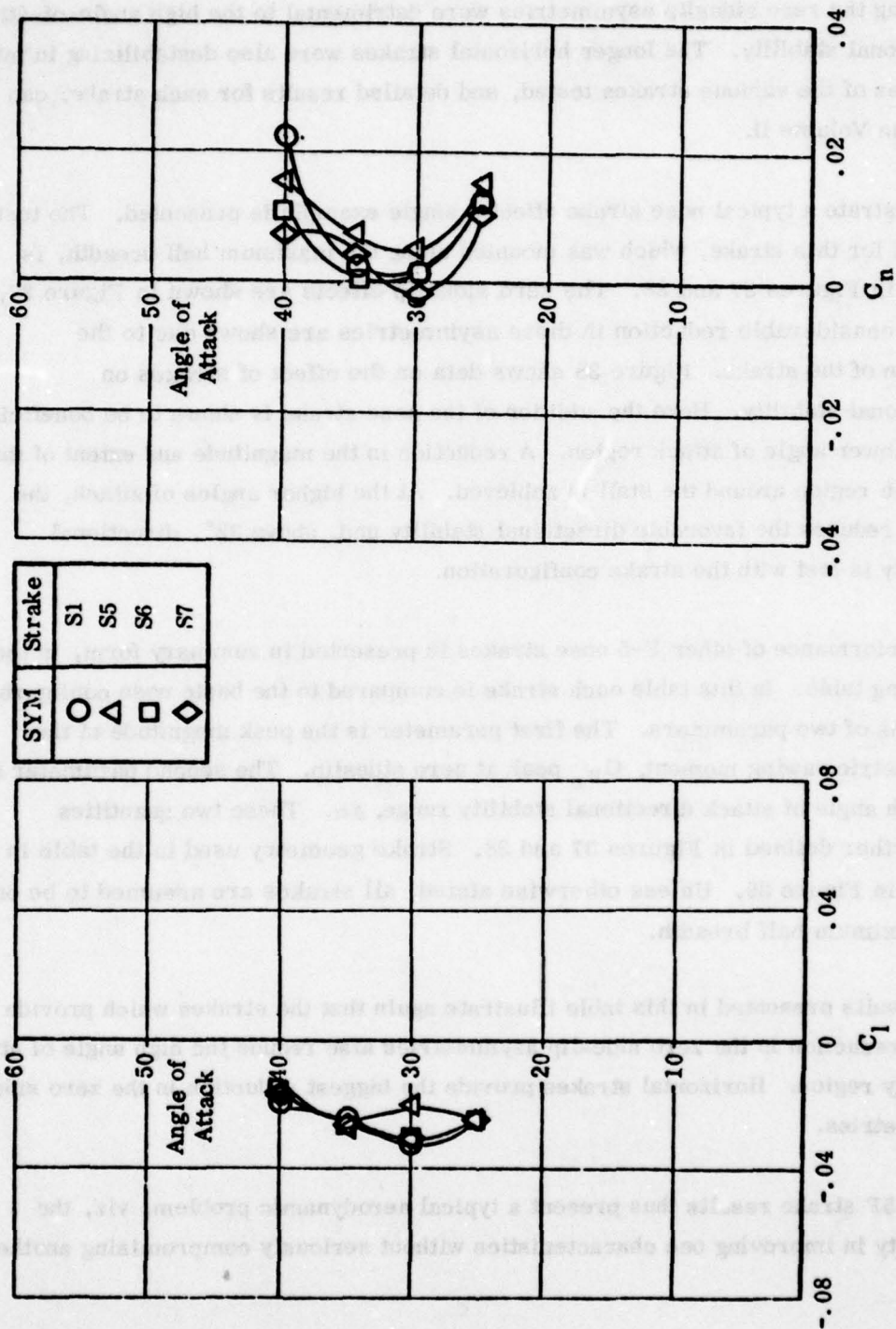


Figure 36. Effect of Strake Configurations at 10° Sideslip

general results obtained in these tests showed that the strakes that were helpful in reducing the zero sideslip asymmetries were detrimental to the high angle-of-attack directional stability. The longer horizontal strakes were also destabilizing in pitch. Sketches of the various strakes tested, and detailed results for each strake, can be found in Volume II.

To illustrate a typical nose strake effect a single example is presented. The test results for this strake, which was mounted along the maximum half breadth, is shown in Figures 37 and 38. The zero sideslip effects are shown in Figure 37, where considerable reduction in these asymmetries are shown due to the addition of the strake. Figure 38 shows data on the effect of strakes on directional stability. Here the addition of the nose strake is shown to be beneficial in the lower angle of attack region. A reduction in the magnitude and extent of the unstable region around the stall is achieved. At the higher angles of attack, the strake reduces the favorable directional stability and, above 32° , directional stability is lost with the strake configuration.

The performance of other F-5 nose strakes is presented in summary form, in the following table. In this table each strake is compared to the basic nose configuration in terms of two parameters. The first parameter is the peak magnitude of the asymmetric yawing moment, C_{n_0} peak at zero sideslip. The second parameter is the high angle of attack directional stability range, $\Delta\alpha$. These two quantities are further defined in Figures 37 and 38. Strake geometry used in the table is shown in Figure 39. Unless otherwise stated, all strakes are assumed to be on the maximum half breadth.

The results presented in this table illustrate again that the strakes which provide a useful reduction in the zero sideslip asymmetries also reduce the high angle of attack stability region. Horizontal strakes provide the biggest reduction in the zero sideslip asymmetries.

The F-5F strake results thus present a typical aerodynamic problem, viz, the difficulty in improving one characteristics without seriously compromising another.

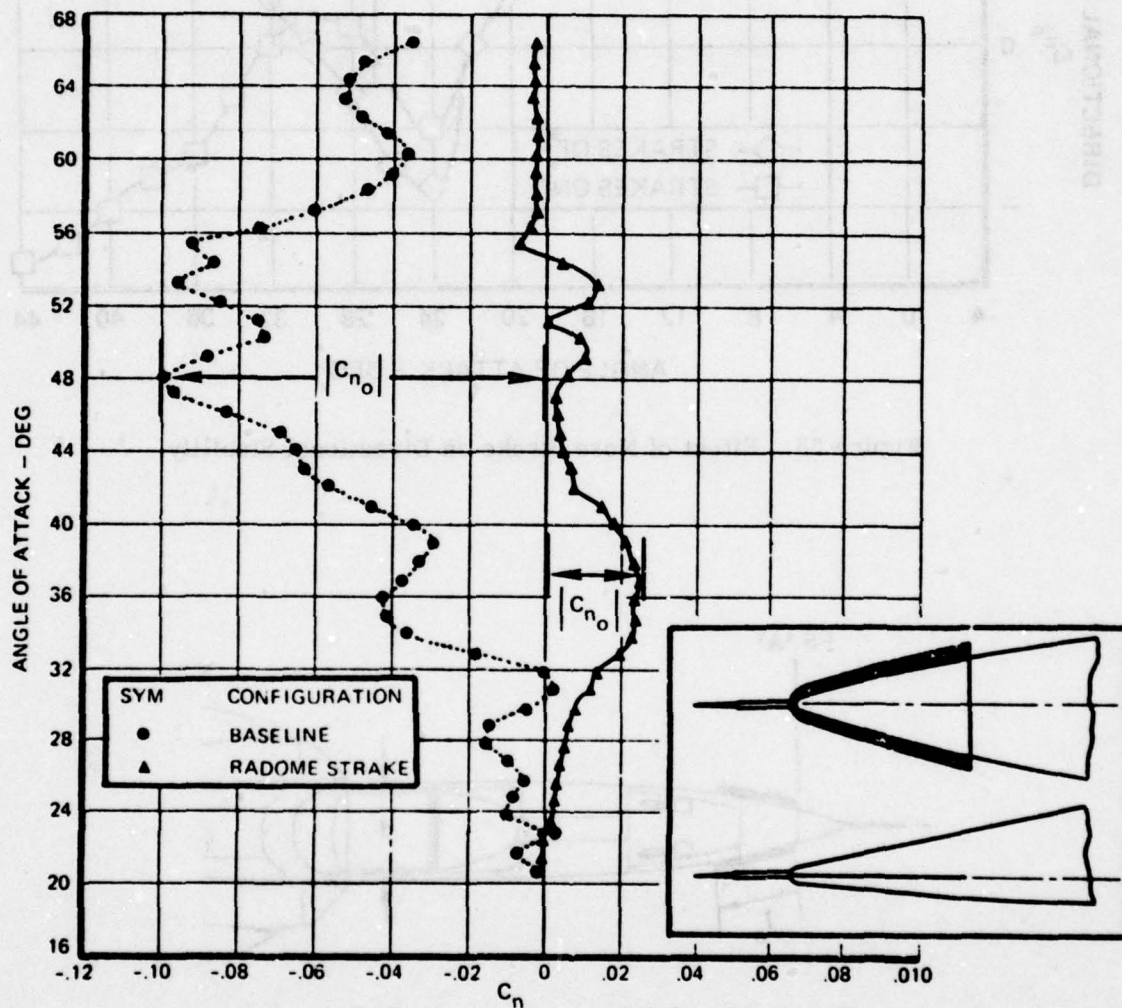


Figure 37. Effect of Nose Strake at Zero Sideslip

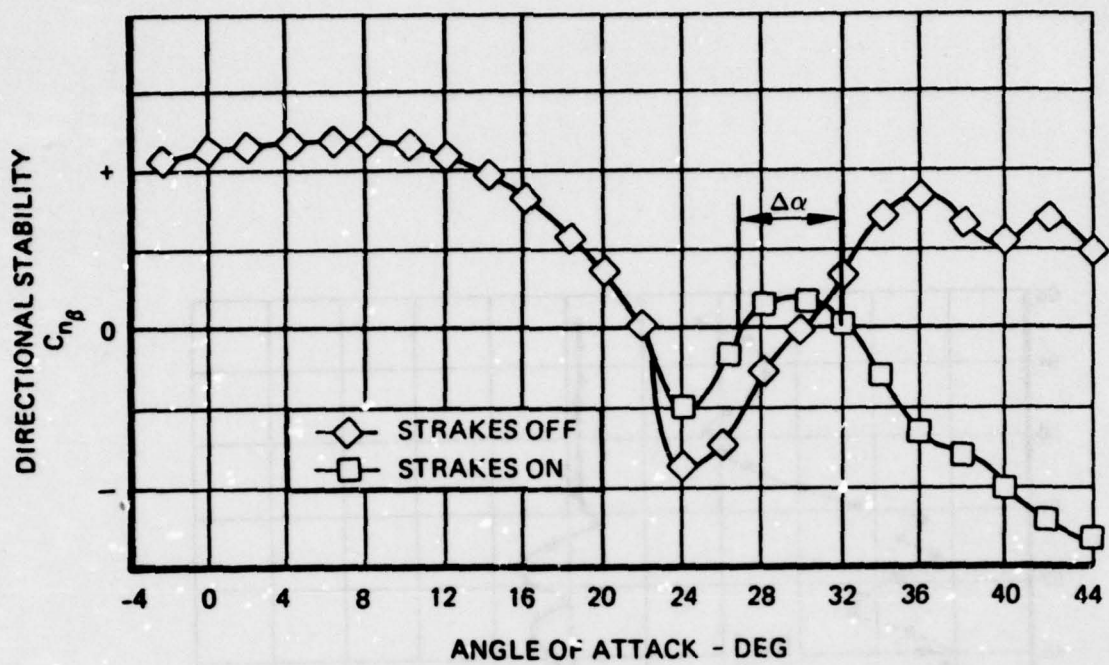


Figure 38. Effect of Nose Strake on Directional Stability

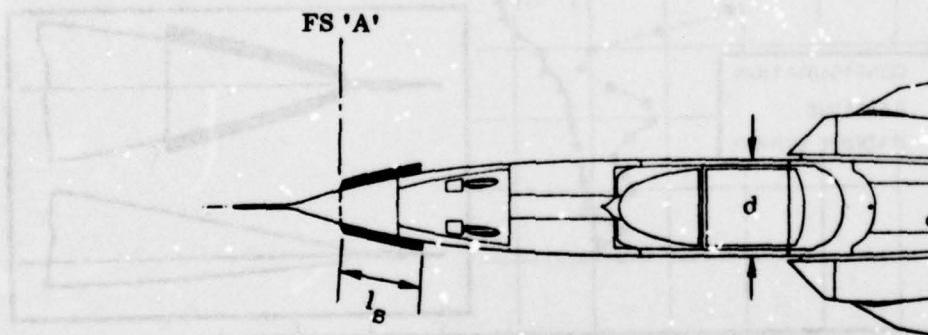








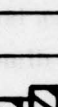








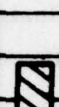








Figure 39. F-5 Strake Geometry Definitions

TABLE II - SUMMARY OF STRAKE DATA - F-5F

STRAKE	F.S. 'A'	l_s	LOCATION	COMMENTS	$ C_{n_0} _{\text{peak}}$					HIGH AOA STABILITY RANGE				
					.02	.04	.06	.08		10	20	30	40	50
S7	-0.23 d	0.46 d												
S8	0	0.72 d												
S9	0	6.05 d												
S10	0.23 d	0.87 d		Data for two runs										
S11	0.23 d	0.87 d												
S12	0.67 d	0.43 d												
S13	0.23 d	0.43 d												
S14	0.23 d	0.43 d		Strake Faired in										
OFF	—	—	—	—										

SUMMARY OF STRAKE DATA - F-5F

d. Blunted Noses

The effects of blunting the nose are shown in the following three sections. The first of these sections will assess the effects of progressively increasing the tip radius of the radome. This was investigated on the F-5F in Reference 54. Because of the flat elliptic cross sectional shape of the radome it was not possible to provide a truly spherical tip on the nose of the wind tunnel model. The tip radius was therefore defined in the profile view, and the planform shape became somewhat blunter, and was composed of both spherical and cylindrical sections. Figure 40 shows a view of the nose, and illustrates the various bluntness shapes tested. Tip radii of 2", 3", 4", and 5" were investigated, these dimensions being full scale.

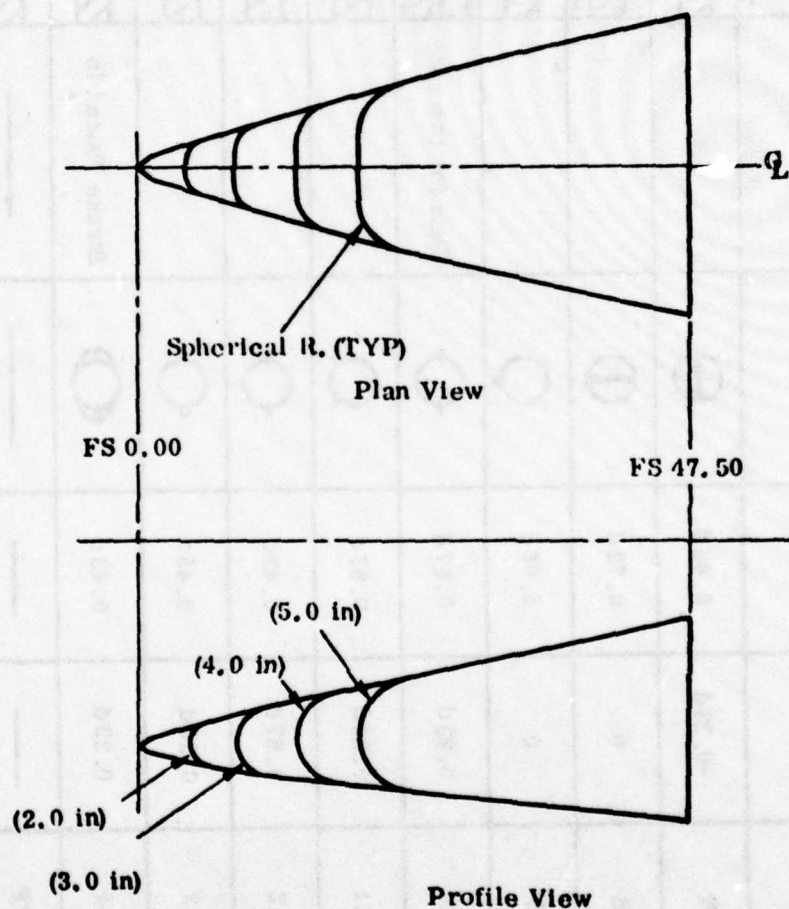


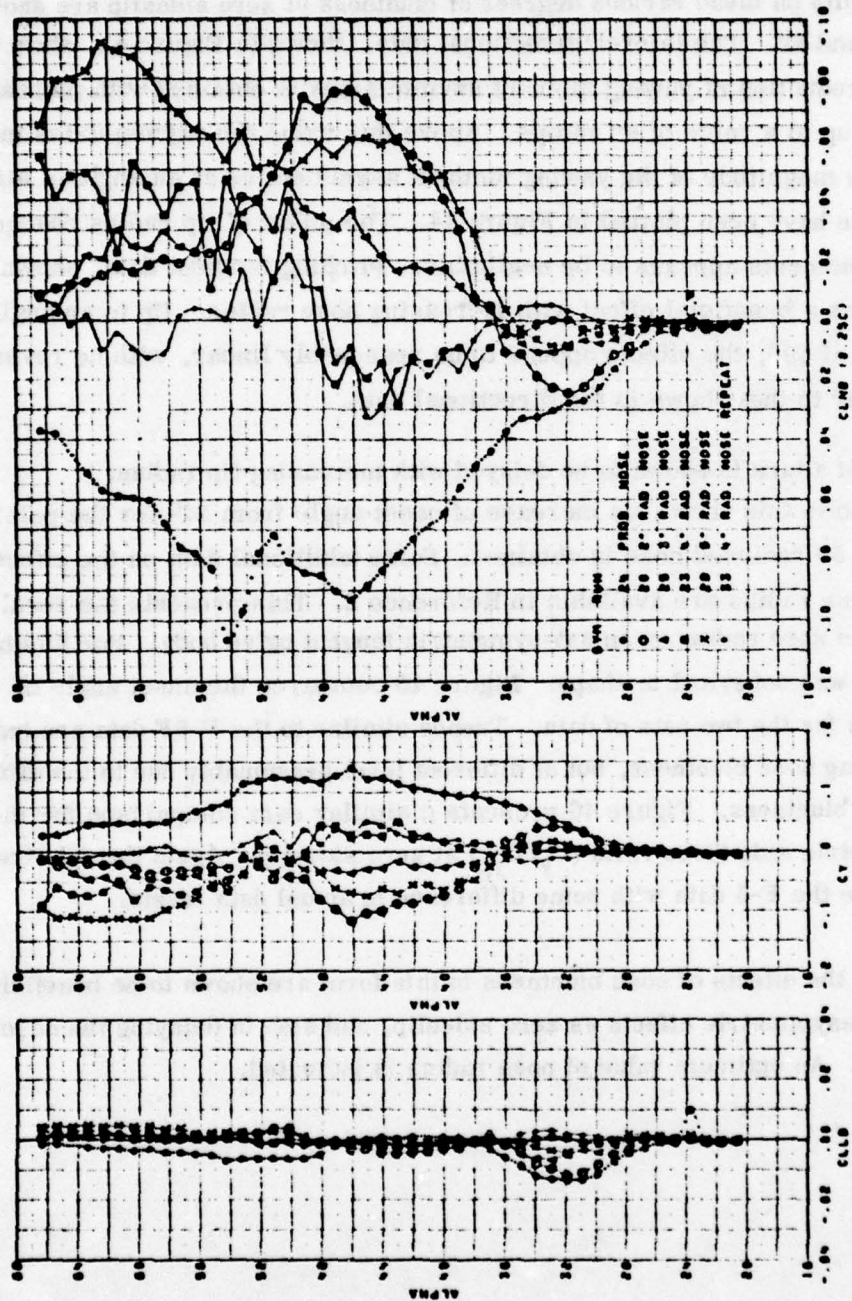
Figure 40. Radiused Nose

(1) Effects at Zero Sideslip

The test results on these various degrees of bluntness at zero sideslip are shown in Figures 41 and 42. The lateral/directional data, shown in Figure 41, show that a worthwhile reduction of yawing moment asymmetries is obtained with increasing nose radius up to a value of 4" radius. Above this value the asymmetries increase. The absolute magnitude of the yawing moment asymmetries at an angle of attack of 46 degrees have been plotted in Figure 44. The effect of tip radius changes on the rolling moments appears to be negligible. Pitching moment data, shown in Figure 42, shows a beneficial effect with increasing nose radius. Up to an angle of attack value of 50°, the effects appear to be reasonably linear, with no reversal of effect similar to that shown in the directional data.

Onset angle of attack is shown to be delayed with increasing tip radius. Figure 43 shows this trend, an increase of onset angle from 24° for the pointed nose to 36 for the 5" radiused nose is obtained. Some additional data on the effects of increased nose radius are available in Reference 2. This presents the results of increasing the nose radius on an axi-symmetric tangent ogive body. For this body the tip bluntness was spherical in shape. Figure 45 compares the onset angle of attack effects for the two sets of data. Trends similar to the F-5F data are indicated with increasing nose bluntness, but at different level presumably due to the different form of nose bluntness. Figure 46 presents a similar data comparison for the peak asymmetric side force ratio (C_y/C_{y0}) at zero sideslip. Again the data trends are similar to the F-5 data with some difference in actual data levels.

In summary, the effects of nose bluntness in this form are shown to be beneficial in reducing the asymmetric effects at zero sideslip, and also in delaying the onset of these effects. An optimum value of nose radius is indicated.



F-5F EFFECT OF NOSE RADIUS AT BETA=0 DEG.
P/-//LR. FLAPS=0/0. DM=-20 DEG. MAL-170

Figure 41. Lateral/Directional Effects of Increased Nose Radius at Zero Sideslip



55

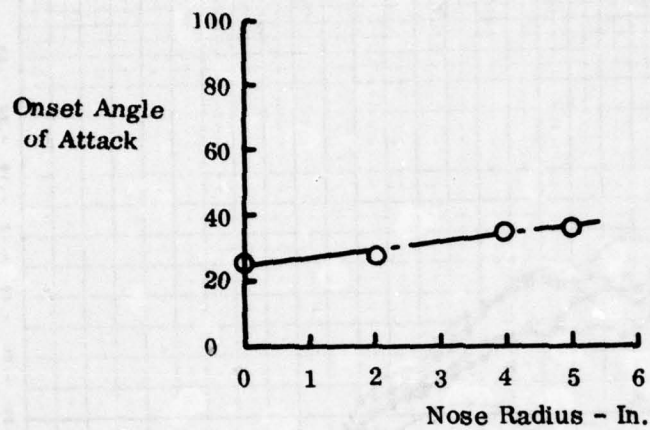


Figure 43. Effect of Nose Radius Increases on Onset Angle of Attack

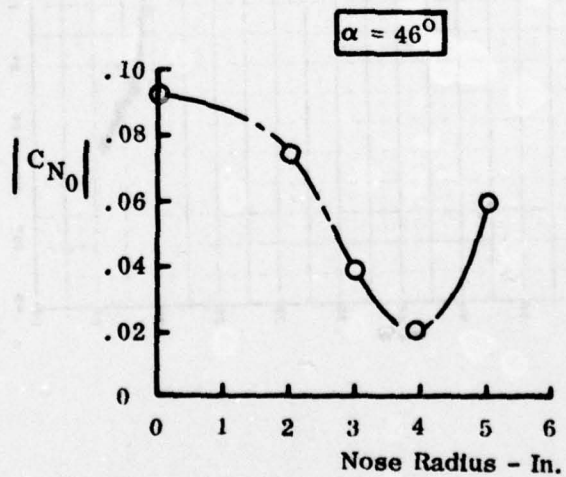


Figure 44. Effect of Nose Radius Increases on Peak Asymmetric Yawing Moments

□ Ref 2
 ▲ Ref 54

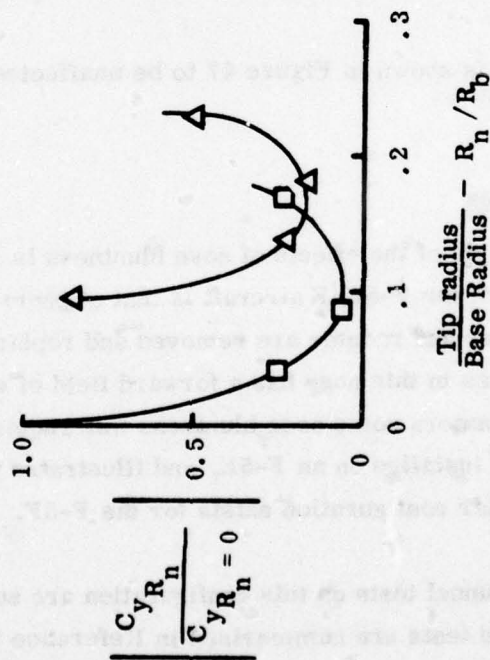


Figure 45. Comparison of Peak Asymmetric Data

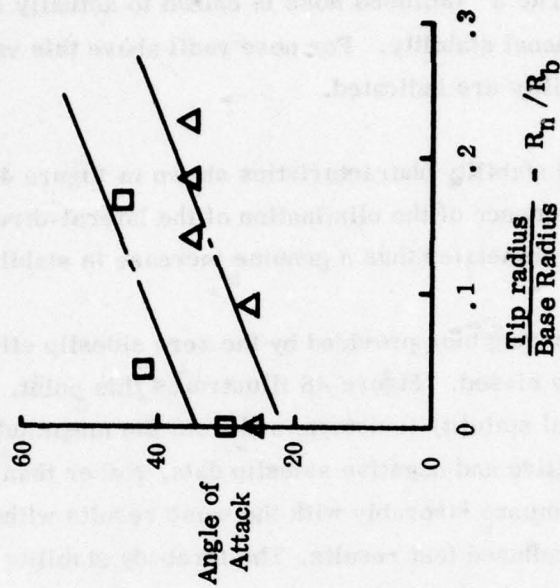


Figure 46. Comparison of Onset Angle of Attack Data

(2) Effects on Non-Zero Sideslip

The effects of an increase in nose radius on lateral/directional stability is presented in Figure 47. The 3" radiused nose is shown to actually reduce the high angle of attack directional stability. For nose radii above this value improvements in directional stability are indicated.

These improved stability characteristics shown in Figure 47 are probably more of a consequence of the elimination of the lateral-directional bias due to the aerodynamic asymmetries than a genuine increase in stability.

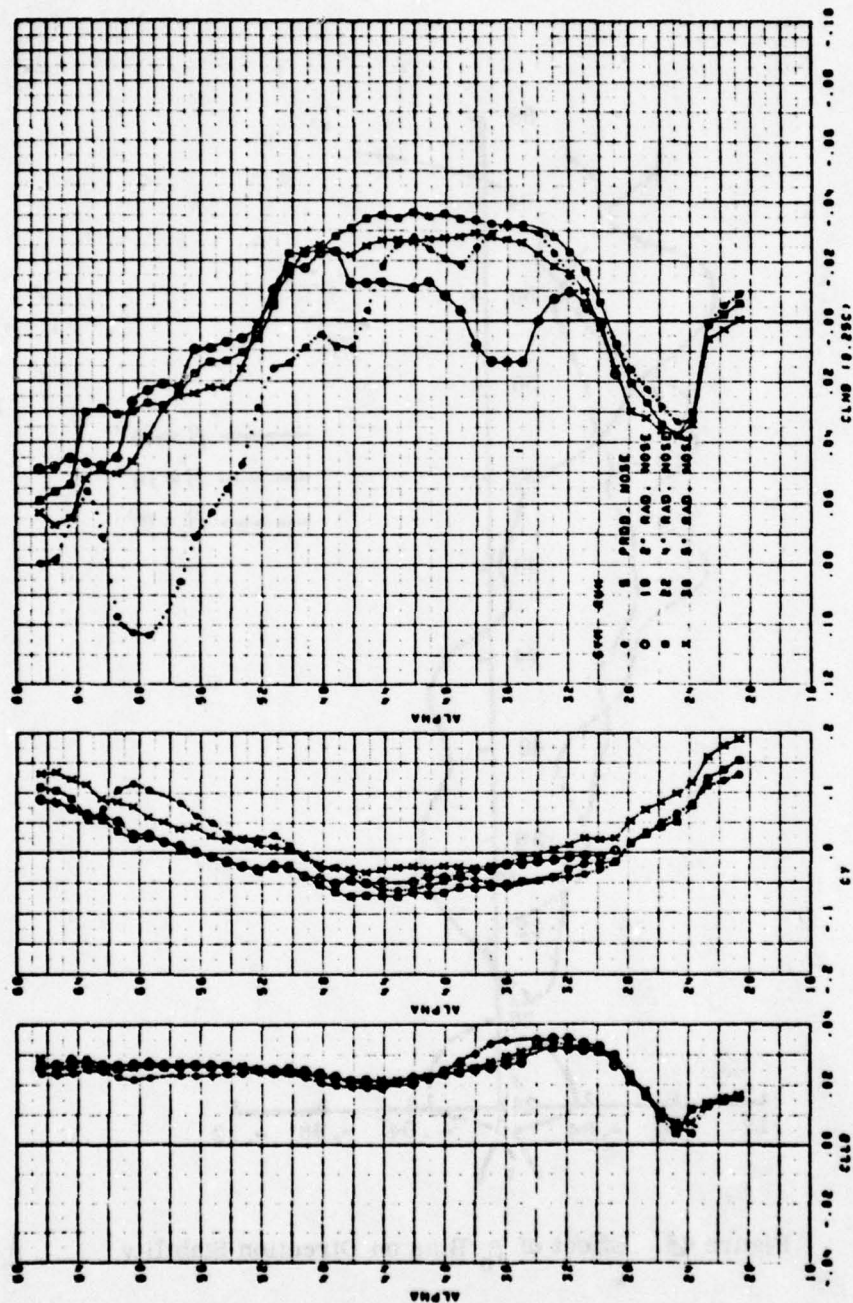
Because of the strong bias provided by the zero sideslip effects, directional stability itself is strongly biased. Figure 48 illustrates this point. If the high angle-of-attack directional stability is determined from the magnitude of the difference between the positive and negative sideslip data, rather than the absolute values, then these results compare favorably with the same results without bias, as typified by the large nose radiused test results. The forebody stability is a stronger function of the forebody cross sectional shapes than the nose tip radius.

Lateral stability is shown in Figure 47 to be unaffected by changes in nose radius.

e. Camera Noses

The second example of the effects of nose bluntness is also provided from F-5 data. One of the roles of the F-5E/F aircraft is that of photo reconnaissance, and for this purpose, the radar and radome are removed and replaced by a special camera nose. One of the cameras in this nose has a forward field of view, and to accommodate the window for this camera some nose bluntness was required. Figure 49 shows this camera nose installed on an F-5E, and illustrates the blunting for the forward camera. A similar configuration exists for the F-5F.

Low speed wind tunnel tests on this configuration are summarized in Reference 51, and the high speed tests are summarized in Reference 59. In general, the camera nose modification was seen to improve both the aerodynamic asymmetries and the directional stability effects at high angles of attack. The results from these tests



7-57 EFFECT OF NOSE RADIUS AT $\beta = 10$ DEG.
 P/L - 1/2, FLAPS - 0/5, 10/15, 20/25, 30/35

Figure 47. Lateral/Directional Stability Effects

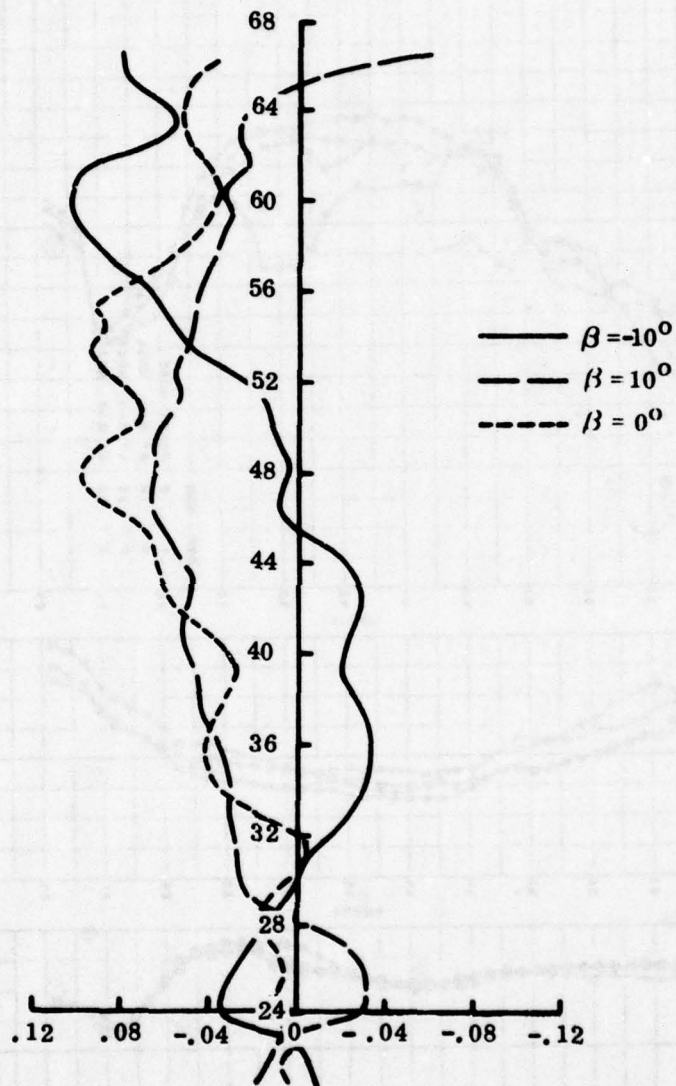


Figure 48. Effect of β_0 Bias on Direction Stability

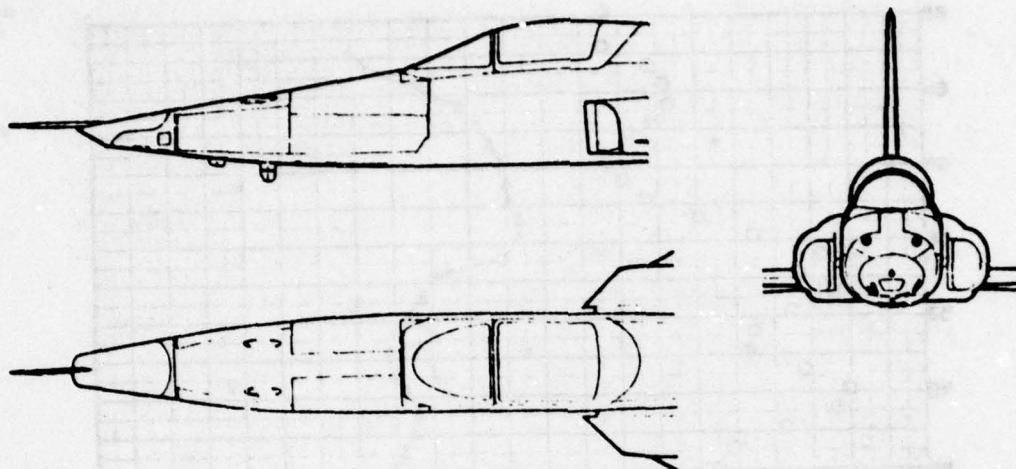


Figure 49. F-5E Camera Nose

are included in this analysis section mainly to show Mach Number trends, and also a further indication of the beneficial nature of a slight blunting of the nose of the aircraft.

The effects on aerodynamic asymmetries of this type of nose geometry at subsonic Mach numbers are shown in Figure 50. The large reduction of the zero sideslip yawing moments is clearly shown.

The effect of Mach number on the zero sideslip yawing moments is shown in Figure 51. Here data are presented for both the camera nose and the base (pointed) nose for a constant angle of attack. The beneficial effects of the addition of nose bluntness in reducing the aerodynamic asymmetries is clearly shown across the Mach number range. For the particular angle of attack chosen, the asymmetries are shown to disappear just below a Mach number of 1.0. To further investigate the effects of Mach number data over a range of angles of attack will be examined.

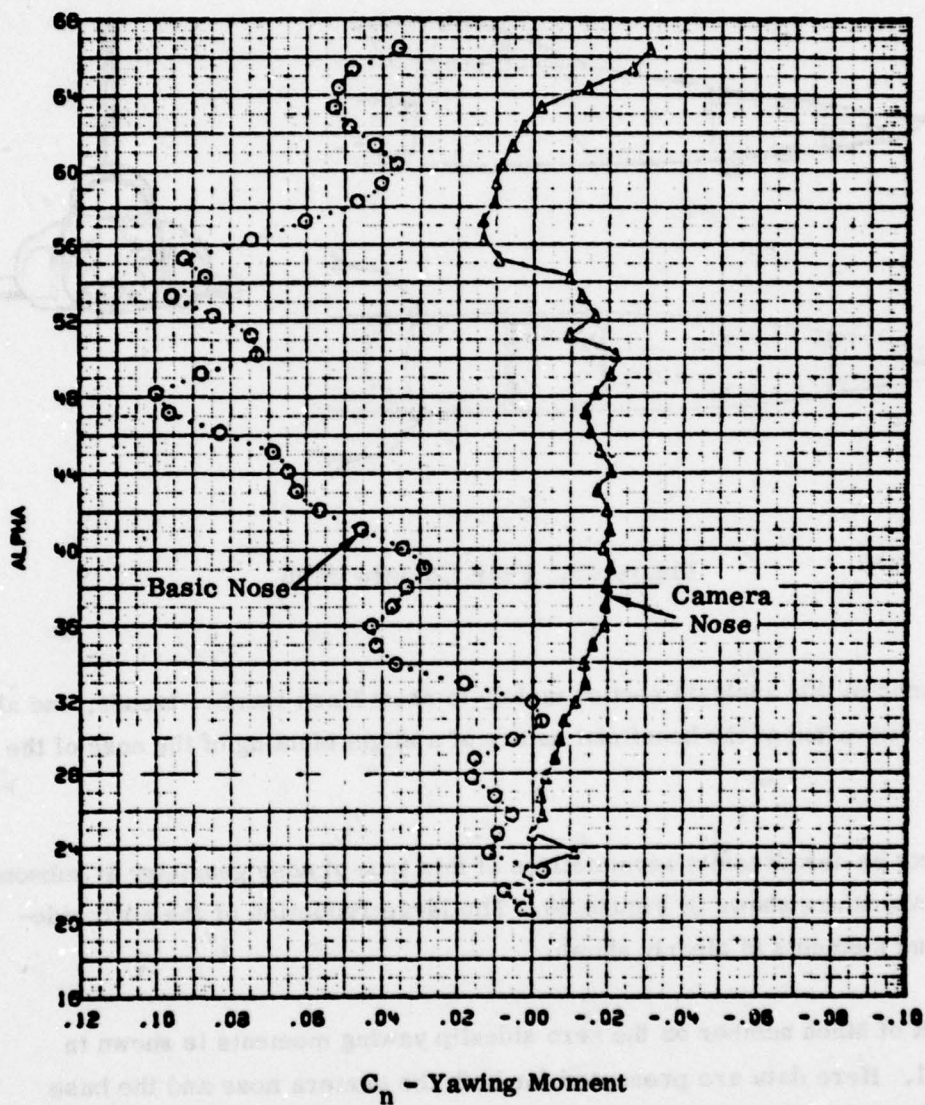


Figure 50. Effect of Camera Nose at Zero Sideslip

□ Camera Nose } Ref 59, Volume II
 ◇ Base Nose

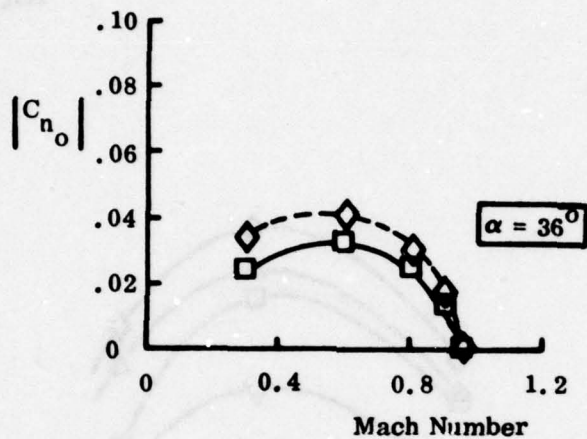


Figure 51. Effect of Camera Nose on Zero Sideslip Asymmetries

Figure 52 shows the zero sideslip yawing moments for angles of attack between 32° and 40° , as a function of Mach number. In general, the effects of Mach number are seen initially to increase the asymmetries, after which rapid decreases in the aerodynamic asymmetries are shown. At a value just below $M = 1.0$, the asymmetries become negligible.

During a previous discussion, mention was made of the data of Reference 2, which suggested that the zero sideslip effects were eliminated when the cross flow Mach number, M_{cf} , reached a value of 0.5. To examine this concept, the data of Figure 52 has been replotted as a function of cross flow Mach number on Figure 53.

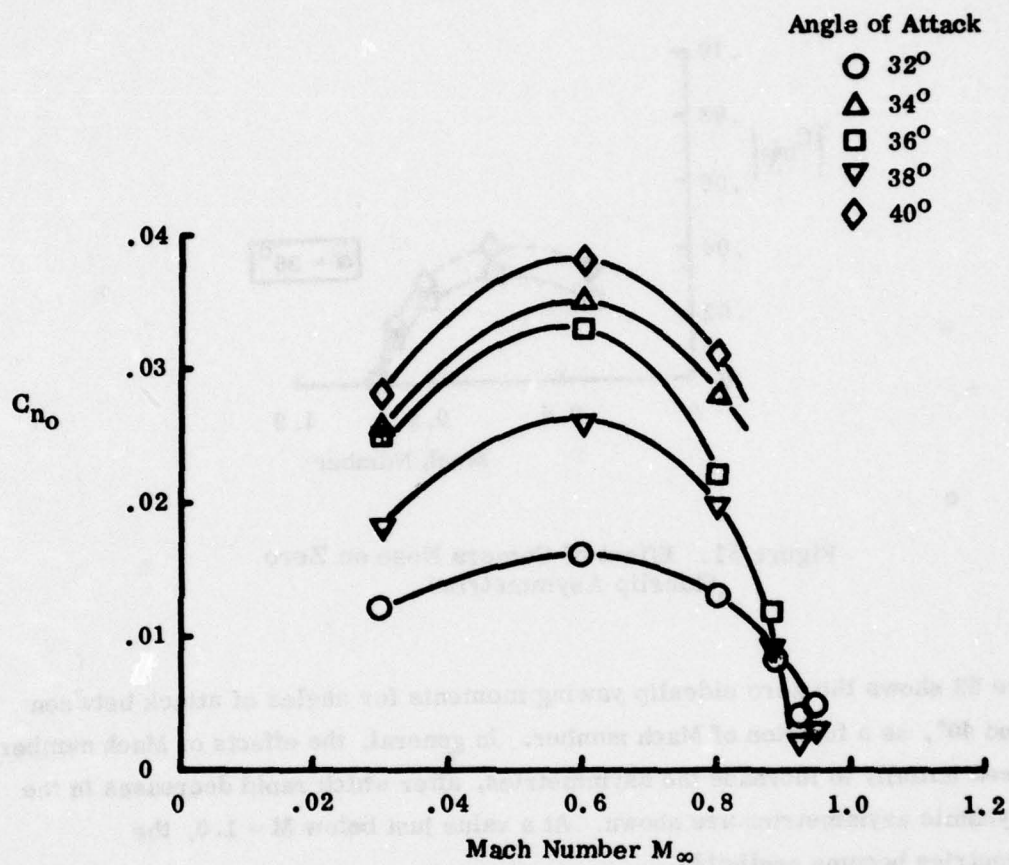


Figure 52. Camera Nose Zero Sideslip Yawing Moments

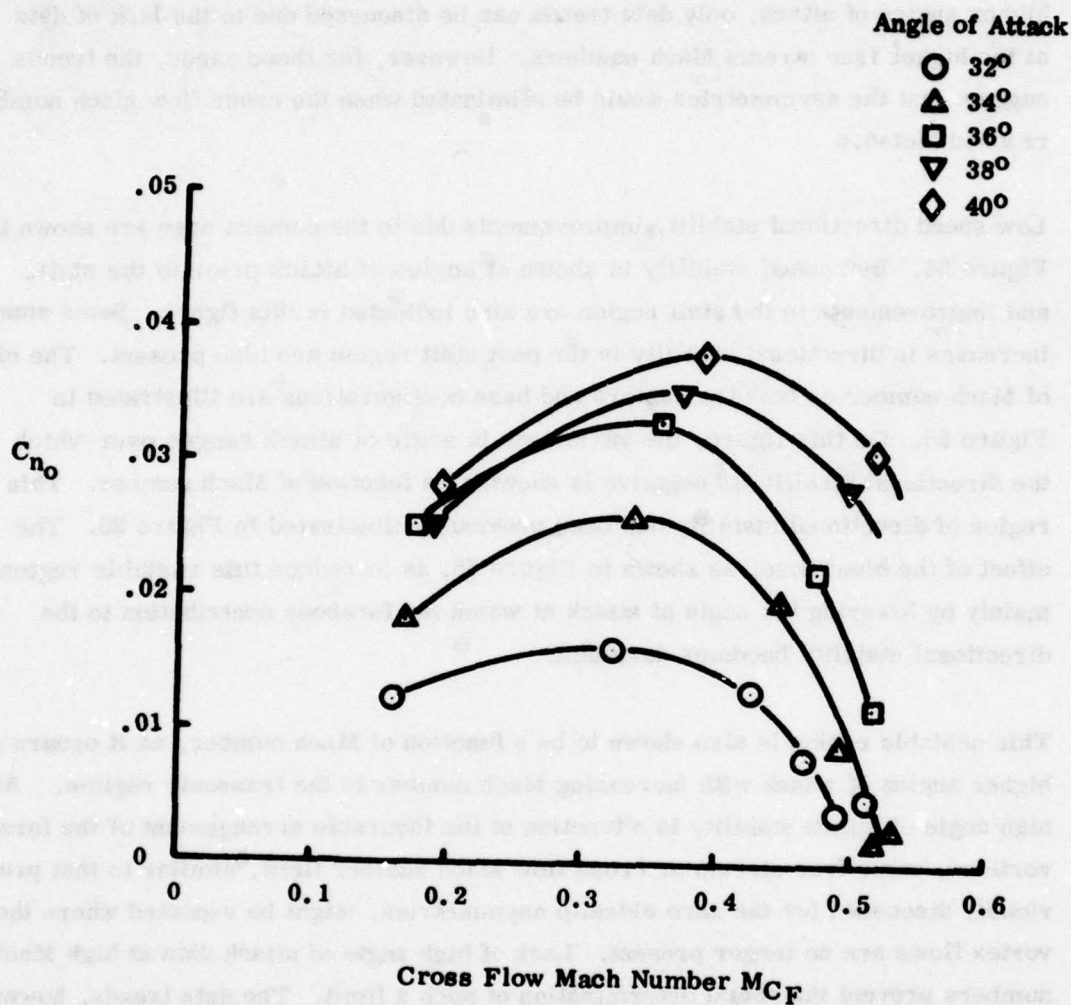


Figure 53. Effects of Cross Flow Mach Number

This figure shows that the zero sideslip yawing moments at the lower angles of attack tend towards zero at a cross flow Mach number slightly greater than 0.5. At the higher angles of attack, only data trends can be discussed due to the lack of data at the higher free stream Mach numbers. However, for these cases, the trends suggest that the asymmetries would be eliminated when the cross flow Mach number reached $M_{cf}=0.6$

Low speed directional stability improvements due to the camera nose are shown in Figure 54. Increased stability is shown at angles of attack prior to the stall, and improvements in the stall region are also indicated in this figure. Some small increases in directional stability in the post stall region are also present. The effects of Mach number on both the camera and base configurations are illustrated in Figure 55. On this figure, the variations in angle of attack ranges over which the directional stability is negative is shown as a function of Mach number. This region of directional stability has been previously illustrated in Figure 25. The effect of the blunt nose, as shown in Figure 55, is to reduce this unstable region, mainly by lowering the angle of attack at which the forebody contribution to the directional stability becomes dominant.

This unstable region is also shown to be a function of Mach number, as it occurs at higher angles of attack with increasing Mach number in the transonic regime. As the high angle of attack stability is a function of the favorable arrangement of the forebody vortices, some free stream or cross flow Mach number limit, similar to that previously discussed for the zero sideslip asymmetries, might be expected where the vortex flows are no longer present. Lack of high angle of attack data at high Mach numbers prevent the actual determination of such a limit. The data trends, however, suggest the limit has almost been reached.

f. Shark Type Noses

As part of the F-5F development, an analytic and experimental program was undertaken with the specific objective of designing a forebody geometry which would minimize the adverse effects of the aerodynamic asymmetries, while maintaining or enhancing the already excellent lateral-directional stability characteristics known to be a property of the F-5 nose cross sectional shape. Additionally, the effects of changes to forebody geometry on radar performance were integrated into this development program. The

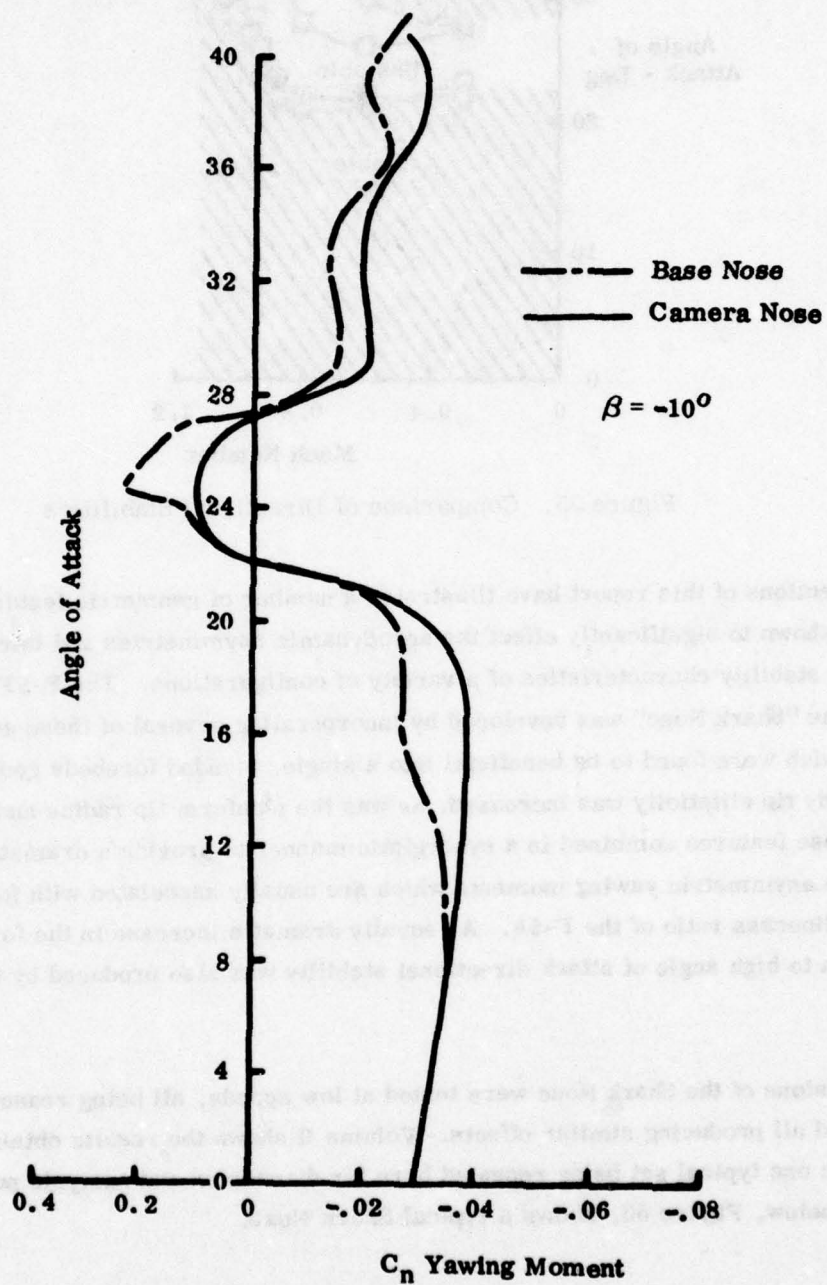


Figure 54. Directional Stability Comparisons

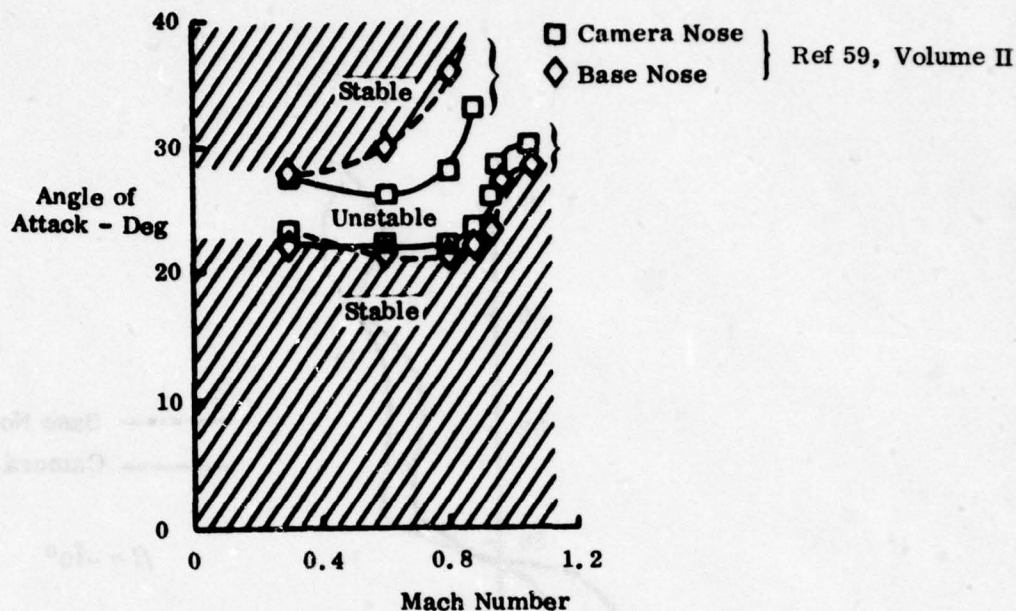


Figure 55. Comparison of Directional Stabilities

previous sections of this report have illustrated a number of geometric features which have been shown to significantly effect the aerodynamic asymmetries and lateral-directional stability characteristics of a variety of configurations. The F-5F forebody known as the "Shark Nose" was developed by incorporating several of these geometric features which were found to be beneficial into a single, blended forebody geometry. The forebody tip ellipticity was increased, as was the planform tip radius and the nose angle. These features combined in a synergistic manner to provide a dramatic reduction in the large asymmetric yawing moments which are usually associated with forebodies having the fineness ratio of the F-5F. An equally dramatic increase in the forebody contribution to high angle of attack directional stability was also produced by the Shark Nose.

Several versions of the Shark Nose were tested at low speeds, all being reasonably similar, and all producing similar effects. Volume II shows the results obtained with these noses; one typical set being repeated here for discussion and analysis purposes. The figure below, Figure 56, shows a typical Shark Nose.

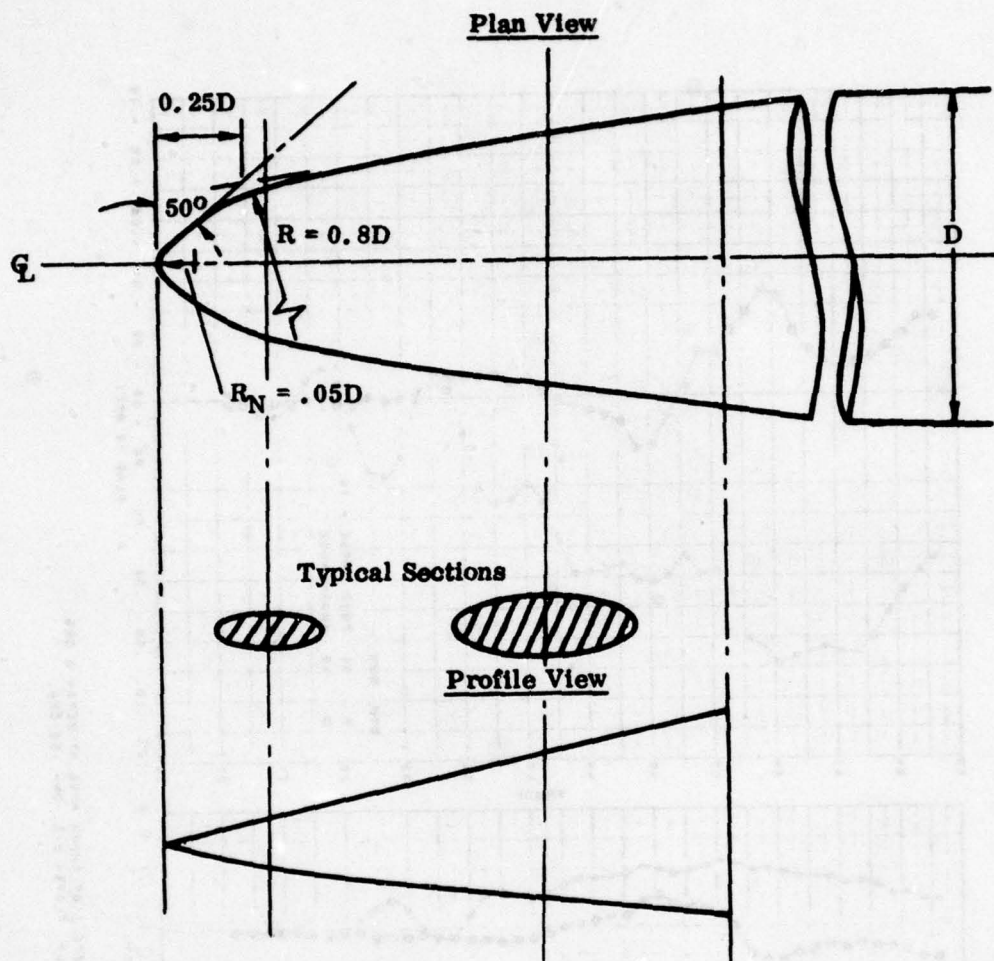
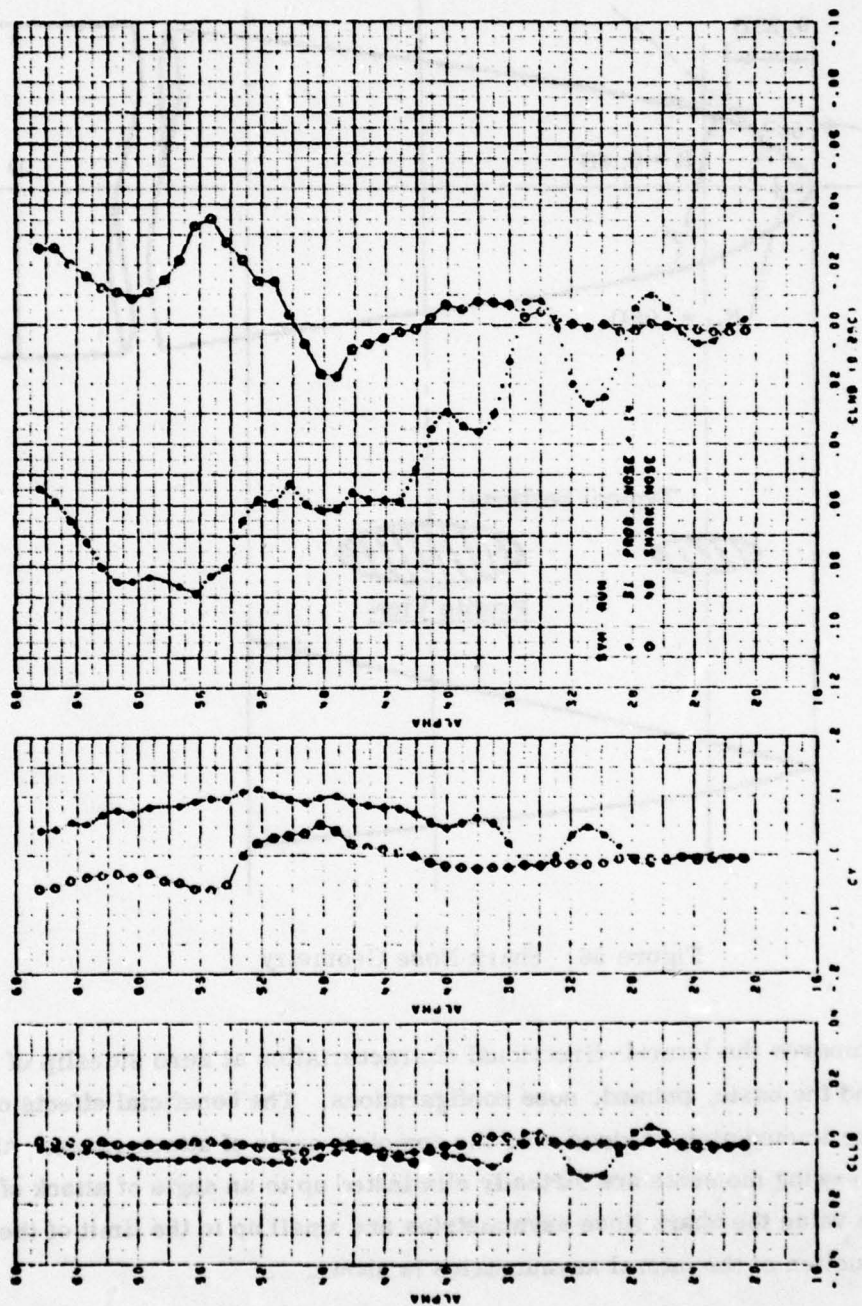


Figure 56. Shark Nose Geometry

Figure 57 compares the lateral-directional characteristics at zero sideslip of the Shark Nose and the basic, pointed, nose configurations. The beneficial effects of the Shark Nose are immediately obvious over the complete angle of attack range. All the zero sideslip yawing moments are virtually eliminated up to an angle of attack of 50° , and above this value the Shark Nose asymmetries are small up to the limit of the data. A similar reduction of the lateral asymmetries is shown.



7-57 EFFECT OF SHARK NOSE AT BETA=0 DEG.
 PITCH=0, FLAPS=0, DM=-20 DEG.

Figure 57. Effect of Shark Nose at Zero Sideslip

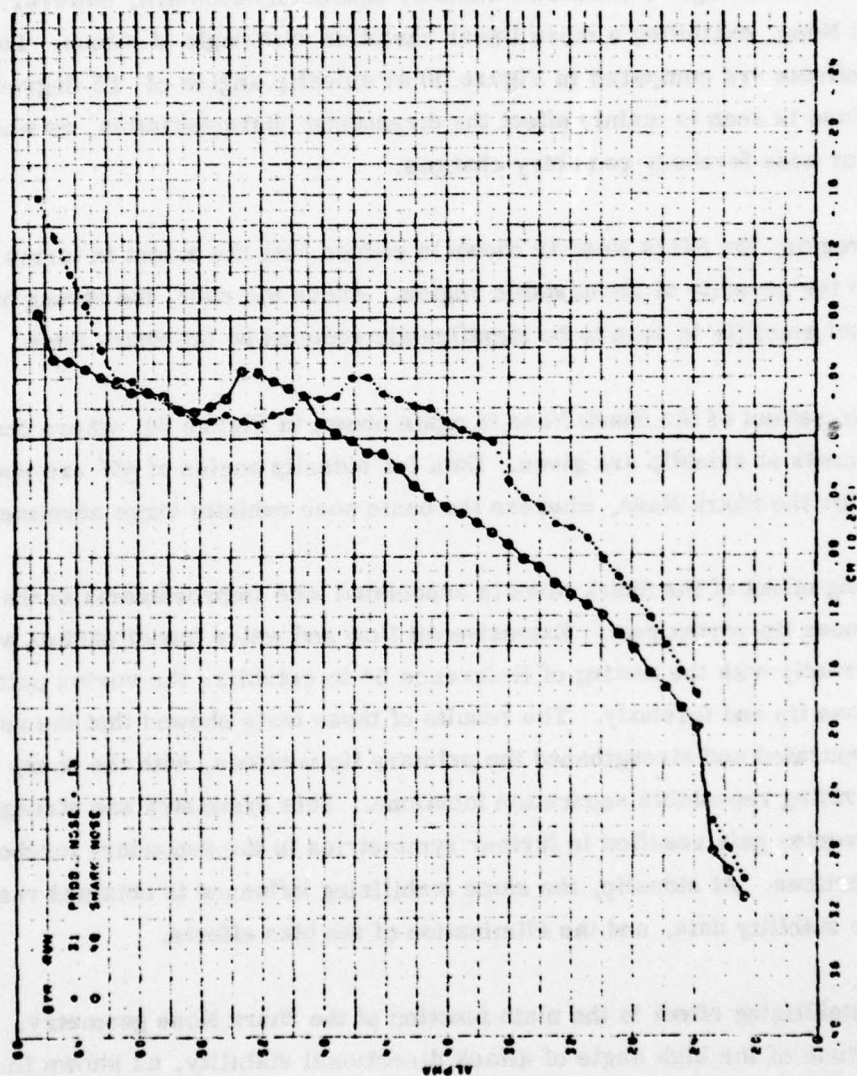
The effects of the Shark Nose on trimmed lift is negligible. However, the effect on the post-stall longitudinal stability is quite large, as illustrated in Figure 58. Just above the stall angle of attack, the Shark Nose is seen to produce a destabilizing shift in the pitching moment, probably due to the additional planform area associated with the nose broadening. The overall stability characteristics are, however, improved by the Shark Nose, exhibiting a more linear variation with angle of attack. Lateral-directional effects are compared in Figure 59 at sideslip angles of ± 5 degrees. The Shark Nose is seen to mainly effect the directional characteristics, as was noted previously for nose forebody geometry changes.

In the stall region, the Shark Nose is shown to reduce both the extent in terms of angle of attack and the severity of the unstable region. Above the stall, the strong bias in the directional stability is seen to be significantly reduced by the Shark Nose.

The stabilizing effect of the Shark Nose is again shown in Figure 60, where the pitching moments at sideslip are given. Data for sideslip angles of $\pm 5^\circ$ are shown to be identical for the Shark Nose, whereas the basic nose exhibits large asymmetries.

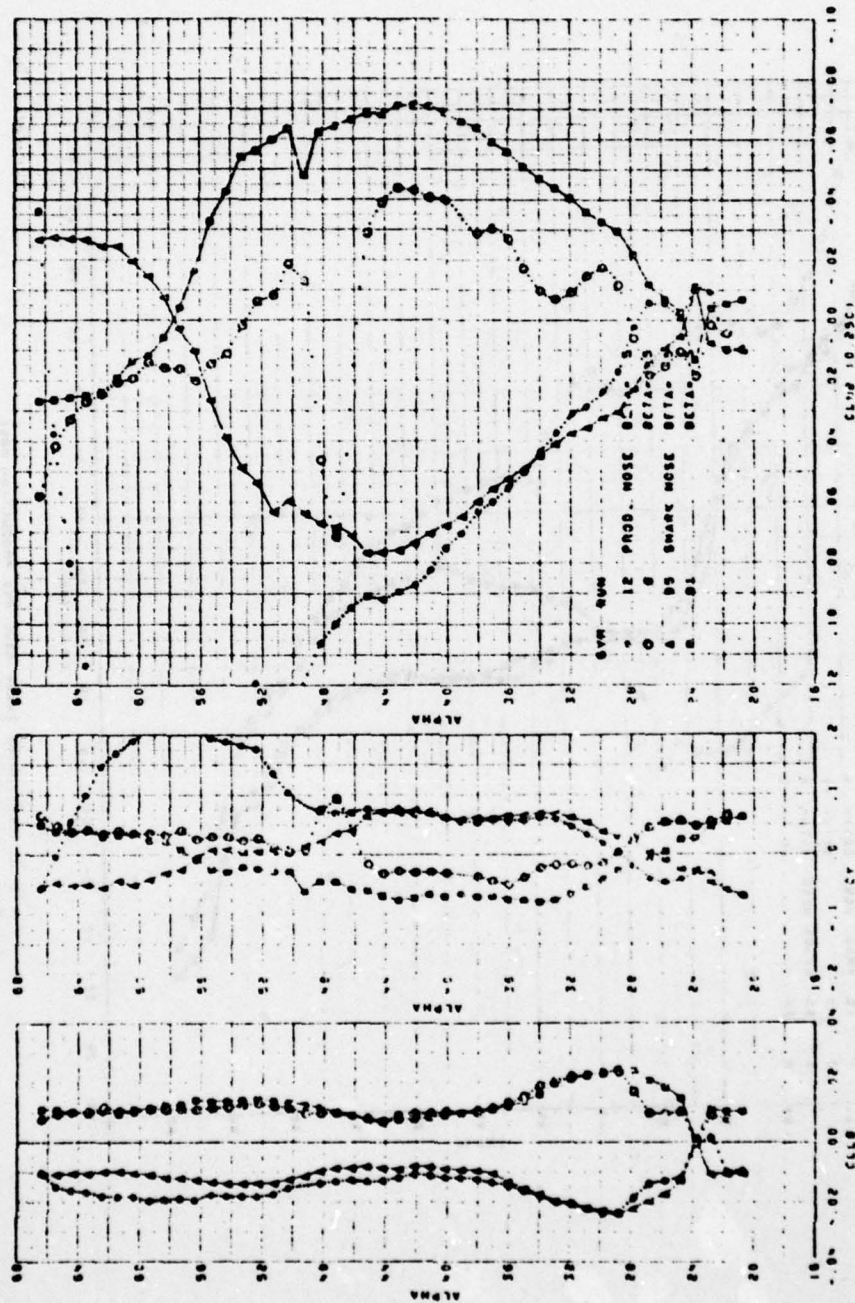
The stabilizing effect of the Shark Nose is associated with improvements in the stability of the nose tip vortex pair. Extensive oil flow and water tunnel studies were made concurrently with the testing of Reference 54 to establish the vortex patterns around the nose tip and forebody. The results of these tests showed that the nose broadness separated and strengthened the primary tip vortices, with the sharp edge contours providing repeatable separation locations. This symmetry and strength of the primary vortex pair resulted in further symmetries in the secondary forebody separation vortices. At sideslip, the same stabilizing influence is obtained resulting in symmetric stability data, and the elimination of the bias effects.

This vortex stabilizing effect is the main function of the Shark Nose geometry. The actual magnitude of the high angle of attack directional stability, as shown in Figure 59, is virtually unchanged by the addition of the Shark Nose, if the bias effects are ignored. This indicates that the basic forebody produces the directional stability in this angle of attack region. The stabilizing effect of the Shark Nose on the forebody vortices is shown in Figure 61 where some typical fluorescent oil flow pictures are presented. These photographs illustrate the surface conditions over the upper section of the forebody at high angle of attack, and zero sideslip. The strength and



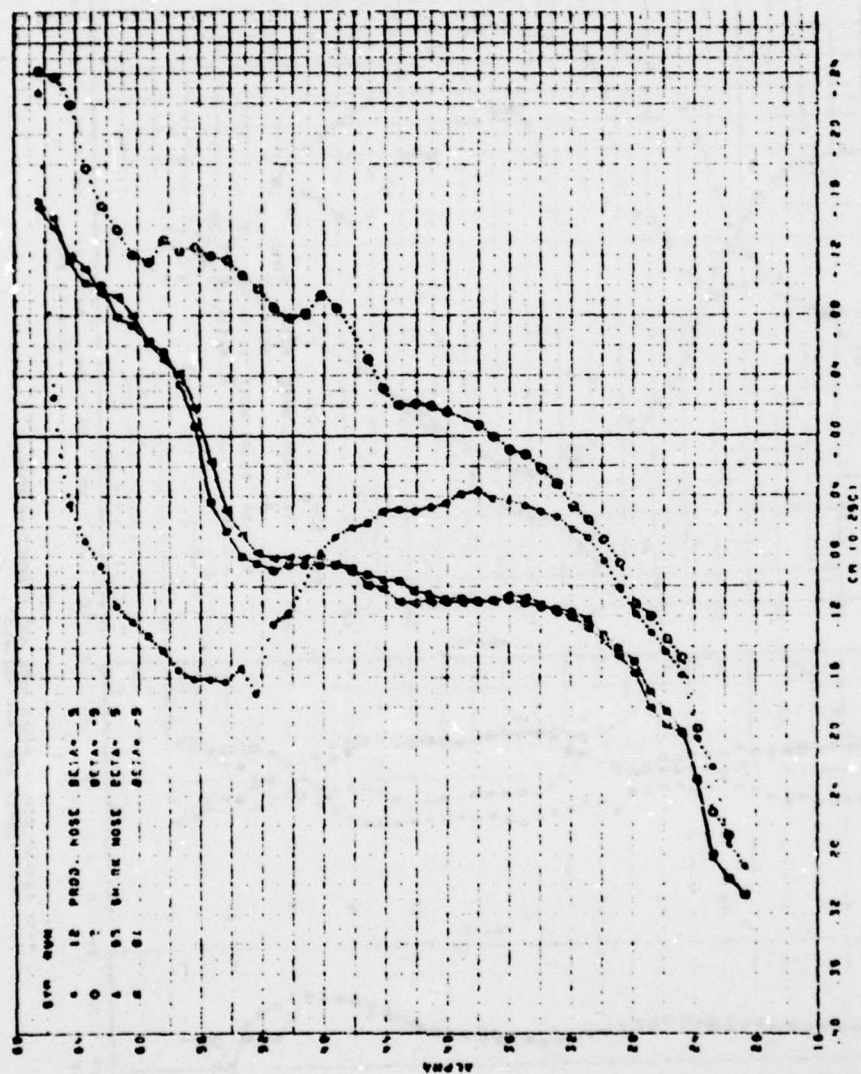
P. 51 EFFECT OF SHARK NOSE AT $\beta = 0$ DEG.
 P. 51-1/2. PLANE 1/2. DMO - 80 DEG

Figure 58. Effect of Shark Nose on Zero Sideslip Pitching Moments



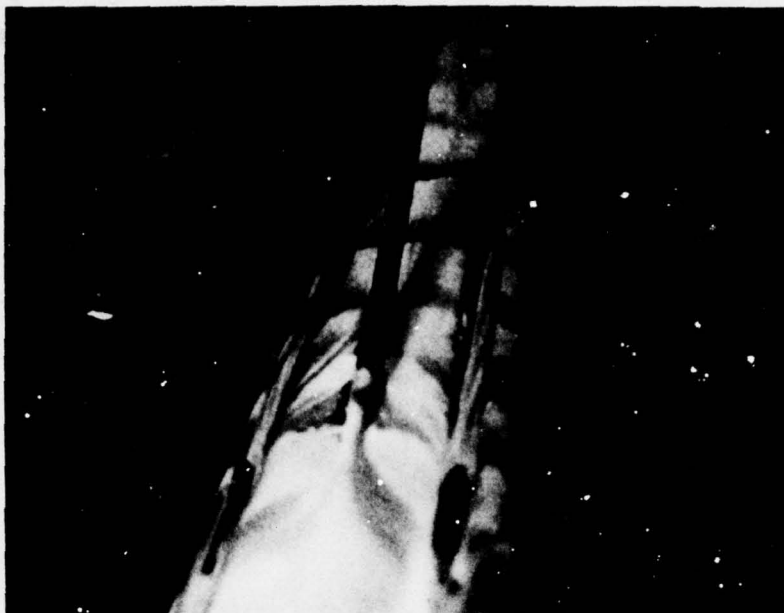
F-35 COMPARISON OF SHARK NOSE AND PRODUCTION NOSE
 PROD. NOSE, FLAPS 3/8, DME -20 DEG

Figure 59. Effect of Shark Nose on Lateral/Directional Stability



P-3F COMPARISON OF SHARK NOSE AND PRODUCTION NOSE
 P-3F, FLAPS 0/0, Dns -20 DEG.

Figure 60. Effect of Shark Nose on Pitching Moments in Sideslip



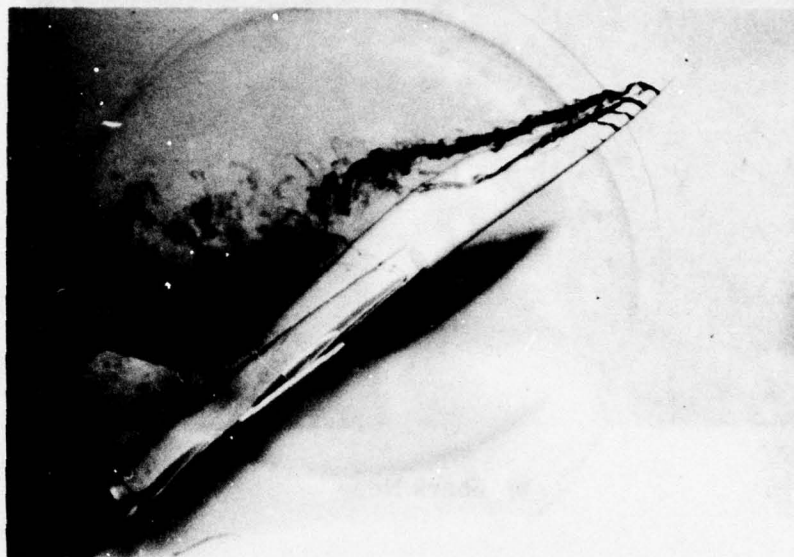
a) Shark Nose



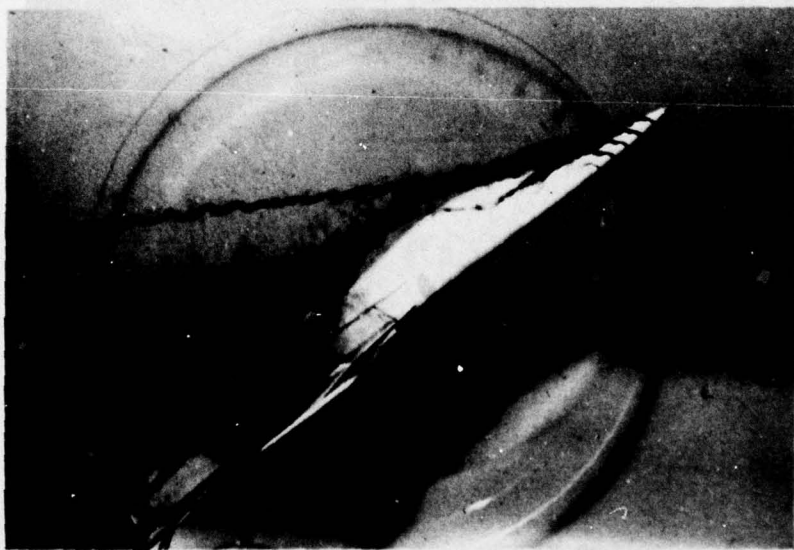
b) Pointed (Production) Nose

Figure 61. Surface Oil Flows on F-5F Nose

symmetry of the vortices on the Shark Nose (upper photo) contrast vividly with the erratic flow patterns obtained on the basic nose (lower photo). These effects are illustrated again in Figure 62, where some typical water tunnel photos for similar conditions are presented.



a) Shark Nose



b) Base Nose

Figure 62. F-5F Model in Northrop Water Tunnel

g. Forebody Design Guidelines Summary

The previous paragraphs have discussed various aspects of forebody geometry changes and the aerodynamic benefits to be obtained. Before summarizing the highlights from this study, a few words regarding use of these results are appropriate. The data survey is based entirely on static wind tunnel measurements, but the effects of airplane dynamics cannot be ignored. In the stall/post stall region, the aircraft may experience heavy buffet and some degree of wing rock, both of which must inevitably modify or mask the trends suggested by the static tunnel data. Exactly how airplane dynamics influence the static aero characteristics is not yet clearly understood. A study of these effects would be a major task in itself, and is also beyond the scope of this investigation. However, these dynamic effects must be remembered when assessing high angle of attack flying characteristics.

The following is, therefore, a summary of the data on forebody effects, based only on the static aerodynamic results.

The forebody is seen to be more than a fairing over a large collection of electronic black boxes and, if properly designed, can be directionally stable at both zero and positive angles of sideslip at high angles of attack.

At zero sideslip, directional stability is obtained by controlling the nose vortex array. This array consists of a pair of primary nose tip vortices, plus the secondary forebody separation vortex pair. For pointed bodies, increasing the forebody length reduces the angle of attack at which vortex instability and resulting asymmetries are noticeable. Blunting the nose, adding small tip strakes, or a local broadening of the tip of the nose (i.e., the Shark Nose) are all shown to be beneficial in correcting the tip vortex instability.

At sideslip, directional stability is obtained at high angles of attack by the use of elliptic forebody cross-sections, with the major axis horizontal. This slope distribution around the forebody interacts with the windward vortex to create restoring sideforce, and hence positive stability. Positive nose stability by this means can be provided in the 30° – 50° angle-of-attack range.

For more circular noses, directional stability can be achieved by the addition of horizontal nose strakes.

These conclusions refer mainly to low subsonic Mach numbers. Increases in Mach number into the transonic region are shown to be beneficial in terms of reducing the zero sideslip asymmetries, but unfavorable to the post stall high angle of attack directional stability. The effects of Mach number are to gradually eliminate the nose vortex system's influence, and to replace it with a shock induced separation pattern. The asymmetries associated with a random vortex arrangement are therefore eliminated. The favorable vortex induced stabilizing forces, present on broad elliptical forebodies, are also eliminated in a similar manner. In general, forebody vortex effects appear to be present if the forebody cross flow Mach number is below $M_{cf} = 0.5-0.6$.

The sensitivity of the nose region at high angles of attack is such that any modification of the tip region by the addition of such items as a flight test nose boom should be avoided.

Following are some specific design guidelines which cover points discussed above.

To obtain a forebody configuration which at high angles-of-attack would have:

- 1) Minimum asymmetric forces at zero sideslip
- 2) Positive directional stability

the following design guidelines are suggested.

The asymmetric side forces and moments are minimized when the forebody $1/d$ ratio is (3.5-4), and this can be achieved either by use of a LEX as a forebody shield, or by shortening the forebody.

If the forebody fineness ratio has to be of the order four then a blended forebody geometry such as the Shark type nose, or the use of nose strakes will be required. The addition of nose strakes to a stable forebody which contributes directional stability is not recommended.

Positive directional stability at high angles of attack can be achieved by using a forebody with flat elliptical nose sections. From the test results, two guidelines are presented. The first being the angle of attack at which positive nose stability occurs, α and this is shown in Figure 63. The second guideline is that of the angle of attack range over which the forebody remains stable, $\Delta\alpha$ and this is shown on Figure 64.

A final guideline is proposed. This defines the region where the forebody vortex flows dominate, and can be used for stabilizing effects. Figure 65 illustrates this region, which essentially is the free stream conditions up to values where the cross flow Mach number is of the order $0.5 \approx 0.6$. For conditions where the cross flow Mach number is greater than these values, shock induced separation effects dominate.

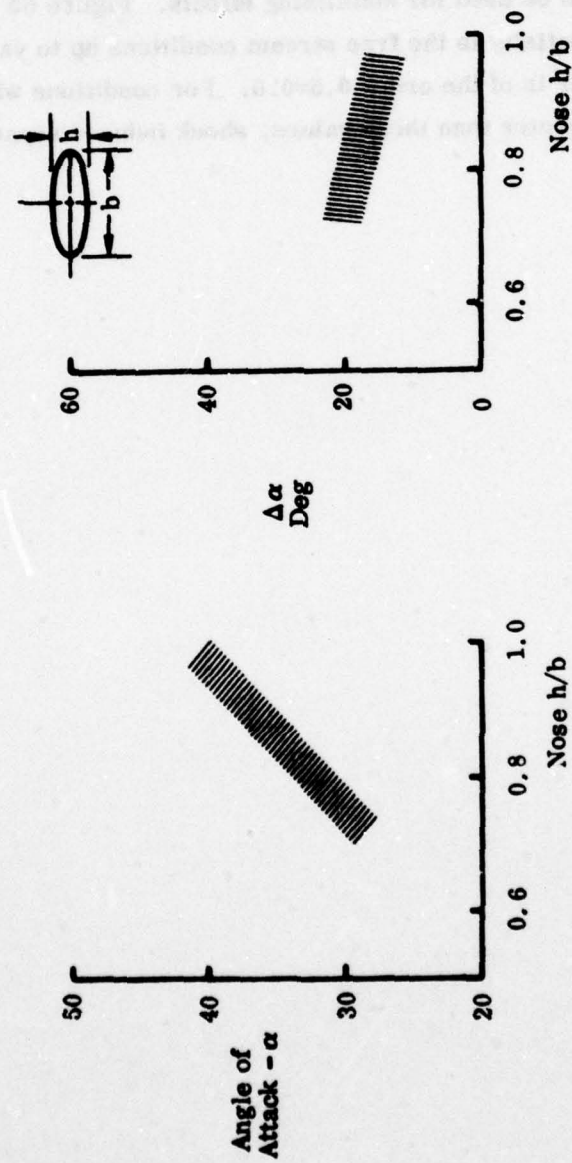


Figure 63. Onset Angle for Nose Stability

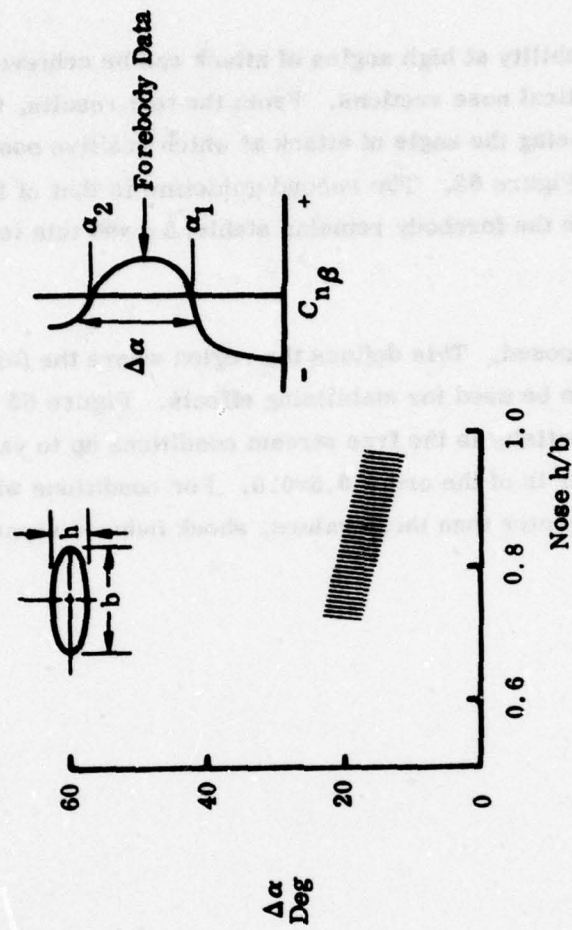


Figure 64. Range of Nose Stability

Effect of Mach number on the flow field around a blunt body is a function of the angle of attack and the Mach number. The flow field is characterized by the presence of shock waves and vortices. The shock waves are formed by the compression of the flow and the vortices are formed by the separation of the flow from the surface of the body. The flow field is characterized by the presence of shock waves and vortices. The shock waves are formed by the compression of the flow and the vortices are formed by the separation of the flow from the surface of the body. The flow field is characterized by the presence of shock waves and vortices. The shock waves are formed by the compression of the flow and the vortices are formed by the separation of the flow from the surface of the body.

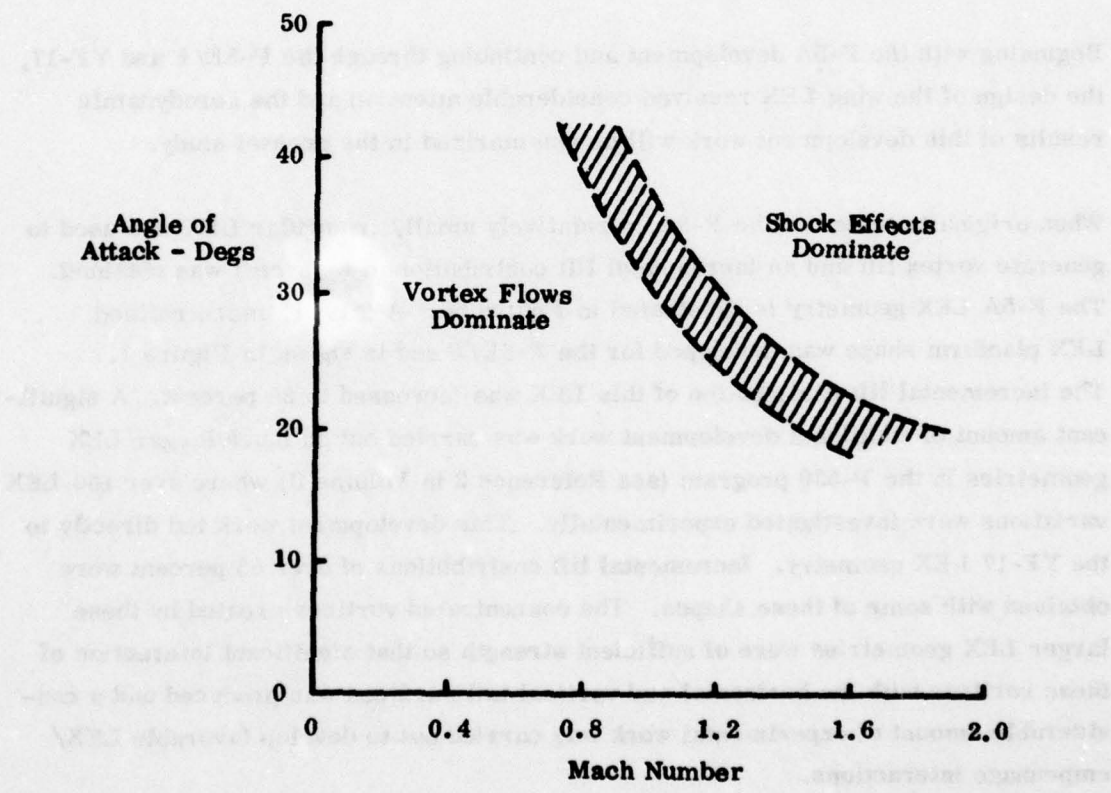


Figure 65. Limiting Regions for Nose Vortex Effects

2. WING LEADING EDGE EXTENSIONS

Fighter aircraft configurations in the past were designed such that a fully attached flow would be maintained over the lifting surfaces in order to maximize both the performance and the maneuvering capability of the design. Experimental studies on a variety of configurations have shown that significant increases in maximum lift coefficient and reductions in drag at high lift can be also obtained by careful generation and control of concentrated vortices which favorably interact with the flow over a low aspect ratio main wing surface. These vortices have been generated by such devices as close coupled canards, wing leading edge discontinuities or snags and wing-body strakes or leading edge extensions (LEX's).

Beginning with the F-5A development and continuing through the F-5E/F and YF-17, the design of the wing LEX received considerable attention and the aerodynamic results of this development work will be summarized in the present study.

When originally tested on the F-5A, a relatively small, triangular LEX was used to generate vortex lift and an incremental lift contribution of 8 percent was obtained. The F-5A LEX geometry is illustrated in Figure 66. A larger, more refined LEX planform shape was developed for the F-5E/F and is shown in Figure 1. The incremental lift contribution of this LEX was increased to 30 percent. A significant amount of additional development work was carried out on much larger LEX geometries in the P-530 program (see Reference 2 in Volume II) where over 100 LEX variations were investigated experimentally. This development work led directly to the YF-17 LEX geometry. Incremental lift contributions of over 85 percent were obtained with some of these shapes. The concentrated vortices created by these larger LEX geometries were of sufficient strength so that significant interaction of these vortices with the horizontal and vertical tail surfaces was produced and a considerable amount of experimental work was carried out to develop favorable LEX/empennage interactions.

This section will discuss the influence of such geometric parameters as LEX planform shape, cross sectional shape, area, aspect ratio and incidence as well as the effects of wing planform variations, leading and trailing edge flaps and vertical and

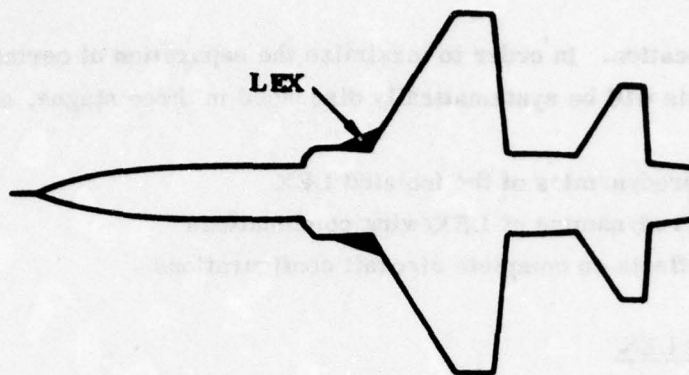


Figure 66. F-5A Wing Leading Edge Extension

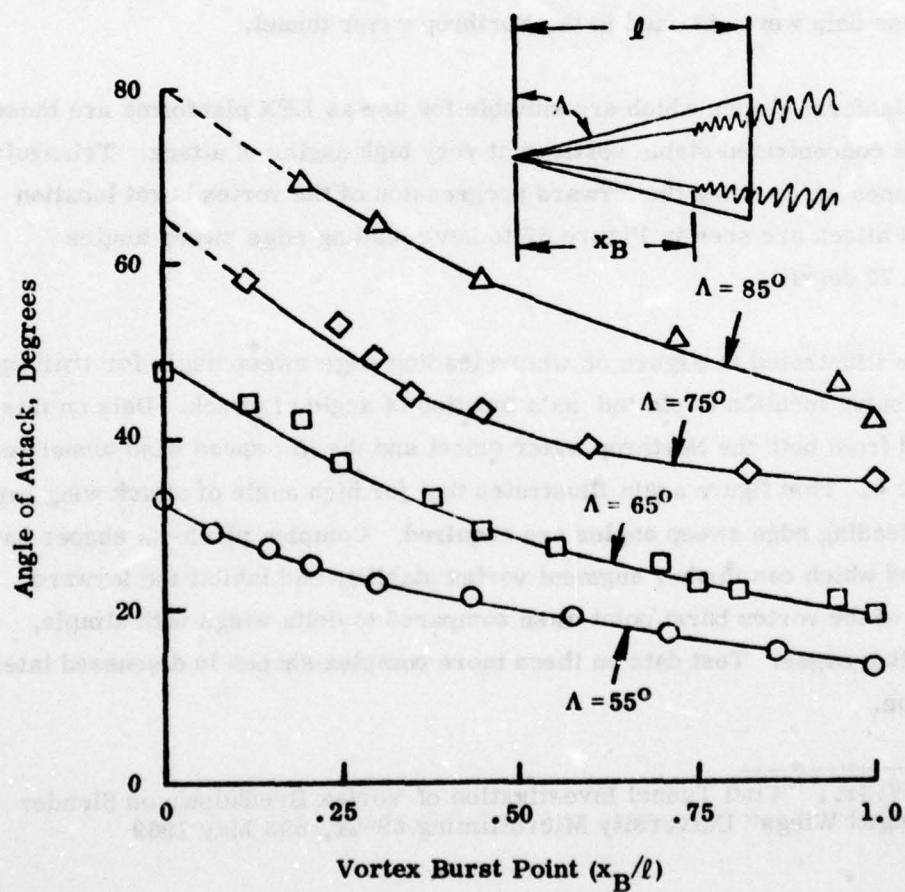


Figure 67. Slender Delta Wing Vortex Burst Locations

horizontal tail location. In order to maximize the separation of certain strong interactions, the analysis will be systematically discussed in three stages, as follows:

- The aerodynamics of the isolated LEX
- The aerodynamics of LEX/wing combinations
- LEX effects on complete aircraft configurations

a. The Isolated LEX

The LEX is essentially a vortex generator, and therefore its geometry is restricted to planform shapes of low aspect ratio on which strong leading edge vortex flows are developed. The vortex generating capabilities of the slender delta can be used as an example of LEX aerodynamics. Figure 67 shows the vortex burst location point for a family of delta wings as a function of leading edge sweep angle and angle of attack. These data were obtained in the Northrop water tunnel.

Delta wing planform shapes which are suitable for use as LEX planforms are those which exhibit concentrated stable vortices at very high angles of attack. Triangular planform shapes which delay the forward progression of the vortex burst location with angle of attack are seen in Figure 67 to have leading edge sweep angles greater than 70 degrees.

This is again illustrated in Figure 68 where leading edge sweep angle for trailing edge vortex burst location is plotted as a function of angle of attack. Data on this plot was obtained from both the Northrop water tunnel and the low speed wind tunnel results of Reference 6. This figure again illustrates that for high angle of attack wing capability, high leading edge sweep angles are required. Complex planform shapes have been designed which can further augment vortex stability and inhibit the forward progression of the vortex burst point when compared to delta wings with simple, straight leading edges. Test data on these more complex shapes is discussed later in this section.

6. Wentz, W. Jr., "Wind Tunnel Investigation of Vortex Breakdown on Slender Sharp-Edged Wings" University Microfilming 69-21, 593 May 1969

AD-A069 646

NORTHROP CORP HAWTHORNE CA AIRCRAFT GROUP

F/G 20/4

ANALYSIS OF WIND TUNNEL DATA PERTAINING TO HIGH ANGLE OF ATTACK--ETC(U)

JUL 78 J W HEADLEY

F33615-77-C-3062

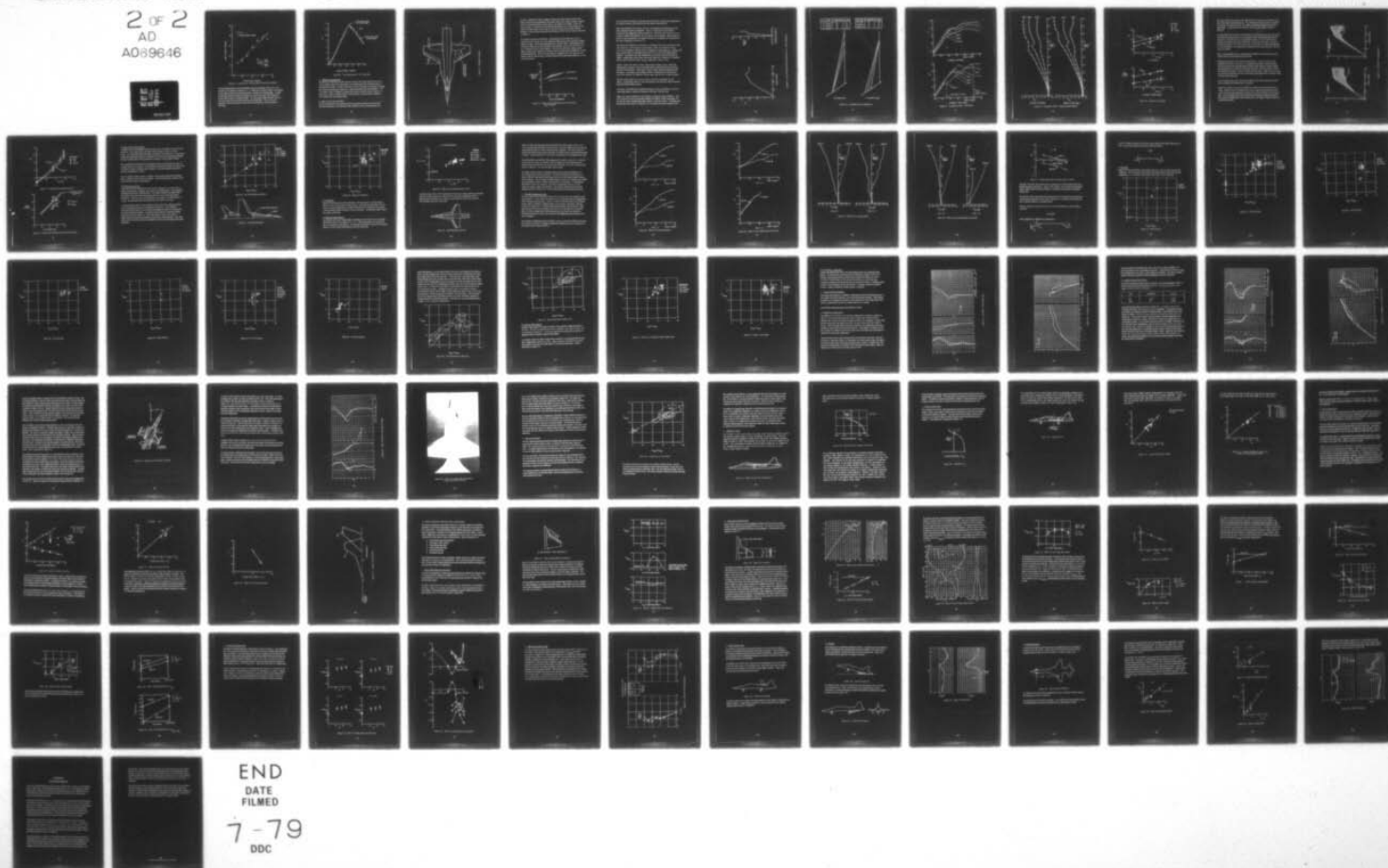
UNCLASSIFIED

NOR-78-69-VOL-1

AFFDL-TR-78-94-VOL-1

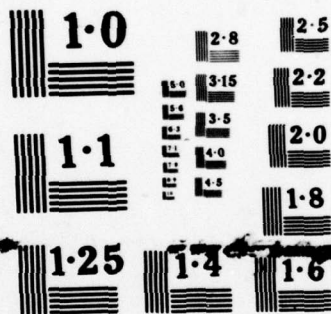
NL

2 OF 2
AD
AD89646



END
DATE
FILMED

7-79
DDC



NATIONAL BUREAU OF STANDARDS
MICROCOPY RESOLUTION TEST CHART

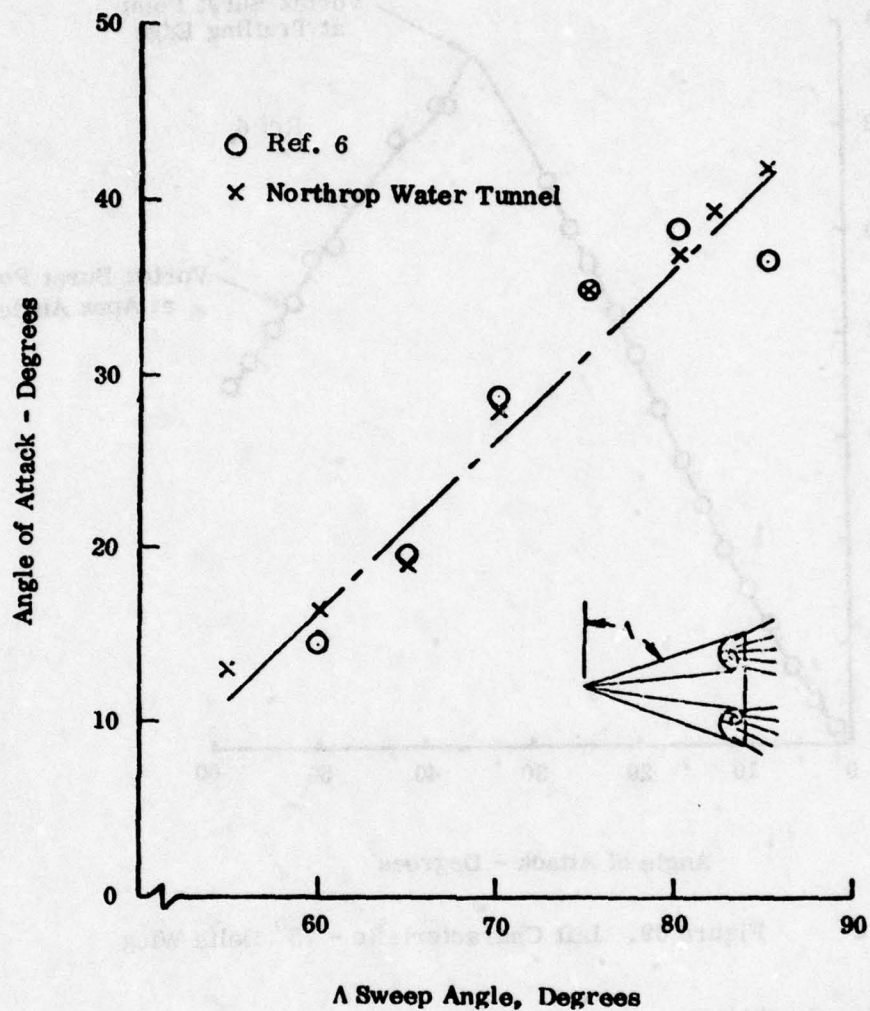


Figure 68. Conditions for Trailing Edge Vortex Burst Location

The lift characteristics of an isolated delta wing are presented in Figure 69. The maximum lift coefficient is shown to be 1.3, obtained at an angle of attack of 35 degrees. At this angle of attack the vortex burst point is located at the trailing edge. As angle of attack increases the vortex burst point moves across the wing, until at about 50 degree angle of attack it reaches the apex. For this isolated delta wing lift is lost as the vortex burst point moves forward from the trailing edge. This is in contradistinction with the performance of the LEX/wing combination, which will now be discussed.

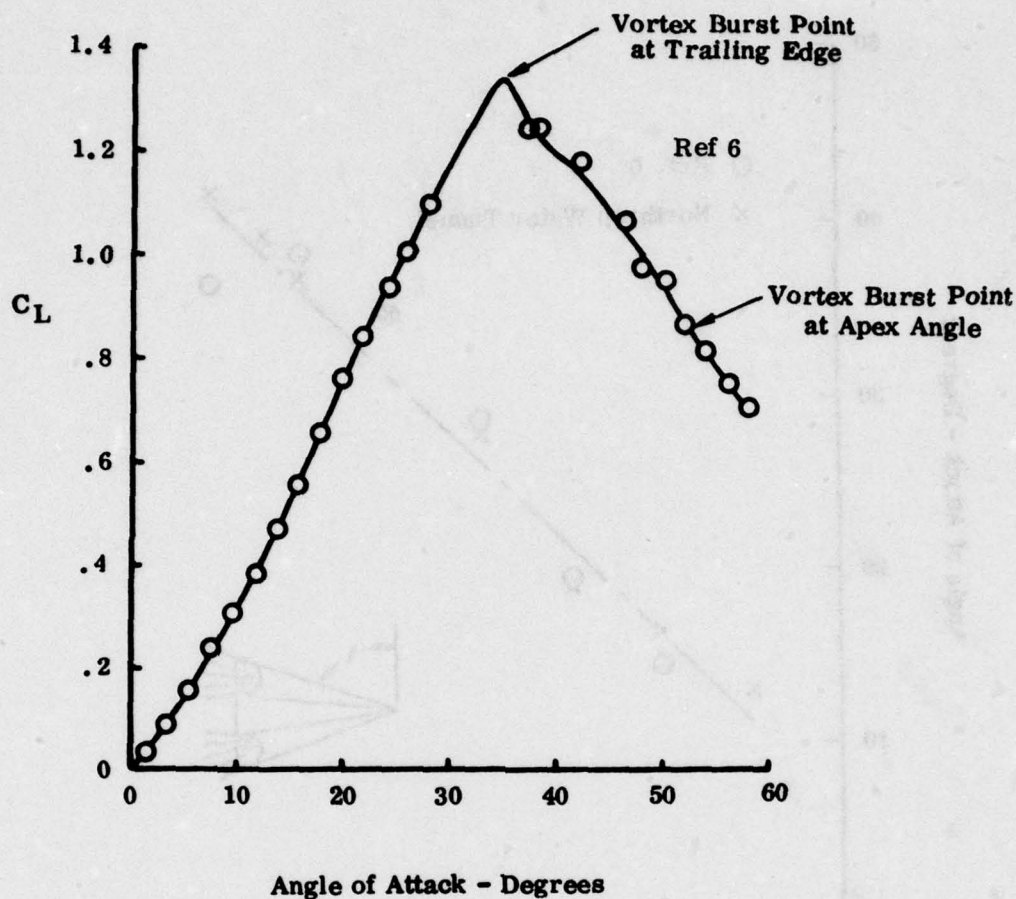


Figure 69. Lift Characteristic - 75° Delta Wing

b. LEX/Wing Combinations

The effects of combining the highly swept low aspect ratio leading edge extension with a basic slightly swept main wing surface can be illustrated by the wing/body data of the P530 and the P610. In these references, data are available on a variety of leading edge extension geometries, attached to a constant geometry basic wing planform. The LEX shapes tested, in addition to slender delta shapes included various complex configurations. Figure 70 shows the basic wing geometry, its flap system, together with a typical LEX and fuselage shape.

(1) Effect of Wing Flap Deflection

One of the first items to be considered when assessing the effectiveness of the LEX and wing combination is the influence of the wing flap system on the performance of

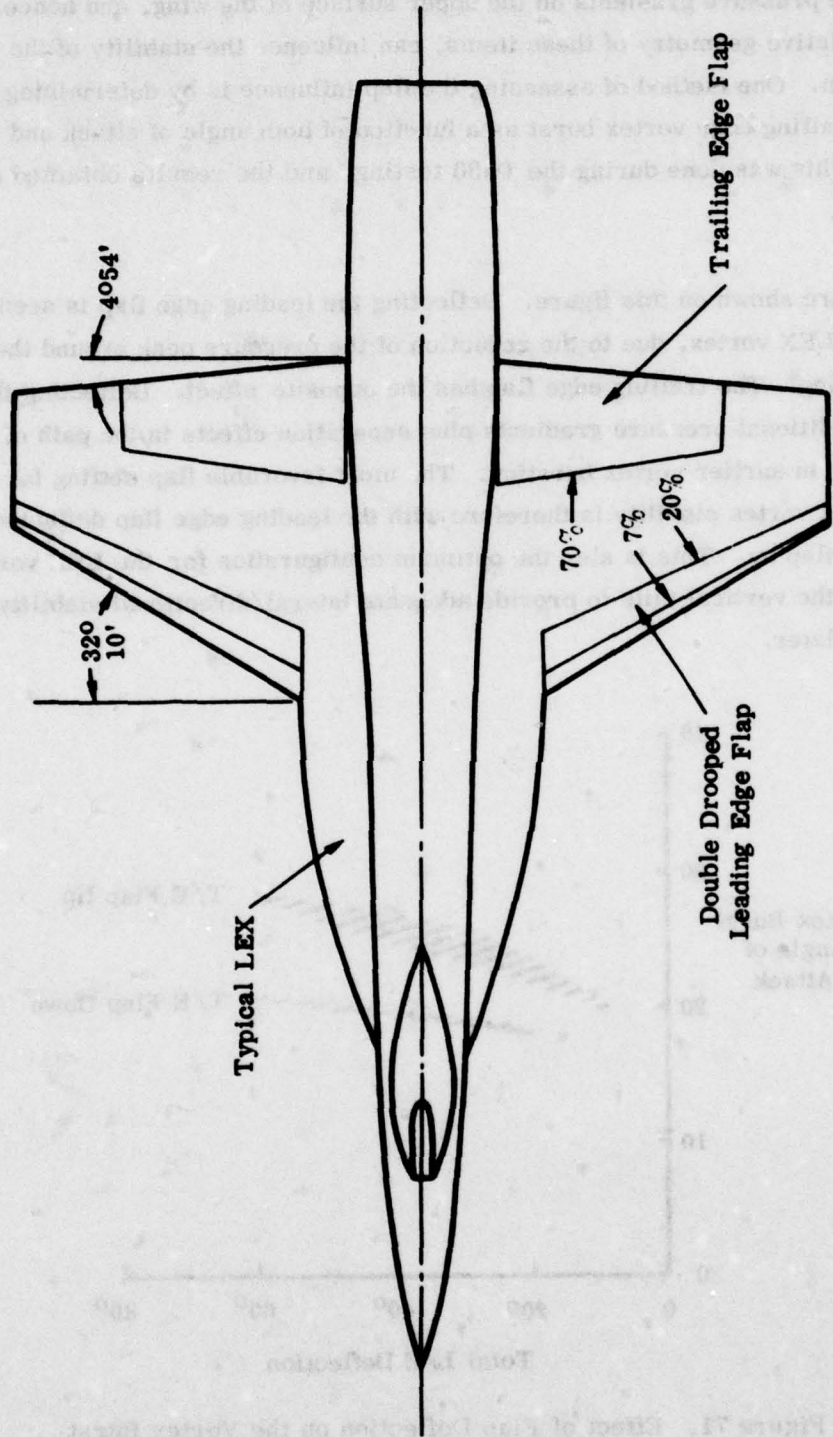


Figure 70. Wing/Body Geometry

the LEX. Deflection of either leading or trailing edge flaps modifies both the flow fields and the pressure gradients on the upper surface of the wing, and hence, depending on the relative geometry of these items, can influence the stability of the LEX vortex system. One method of assessing the flap influence is by determining the conditions for trailing edge vortex burst as a function of both angle of attack and flap deflection. This was done during the P530 testing, and the results obtained are shown in Figure 71.

Two effects are shown on this figure. Deflecting the leading edge flap is seen to stabilize the LEX vortex, due to the reduction of the pressure peak around the leading edge of the wing. The trailing edge flap has the opposite effect. Deflecting this flap introduces additional pressure gradients plus separation effects in the path of the vortex, resulting in earlier vortex bursting. The most favorable flap setting for high angle-of-attack vortex stability is therefore with the leading edge flap deflected, and the trailing edge flap up. This is also the optimum configuration for the LEX vortex to interact with the vertical tails to provide adequate lateral/directional stability, as will be discussed later.

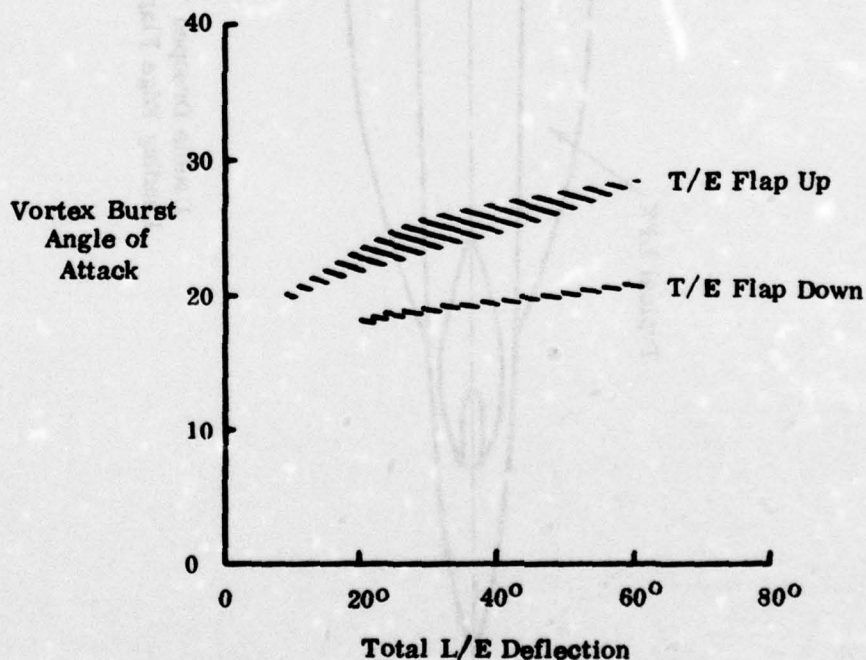


Figure 71. Effect of Flap Deflection on the Vortex Burst Angle of Attack

The data analysis following, which deals with LEX effects on wing/body configurations, is in general based on data obtained with this optimum flap deflection.

Before discussing the LEX effects, however, the longitudinal characteristics of the basic wing/body should be established. Figure 72 shows the lift and pitching moments of the configuration shown on Figure 70. Maximum lift is seen to occur at an angle of attack of 30 degrees, and a C_L max of 1.38 is obtained. The aerodynamic center for this configuration, for angles of attack up to 22 degrees is at 20 percent of the mean aerodynamic chord (M.A.C.).

The effect of the addition of two families of triangular LEX shapes is shown on Figures 74 and 75. These families of LEX shapes, which are illustrated on Figure 73 were designed so that the effect of changing the LEX length for a constant LEX span, and the effects of changing the LEX span for a constant LEX length could be obtained. An identical base LEX configuration was used for both these families of shapes. Leading edge sweep values covered the range from 74 degrees to 80 degrees, and the LEX to wing area ratios, S_L/S_W , ranged from 0.086 to 0.142.

Figure 74 shows the effects of these LEX geometry changes on lift coefficient. Increasing the LEX span is seen to increase both the slope of the lift curve and the maximum lift coefficient. Stall angles of attack remain virtually unchanged around 26 degrees. Increasing the LEX length is shown to change both the stall angle of attack and maximum lift coefficient, but the slope of the lift curve remains constant.

Pitching moment effects are shown on Figure 75 for the two families of LEX shapes. In general the effects of LEX area dominate, the larger the LEX, the greater the incremental pitching moment.

A summary of the lift data is presented on Figure 76 where in addition to area and sweep angle effects, the data is compared to the basic, LEX off, case.

Figure 76a shows the effects of LEX geometry variations on lift coefficient. LEX area is seen to be the most important variable, the effects of LEX sweep angle, for this narrow range of leading edge angles tested, is seen to be minor. A maximum lift increase due to the LEX of 16 percent, for a 10 percent increase in planform area.

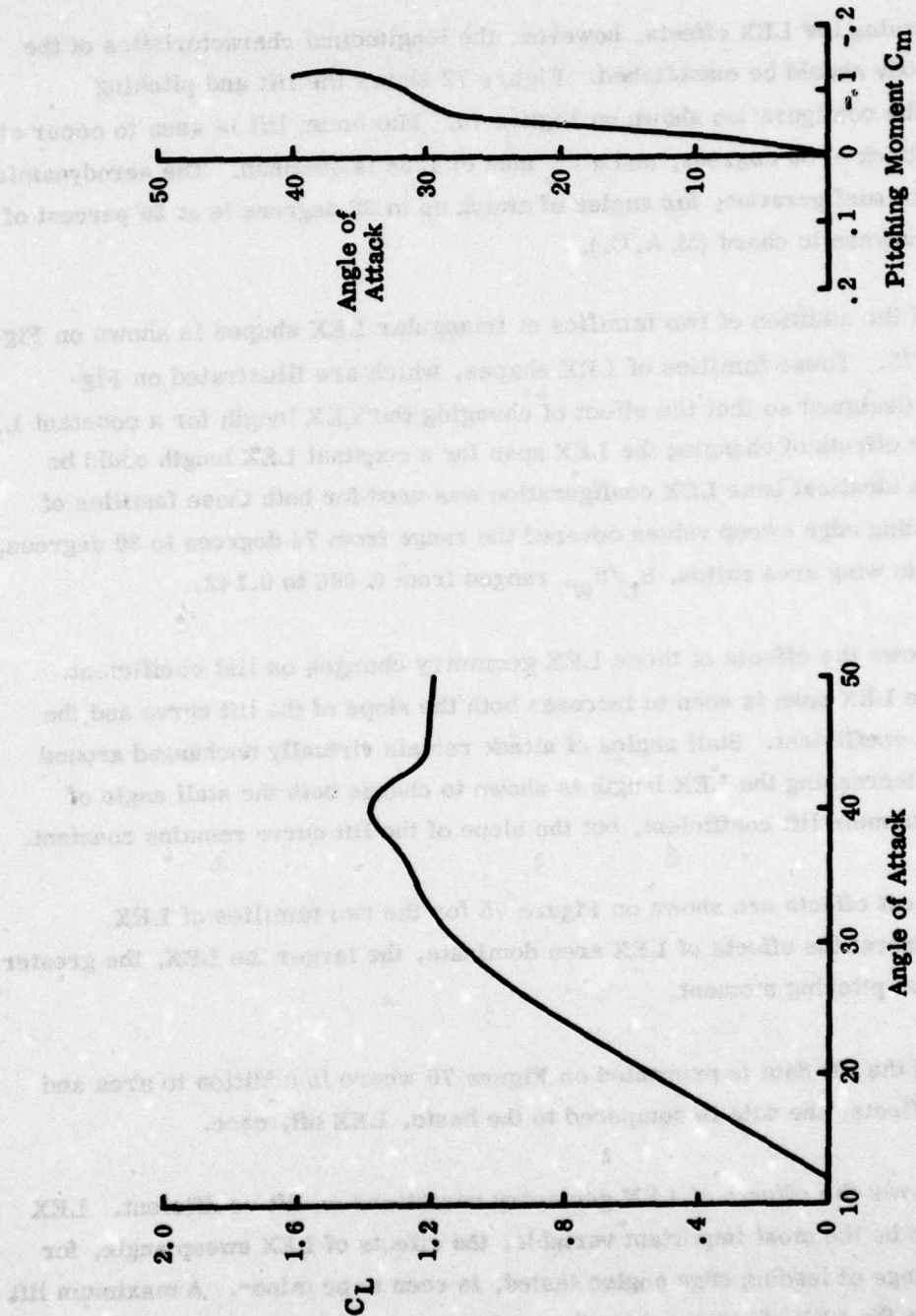


Figure 72. Basic Wing (LEX Off) Performance L. E. Flaps Deflected

W	LEX	L/E Sweep	S_L/S_W
67	Long	79°	.142
63	Basic	76°	.124
65	Short	74°	.086

W	LEX	L/E Sweep	S_L/S_W
64	Wide	74°	.142
63	Basic	76°	.124
66	Narrow	80°	.086

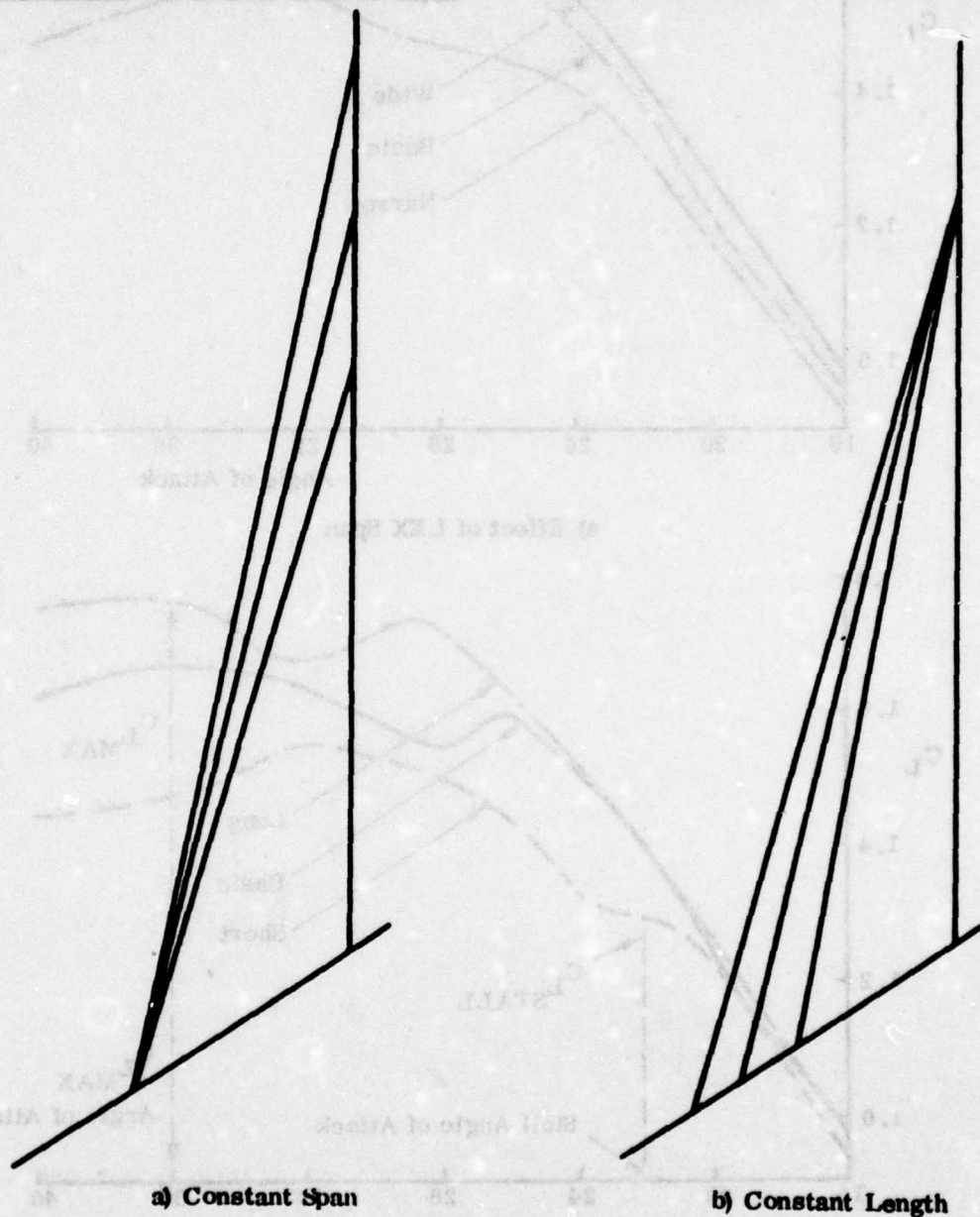
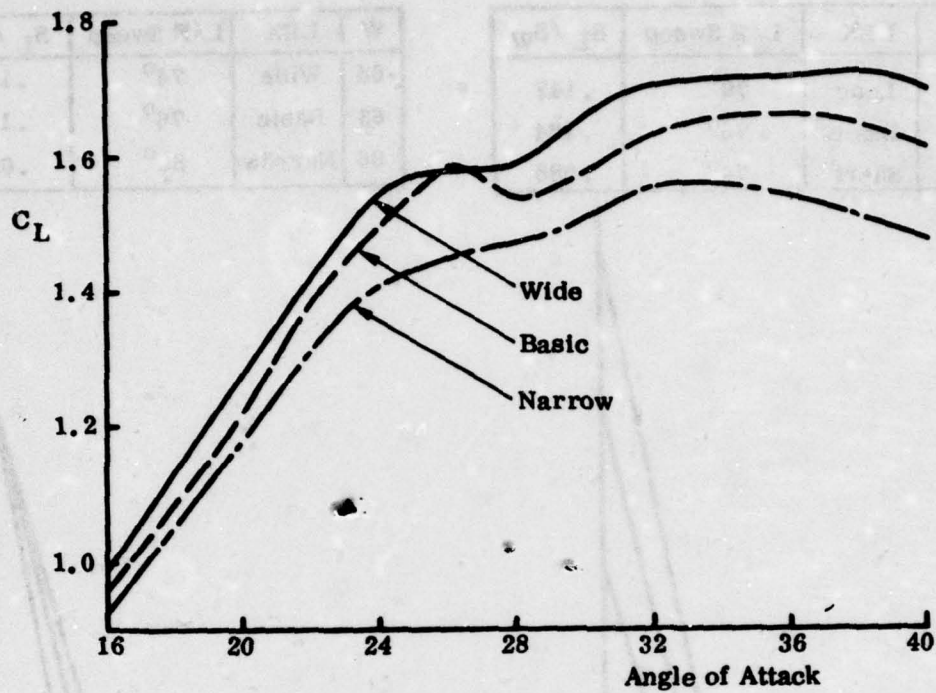
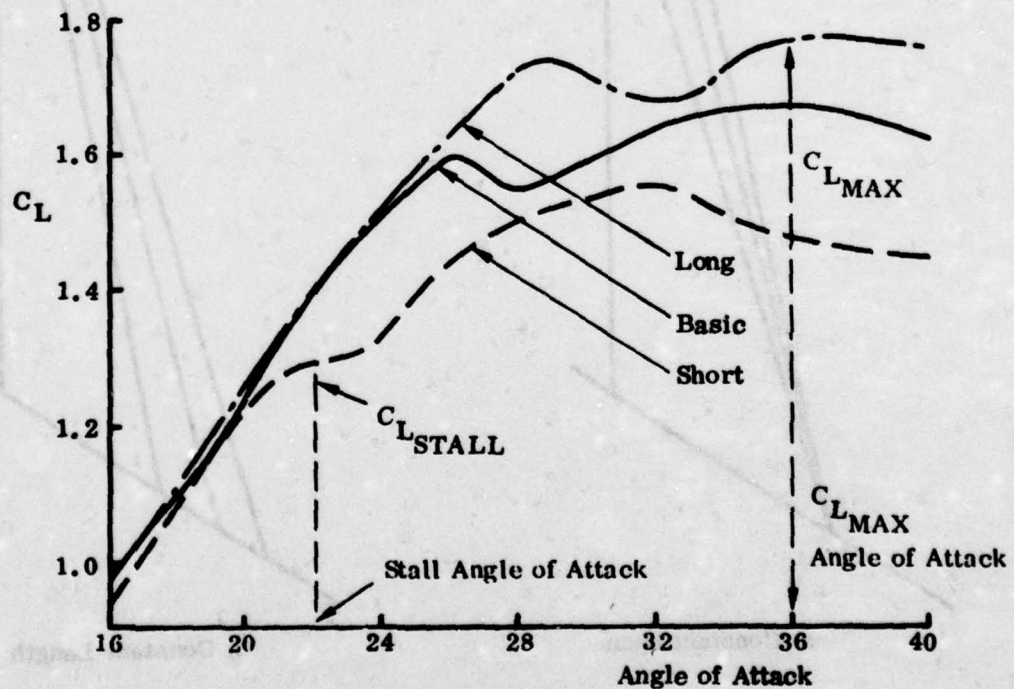


Figure 73. Triangular LEX Configurations



a) Effect of LEX Span



b) Effect of LEX Length

Figure 74. Triangular LEX's - Lift Effects

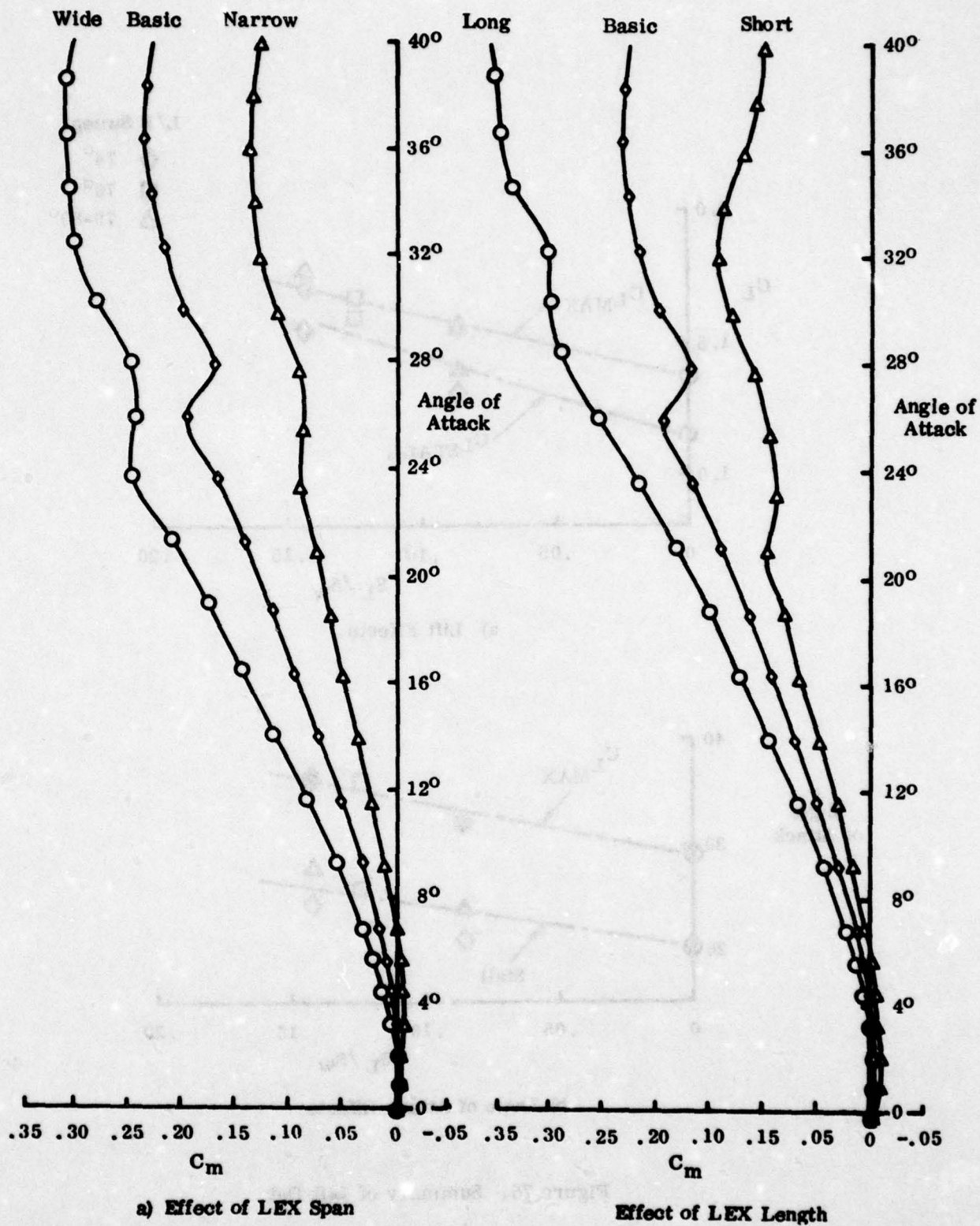
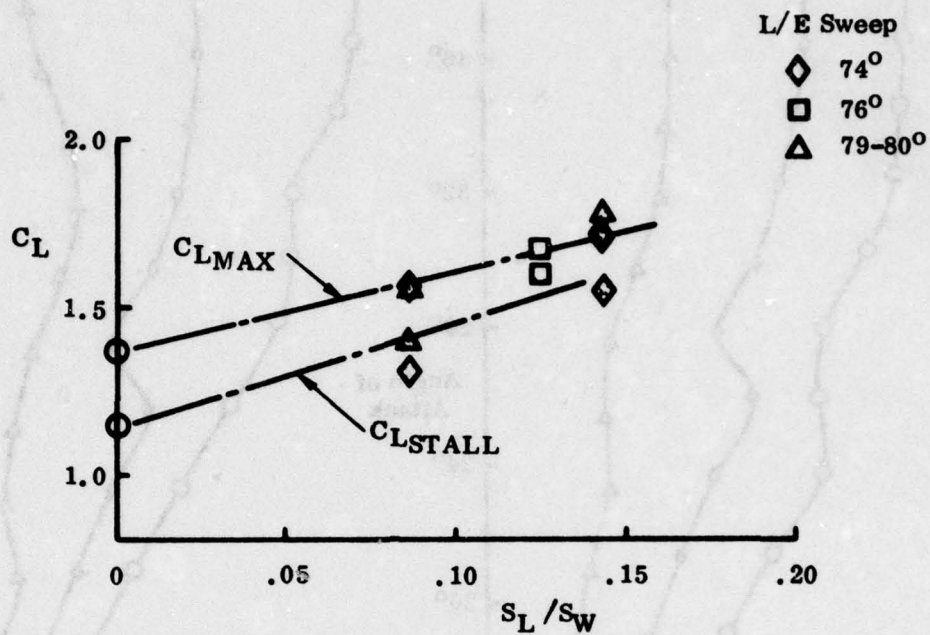
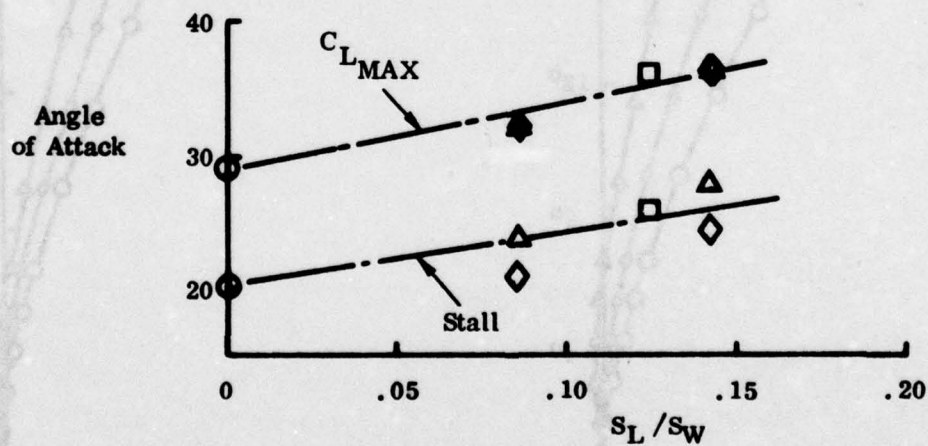


Figure 75. Triangular LEX's - Pitching Moment Effects



a) Lift Effects



b) Angle of Attack Effects

Figure 76. Summary of Lift Data

The angle of attack for maximum lift coefficient is also shown to be a function of LEX area, rather than leading edge sweep. The stall angle of attack is however a function of both area ratio and sweep angle, the higher sweep angles producing the greatest stall angles. A constant increment between stall and $C_{L \text{ max}}$ angle of attack is indicated.

The apparently small increase in lift produced by the LEX (16 percent for a 10 percent area increase) mentioned above is a consequence of the wing/leading edge flap/LEX interaction. This interaction is demonstrated on Figure 77 where the lift characteristics of the basic wing, flaps up and down, LEX on and off is shown. The incremental lift produced by the LEX is seen to be much greater when the leading edge flap is in the up position. The maximum lift coefficient of both wings (LEX on) is however seen to be similar.

Thus a nonsynergistic effect is created when lift additions to the basic wing are provided by both the leading edge flap and the LEX.

Pitching moment effects are summarized on Figure 78. Here the data are also compared to the basic, LEX off case. Pitching moment effects, taken at both the stall and maximum lift coefficient angles of attack, show similar, nonlinear trends, increasing pitch-up is produced by increased LEX area. This is contrary to the lift data discussed previously, where all data trends were linear. Again LEX size is seen to be the most important parameter for pitching moment effects with a secondary effect of leading edge sweep angle.

These nonlinear trends show that pitch-up effects, rather than maximum lift coefficient is probably the limiting factor on LEX size.

Figure 79 presents a comparison of stall and maximum lift coefficient angles of attack, obtained from the wing body test results, with the delta wing data of Figure 68, the latter data showing the conditions for vortex breakdown at the trailing edge. This comparison shows that the wing-body stall angle of attack is generally lower than the isolated delta result, whereas the $C_{L \text{ max}}$ angle of attack is seen to be reasonable agreement.

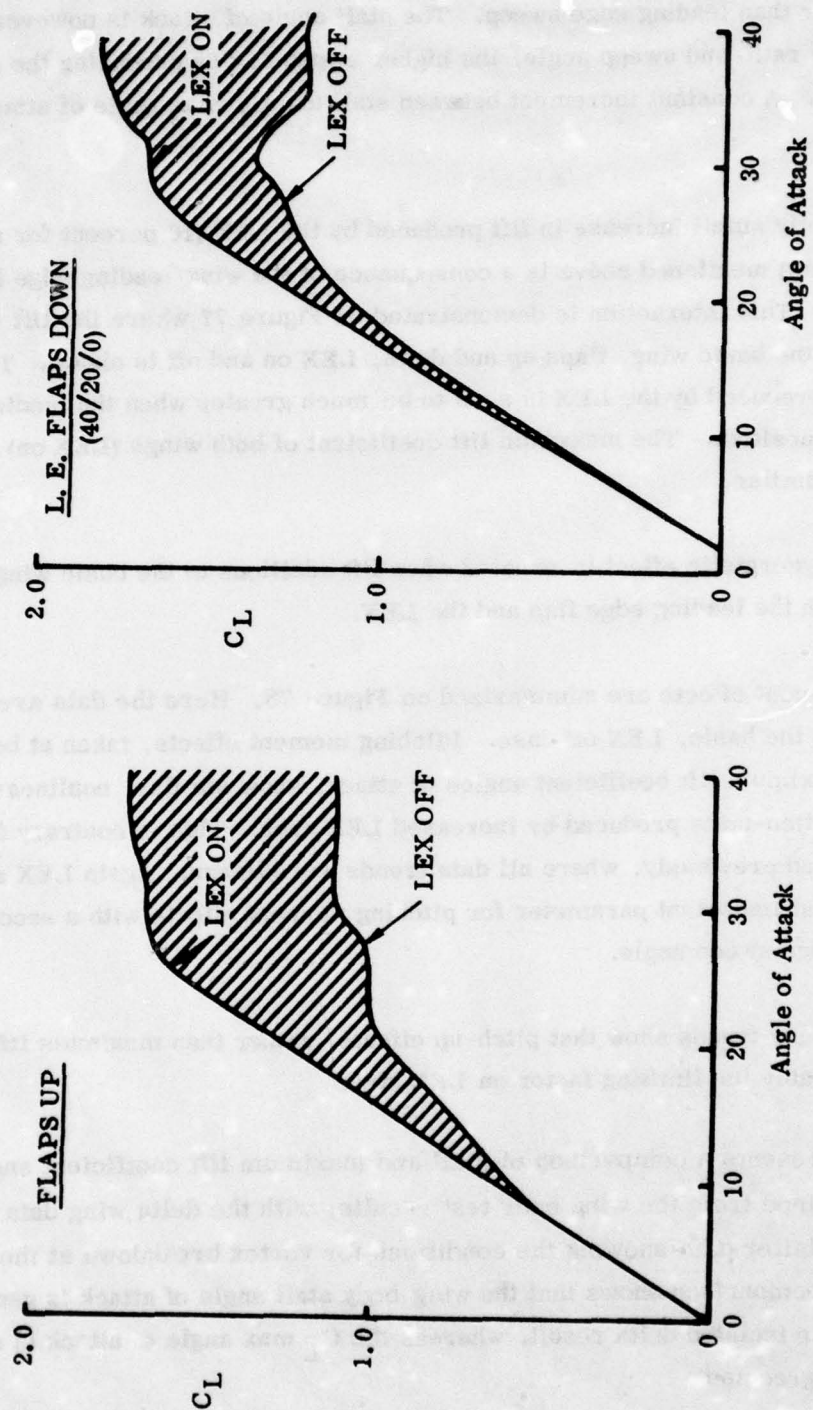


Figure 77. LEX Effect - Empennage Off

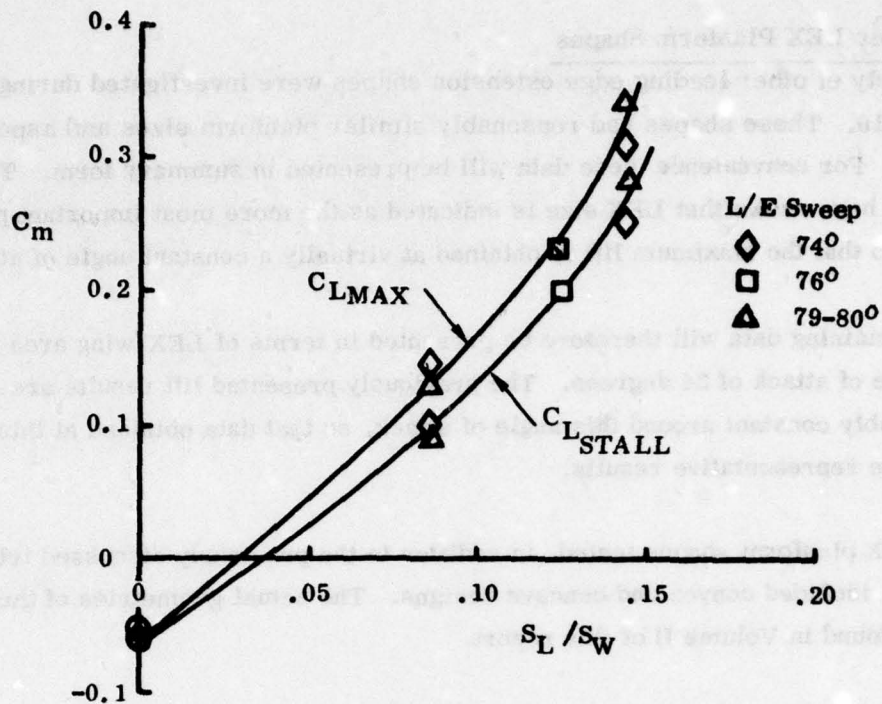


Figure 78. Pitching Moment Effects of LEX

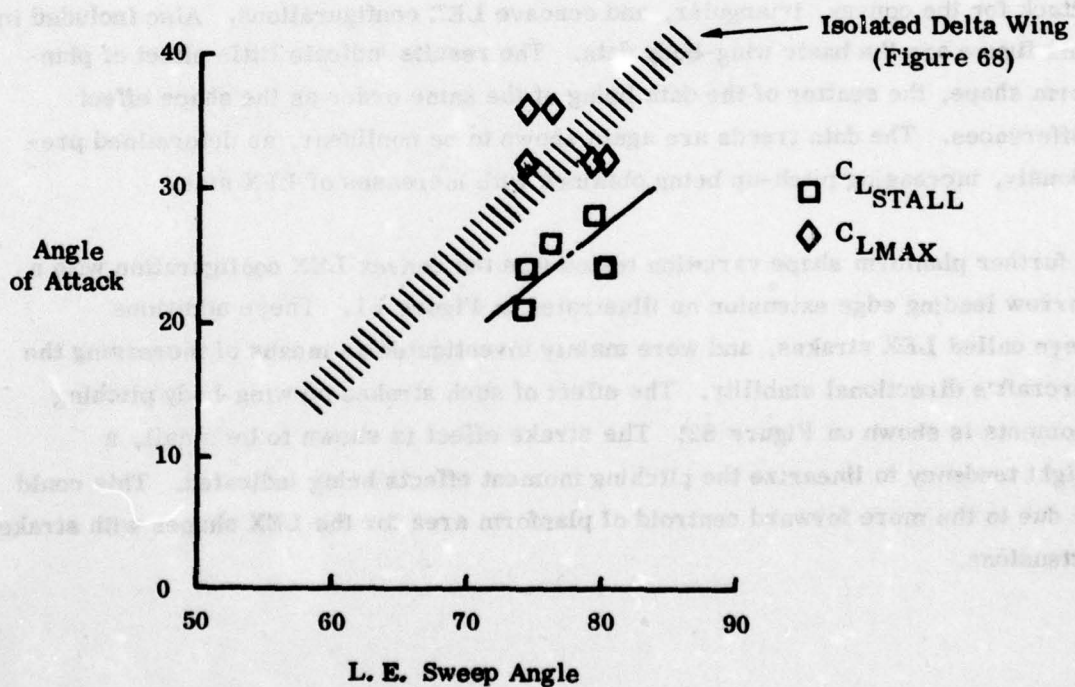


Figure 79. Comparison of Wing Body and Delta Wing Data

(2) Other LEX Planform Shapes

A variety of other leading edge extension shapes were investigated during the P530 and P610. These shapes had reasonably similar planform sizes and aspect ratios. For convenience these data will be presented in summary form. The previous results have shown that LEX size is indicated as the more most important parameter, and also that the maximum lift is obtained at virtually a constant angle of attack.

The remaining data will therefore be presented in terms of LEX/wing area ratio, at an angle of attack of 34 degrees. The previously presented lift results are shown to be reasonably constant around this angle of attack, so that data obtained at this value will give representative results.

The LEX planform shapes tested, in addition to the previously discussed triangular shapes, included convex and concave designs. The actual geometries of these LEX's can be found in Volume II of this report.

(3) Pitching Moment Data

Figure 80 presents the pitching moment results, obtained at a constant angle of attack for the convex, triangular, and concave LEX configurations. Also included in this figure are the basic wing-body data. The results indicate little effect of planform shape, the scatter of the data being of the same order as the shape effect differences. The data trends are again shown to be nonlinear, as determined previously, increasing pitch-up being obtained with increases of LEX size.

A further planform shape variation tested was the convex LEX configuration with a narrow leading edge extension as illustrated in Figure 81. These additions were called LEX strakes, and were mainly investigated as means of increasing the aircraft's directional stability. The effect of such strakes on wing-body pitching moments is shown on Figure 82. The strake effect is shown to be small, a slight tendency to linearize the pitching moment effects being indicated. This could be due to the more forward centroid of planform area for the LEX shapes with strake extensions.

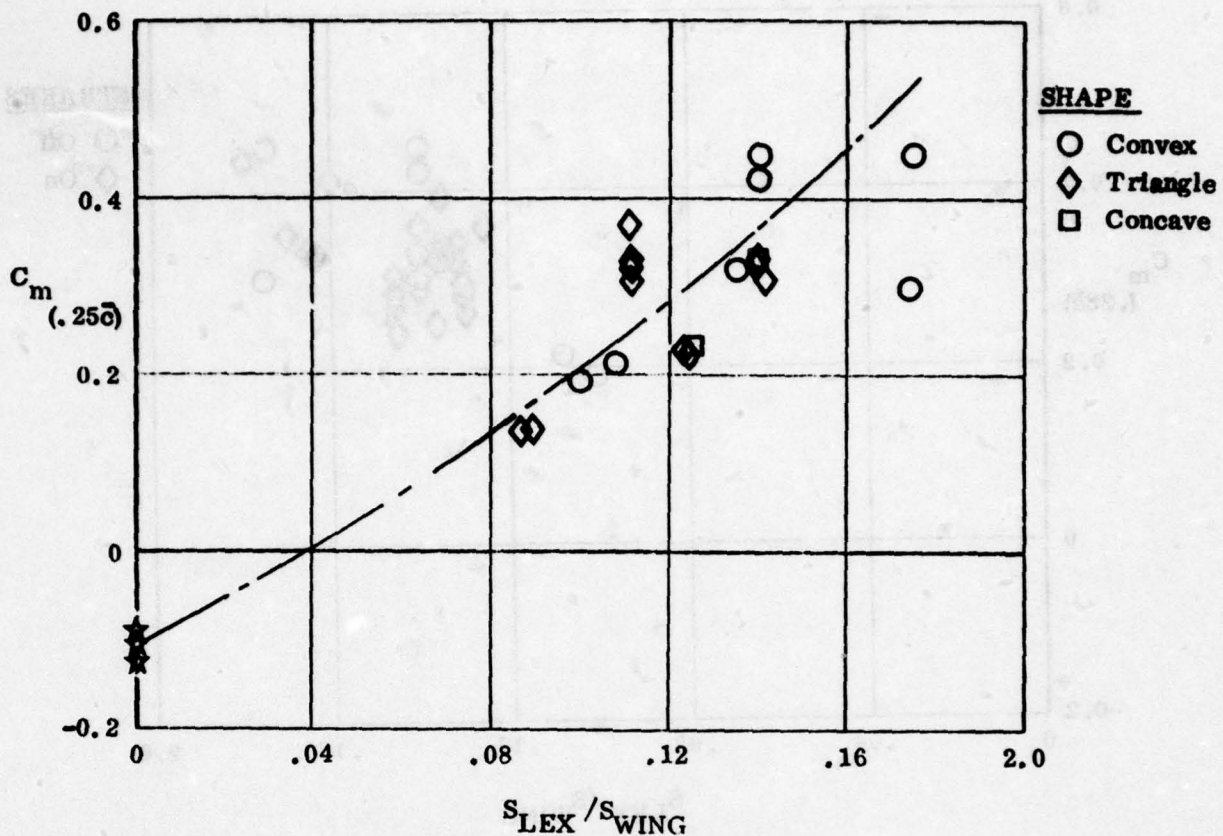


Figure 80. Lex Pitching Moment Effects

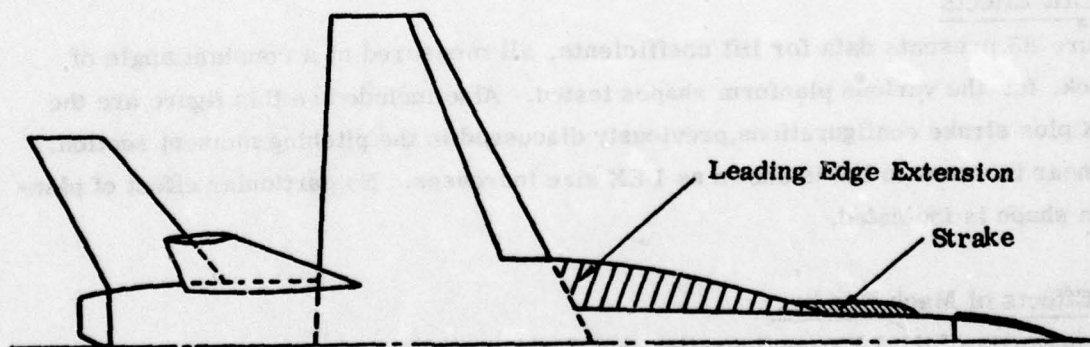


Figure 81. Lex Strake Geometry

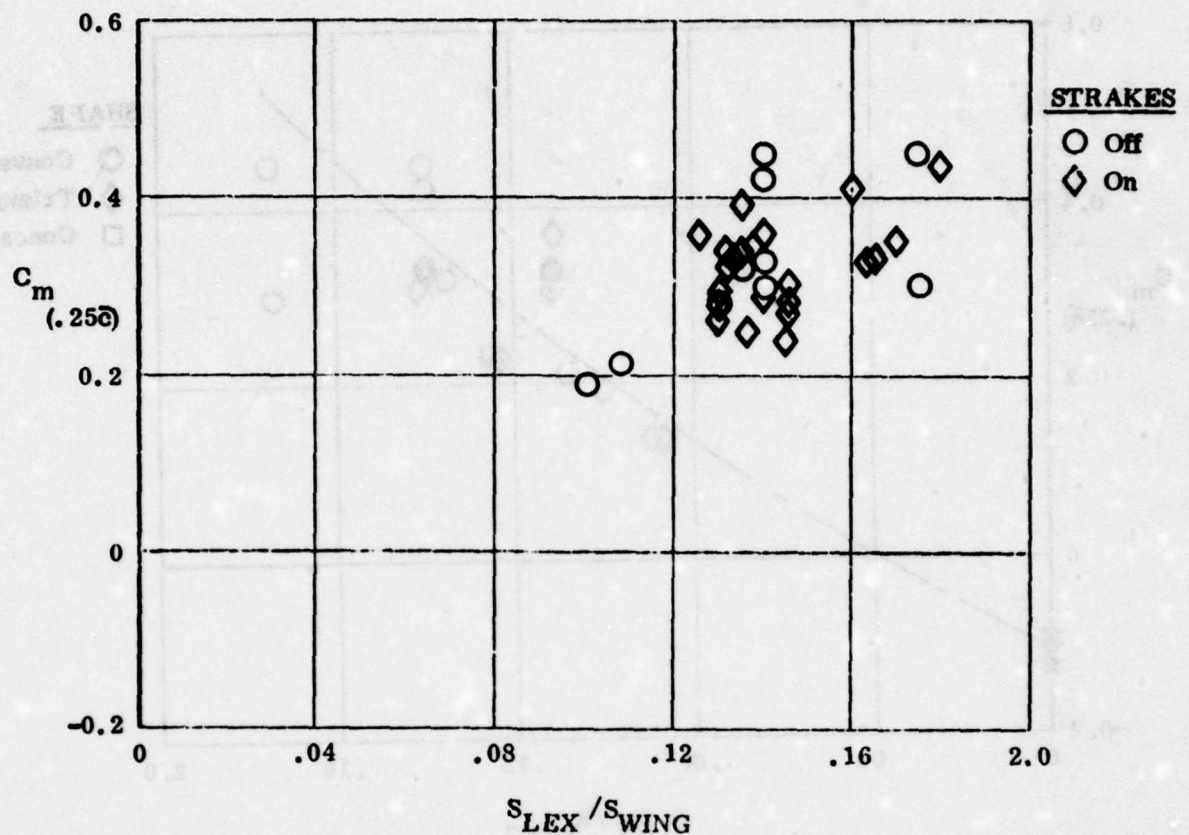


Figure 82. Effect of Lex Strakes

(4) Lift Effects

Figure 83 presents data for lift coefficients, all measured at a constant angle of attack, for the various planform shapes tested. Also included on this figure are the LEX plus strake configurations previously discussed in the pitching moment section. A linear increase in lift is shown as LEX size increases. No particular effect of planform shape is indicated.

(5) Effects of Mach Number

The majority of the LEX configuration investigations were carried out at low speeds, with Mach numbers in the region of 0.2 ~ 0.3. High speed testing was reserved for the more promising configurations. It is therefore impossible to present Mach number effects on all the various configurations previously discussed.

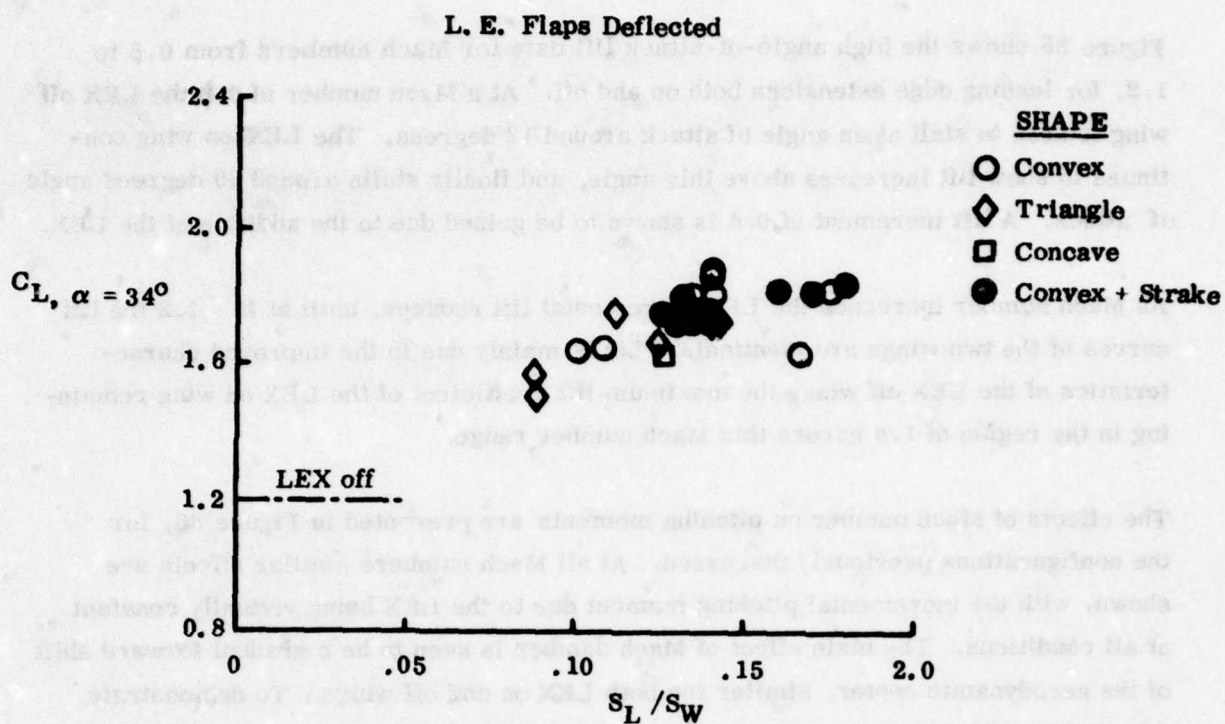


Figure 83. Effect of Lex Planform Shape on Lift

A single example will be used to illustrate general trend as Mach number is increased. Data used in this example was obtained for the wing-body combination shown in Figure 84 from Reference 60. Results are presented for both LEX on and off. The wing flaps were up for these data.

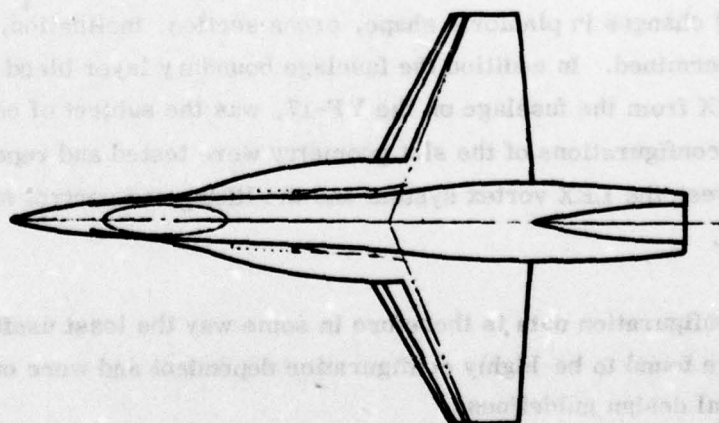


Figure 84. Lex/Wing/Body Geometry

Figure 85 shows the high angle-of-attack lift data for Mach numbers from 0.6 to 1.2, for leading edge extensions both on and off. At a Mach number of 0.6 the LEX off wing is seen to stall at an angle of attack around 12 degrees. The LEX-on wing continues to show lift increases above this angle, and finally stalls around 30 degrees angle of attack. A lift increment of 0.4 is shown to be gained due to the addition of the LEX.

As Mach number increases the LEX incremental lift reduces, until at $M = 1.2$ the lift curves of the two wings are identical. This is mainly due to the improved characteristics of the LEX off wing, the maximum lift coefficient of the LEX on wing remaining in the region of 1.4 across this Mach number range.

The effects of Mach number on pitching moments are presented in Figure 86, for the configurations previously discussed. At all Mach numbers similar effects are shown, with the incremental pitching moment due to the LEX being virtually constant at all conditions. The main effect of Mach number is seen to be a gradual forward shift of the aerodynamic center, similar for both LEX on and off wings. To demonstrate this Figure 87 has been compiled. This shows the pitching moments for both wings at an angle of attack of 20 degrees. The virtually constant LEX incremental pitching moment is clearly seen, as is the forward shift of the aerodynamic center.

c. Complete Configuration Data

By far the largest body of data generated in this test period was with complete model configurations. In this section the pertinent LEX data obtained on these configurations will be presented and discussed. Data on a variety of LEX geometries are available, and the effects of changes in planform shape, cross section, inclination, twist and camber were determined. In addition the fuselage boundary layer bleed slot, which separated the LEX from the fuselage on the YF-17, was the subject of considerable study, and many configurations of the slot geometry were tested and reported on. Interactions between the LEX vortex system and the lifting and control surfaces were also investigated.

This complete configuration data is therefore in some way the least useful of this study. Many effects were found to be highly configuration dependent and were of little use in developing general design guidelines.

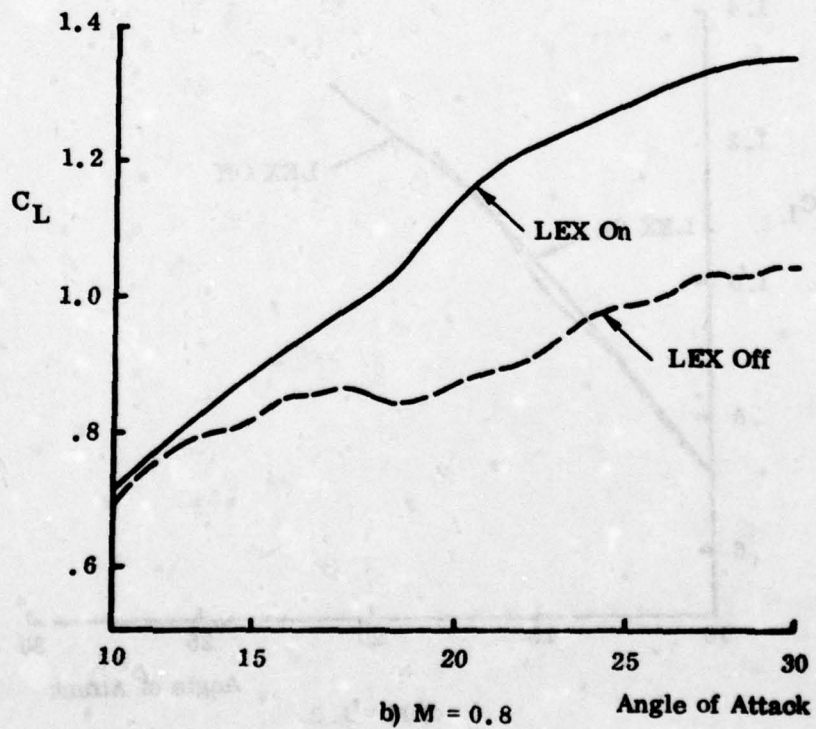
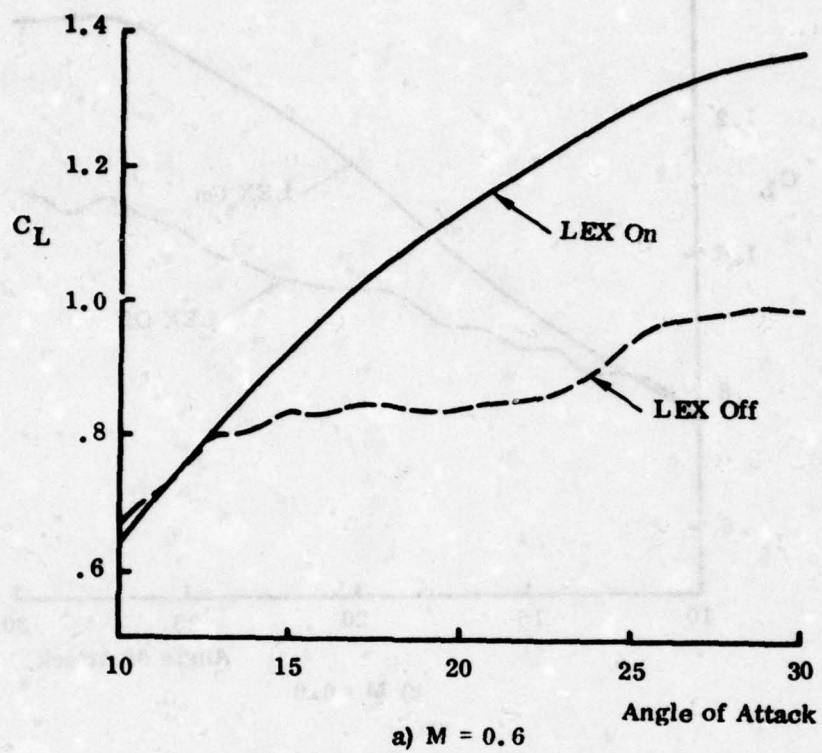


Figure 85. Effect of Lex at High Speeds

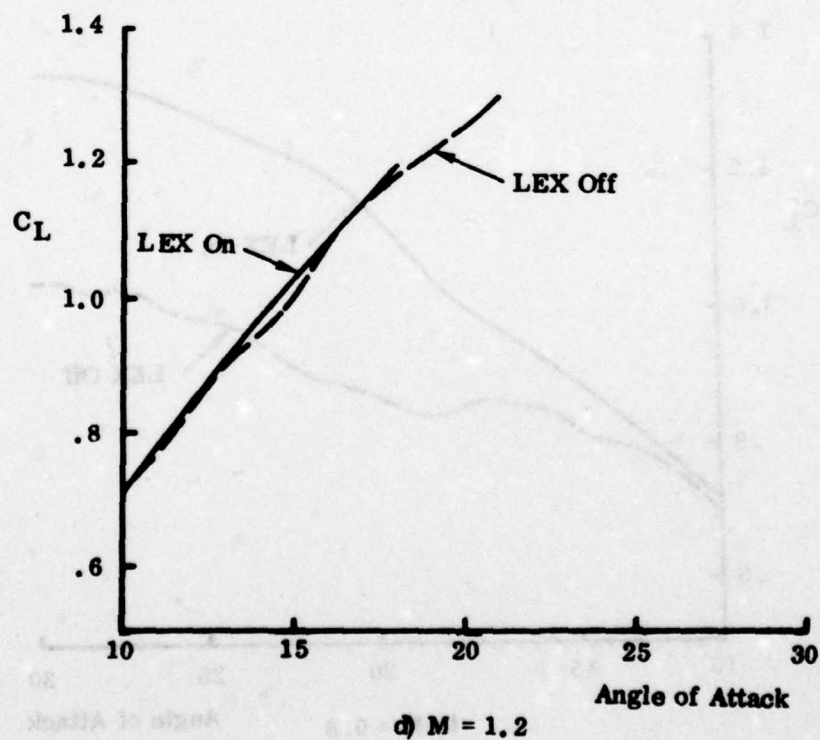
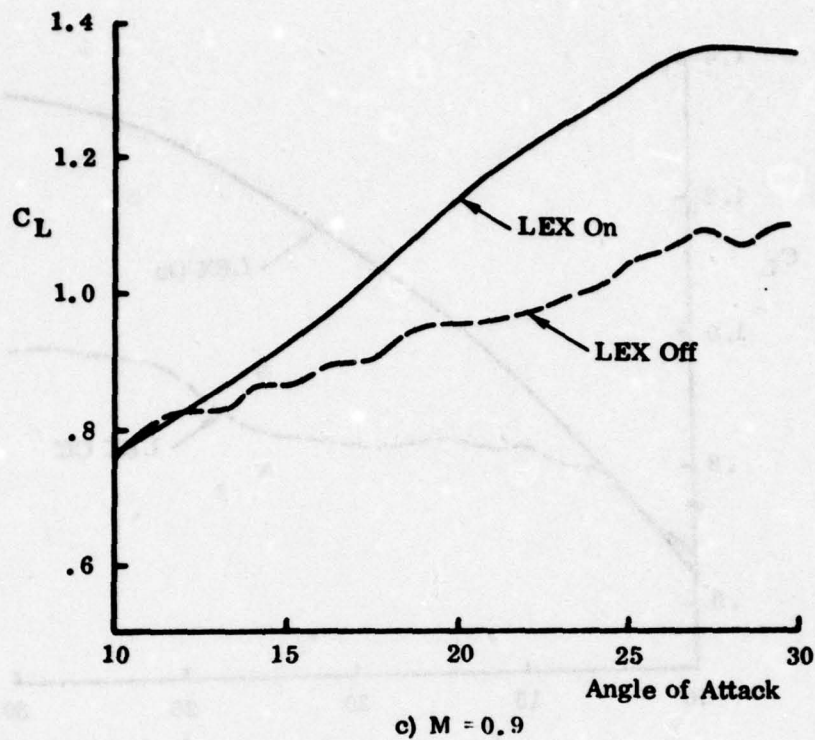


Figure 85. Effect of Lex at High Speeds (Continued)

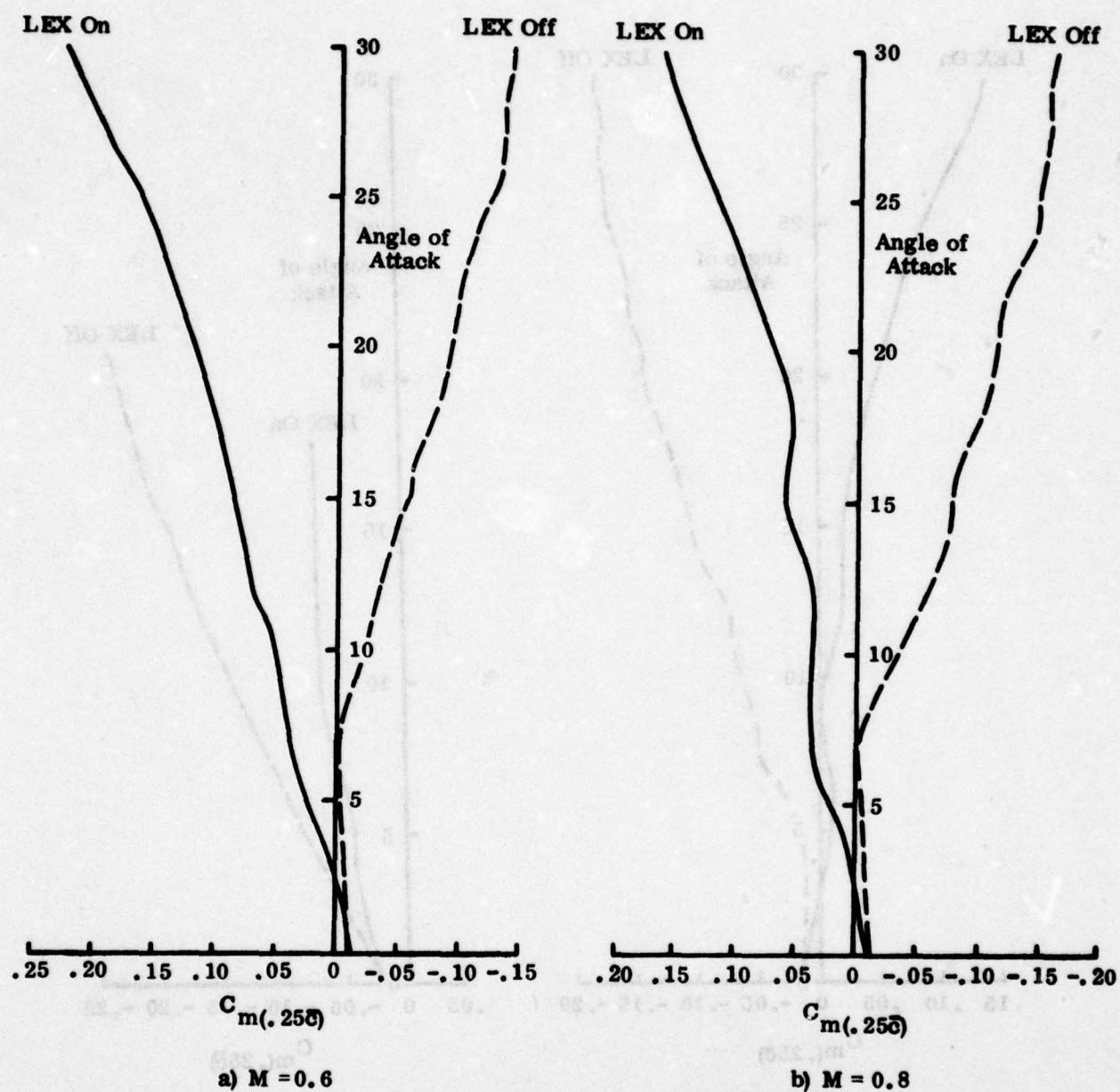
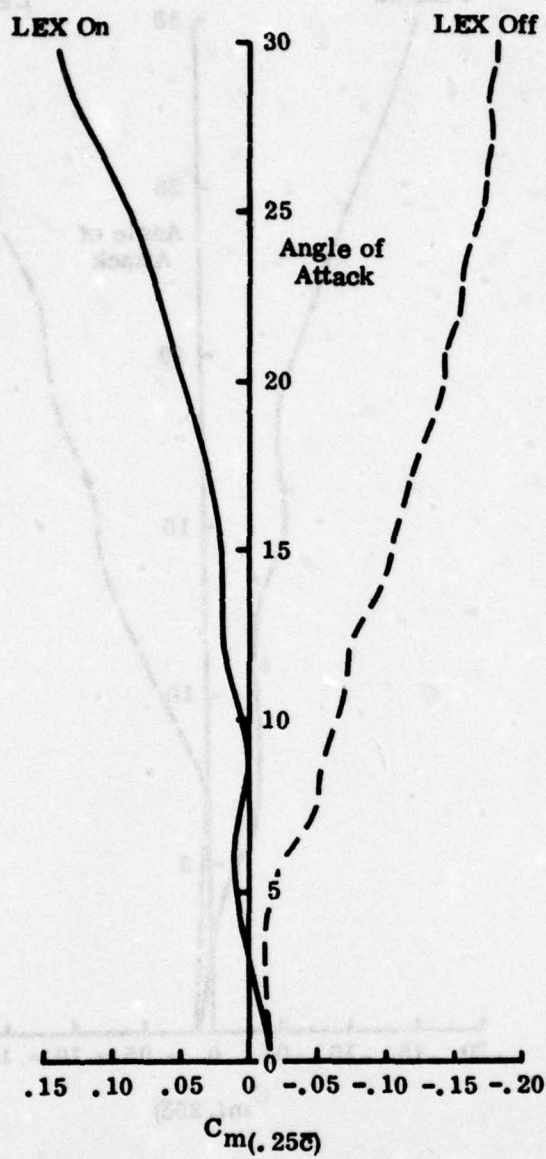
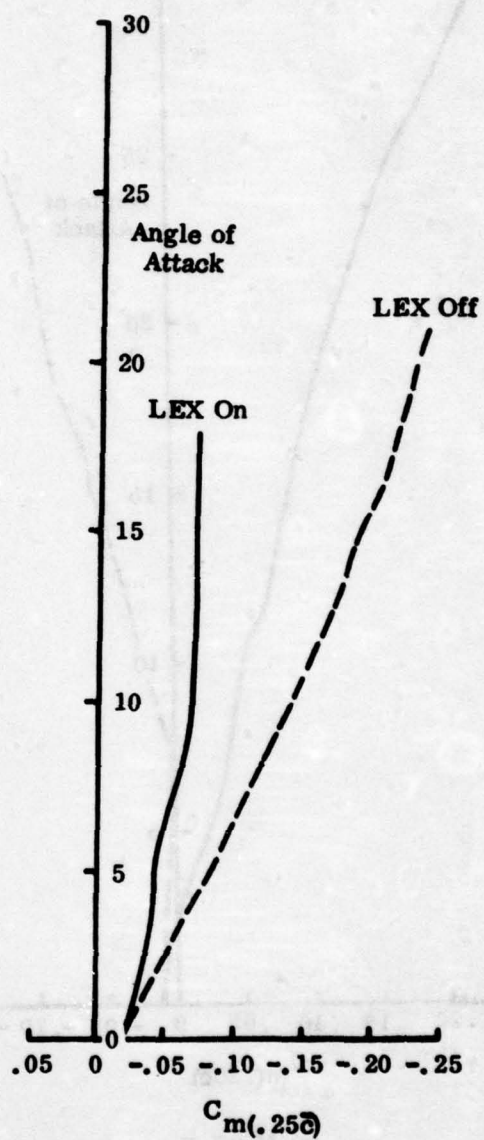


Figure 86. Effect of Lex at High Speeds



c) $M = 0.9$



d) $M = 1.2$

Figure 86. Effect of Lex at High Speeds (Continued)

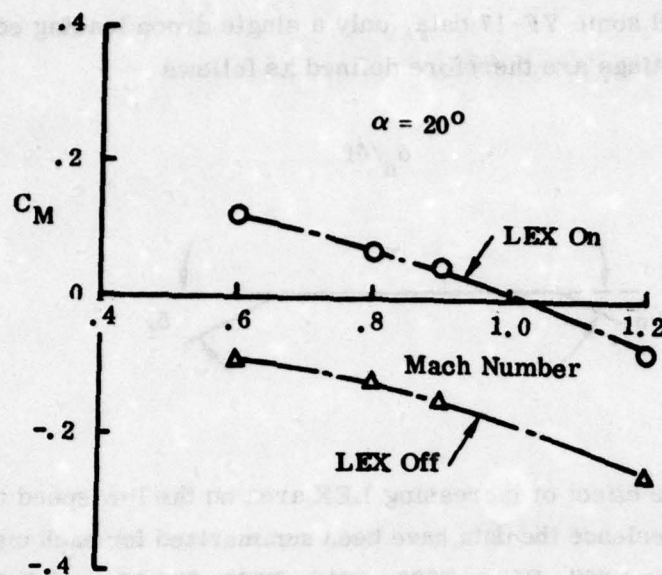


Figure 87. Pitching Moments at Constant Angle of Attack

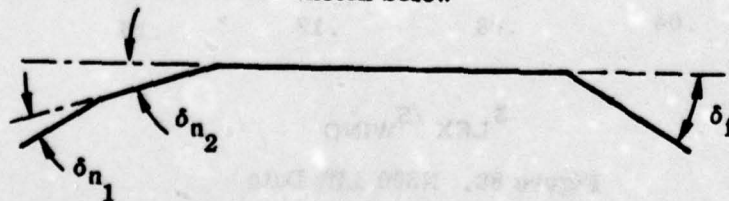
Generally, therefore, this section will be concerned only with the effects of the more primary geometric parameters. Data for other effects, such as LEX cross sectional shapes, glutter slots are found in Volume II, and will not be analyzed or discussed further here.

The previous section showed that the primary geometric LEX parameter was the area. The data will be presented in this section, therefore, as a function of LEX/wing area ratio, with flap setting as a secondary effect.

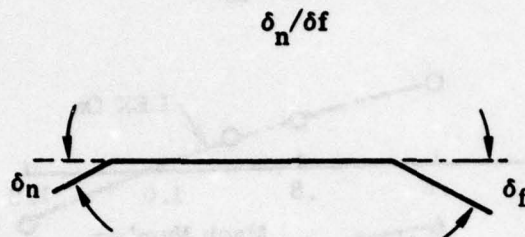
Wing flap settings are presented in terms of the actual deflections, and are written as follows

$$\delta_{n1}/\delta_{n2}/\delta_f$$

These quantities are defined in the sketch below



For the F-5 data, and some YF-17 data, only a single droop leading edge flap was used. These flap settings are therefore defined as follows



(1) Lift Data

Figure 88-94 show the effect of increasing LEX area on the low speed trimmed lift coefficient. For convenience the data have been summarized for each major aircraft configuration, i.e., the N300, P530, P600, P610, P630, YF-17, and F-5F.

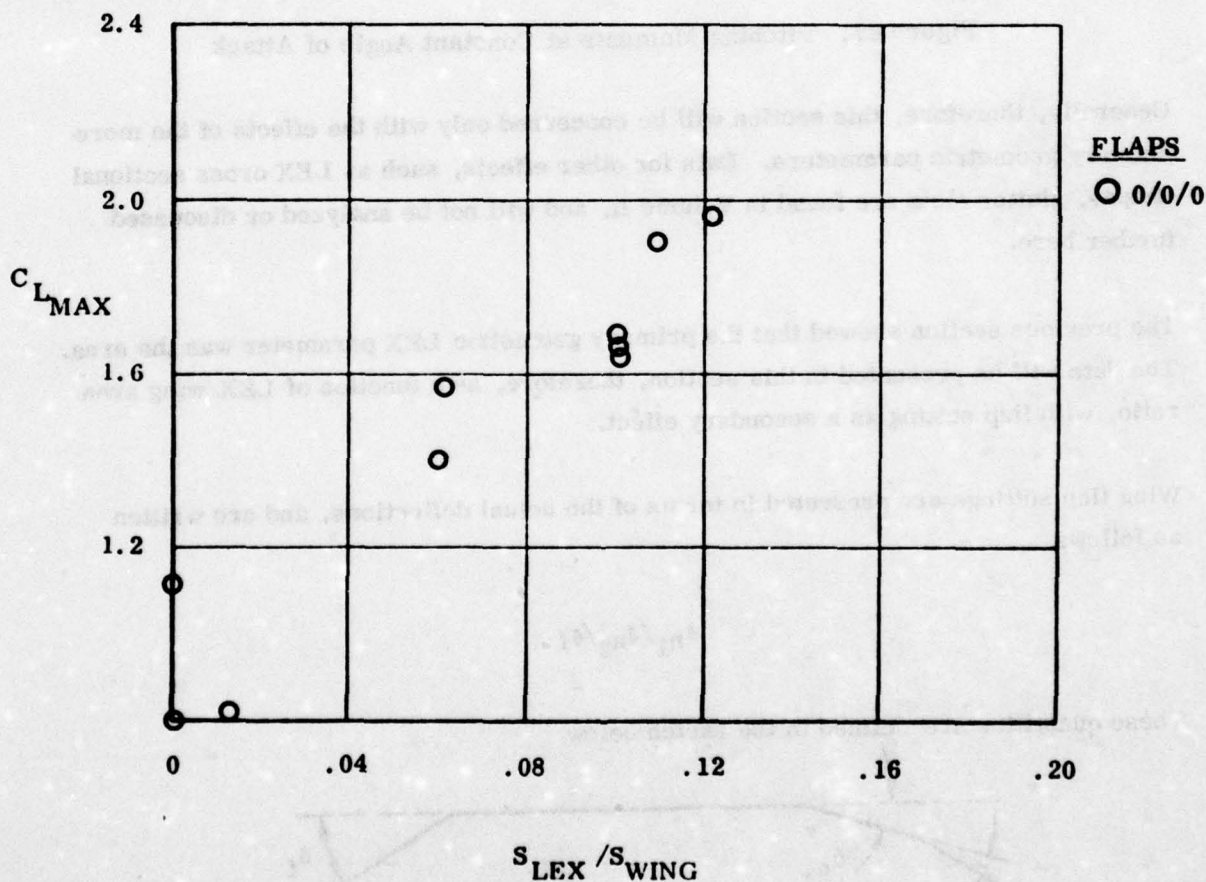


Figure 88. N300 Lift Data

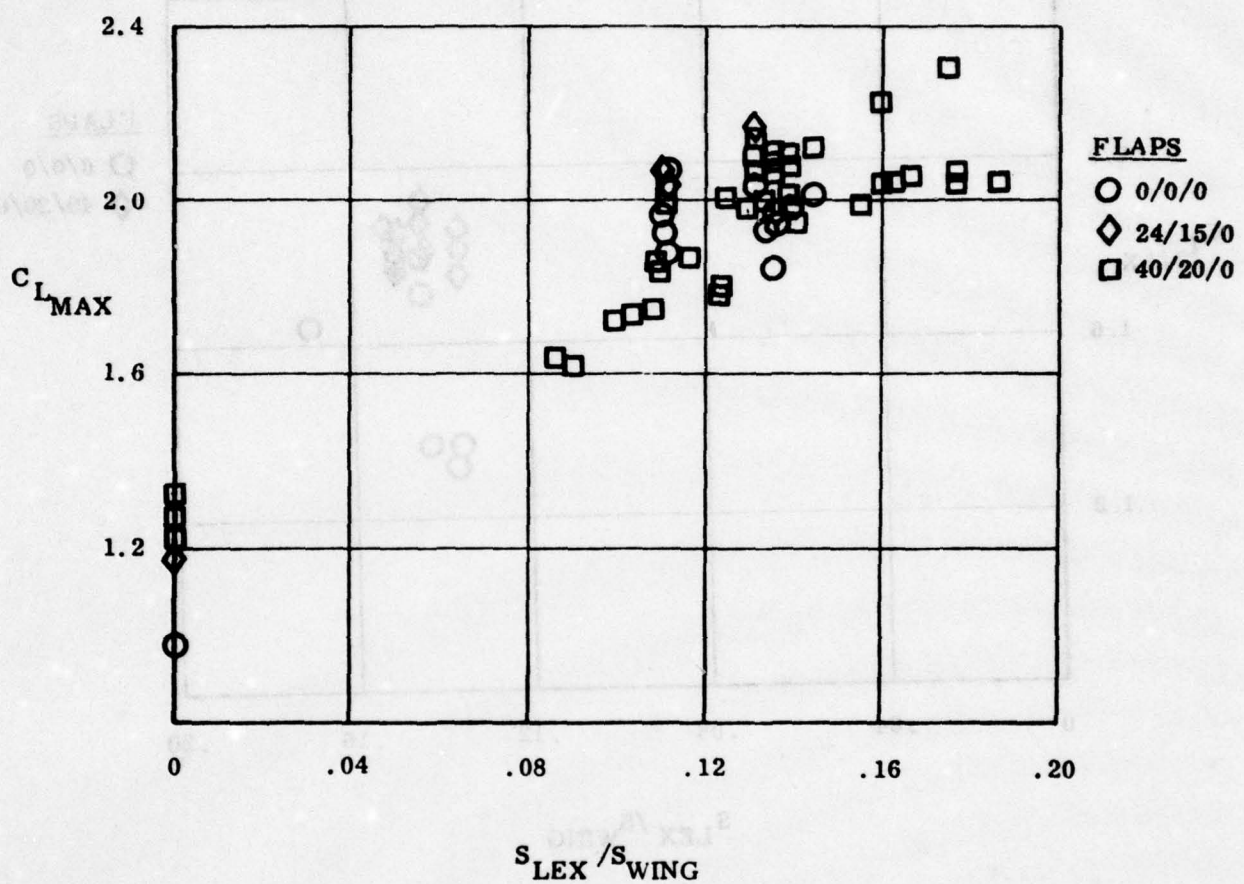


Figure 89. P530 Lift Data

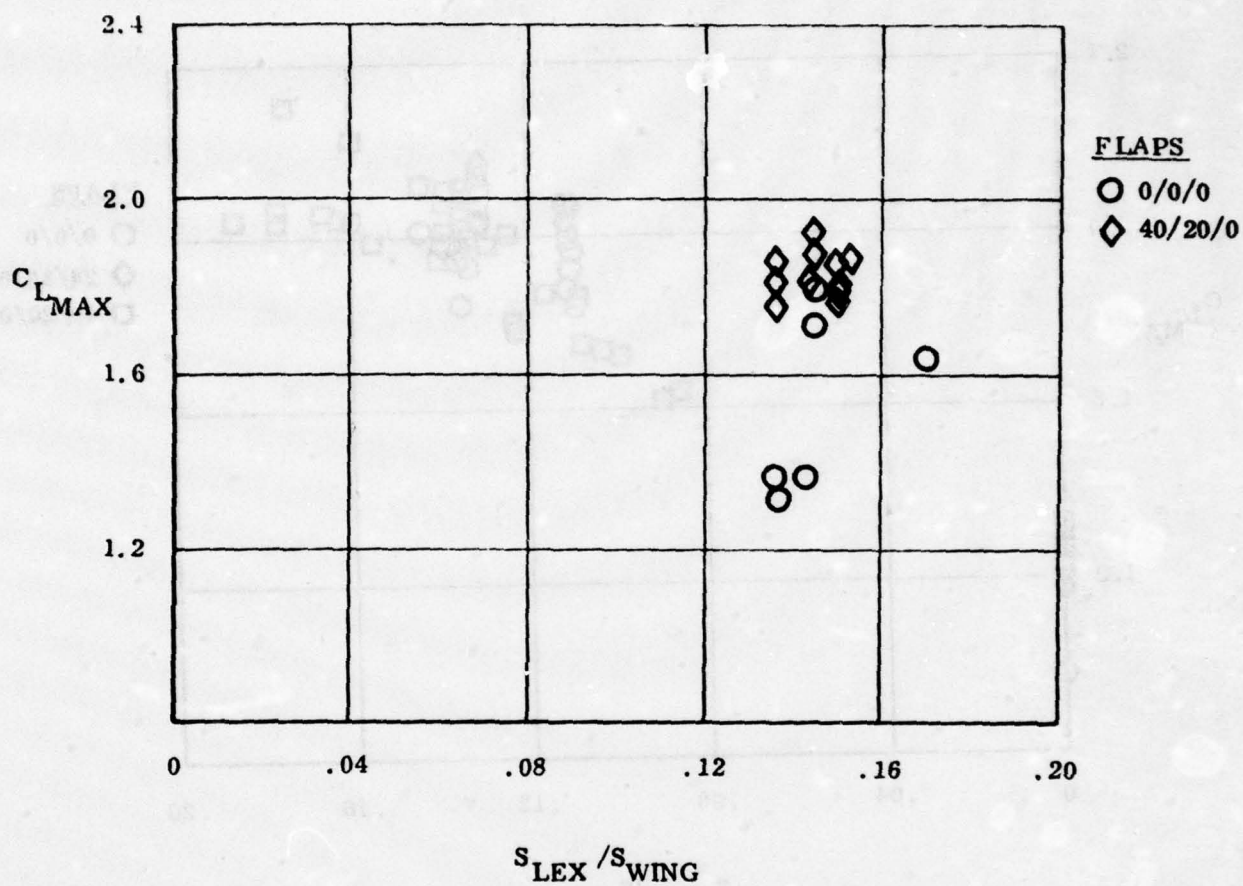


Figure 90. P600 Lift Data

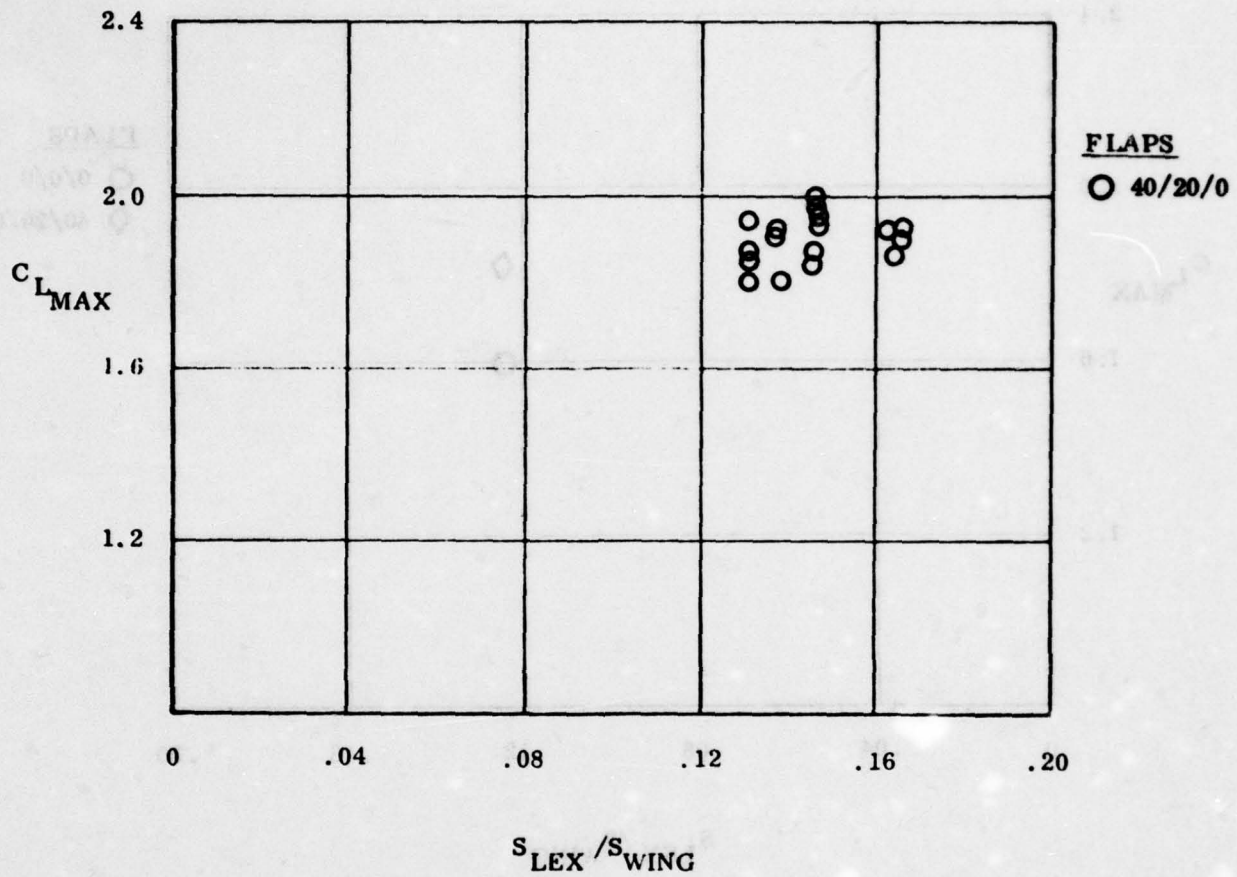


Figure 91. P610 Lift Data

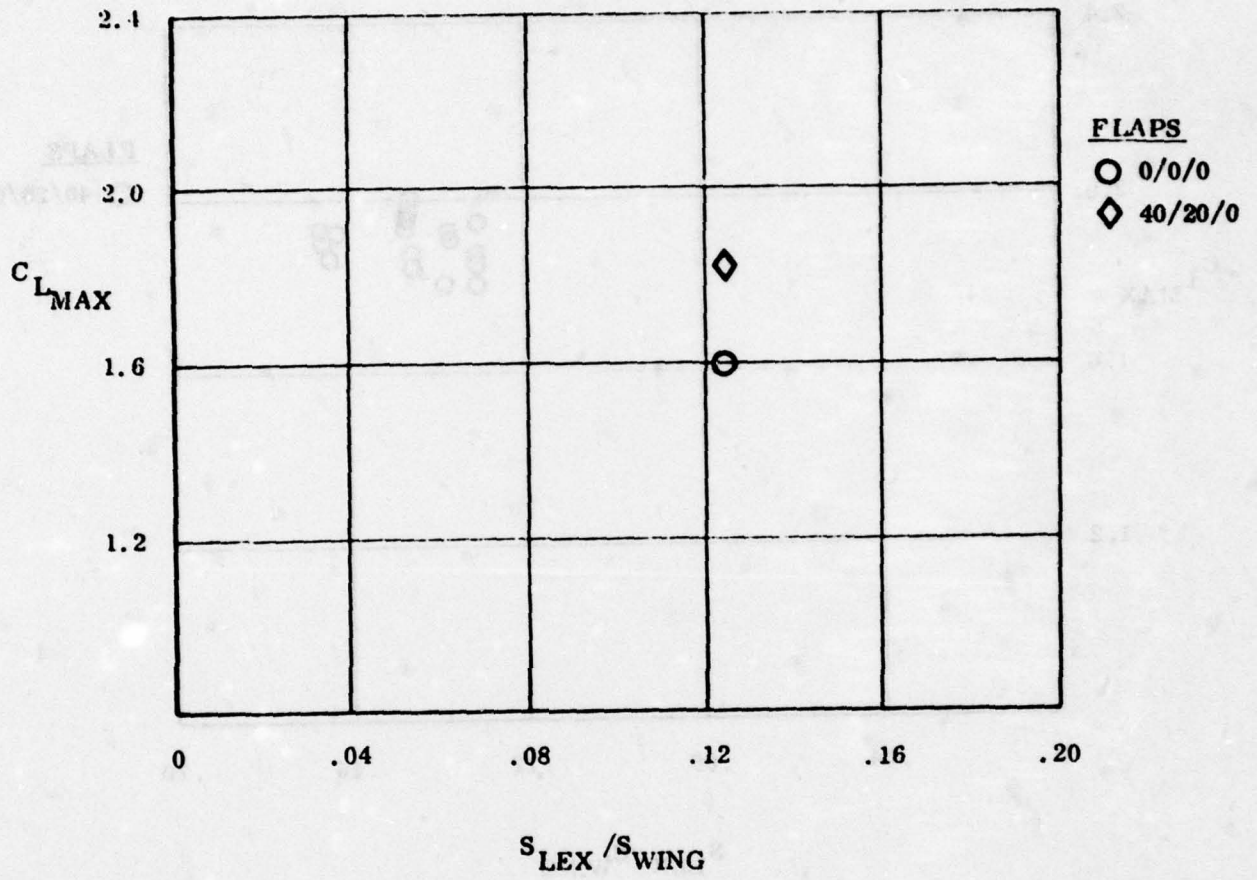


Figure 92. P630 Lift Data

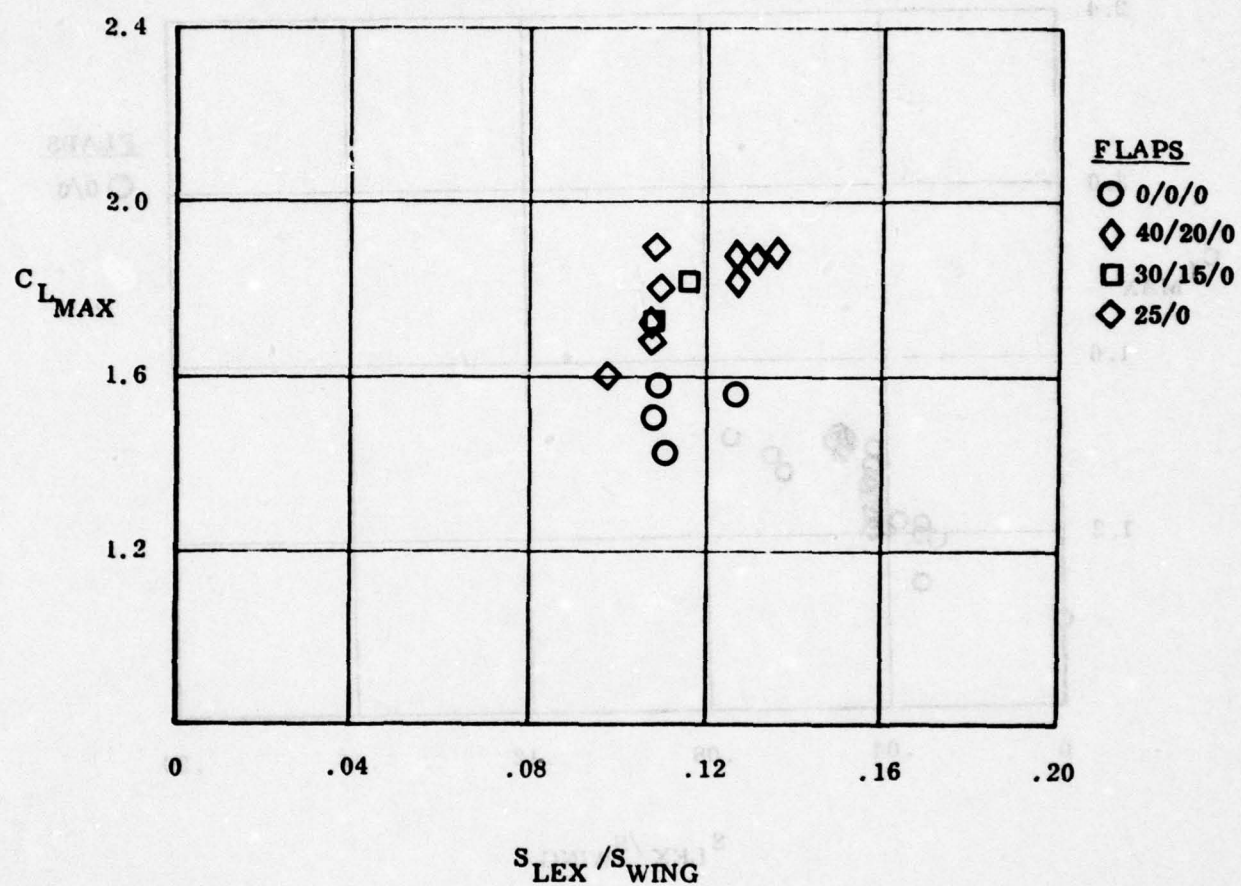
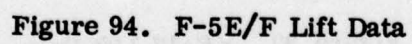


Figure 93. YF-17 Lift Data



From these figures, it is seen that the bulk of test data were obtained in the P530 program, and that configurations after this model concentrated in refining the size/shape for an approximate 14 percent area LEX. All the data show a basically linear trend with increasing LEX size, and also show for the P530 data, little effect of flap setting. For the YF-17, the flap effect is more pronounced, and this is possibly due to a wing planform change, the YF-17 wing having a smaller taper and LEX span ratio and larger aspect ratio. To isolate the actual effect of deflecting the leading edge flaps Figures 95 and 96 are given. Although the flaps up data are somewhat scattered, the trend shows that the effect of flaps is much larger with small LEX's, and, as LEX size increases, the flap incremental contribution to lift decreases. This is probably due to some natural limit in lift being reached on the wing, and further attempts to increase the lift show diminishing returns. This effect as was previously illustrated in Figure 77 for a wing body configuration.

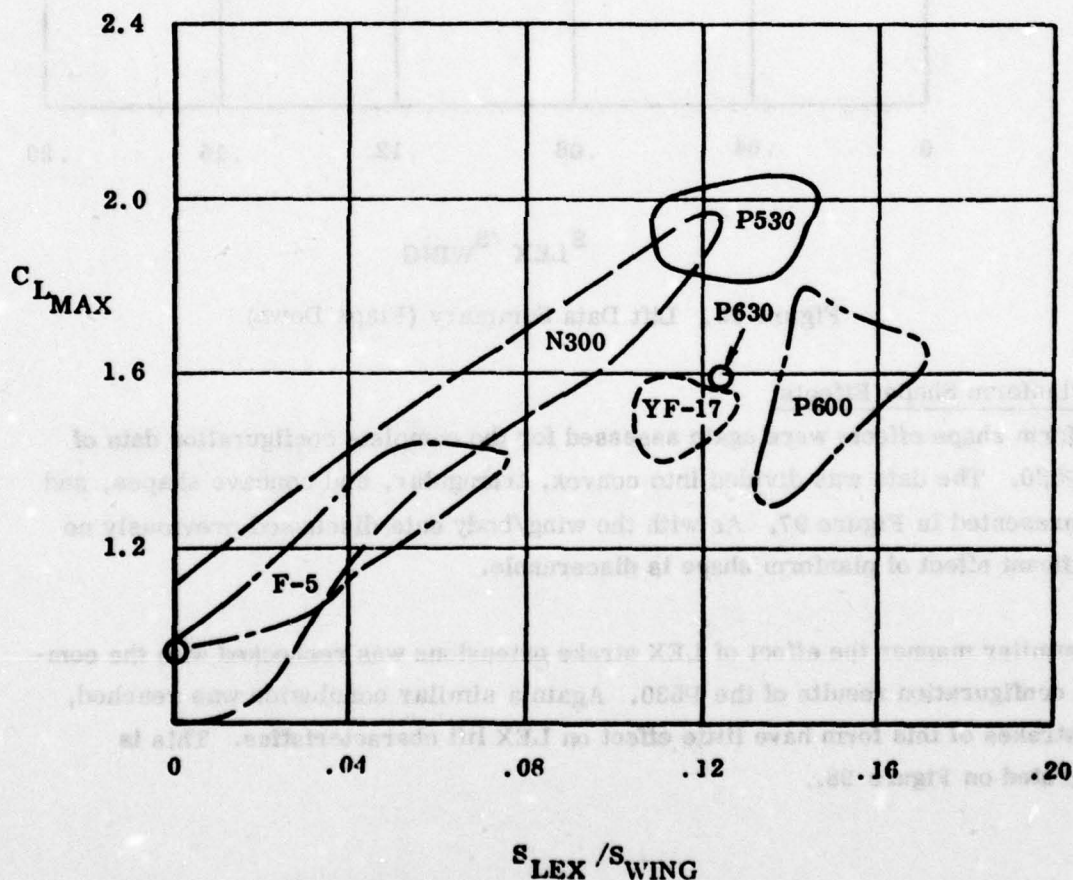


Figure 95. Lift Data Summary (Flaps Up)

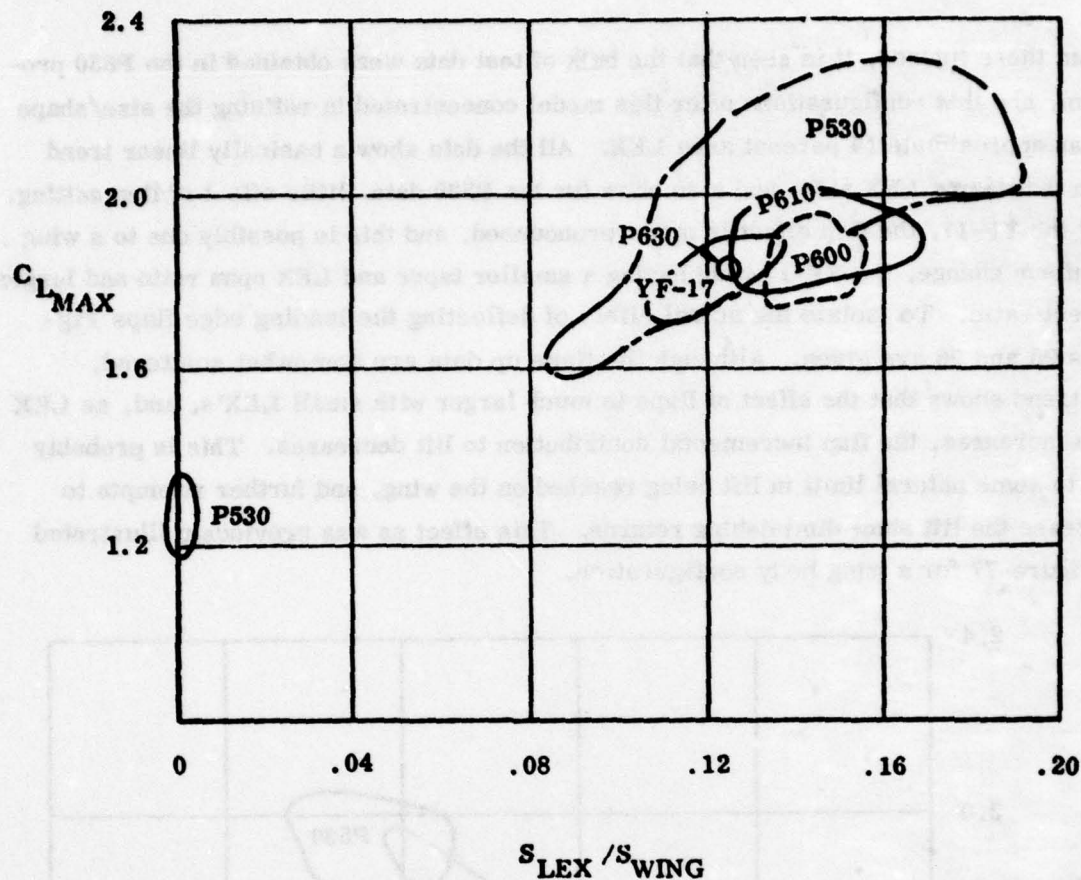


Figure 96. Lift Data Summary (Flaps Down)

(2) Planform Shape Effects

Planform shape effects were again assessed for the complete configuration data of the P530. The data was divided into convex, triangular, and concave shapes, and are presented in Figure 97. As with the wing/body data discussed previously no significant effect of planform shape is discernable.

In a similar manner the effect of LEX strake extensions was rechecked with the complete configuration results of the P530. Again a similar conclusion was reached, that strakes of this form have little effect on LEX lift characteristics. This is illustrated on Figure 98.

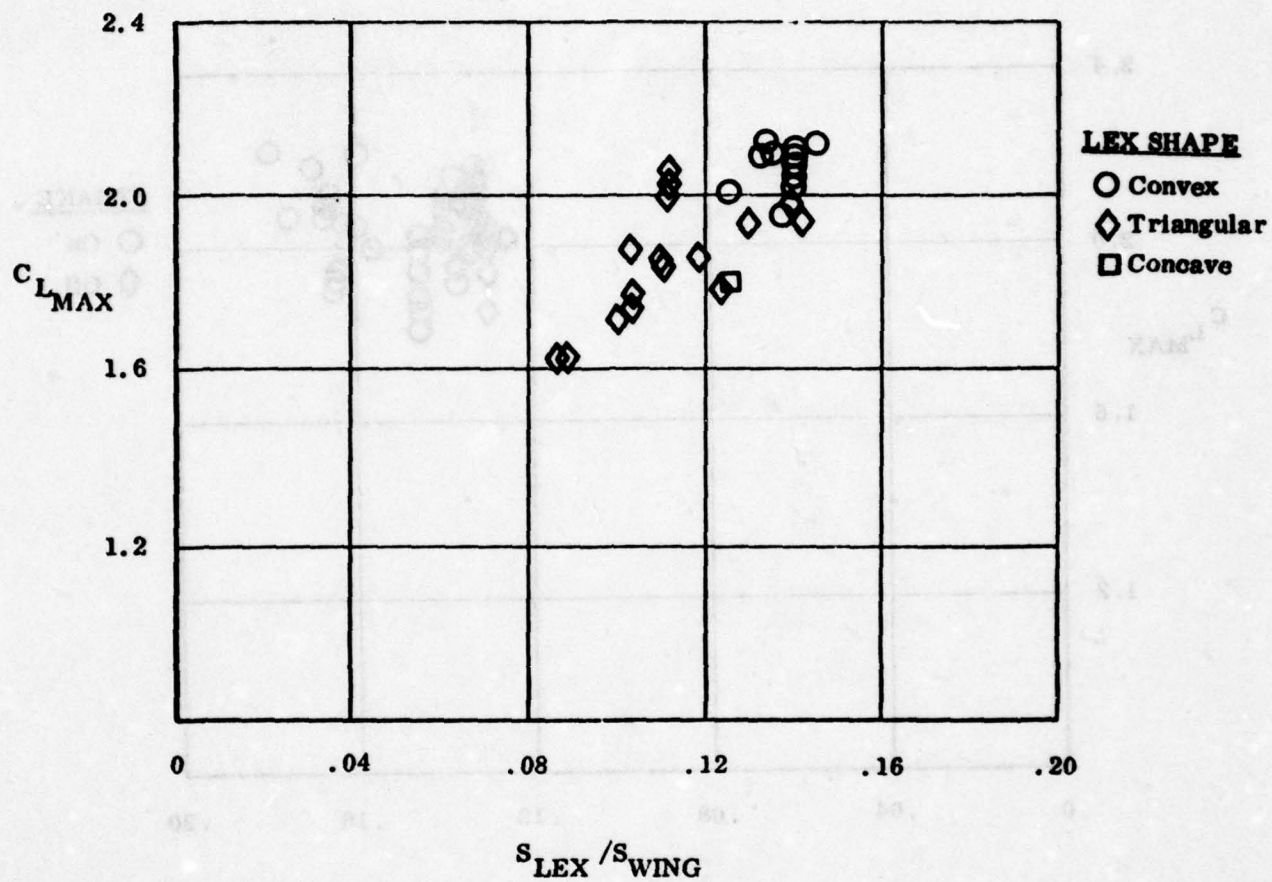


Figure 97. Effect of Lex Planform Shape (Flaps Down)

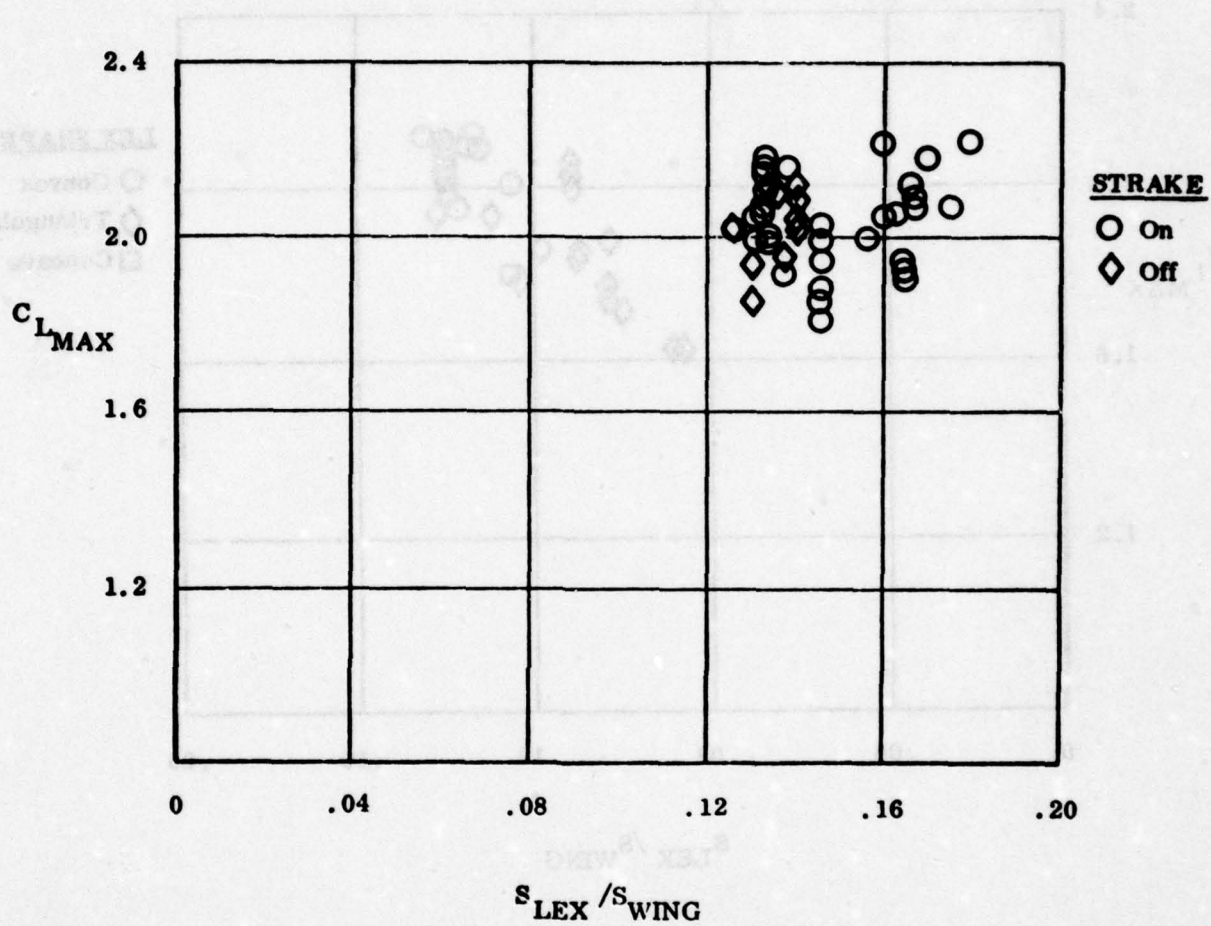


Figure 98. Effect of Lex Strake

(3) LEX Effects, High Speed

Data for the effects of the LEX on lift and pitching moment were obtained at high speeds. The model used was that previously illustrated in Figure 70 with tail on. The test results showed similar trends to those presented in Figures 85 and 86. The effect of Mach number on the LEX lift increment is as previously seen. A gradual collapsing of the lift curves into one common line occurs. Pitching moment trends are also consistent with the tail-off data. A constant increment in pitching moment, virtually independent of Mach number is indicated.

d. Lateral/Directional Effects

The leading edge extension, in addition to influencing the lift and pitching moments on the aircraft, has also an influence on the lateral/directional stability. These effects are shown to be configuration dependent, being detrimental on the single vertical tail F-5E/F, and beneficial on the twin vertical tailed YF-17 aircraft.

The following paragraphs discuss these effects in detail.

(1) Wing-Body Configurations

The addition of a LEX to the F-5E wing body configuration are shown on Figures 99 and 100. The lateral/directional data, seen on Figure 99, indicates that the addition of the LEX has little effect at angles of attack up to 14 degrees. At this angle the basic wing stalls (see Figure 100) and a reduction of the directional stability occurs. With increasing angle of attack the wing-plus-LEX configuration also stalls, causing a similar shift in the directional stability. These effects are small, however, and in general the addition of the LEX is seen to have little effect on the directional in stability of the wing body configuration.

The lateral data shows a much stronger effect of the addition of the LEX. The basic wing body is essentially stable in roll throughout the angle of attack range, the degree of stability being smallest around the wing stall angle of attack. Addition of the LEX causes the configuration to be unstable in the stall angle-of-attack region. Both configurations are stable above 25 degrees angle of attack.

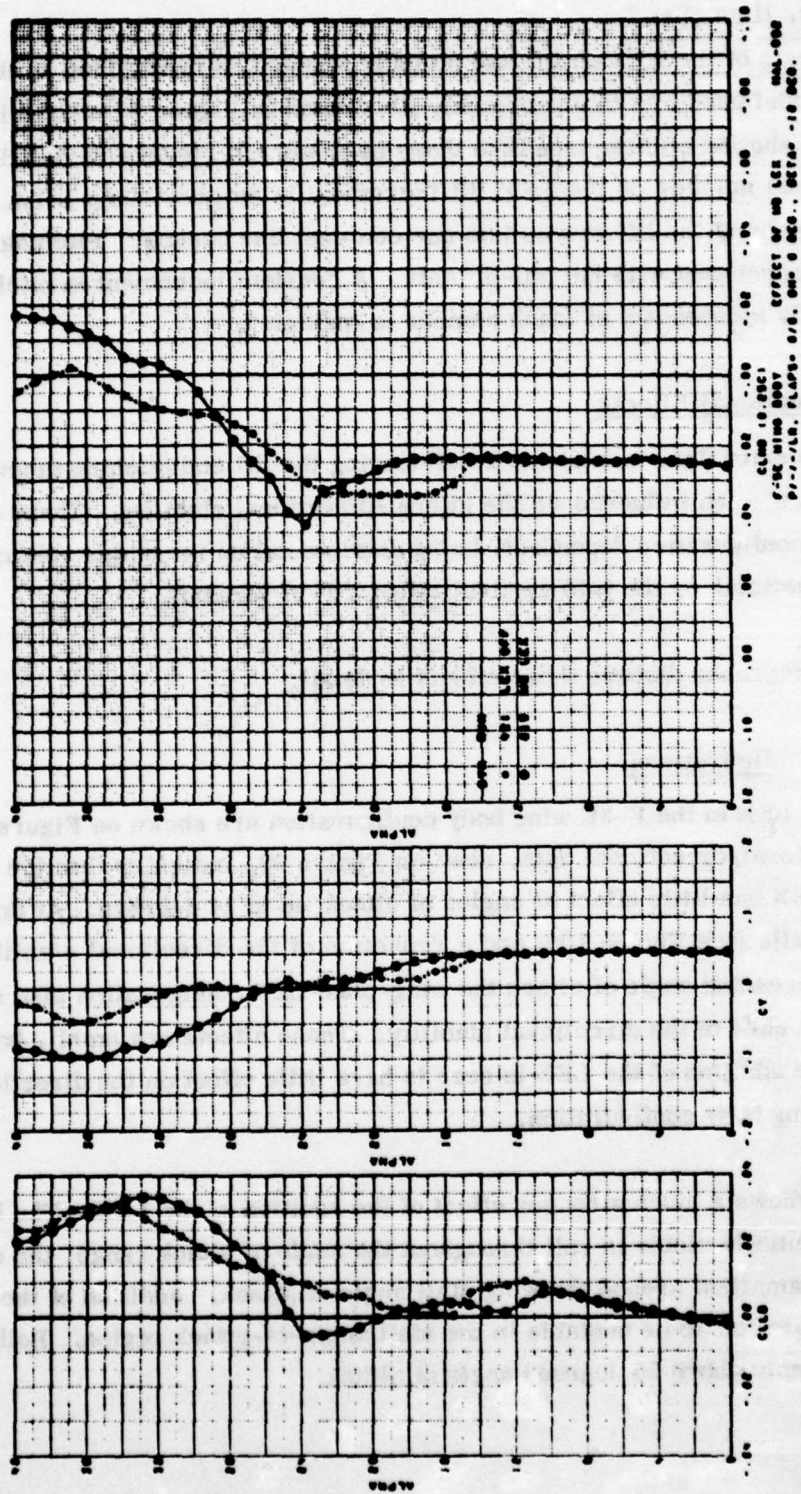


Figure 99. Lex Effect of Wing Body Data

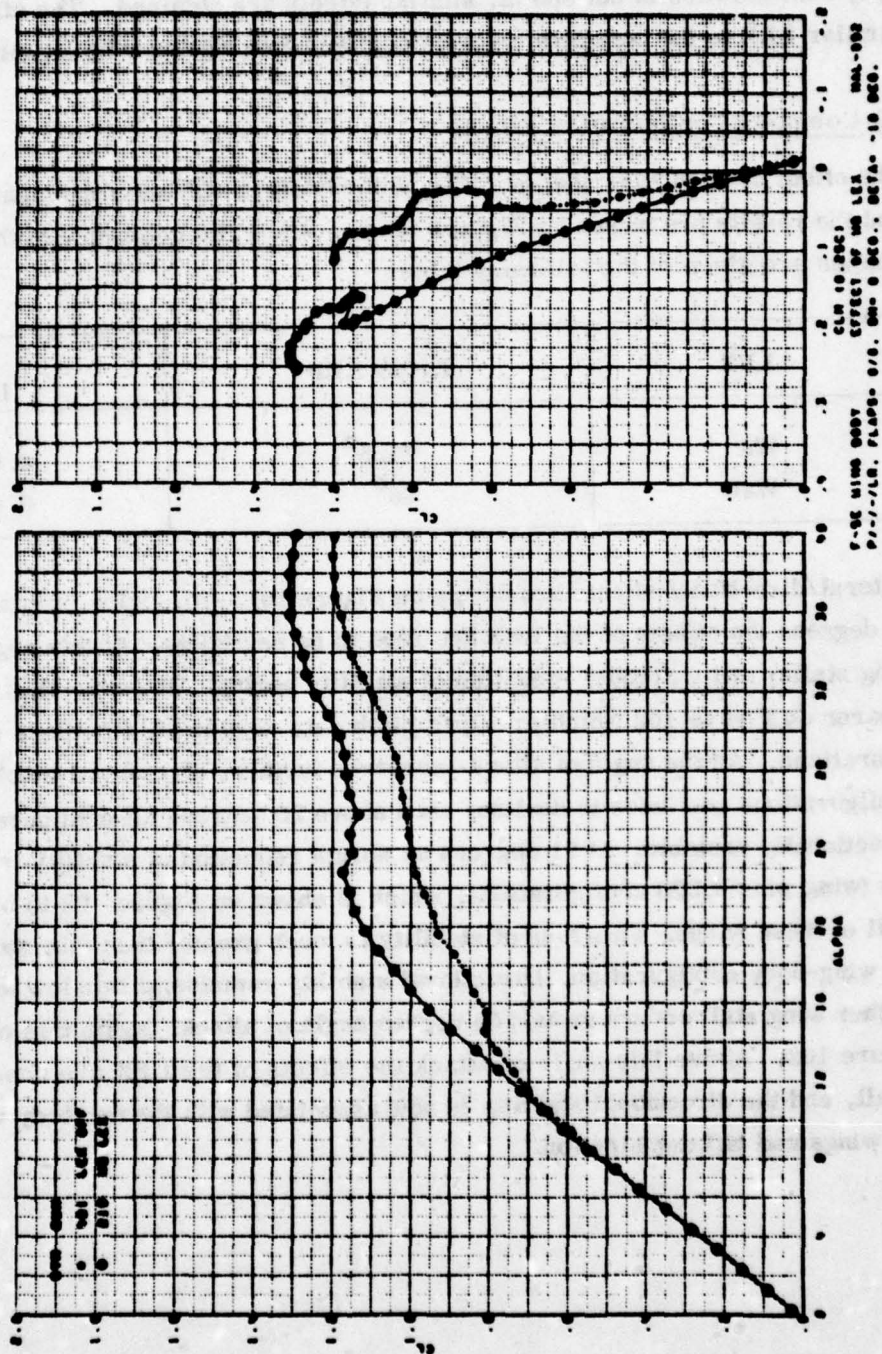


Figure 100. Lex Effect on Wing Body Data

The main effect of the addition of the LEX is seen to be in lateral stability, the directional effects of the LEX addition being small. Although data for the YF-17 wing body configuration is not shown, similar effects are obtained. The effect of adding a similar LEX to the complete aircraft configuration will now be examined.

(2) Complete Configuration Effects

The effect of triangular shaped LEXs on the basic F-5F was investigated in Ref 7-9 and the results are shown on Figures 99 and 100. The geometry of these LEX shapes are given in the following table.

LEX	LE SWEEP	S_L/S_W
W2	71.5°	0.031
W26	66°	0.043

Lateral/directional effects are shown on Figure 101. At angles of attack up to 12 degrees the effects of the LEX are seen to be negligible. At this angle the basic wing stalls, and a gradual reduction of stability begins. The wing stall can be seen clearer on Figure 102 which presents pitch data at sideslip for these same configurations. As the angle of attack increases further, directional stability on all configurations continues to decline, until above 20 degrees all configurations are directionally unstable. At 21 degrees an abrupt reduction of stability is shown for the two (wing-plus-LEX) configurations, which is shown on Figure 102 to be the first stall of these wings. This loss of stability is much greater than that shown earlier on the wing-body configuration. Directional stability remains at this low level until a further wing stall occurs around 26 degree angle of attack. Again this can be seen on Figure 102. Above this angle of attack the effects of the LEX are shown to be small, and the directional stability is now associated with the forebody rather than the wings and tail combination.

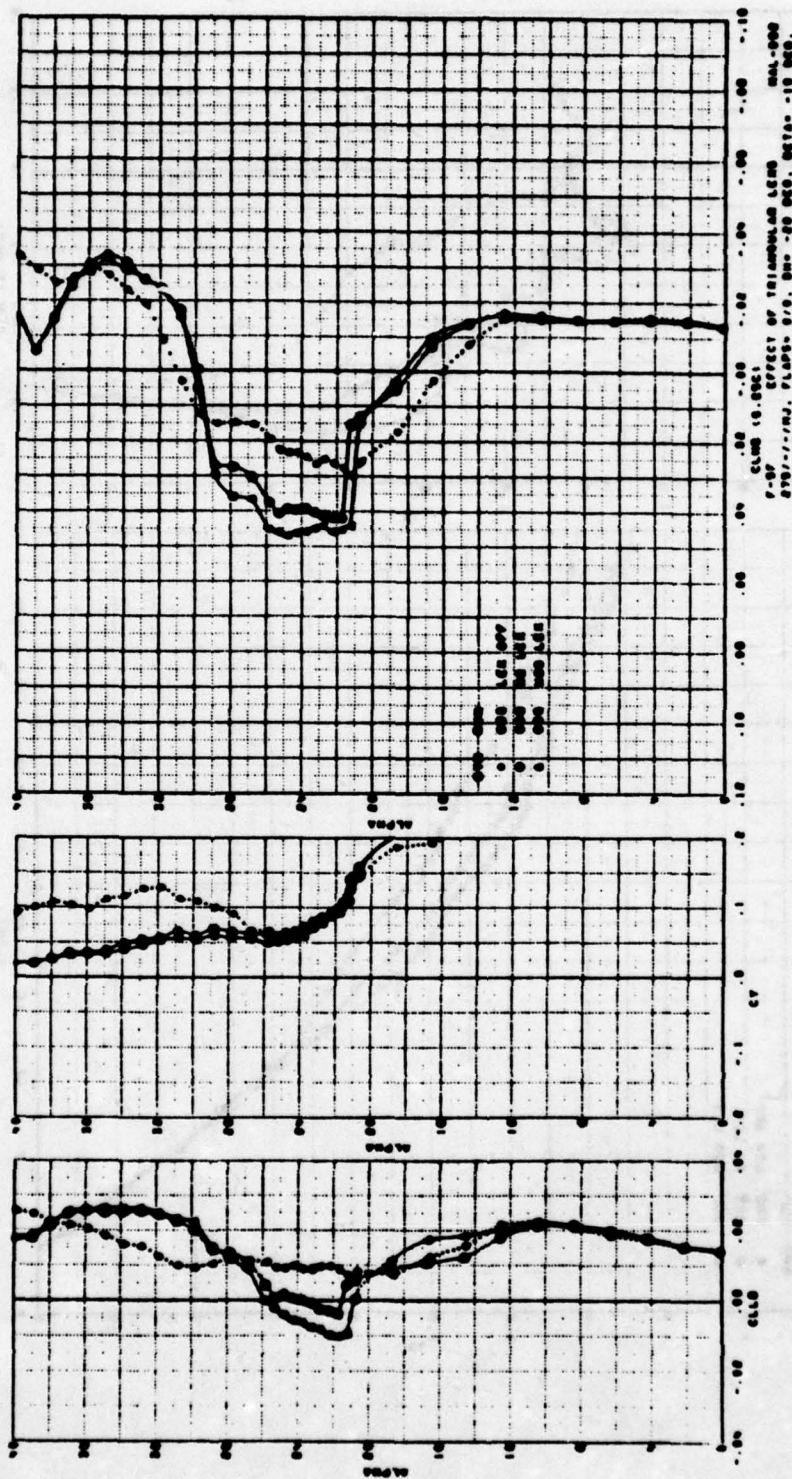


Figure 101. Triangular Lex Effects in Sideslip

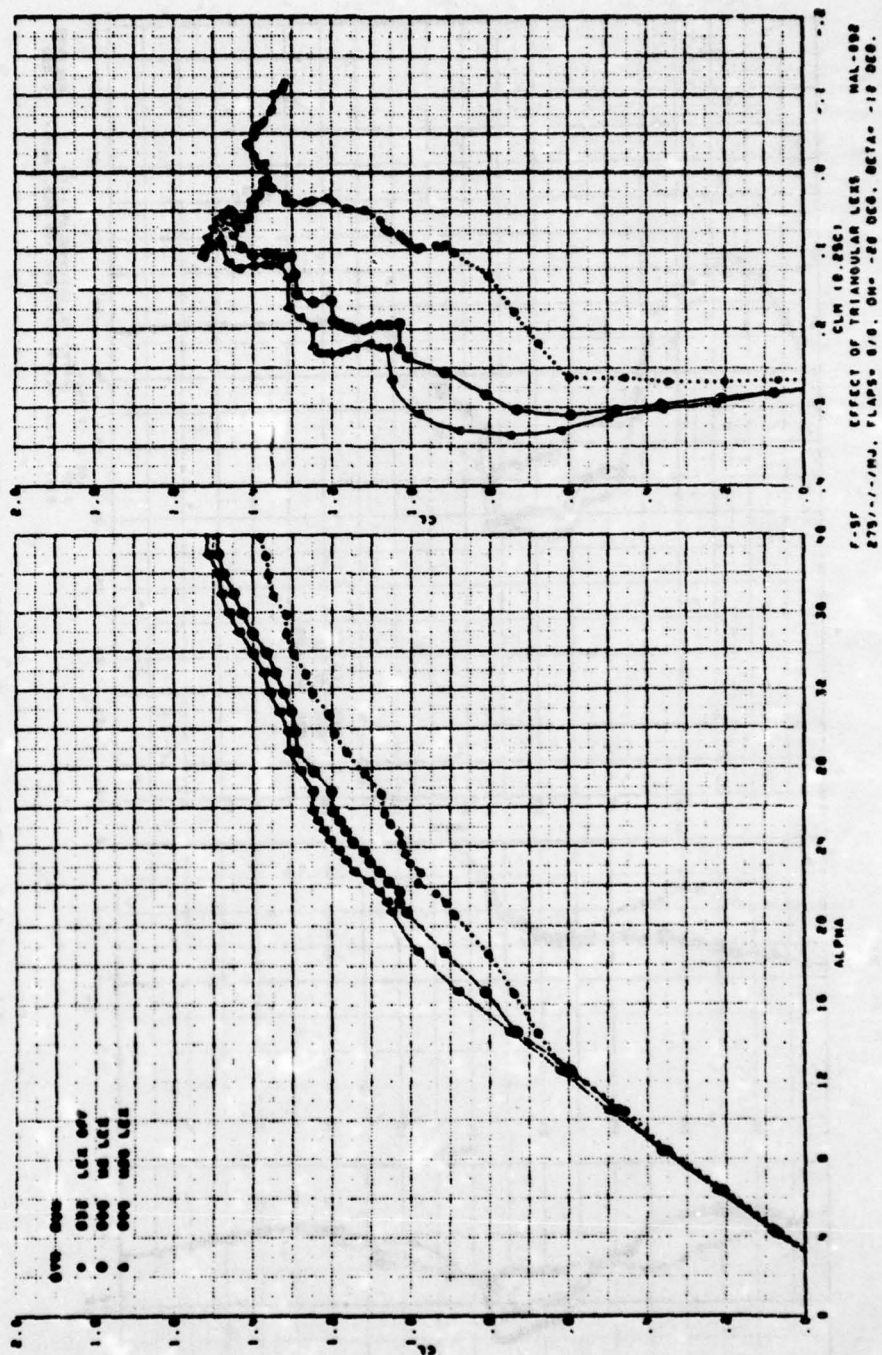


Figure 102. Triangular Lex Effects in Sideslip

The lateral stability shows a similar trend, but with different levels of results. The directional stability for both the LEX-on and-off wings was seen to be first stable and then unstable as angle of attack increased through the stall region, the actual degree of instability being influenced mainly by the presence of the LEX, and only slightly influenced by actual LEX size. Lateral stability is seen to change from positive to negative due to the presence of the LEX with a major effect of LEX size in the stall region. Again the effect of the two wing stall angles on the (wing-plus-LEX) configurations is seen, at the second stall lateral stability is regained. For post-stall angles of attack, the LEX effect is seen to be beneficial, with improved lateral stability up to around 40 degree angle of attack.

The LEX effects on lateral/directional stability are seen to be similar to the LEX effects on longitudinal stability. The basic wing with its low stall angle of attack and gradual stall progression also has a low break point and a gradual loss of directional stability. The LEX-on wings have a higher stall angle of attack, and an abrupt stall, with a similar abrupt loss of both lateral and directional stability. The LEX wing in sideslip is seen to have two stall angles, the windward wing stalling before the leeward wing. This differential stall pattern is associated with differential bursting of the LEX vortex. During the previous discussions it was shown that the LEX vortex burst point was a function of both angle of attack and leading edge sweep. Yawing the aircraft produces essentially different sweep angle on the windward and leeward LEXs. This is illustrated on Figure 103.

This different apparent sweep angle of the LEX therefore results in different vortex burst locations, and hence different stall angle of attack for each wing. The vortex burst location as shown on Figure 67 for simple delta wings indicates the greater sensitivity of the lower leading edge sweep angles. Hence the windward LEX having the smaller sweep has a more abrupt stall pattern, due to the rapid forward movement of the burst point. The abrupt wing stall in turn causes an abrupt change in the sidewash on the vertical, and hence the rapid loss in directional stability. A further effect compounding the loss of directional stability is the low energy wake resulting from the wing stall reducing the dynamic pressure at the vertical tail.

The discussion so far has been concerned with triangular shaped LEX configurations on the F-5F. Other LEX shapes were investigated during the tests of Reference 49

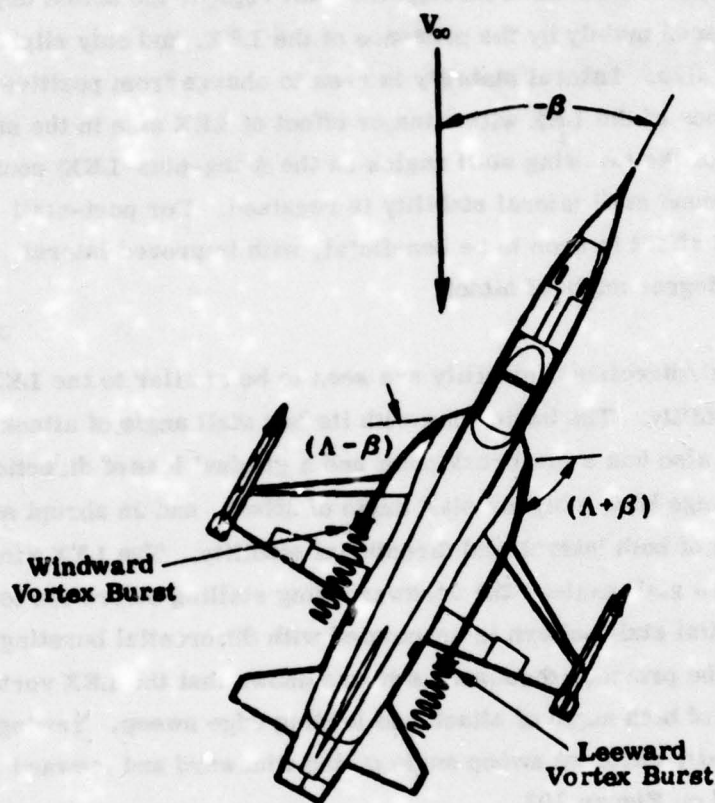


Figure 103. Schematic of Lex Effect in Sideslip

to determine what factors improved the stability loss in the stall region. One such technique was to reduce the angle of incidence of the LEX. This LEX droop delayed the stalling of the wing approximately by the angle of droop, as shown on Figure 104. This effective delay in the stall angle of attack eliminated the loss of lateral stability in the stall region. A considerable reduction in the directional instability around the stall is also seen, due to this increased stall angle of attack. This latter effect is F-5F configuration dependent, however, because of the stable forebody configuration.

Delaying the stall angle can also be accomplished by increasing the size of the LEX, and in addition increasing its leading edge sweep angle. A typical example of this is LEX W6 on the F-5F. Data for this LEX can be found in Volume II. On the YF-17 configuration effect of increasing the leading edge sweep angle by the adoption of a convex curved LEX leading edge was investigated in detail. This is essentially the same as increasing the leading edge sweep angle mentioned above. The effect of the convex contouring of the LEX was determined by flow visualization during the P530 tests.

A typical result is shown in Figure 105. Here the vortex generated by the triangular LEX is seen to be burst, with the burst location at the junction of the wing and LEX. The vortex generated by the convex LEX passes over the complete chord before bursting around the wing trailing edge.

For this particular configuration the triangular LEX vortex burst point moved from the trailing edge to the leading edge of the wing within the angle of attack range from 20 to 25 degrees. With the convex planform, vortex bursting started at a much higher angle of attack (25 degrees) and at 30 degrees had only reached the mid-chord station of the wing. The data shown by the flow visualization was at zero sideslip.

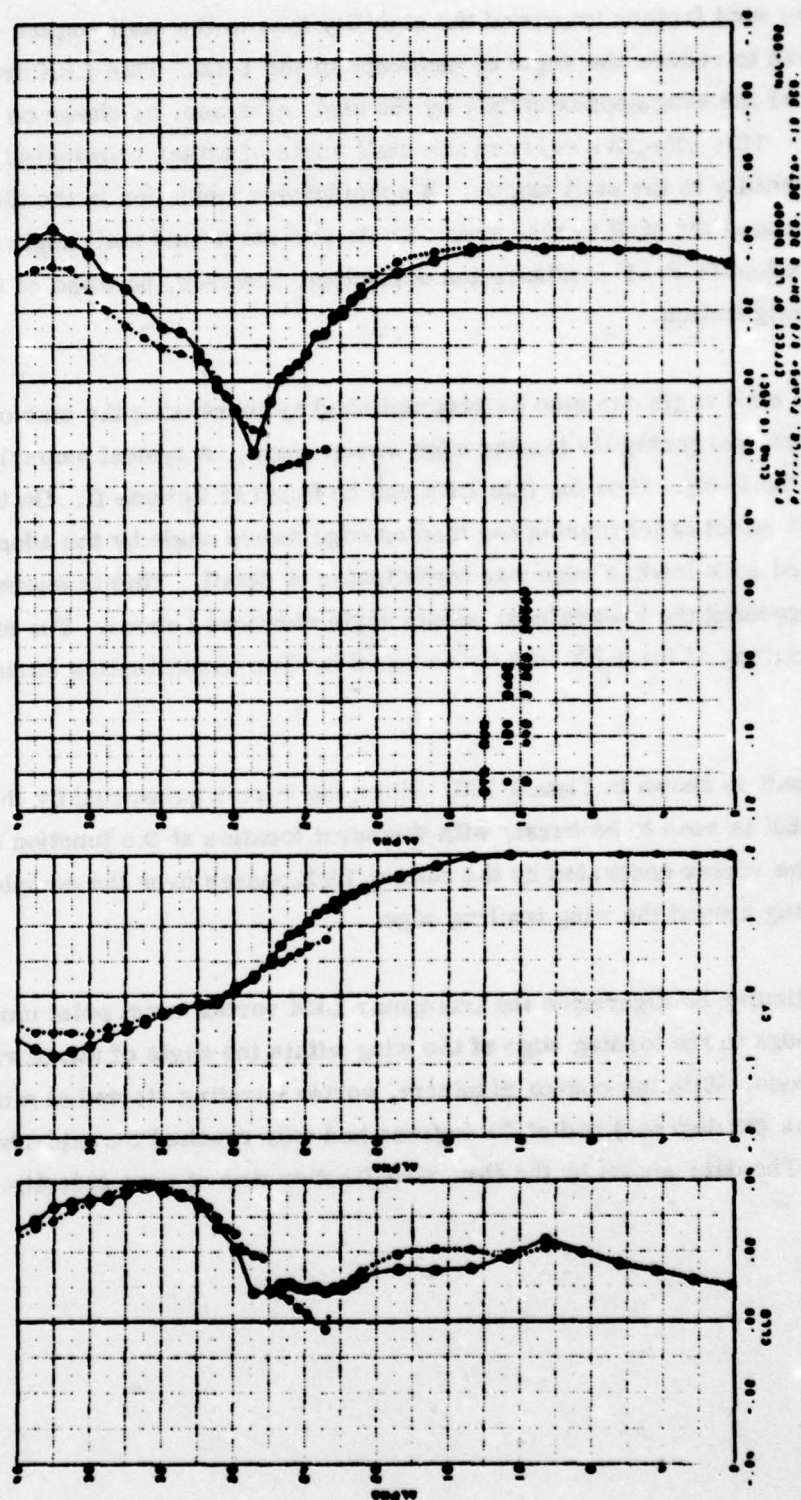


Figure 104. Effect of Reduced Lex Angle of Attack



Figure 105. Effect of Leading Edge Curvature on
Vortex Burst Point ($\alpha = 25^\circ$)

At non-zero sideslip such a planform should not be as sensitive to the loss of leading edge sweep previously mentioned on the triangular shaped LEX. Two effects are present here. The first is that the sensitivity of the LEX to vortex burst is reduced with increased leading edge sweep angle, as shown on Figure 67. The second point is that the leading edge sweep of the leeward wing, with such a LEX planform shape exceeds 90 degrees when sideslipped, thus weakening the leeward vortex, and reducing the asymmetries associated with differential vortex bursting.

Because of the high degree of configuration dependence, further detailed discussion of the lateral/directional effects of the LEX configuration on the YF-17 is not appropriate. Isolated effects of the LEX may not be relevant on such a configuration, which was developed to have highly interactive component effects. The lateral/directional stability of the YF-17 is influenced by the wing leading edge extension, the vertical tail and leading edge flap system in a highly complex manner. Further discussion of these components and their effects will be made in the sections on vertical tails and leading edge flaps.

e. Summary of Results

The test results presented show that the leading edge extension is a powerful way of increasing the maximum lift of a wing. A summary of this test data, shown in Figure 106, presents maximum lift coefficients as a function of LEX/wing area ratio. This figure indicates that a unit increase in LEX area produces a 5.5 increase in maximum lift coefficient as does a unit increase in wing area.

The test data covers LEX geometries which are subject to many constraints due to the particular aircraft configurations which they have been applied to, and, therefore, do not necessarily represent the optimum LEX geometries. For the particular configurations tested LEX area appears to be the more significant factor in obtaining increases in maximum lift coefficient.

The pitching moments associated with the LEX are shown to be non-linear, in contra-distinction to the lift increments, and show increasing pitch-up tendencies with increased LEX area.

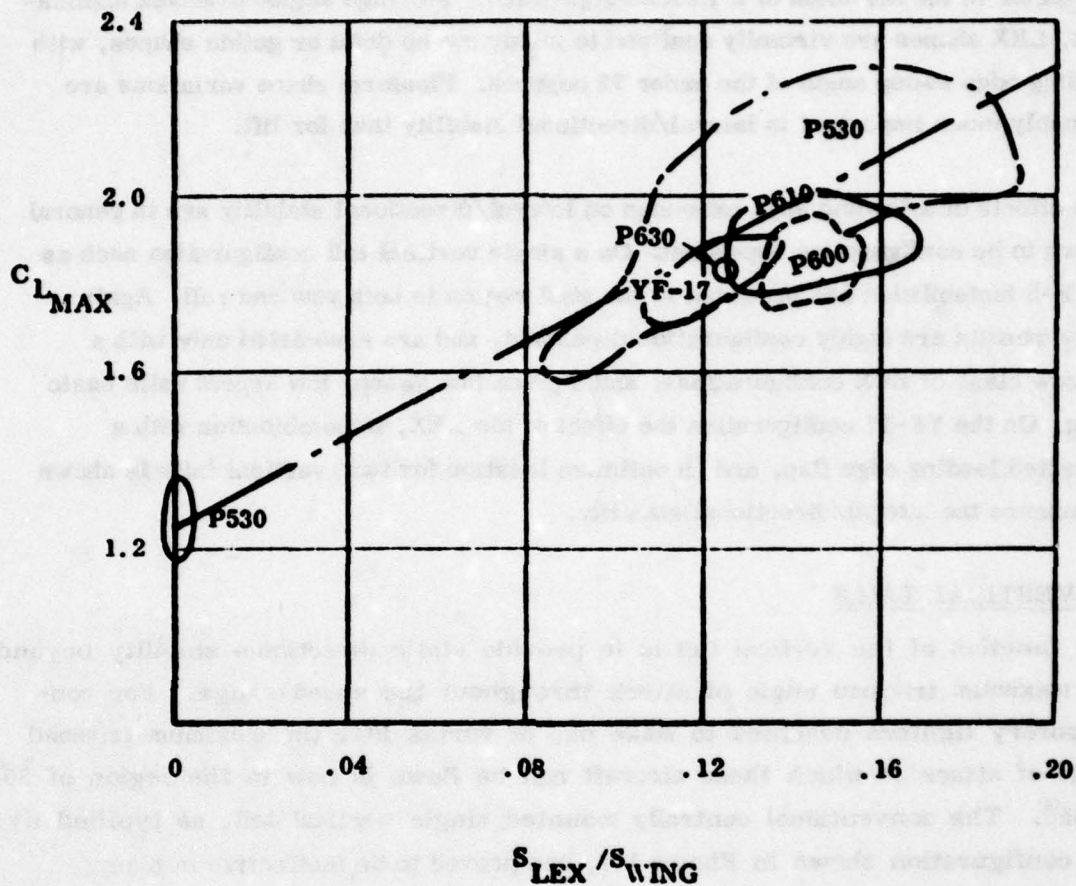


Figure 106. Linearized Lex Lift Effects

The effects of the LEX are shown to be a function of Mach number. The lift increases due to the LEX diminish as Mach number increases, mainly due to the improved characteristics of the basic wing. The LEX pitching moments, however, are unaffected by Mach number, and remain virtually constant across the test range of Mach numbers.

Thus pitching moment effects are more significant than the lift increments as a limiting factor in the selection of a LEX configuration. For high angle-of-attack application, LEX shapes are virtually confined to highly sweep delta or gothic shapes, with leading edge sweep angle of the order 75 degrees. Planform shape variations are probably more important in lateral/directional stability than for lift.

The effects of a leading edge extension on lateral/directional stability are in general shown to be configuration dependent. On a single vertical tail configuration such as the F-5 instabilities are produced in the stall region in both yaw and roll. Again these results are highly configuration dependent, and are associated only with a narrow class of LEX configurations, and a given low sweep, low aspect ratio basic wing. On the YF-17 configuration the effect of the LEX, in combination with a deflected leading edge flap, and an optimum location for twin vertical tails is shown to enhance the lateral/directional stability.

3. VERTICAL TAILS

The function of the vertical tail is to provide static directional stability beyond the maximum trimmed angle of attack throughout the speed range. For contemporary fighters designed to make use of vortex lift, the maximum trimmed angle of attack to which these aircraft can be flown is now in the region of 30° to 35° . The conventional centrally mounted single vertical tail, as typified by the configuration shown in Figure 107, has proved to be ineffective in many cases at these angles of attack.

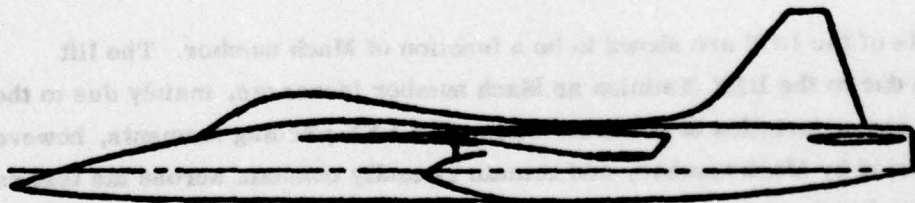


Figure 107. Single Vertical Tail Configuration

Figure 108 illustrates the directional stability of this configuration, taken from Reference 6, and shows that stability is lost above 18 degrees angle of attack.

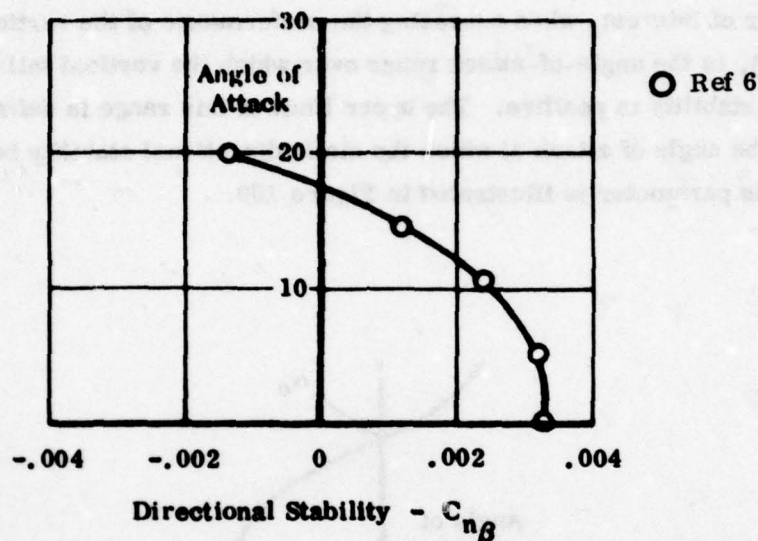


Figure 108. Effectiveness of a Single Vertical Tail

As an alternate approach to the problem of providing adequate directional stability at high angles of attack, the development of a twin vertical tail system, which benefited from favorable interference from the wing LEX flows, was initiated. The majority of the test data presented in Volume II is associated with the development of twin-tailed configurations, and the determination of the optimum location of the vertical tail/LEX assembly. A large number of twin vertical tail configurations were tested at low speeds. Analysis of this very large data base showed the results to be highly configuration dependent and, as such, not amenable to generalization. However, the basic result of the twin vertical tail development program was that a suitable twin vertical tail system could be developed which would provide adequate directional stability in the $30^\circ \sim 35^\circ$ angle of attack range.

In the following paragraphs a general discussion of both single and twin vertical tail configurations is presented. The major topic of discussion will be directional stability effects. The effects of vertical tail geometry changes on other parameters, such as rolling moments, are given in Volume II and will not be discussed further here.

a. Single Vertical Tails

The parameter of interest, when assessing the performance of the vertical tail (either single or twin), is the angle-of-attack range over which the vertical tail contribution of directional stability is positive. The upper limit of this range is defined in this study as α_c , the angle of attack at which the static directional stability becomes negative. This parameter is illustrated in Figure 109.

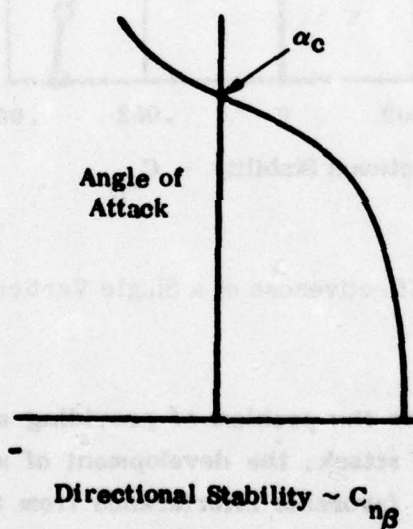


Figure 109 Definition of α_c

The performance of the various single vertical tail geometries available from this study will be assessed in terms of and a further parameter, the angle of attack at which the vertical tail becomes immersed in the wake of the wing. This is represented here as the angle between the tip of the vertical tail and the wing root fuselage junction, θ_v , and is illustrated in Figure 110.

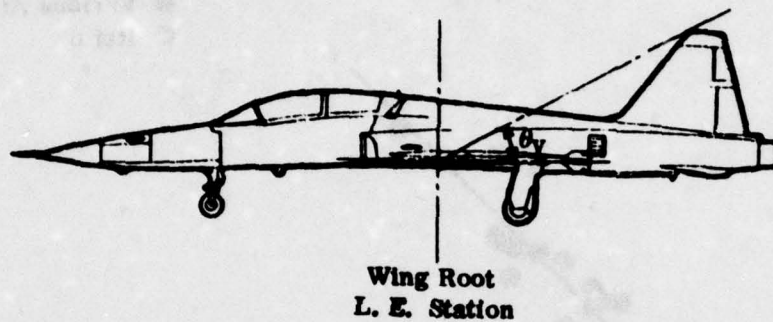


Figure 110. Definition of θ_v

Data from various fighter aircraft configurations not associated with this study indicated that these two angles were of similar magnitude. These data, taken from various NASA references, are plotted in Figure 111, together with the data point from Figure 108 presented earlier, and illustrate this equivalence.

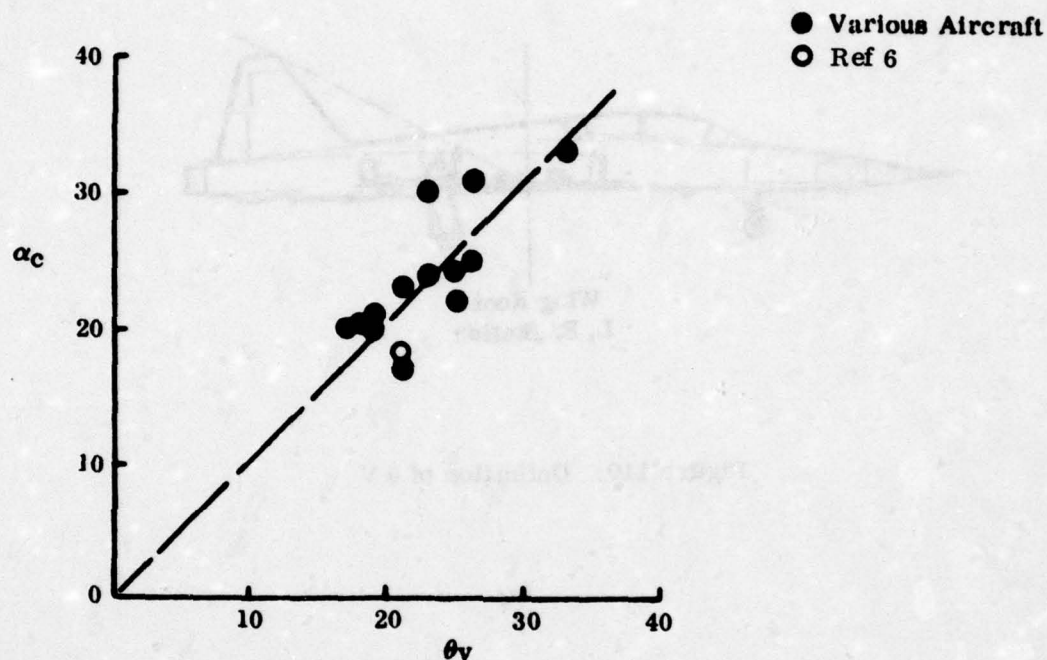


Figure 111. Vertical Tail Effective Range

A similar comparison is made in Figure 112 using data for single vertical tail configurations from tests on the P530, P600, YF-17, and F-5E/F.

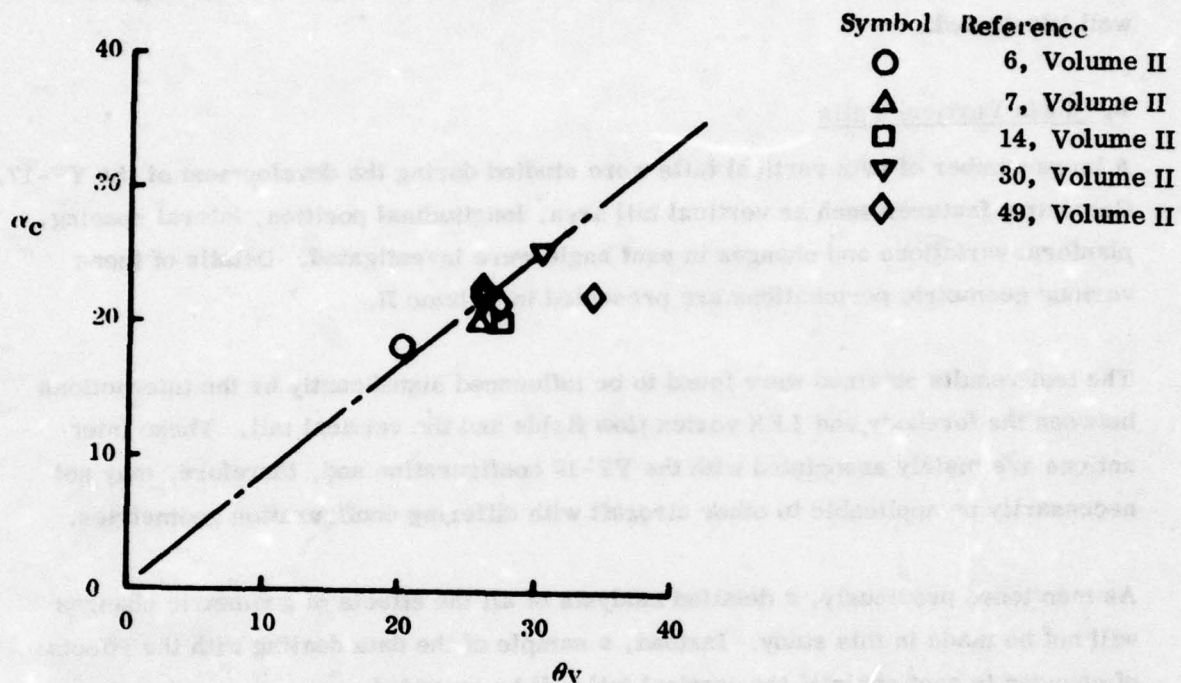


Figure 112. Vertical Tail Effective Range As A Function of Wing Blanketing Angle

This figure indicates that although a slightly different relationship exists between α_c and θ_v , the equivalence is still indicated.

Based on the data from Figure 111 and 112, the impracticality of using a single vertical tail for positive directional stability in the higher angle of attack regions is well illustrated.

b. Twin Vertical Tails

A large number of twin vertical tails were studied during the development of the YF-17. Geometric features such as vertical tail area, longitudinal position, lateral spacing, planform variations and changes in cant angle were investigated. Details of these various geometric perturbations are presented in Volume II.

The test results obtained were found to be influenced significantly by the interactions between the forebody and LEX vortex flow fields and the vertical tail. These interactions are mainly associated with the YF-17 configuration and, therefore, may not necessarily be applicable to other aircraft with differing configuration geometries.

As mentioned previously, a detailed analysis of all the effects of geometric changes will not be made in this study. Instead, a sample of the data dealing with the effects of changes in cant angle of the vertical tail will be provided.

Figure 113 presents the effect of variations of cant angle on α_c , the angle of attack at which directional stability becomes negative. Data are presented for two groups of vertical tail areas, these being $S_v \sim 0.08 S_w$ and $S_v \sim 0.14 S_w$. The tail moment arm for all data is essentially constant, at $lv/\bar{c} \approx 1.2$. Two trends are shown. The group of smaller vertical tails indicates a reduction in the vertical tail contribution to directional stability with increasing cant angle. Increasing the cant angle effectively reduces the side area of the vertical tail. This effect is not overcome by any favorable vortex interaction from the LEX or forebody, presumably due to the small size of these verticals.

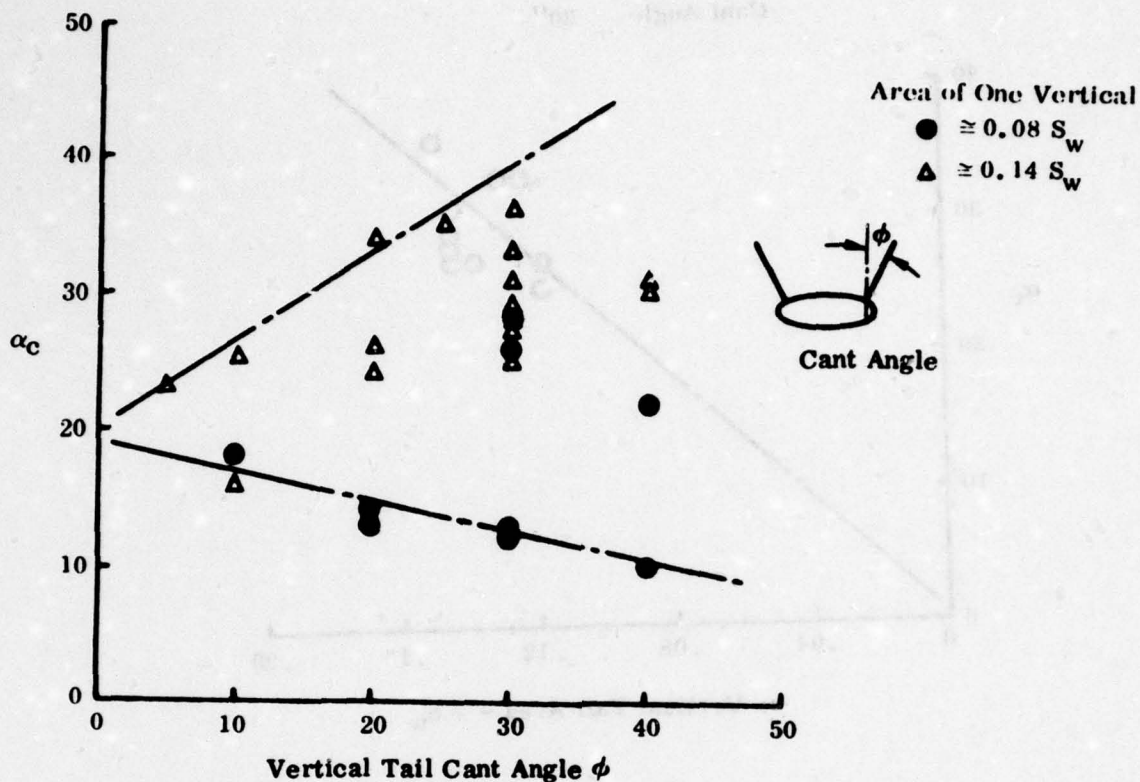


Figure 113. Effect of Vertical Tail Area

The data for the group of larger vertical tails, however, indicate that increasing cant angle up to approximately 40 degrees produces a favorable effect on the vertical tail contribution to directional stability. A significant variation, at a constant cant angle, in the angle of attack at which directional stability is lost is exhibited by the data, again illustrating the sensitivity of this parameter to LEX/forebody vortex interactions.

This is also illustrated in Figure 114, where the variation in α_c is plotted against the actual vertical tail area for a constant cant angle of 30 degrees. Some effect of area increase is shown, but again the vortex flow effects are shown to be significant.

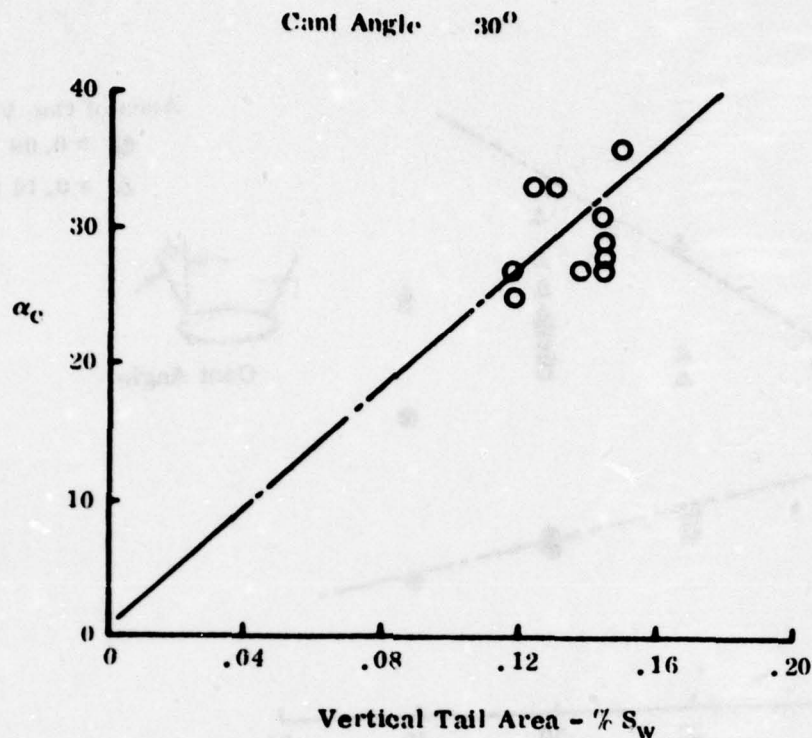


Figure 114. Effect of Vertical Tail Area

Examining again the data in Figure 113 at a constant cant angle of 30 degrees, two points for the smaller vertical tail area show a wide divergence of results. This effect is shown to be due to a variation in longitudinal location, as shown in Figure 115. Figure 116 presents a description of the vertical tail geometries which correspond to these data. Figure 116 shows that a significant improvement in the vertical tail contribution to directional stability is achieved by moving the tails forward into a region of favorable interaction with the forebody/LEX/wing flow field system. This is in spite of the fact that this forward location represents a reduction in vertical tail moment arm.

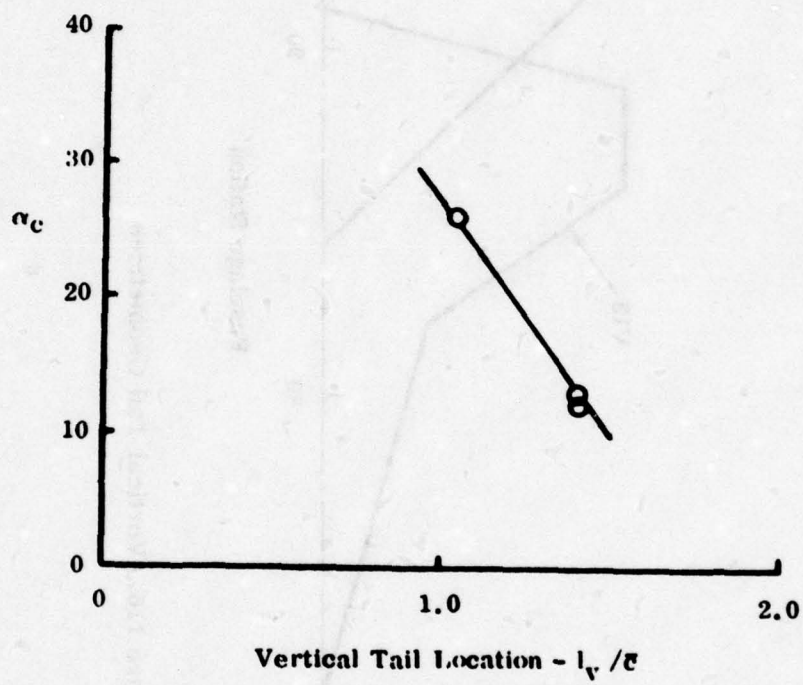


Figure 115. Effect of Fore and Aft Location

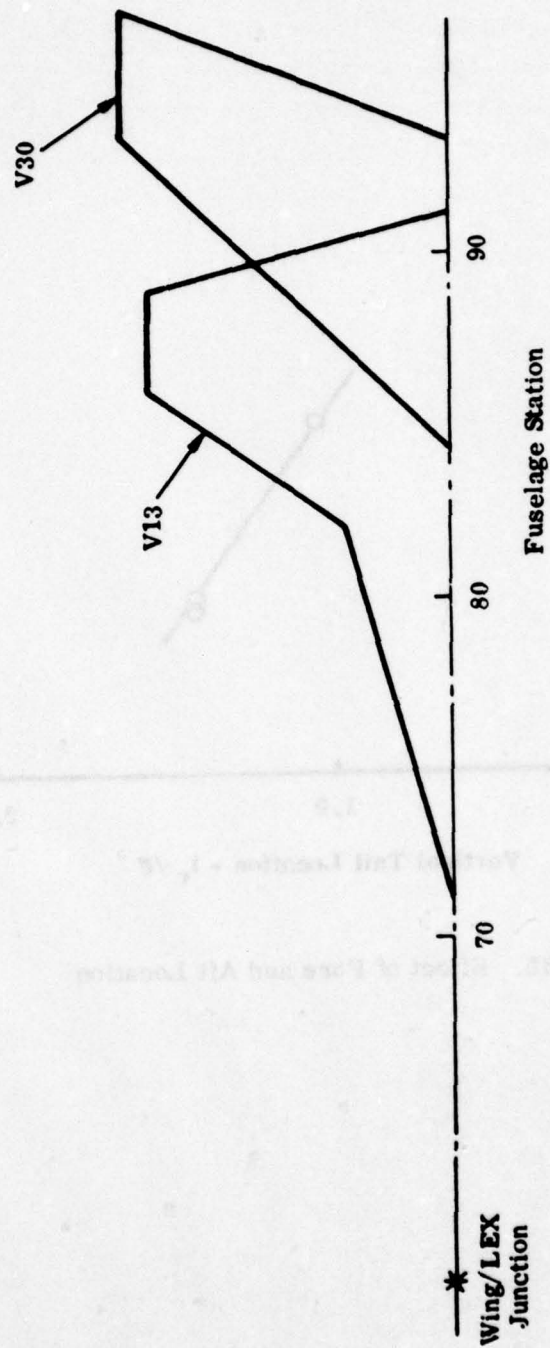


Figure 116. Vertical Tail Geometries

4. MISCELLANEOUS CONFIGURATION COMPONENTS

The major configuration components which have a dominant influence on the flying qualities of an aircraft at high angles of attack are the wing LEX, the forebody and the vertical tails. A detailed discussion of the effects of geometric variations of these components is contained in the foregoing paragraphs of this report. Certain other configuration components are responsible for a more minor, but still important, contribution to high angle-of-attack characteristics. These components are:

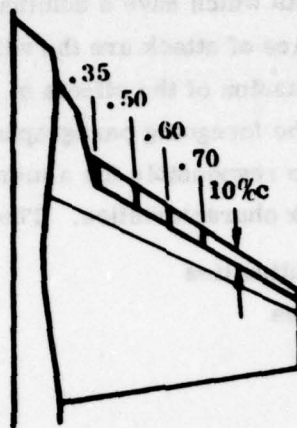
- 1) Wing leading edge discontinuities
- 2) Wing upper surface fences
- 3) Wing leading edge flaps
- 4) Wing trailing edge flaps
- 5) Dorsal/ventral fins
- 6) Decoupled canards

The existing data base for these components consists mainly of low speed wind tunnel tests and is, in general, not comprehensive. Due to the limited nature of the data base, in many cases, design guidelines for these components cannot be developed and only general comments are appropriate.

a. Wing Leading Edge Discontinuities

A series of wing planform leading edge discontinuities was tested at low speeds on the F-5 aircraft and the results are reported in References 49, 51, and 52. These discontinuities are also referred to as wing leading edge sawteeth or snags in Volume II of this report.

The data of Reference 49 are representative of the results which were obtained in all tests. Figure 117 presents a description of four sawtooth geometries which were tested. The local wing chord was extended 10 percent outboard of wing semi-span stations of 35, 50, 60 and 70 percent, respectively.

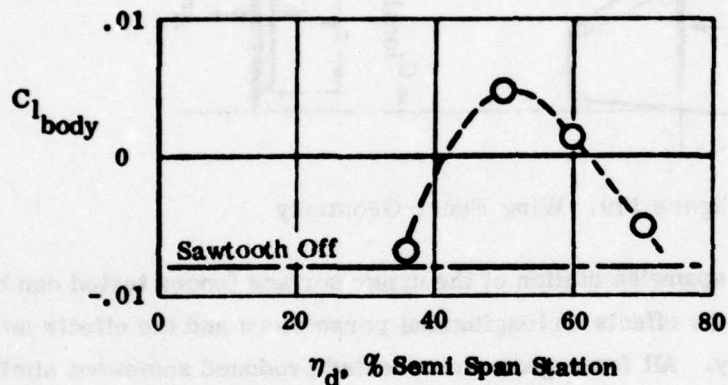
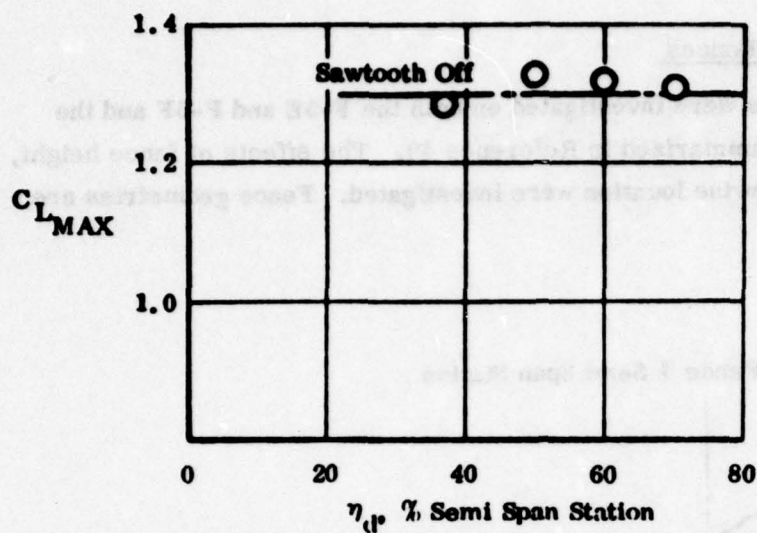


η_d , Discontinuity, % Semi-Span Station

Figure 117. Wing Leading Edge Discontinuities

Figure 118 presents a summary of the results obtained. The lateral/directional data are at an angle of attack of 22 degrees and an angle of sideslip of -10 degrees. These data indicate that the primary effect of the sawtooth is to improve the wing contribution to dihedral effect (Cl_β). A minor improvement in maximum lift coefficient and a minor loss of directional stability in the stall region is indicated. The optimum semi-span station for the sawtooth is shown to be at approximately the mid-span of the wing.

The discontinuity of the sawtooth at the wing leading edge produces a vortex, rotating in a sense opposite to the wing tip and LEX vortices. This vortex acts as an aerodynamic fence, inhibiting the spanwise growth of the boundary layer, thus improving the wing flow characteristics.



Lateral/Directional Data

Angle of Attack = 22°
Angle of Sideslip = -10°

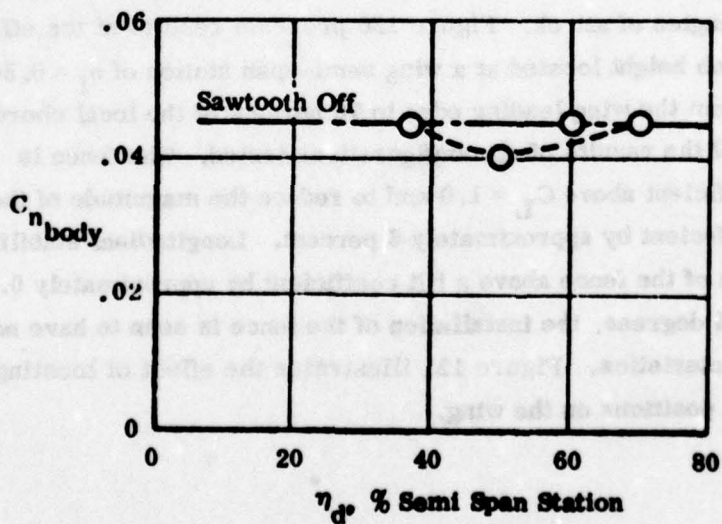


Figure 118. Effect of Leading Edge Discontinuities

b. Wing Upper Surface Fences

Upper surface wing fences were investigated on both the F-5E and F-5F and the results of the tests are summarized in Reference 49. The effects of fence height, chordwise length and spanwise location were investigated. Fence geometries are defined in Figure 119.

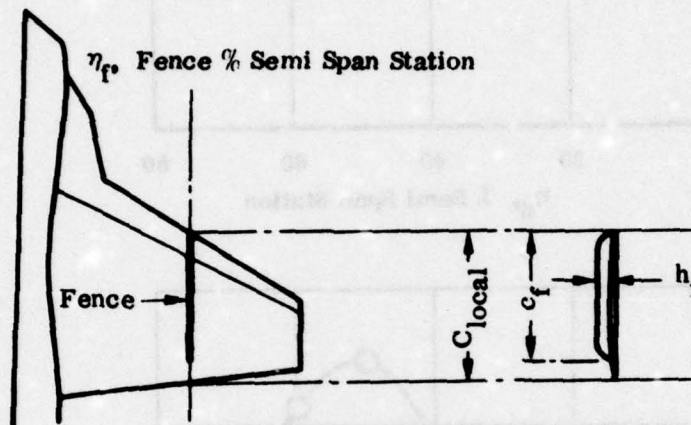


Figure 119. Wing Fence Geometry

The effects of varying the spanwise station of the upper surface fences tested can be separated into two areas, the effects on longitudinal parameters and the effects on lateral/directional stability. All fence geometries tested produced somewhat similar effects on the maximum lift coefficient achieved and on the level of longitudinal stability at moderate to high angles of attack. Figure 120 presents results of the effect of adding a fence of five-inch height located at a wing semi-span station of $\eta_f = 0.50$ and extending chordwise from the wing leading edge to 70 percent of the local chord. These results are typical of the results of all configurations tested. The fence is seen to reduce the lift coefficient above $C_L = 1.0$ and to reduce the magnitude of the maximum value of lift coefficient by approximately 6 percent. Longitudinal stability is increased by the addition of the fence above a lift coefficient by approximately 0.7. At angles of attack above 24 degrees, the installation of the fence is seen to have no effect on longitudinal characteristics. Figure 121 illustrates the effect of locating the fence at other spanwise positions on the wing.

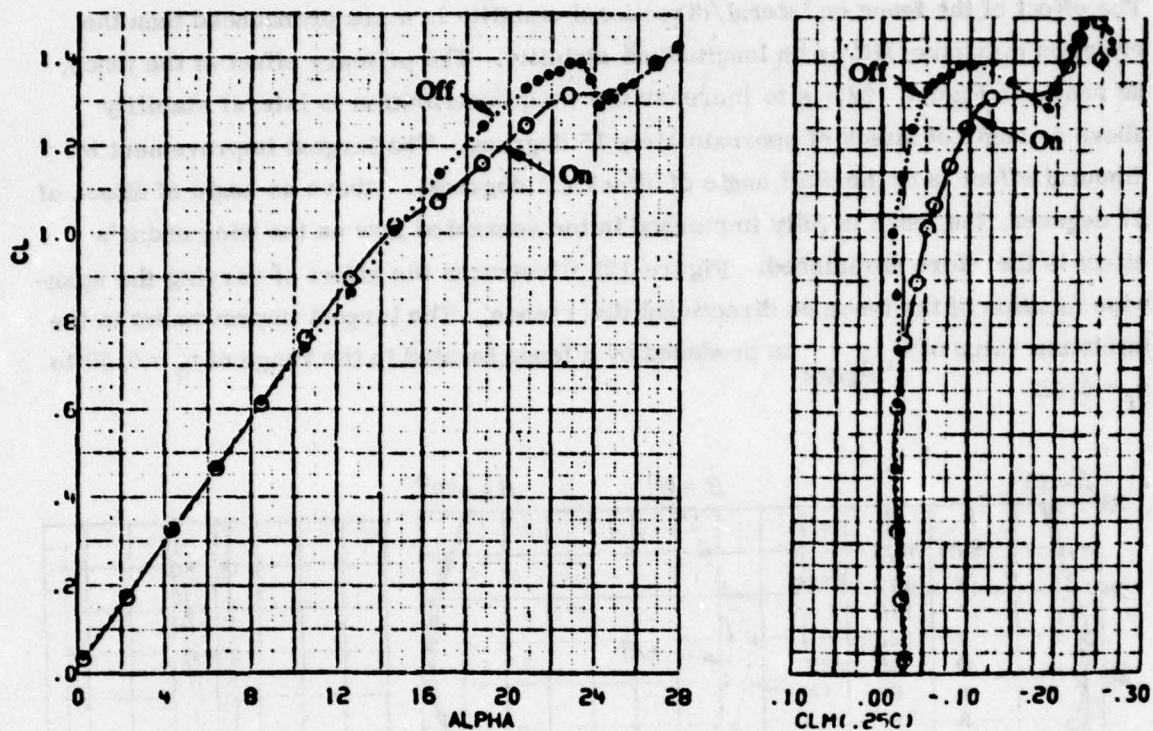


Figure 120. Effect of Upper Surface Wing Fences S

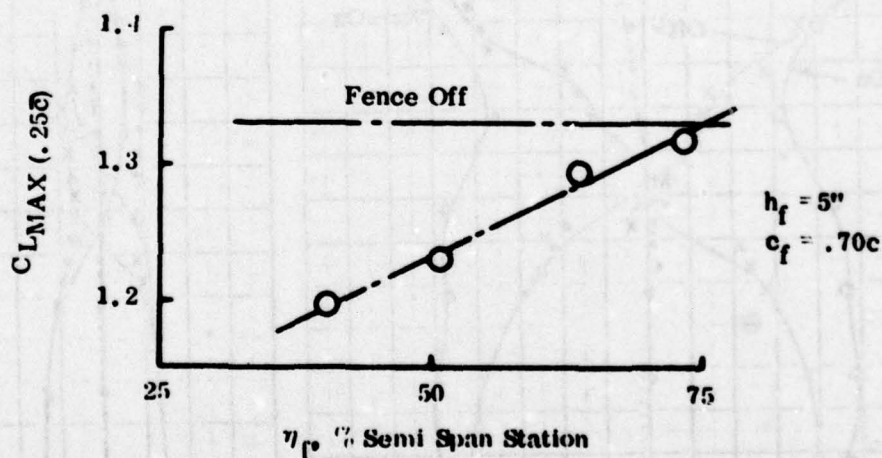


Figure 121. Effect of Fence Semi-Span Station

The effect of the fence on lateral/directional stability is more pronounced than the effect on maximum lift or on longitudinal stability. The primary effect of the fence, as shown in Figure 122, is to increase the wing contribution to lateral stability above an angle of attack of approximately 15 degrees. The largest improvement in dihedral effect is at the stall angle of attack (23 degrees). Above an angle of attack of 27 degrees, the fence is fully immersed in the separated flow on the wing and its effect is therefore diminished. Figure 123 illustrates the effect of varying the spanwise location of the fence on directional divergence. The largest improvement in the minimum value of $C_{n\beta_{DYN}}$ is produced by a fence located in the range of $\eta_f = 0.50$ to $\eta_f = 0.60$.

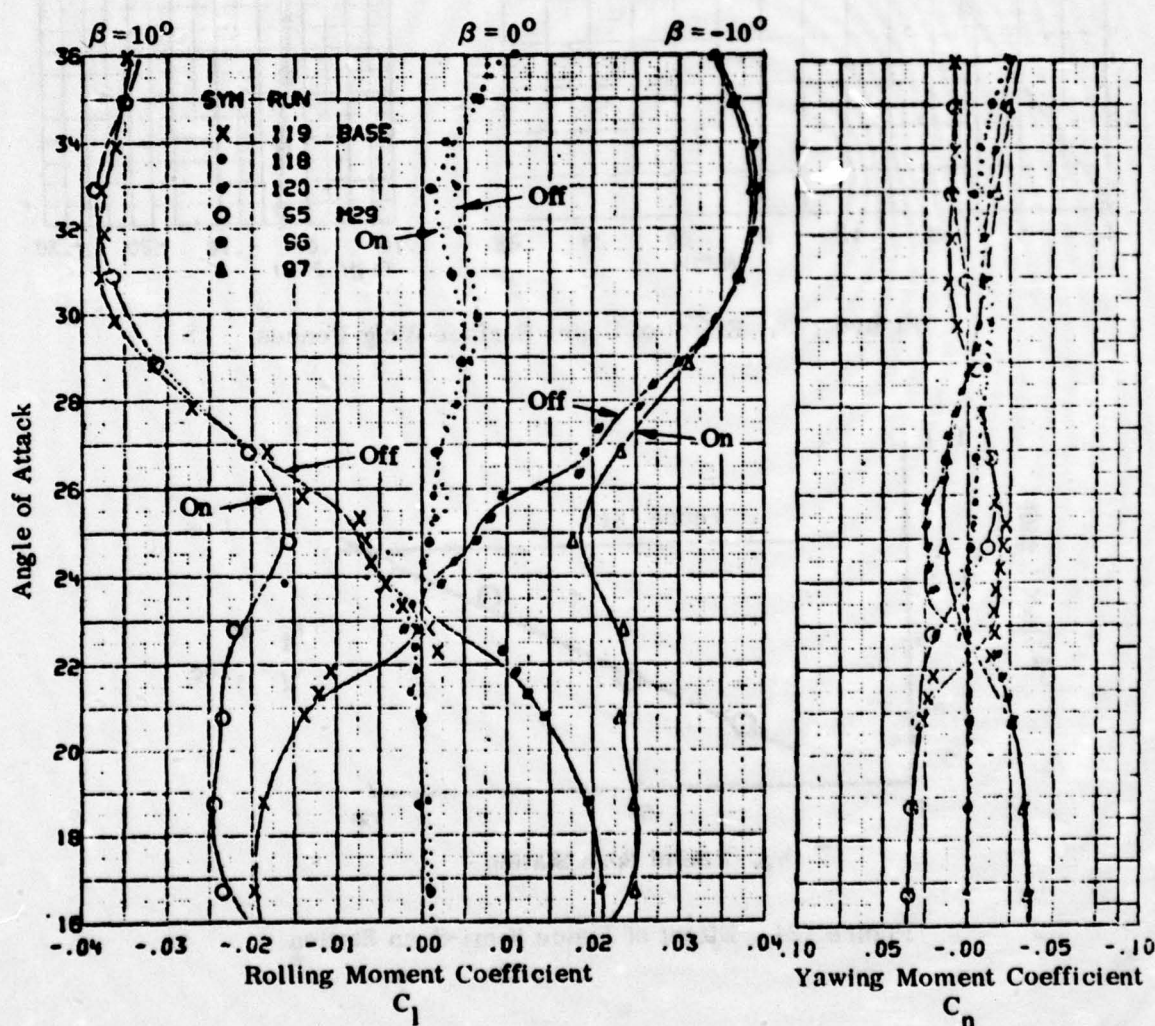


Figure 122. Effect of Upper Surface Wing Fences

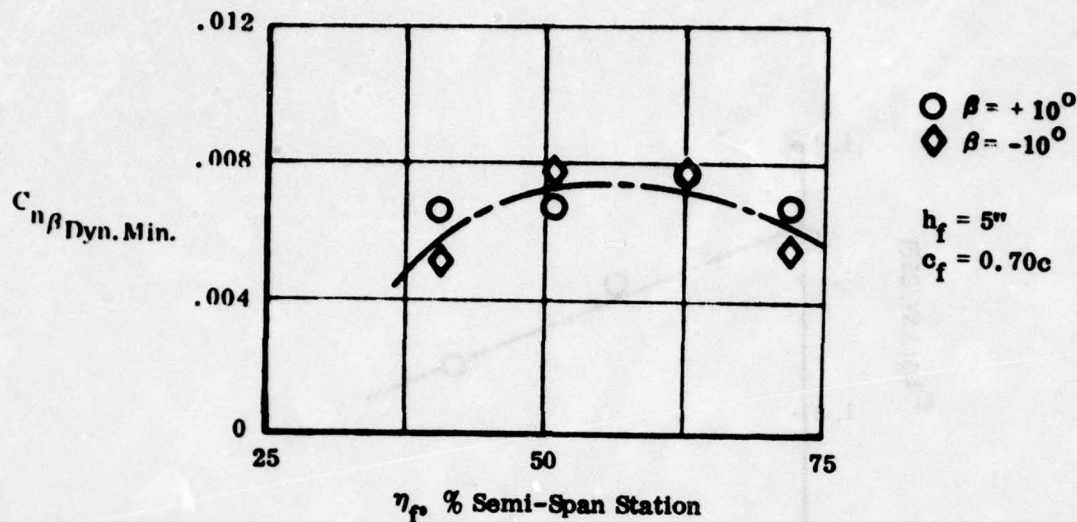


Figure 123. Effect of Fence Semi-Span Station

As discussed in the preceding paragraph, the optimum fence location was found to be at approximately the wing mid-semi-span. This mid-semi-span location resulted in the maximum improvement in lateral/directional stability and resulted in only a small penalty in maximum lift coefficient. With the fence semi-span fixed at $\eta_f = 0.50$ and the fence length fixed at $c_f = 0.70C$, the effect of varying fence height was studied in the tests of Reference 49. Figure 124 illustrates the effect of reducing the fence height on the maximum lift coefficient. Reducing the fence height by 50 percent produced a corresponding 50 percent reduction in the fence penalty to $C_{L_{\max}}$. Figure 125 shows that this reduction in fence height results in only a small degradation in the minimum value of $C_{n\beta \text{ DYN}}$, indicating that the shorter fence is more desirable, overall.

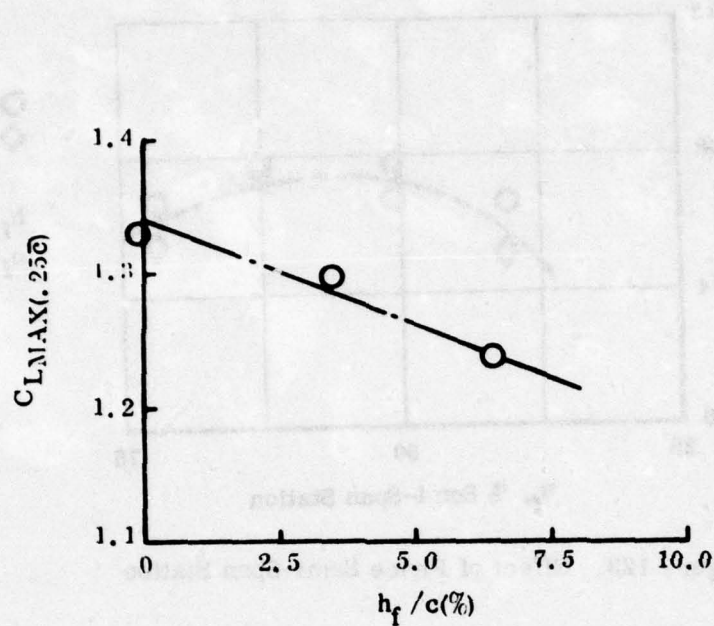


Figure 124. Effect of Fence Height

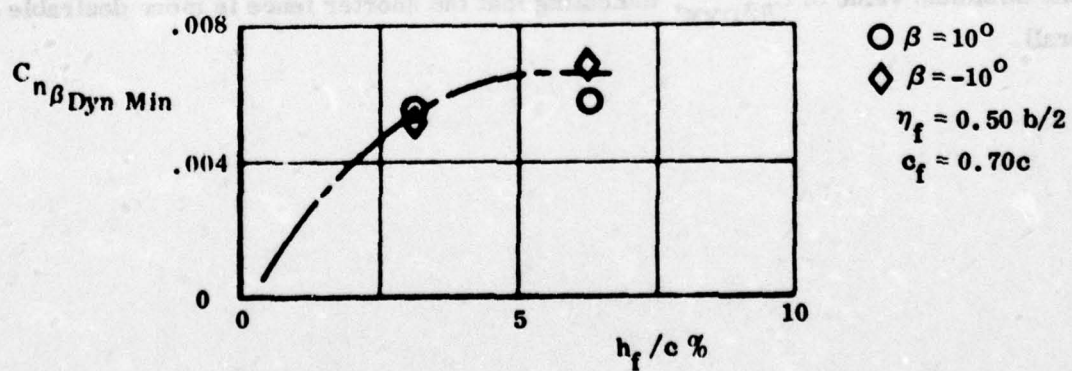


Figure 125. Effect of Fence Height

The effect of varying the chordwise extent of the fence was also studied.

Figures 126 and 128 illustrate the effect of reducing the chord length of the fence by varying the local chord position of the leading edge of the fence. Figures 127 and 129 illustrate the effect of reducing the chord length of the fence by varying the chord location of the aft end of the fence. As seen in Figures 126 and 127, any reduction in the chordwise length of the fence, whether from the forward of the aft end, results in a reduction in the fence C_{Lmax} penalty. Figures 128 and 129 show, similarly, that reduction of fence chord length degrades the value of minimum $C_{n\beta DYN}$ for these configurations.

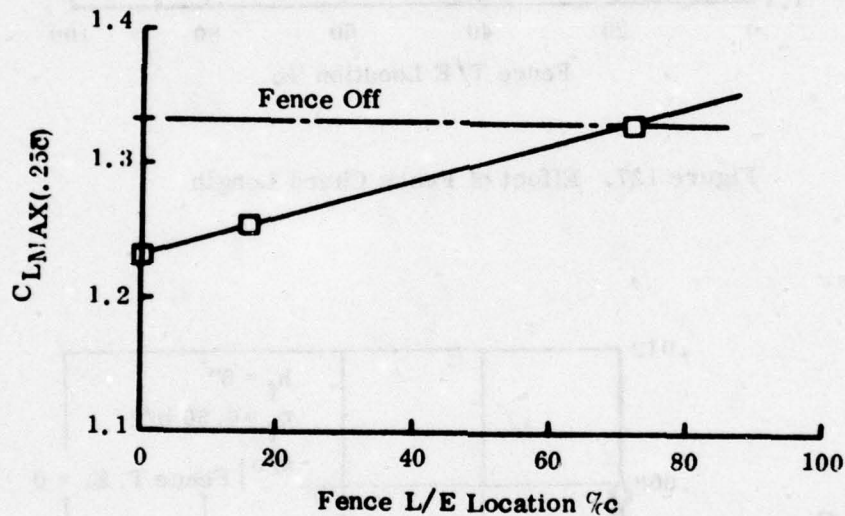


Figure 126. Effect of Fence Chord Length

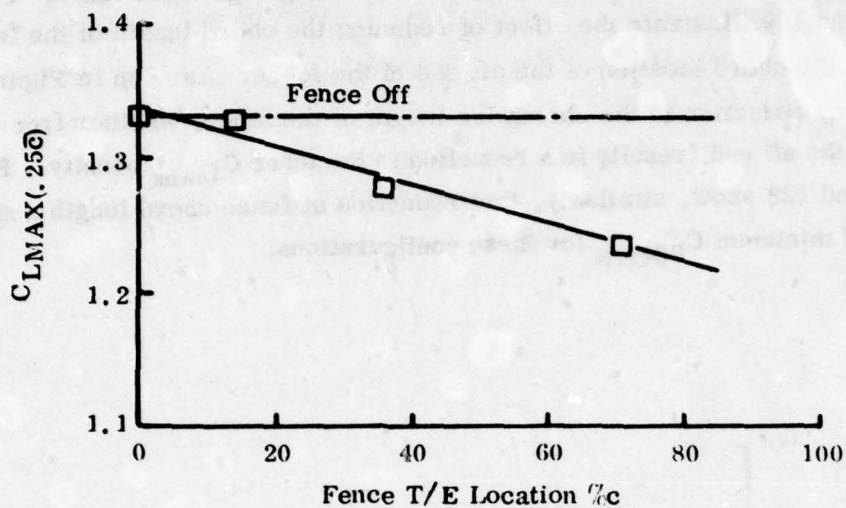


Figure 127. Effect of Fence Chord Length

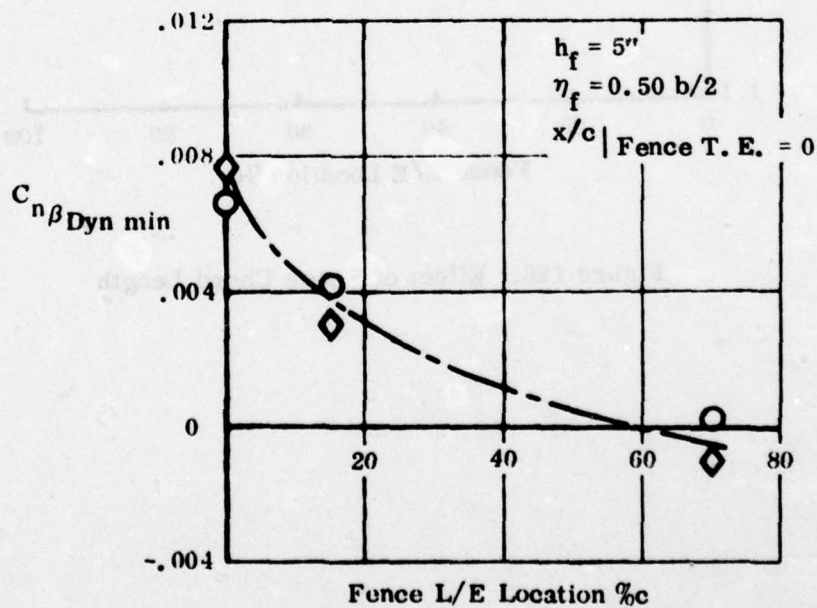


Figure 128. Effect of Fence Chord Length

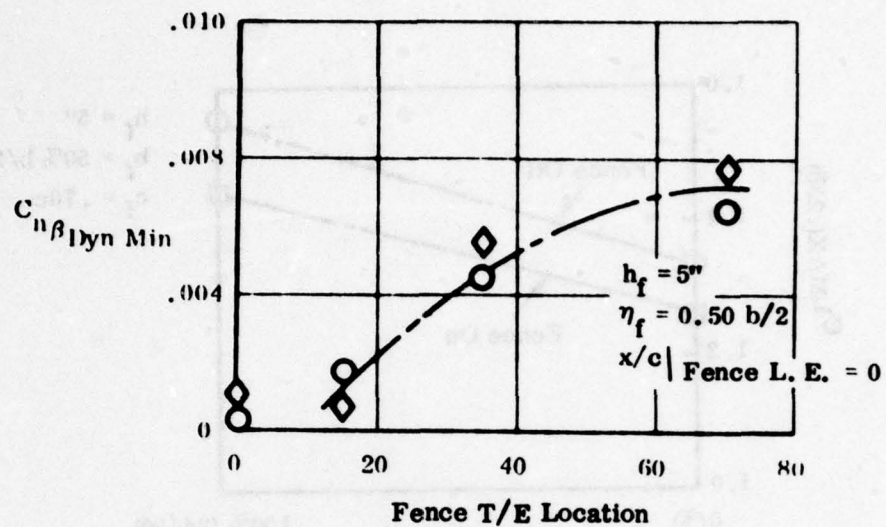


Figure 129. Effect of Fence Chord Length

The previously presented increments due to fence installation are modified when data are compared with leading and trailing edge flap deflected. Figures 130 and 131 illustrate this effect.

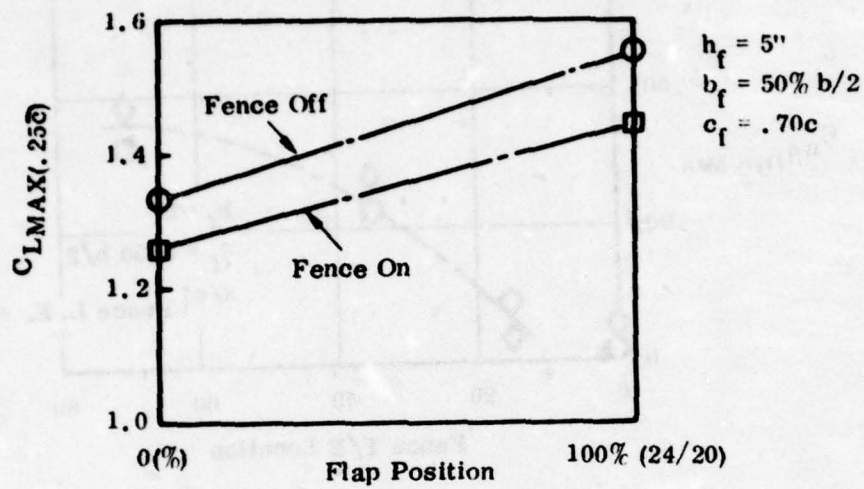


Figure 130. Effect of Slap Deflection on C_{LMax}

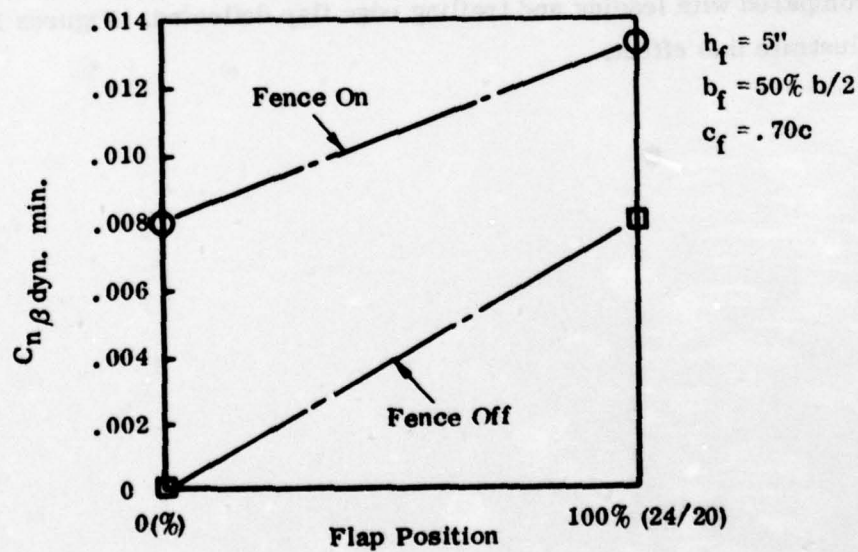
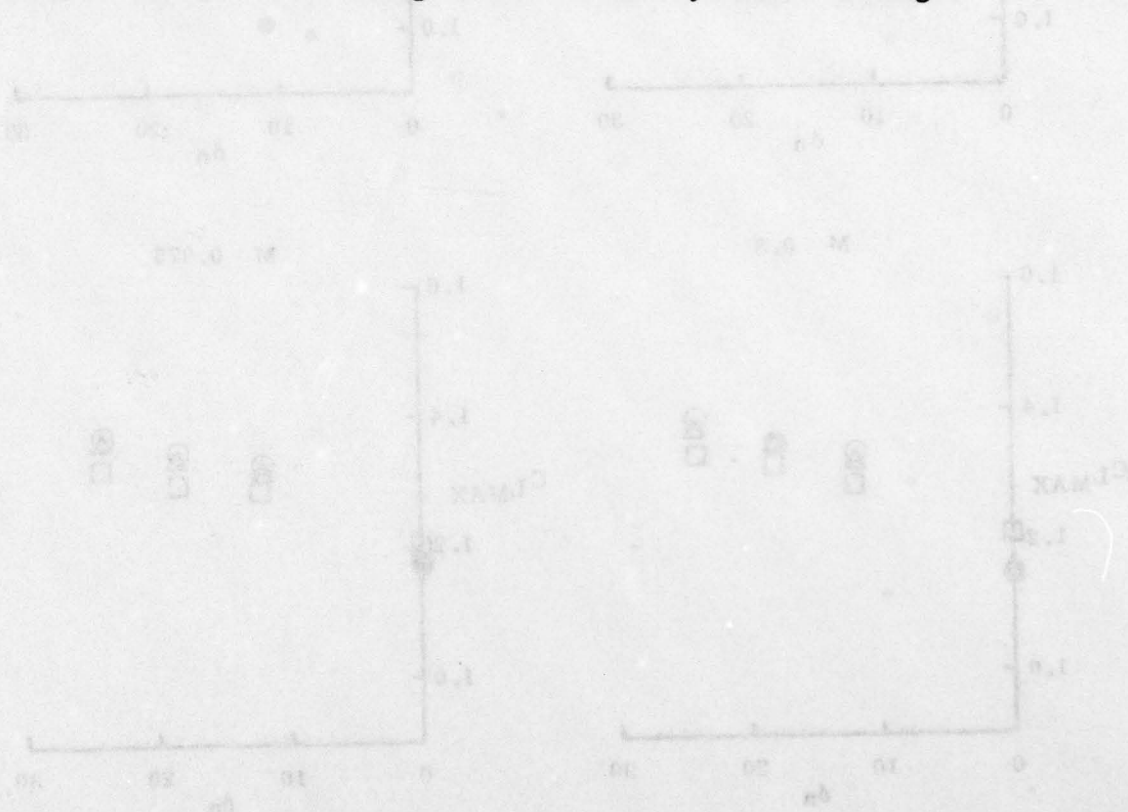


Figure 131. Effect of Flap Deflection on $C_{N\beta \text{ Dyn. Min.}}$

c. Wing Leading-Edge Flaps

The effect of leading-edge flaps at high angles of attack is two-fold. In the longitudinal axis, the maximum lift coefficient of the wing is increased as leading-edge flap deflection is increased. In the lateral/directional axes, increasing the leading-edge flap deflection increases the wing contribution to dihedral effect and the vertical tail contribution to static directional stability. Figure 132 presents the effect of leading-edge flap deflection on CL_{MAX} for several values of trailing-edge flap deflection at Mach numbers of 0.6, 0.7, 0.8 and 0.875. These data are for the F-5 configuration.

Figure 133 illustrates the effect of leading-edge flap deflection on directional and lateral stability. These data are for the YF-17 configuration. As shown, a significant increase in the levels of stability are produced by deflecting the leading-edge flaps by 20 degrees. Increasing the deflection in 5 degree increments is seen to further improve dihedral effect although directional stability remains unchanged.



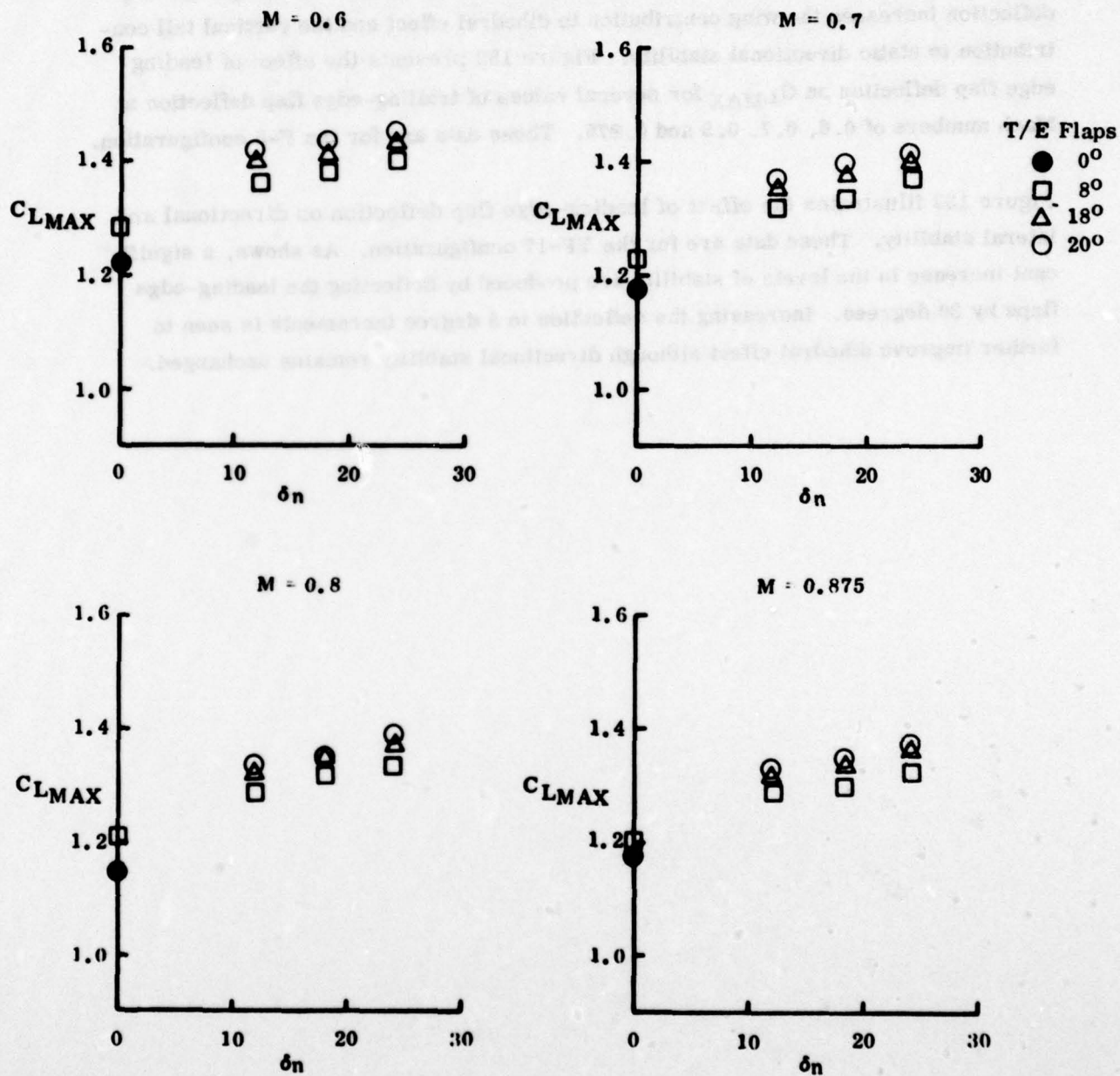


Figure 132. Effect of Leading Edge Flap Deflection

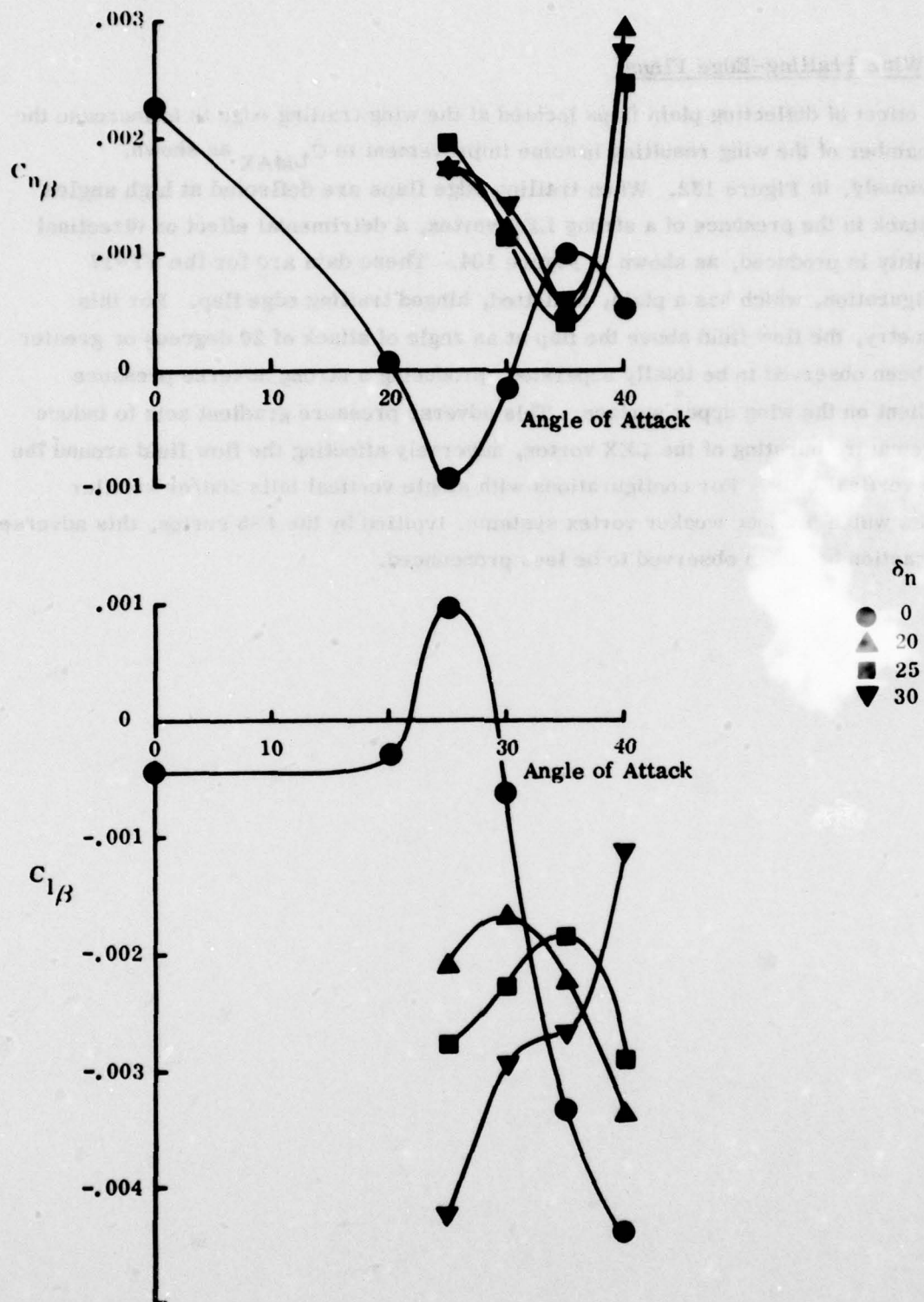


Figure 133. Effect of Leading Edge Flap Deflection

d. Wing Trailing-Edge Flaps

The effect of deflecting plain flaps located at the wing trailing edge is to increase the aft camber of the wing resulting in some improvement in C_{LMAX} as shown, previously, in Figure 132. When trailing edge flaps are deflected at high angles of attack in the presence of a strong LEX vortex, a detrimental effect on directinal stability is produced, as shown in Figure 134. These data are for the YF-17 configuration, which has a plain, unslotted, hinged trailing edge flap. For this geometry, the flow field above the flap at an angle of attack of 20 degrees or greater has been observed to be totally separated, producing a strong adverse pressure gradient on the wing upper surface. This adverse pressure gradient acts to induce a premature bursting of the LEX vortex, adversely affecting the flow field around the twin vertical tails. For configurations with single vertical tails and/or smaller LEX's which produce weaker vortex systems, typified by the F-5 series, this adverse interaction has been observed to be less pronounced.



Figure 134. Effect of Leading Edge Flap Deflection

DATA IS FOR $\beta = 10^\circ$
L/E Flaps 40/20

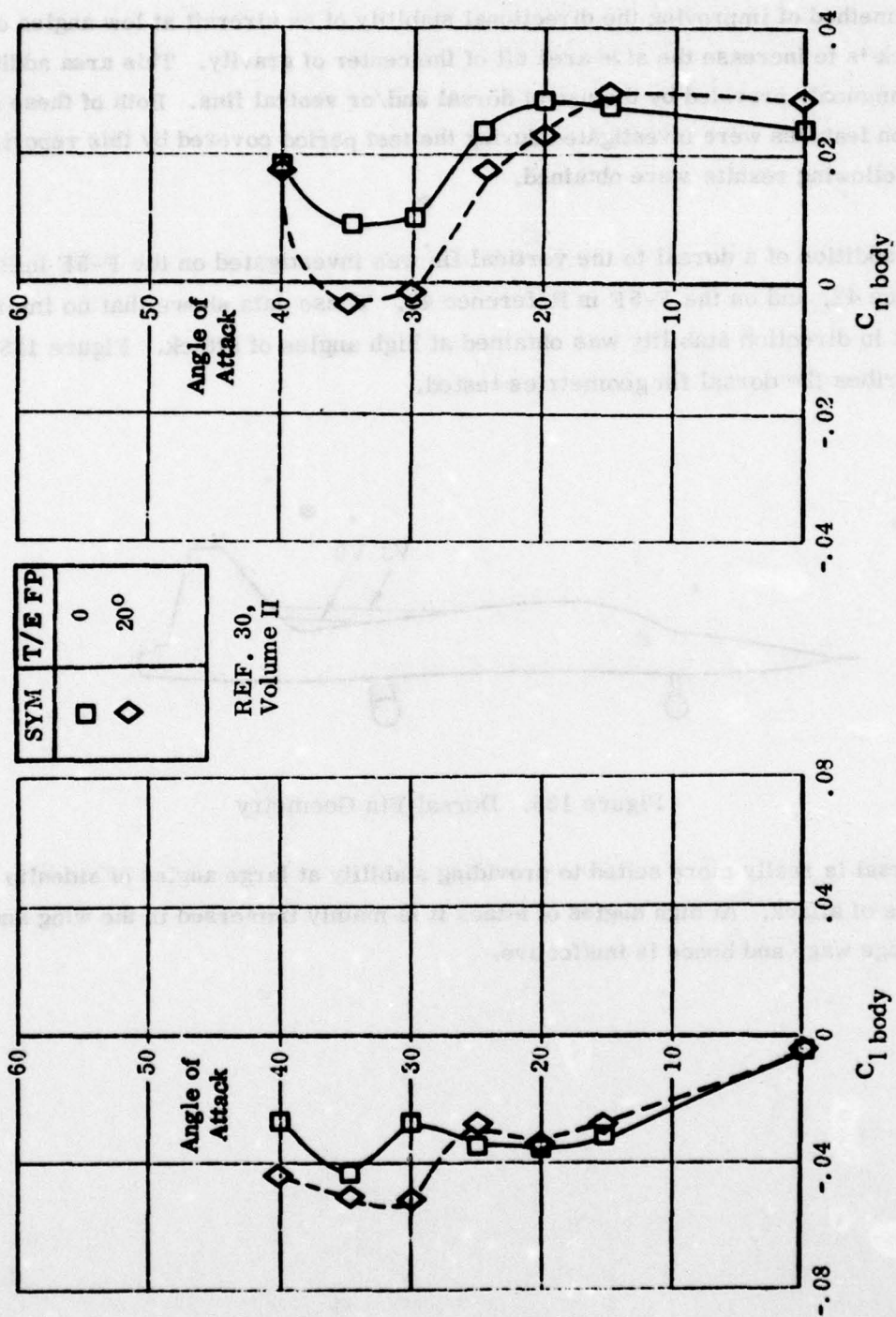


Figure 134. Effect of T/E Flap Deflection

e. Dorsal/Ventral Fins

One method of improving the directional stability of an aircraft at low angles of attack is to increase the side area aft of the center of gravity. This area addition is commonly provided by the use of dorsal and/or ventral fins. Both of these configuration features were investigated during the test period covered by this report, and the following results were obtained.

The addition of a dorsal to the vertical fin was investigated on the F-5F in Reference 42, and on the F-5F in Reference 49. These data shown that no improvement in direction stability was obtained at high angles of attack. Figure 135 describes the dorsal fin geometries tested.

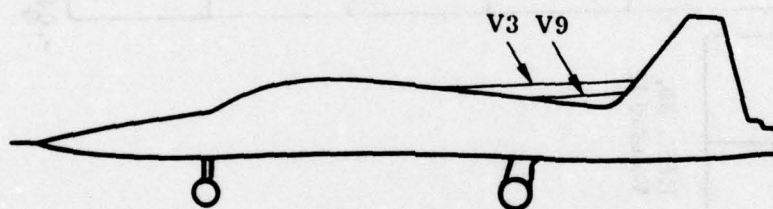


Figure 135. Dorsal Fin Geometry

A dorsal is really more suited to providing stability at large angles of sideslip at low angles of attack. At high angles of attack it is mainly immersed in the wing and fuselage wake and hence is ineffective.

(1) Ventrals

The ventral fin is an inefficient stabilizing surface. Confined to an area bounded by the rear fuselage and the maximum take-off angle of attack, it is by nature a low aspect ratio surface, with the maximum area at the forward end. Figure 136 below illustrates the geometry of a typical ventral fin.

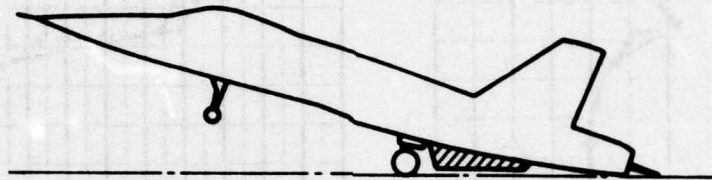


Figure 136. Typical Ventral Fin

The effect of large, side by side ventral fins was determined on the F-5F in the test of Reference 49. Figure 137 illustrates the actual geometry of these ventral fins. A small improvement in directional stability is obtained at all angles of attack as seen in Figure 138.

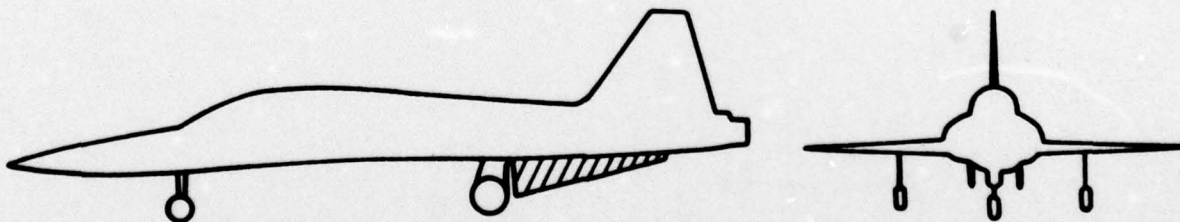


Figure 137. Ventral Fin Geometry

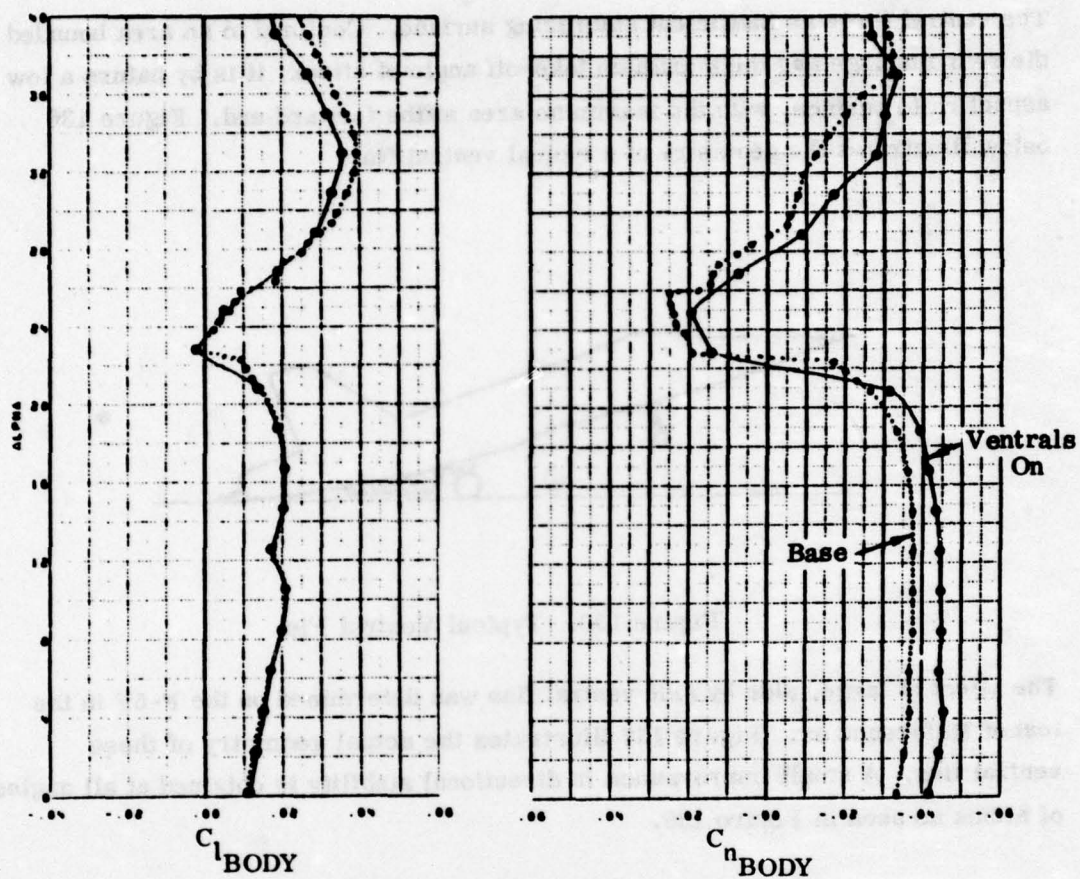


Figure 138. Effect of Ventral Fins

f. Decoupled Canards

A series of decoupled canard surfaces were investigated on the F-5F model in References 45, 46, and 49. These canards were all located on the forebody maximum half breadth just aft of the radome, as shown in Figure 139.

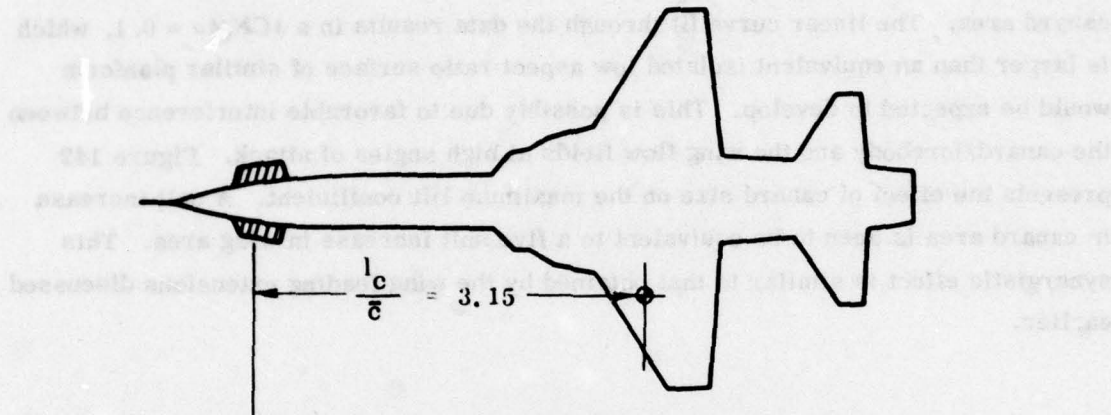


Figure 139. Typical Canard Geometry

For details of the actual canard configurations tested, reference should be made to the appropriate sections in Volume II.

The canards were all tested at low speeds. The results have been analyzed in terms of both longitudinal and lateral/directional effects at high angles of attack.

The canard incremental normal force and pitching moment, obtained at a constant angle of attack, just below the wing stall, are presented in Figure 140. These data are shown to be reasonably linear. The center of pressure for the normal force on the canard is in good agreement with the actual physical moment are of the canard ($l_c/c = 3.15$).

The normal force increment (C_{N_c}) is presented in Figure 141 as a function of canard area. The linear curve fit through the data results in a $\delta C_N / \delta \alpha = 0.1$, which is larger than an equivalent isolated low aspect ratio surface of similar planform would be expected to develop. This is possibly due to favorable interference between the canard/forebody and the wing flow fields at high angles of attack. Figure 142 presents the effect of canard size on the maximum lift coefficient. A unit increase in canard area is seen to be equivalent to a five unit increase in wing area. This synergistic effect is similar to that obtained by the wing leading extensions discussed earlier.

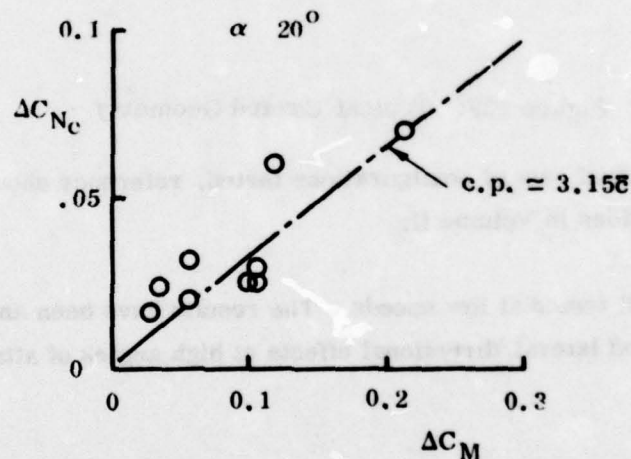


Figure 140. Effect of Decoupled Canards

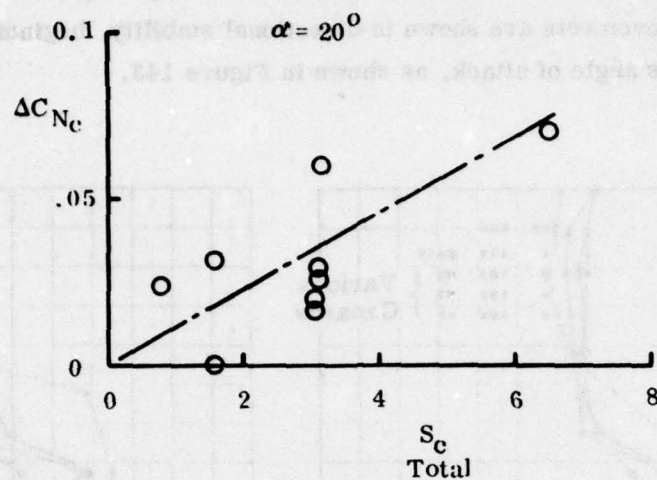


Figure 141. Effect of Decoupled Canards

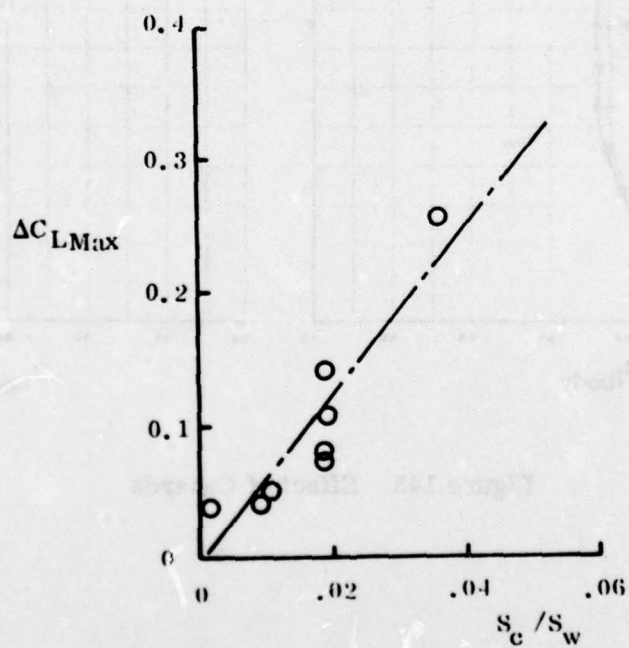


Figure 142. Effect of Canard Size

The small, decoupled canard surfaces tested on the F-5 were found to provide benefits in both lateral and directional stability in the high angle-of-attack region. The largest improvements are shown in directional stability, beginning at approximately 10 degrees angle of attack, as shown in Figure 143.

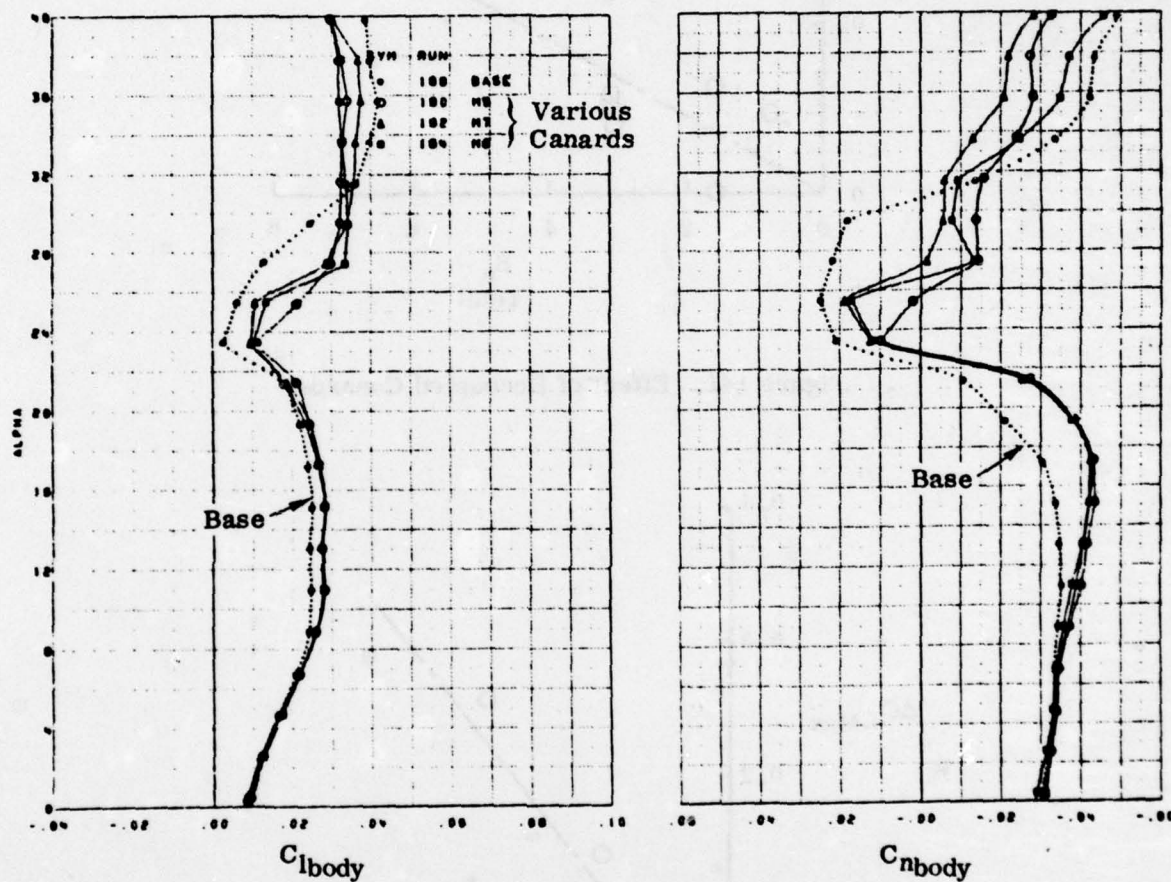


Figure 143. Effect of Canards

SECTION III

CONCLUDING REMARKS

One of the most frequently used words in this report has been "vortex," as in forebody vortex, LEX vortex, leading-edge discontinuity vortex, etc. The high angle-of-attack flight regime is shown to be intimately involved with vortex flows. Stability and control in this area involves the correct production and control of the various vortex systems surrounding the airframe.

Any future work in this area, i.e., the angle-of-attack range between 30 and 60 degrees, cannot ignore vortex phenomena and a basic understanding of the vortex and its usefulness must be obtained. Currently the only vortex under partial control is that generated by the LEX. Large increases in lift by vortex interaction have been demonstrated. Through the use of the guidelines derived in this report, these can be predicted for a certain class of wing configurations. The generation and placement of the optimum lift enhancing LEX vortex for any form of wing planform is still not possible.

The forebody vortex flows are currently partially understood and some means to ensure their symmetry are available, e.g., the Shark nose. However, the ability to design a specific stability into the nose of an aircraft is not presently possible. The use of the LEX vortex to provide additional high angle of attack directional stability through favorable interaction with twin vertical tails has been demonstrated. This is the least understood of all the interactions.

The ultimate goal is, therefore, a full understanding of all the various vortex flows around the aircraft. This can only come after a further series of investigations, both experimental and theoretical, have been carried out and the results thoroughly analyzed. As a first step in this process, it is suggested that a more detailed understanding of the force and moment distributions around the aircraft be obtained. For

this purpose a wind tunnel investigation with a more comprehensive balance system could be used, where in addition to the total body forces, the forebody forces and moment are measured. By this means the effect of the nose vortex system could be partially isolated and the effects of variations in forebody geometry could be investigated. Similar techniques could be used to determine the optimum LEX vortex conditions.

Any study of vortex flows would be incomplete without some form of flow visualization and currently the best technique appears to be the water tunnel, where the vortices are observed by the injection of various dyes into the flow field's regions of interest. Therefore, future wind tunnel investigations of vortex flows must be supported by water tunnel flow visualization studies as a parallel effort.